

**Structural Characterization of
17 β -Hydroxysteroid Dehydrogenase Type 14
and Inhibitor Optimization Using Crystallography
and Computational Techniques**

Dissertation

zur Erlangung des Doktorgrades
der Naturwissenschaften
(Dr. rer. nat.)

dem
Fachbereich Pharmazie der
Philipps-Universität Marburg
vorgelegt

von
Nicole Bertoletti
aus
Sarzana

Marburg/Lahn 2017

Erstgutachter Prof. Dr. Gerhard Klebe
Institut für Pharmazeutische Chemie
Philipps-Universität Marburg

Zweitgutachter Dr. Sarndrine Marchais-Oberwinkler
Institut für Pharmazeutische Chemie
Philipps-Universität Marburg

Eingereicht am 22.8.2017

Tag der Mündlichen Prüfung am 4.10.2017

Hochschulkennziffer: 1180

Die Untersuchungen zur vorliegenden Arbeit wurden auf Anregung von Herrn Prof. Dr. Gerhard Klebe am Institut für Pharmazeutische Chemie des Fachbereichs Pharmazie der Philipps-Universität Marburg in der Zeit von Januar 2014 bis August 2017 durchgeführt.

Summary

17 β -Hydroxysteroid dehydrogenase type 14 (17 β -HSD14) is the latest identified subtype of 17 β -HSDs. *In vivo* this enzyme oxidizes the hydroxyl group at position 17 of estradiol (E2) and 5-androstenediol (5-diol) in the presence of NAD⁺ as cofactor. Two isoforms of this cytosolic protein exist that differ only in sequence position 205: S205 and T205. So far, the protein has not been thoroughly investigated in detail and its physiological role remains unknown. Prior to this thesis, the 17 β -HSD14 apoenzyme (S205) had already been crystallized. The determined structure revealed a very broad and open active site and the conserved catalytic triad and the Rossmann-fold motif. However, all C-terminal tails and for some chains also amino acids in the flexible loop (189-212) were not defined in the electron density. Moreover, it is impossible to derive information regarding a potential substrate from this apo structure. Therefore, the renewed structural determination of the 17 β -HSD14 apo protein as well as in complex with its cofactor and substrate was of utmost importance.

After successful establishment of the expression and purification protocols for 17 β -HSD14 protein, the two enzyme isoforms (S205 and T205) were characterized biochemically. The structures of the S205 apoenzyme and the binary complexes with NAD⁺ of both isoforms were determined. In these complex structures the flexible loop adopts a unique closed conformation differing from the apo structure. Binding of the cofactor is accompanied by a shift of the flexible loop and of the C-terminal Tyr253' of the adjacent monomer, thereby reducing the size of the active site. The ternary complex of the enzyme with estrone (E1) and NAD⁺ was also determined. E1 binds to the active site in an atypical fashion, in so far as its A-ring and not the enzymatically modified position 17 close to the nicotinamide moiety of NAD⁺.

Enzyme inhibitors are useful tools to study the consequences of enzyme inhibition *in vivo*. This allows to clarify whether this enzyme may be interesting as a new drug target for a certain disease. In addition, potent and selective 17 β -HSD14 inhibitors may help understand the selectivity issue with other 17 β -HSDs. As no 17 β -HSD14 inhibitor was known prior to this study, the goal was to identify and optimize nonsteroidal 17 β -HSD14 inhibitors. To that, a library of 17 β -HSD1 and 17 β -HSD2 inhibitors was screened against 17 β -HSD14. The most promising hit was taken as the starting point for further chemical modification applying a ligand-based approach. Newly designed compounds were synthesized and subsequently

tested for their 17 β -HSD14 inhibitory activity. Prior to this thesis, no human 17 β -HSD structure in complex with a nonsteroidal ligand was published. The crystal structures confirmed that the inhibitors bind to the substrate binding site and allowed to rationalize the strong affinity of these inhibitors.

Subsequently, two different structure-based strategies were pursued for inhibitor design. The first structure-based modifications of the initial pyridine-based scaffold led to a ten-fold more potent inhibitor. The goal of the second structure-based optimization strategy was to extend the central pyridine core to interact with the empty binding pocket adjacent to the steroid A and B-ring. The predicted binding mode was verified by co-crystal structures and the low nanomolar potency was confirmed by biophysical characterization. The new crystal structures revealed how small changes of the inhibitors affect the adopted binding mode. The characterization of the most promising 17 β -HSD14 inhibitors against 17 β -HSD1, 17 β -HSD2, and 17 β -HSD10 revealed varying degrees of selectivity. In addition, some of these inhibitors showed very low cytotoxicity and did not interact with the multi-drug resistance protein Pgp, indicating these compounds might not be effluxed from the brain and that the risk of potential side effects is reduced. This suggests these inhibitors as tool compounds for further investigation *in vivo*.

To explain the selectivity profiles of the ligands towards 17 β -HSD14 and other 17 β -HSDs we conducted a structural comparison. The typical V-like shape of the binding pocket of 17 β -HSD14 is determined by His93 and Gln148, which are not present in 17 β -HSD1, 17 β -HSD8 and 17 β -HSD10. In addition, the latter three enzymes have a rather flat binding pocket. This suggests that matching the characteristic three-dimensional requirements of 17 β -HSD14 and optionally addressing His93 and/or Gln148 will increase the selectivity toward this target. Such inhibitors were predicted by docking a library of about 400 17 β -HSD1 and 17 β -HSD2 inhibitors with GOLD followed by *in vitro* screening of docking hits and related compounds. Remarkably, predicted binding modes were in poor agreement with the subsequently determined crystal structures due to the adaptability of the binding pocket caused by the flexible loop.

Finally, a large fragment screening campaign by X-ray crystallography with the aim to discover new inhibitor scaffolds bound to 17 β -HSD14 was performed. This resulted in two fragments that could be clearly identified in the electron density. However, these fragments did not significantly inhibit 17 β -HSD14. In order to enhance affinity, fragment growing and fragment linking strategies were applied, resulting in two new inhibitors with better affinity than the starting fragments.

In summary, both isoforms of 17 β -HSD14, S205 and T205, were characterized biochemically and structurally resulting in four new crystal structures. The first two classes of inhibitor for this enzyme were discovered and the ligands were thoroughly profiled. In addition, the

structures of 12 nonsteroidal inhibitors in complex with the protein were elucidated for the first time for this protein family. The fragment screening by determining 96 fragment-soaked structures, resulted in two fragment hits that were successfully optimize culminating in two inhibitors more active than their precursor fragments.

Zusammenfassung

Die 17 β -Hydroxysteroid Dehydrogenase Typ 14 (17 β -HSD14) ist der zuletzt identifizierte Subtyp der 17 β -HSDs. *In vivo* oxidiert dieses Enzym die Hydroxyl-Gruppe von Estradiol (E2) und 5-Androstendiol (5-Diol) an Position 17 in Gegenwart des Kofaktors NAD⁺. Es existieren zwei Isoformen dieses zytosolischen Proteins, die sich ausschließlich in Sequenzposition 205 unterscheiden: S205 und T205. Bis jetzt wurde das Protein noch nicht gründlich und im Detail untersucht und seine physiologische Rolle bleibt unbekannt. Vor der Durchführung dieser Doktorarbeit war das 17 β -HSD14 Apoenzym (S205) bereits kristallisiert worden. Die gelöste Struktur zeigte ein sehr weites und offenes aktives Zentrum sowie die konservierte katalytische Triade und das Rossmann-Faltmotiv. Jedoch waren alle C-terminalen Enden und bei einigen Ketten auch Aminosäuren der flexiblen Schleife (189-212) nicht in der Elektronendichte definiert. Darüber hinaus ist es unmöglich, Informationen bezüglich eines potentiellen Substrats von dieser Apostruktur abzuleiten. Deshalb war die erneute Strukturbestimmung des 17 β -HSD14 Apoproteins sowie seiner Komplexe mit Kofaktor und Substrat von größter Wichtigkeit.

Nach erfolgreicher Etablierung der Expressions- und Aufreinigungsprotokolle für 17 β -HSD14 wurden die beiden Isoformen (S205 und T205) biochemisch charakterisiert. Die Strukturen des S205 Apoenzyms und der binären Komplexe beider Isoformen mit NAD⁺ wurden aufgeklärt. In diesen Strukturen nimmt die flexible Schleife eine einzigartige geschlossene Konformation ein, die sich von der Apostruktur unterscheidet. Die Bindung des Kofaktors geht einher mit einer Verschiebung der flexiblen Schleife und des C-terminalen Tyr253' des benachbarten Monomers, wodurch die Größe des aktiven Zentrums vermindert wird. Der ternäre Komplex des Enzyms mit Estron (E1) und NAD⁺ wurde ebenfalls aufgeklärt. E1 bindet auf untypische Weise in das aktive Zentrum, insofern als sein A-Ring und nicht die enzymatisch modifizierte Position 17 nahe dem Nikotinamid-Baustein des NAD⁺ positioniert ist.

Enzyminhibitoren sind nützliche Werkzeuge, um die Konsequenzen einer Enzymhemmung *in vivo* zu studieren. Dies erlaubt zu klären, ob dieses Enzym als neues Arzneistofftarget für bestimmte Krankheiten interessant sein könnte. Außerdem könnten potente und selektive 17 β -HSD14 Inhibitoren auch helfen, das Selektivitätsproblem anderen 17 β -HSDs zu verstehen. Da vor dieser Studie kein 17 β -HSD14 Inhibitor bekannt war, war das Ziel die

Identifizierung und Optimierung nicht-steroidaler 17 β -HSD14 Inhibitoren. Dafür wurden 17 β -HSD1 und 17 β -HSD2 Inhibitorbibliotheken gegen 17 β -HSD14 gescreent. Der vielversprechendste Treffer wurde als Startpunkt für weitere chemische Modifizierung unter Anwendung eines ligandbasierten Ansatzes verwendet. Neu designte Verbindungen wurden synthetisiert und anschließend auf ihre inhibitorische Aktivität gegen 17 β -HSD14 getestet. Vor dieser Doktorarbeit waren keine Strukturen einer humanen 17 β -HSD im Komplex mit einem nicht-steroidalen Liganden veröffentlicht. Die Kristallstrukturen bestätigten, dass die Inhibitoren an die Substratbindestelle binden und ermöglichten die hohe Affinität dieser Inhibitoren zu erklären.

Anschließend wurden zwei unterschiedliche Strategien zum Inhibitor-Design verfolgt. Die ersten struktur-basierten Modifikationen des ursprünglichen Pyridin-Grundgerüsts führten zu 10-fach potenteren Inhibitoren. Das Ziel der zweiten struktur-basierten Optimierungsstrategie war die Erweiterung des zentralen Pyridin-Kerns, um eine Interaktion mit der leeren Tasche neben den Steroid-Ringen A und B zu gewährleisten. Der vorhergesagte Bindungsmodus wurde durch Kokristallstrukturen verifiziert und die niedrig-nanomolare Affinität durch biophysikalische Charakterisierung bestätigt. Die neuen Kristallstrukturen offenbarten, wie kleine Änderungen der Inhibitoren den eingenommenen Bindungsmodus beeinflussen. Die Charakterisierung der vielversprechendsten 17 β -HSD14 Inhibitoren bezüglich 17 β -HSD1, 17 β -HSD2 und 17 β -HSD10 offenbarte unterschiedliche Grade an Selektivität. Zusätzlich zeigten einige dieser Inhibitoren eine sehr niedrige Zytotoxizität und keine Wechselwirkung mit dem Multidrug-Resistance-Protein Pgp, was darauf hindeutet, dass diese Verbindungen nicht aus dem Gehirn ausgeschleust werden und dass das Risiko möglicher Nebenwirkungen erniedrigt ist. Dies legt die Nutzung dieser Inhibitoren als Werkzeuge für weitere *in vivo* Untersuchungen nahe.

Um die Selektivitätsprofile dieser Liganden hinsichtlich 17 β -HSD14 und anderen 17 β -HSDs zu erklären, führten wir einen strukturellen Vergleich durch. Die typische V-ähnliche Form der Bindetasche von 17 β -HSD14 wird durch His93 und Gln148 bestimmt, welche in 17 β -HSD1, 17 β -HSD8 und 17 β -HSD10 fehlen. Zusätzlich haben diese drei Enzyme eine eher flache Bindetasche. Dies legt nahe, dass eine Anpassung an die charakteristischen dreidimensionalen Anforderungen von 17 β -HSD14 und wahlweise die Adressierung von His93 und/oder Gln148 die Selektivität für dieses Target erhöhen werden. Solche Inhibitoren wurden durch Docking einer Bibliothek von 400 17 β -HSD1 und 17 β -HSD2 Inhibitoren mit GOLD vorhergesagt, gefolgt von einem *in vitro* Screening der Docking-Hits und verwandter Verbindungen. Bemerkenswerterweise waren die vorhergesagten Bindemoden in schlechter Übereinstimmung mit den nachfolgend ermittelten Kristallstrukturen, bedingt durch die Anpassungsfähigkeit der Bindetasche, welche durch die flexible Schleife verursacht wird.

Schließlich wurde eine großangelegte röntgenkristallographische Fragment-Screening Kampagne durchgeführt, mit dem Ziel neue Inhibitor-Grundgerüste die an 17 β -HSD14 binden zu entdecken. Dies führte zu zwei Fragmenten die deutlich in der Elektronendichte identifiziert werden konnten. Jedoch zeigten diese Fragmente keine signifikante Inhibition von 17 β -HSD14. Um die Affinität zu erhöhen, wurden Strategien zum Fragment-Wachstum und zur Fragment-Kopplung (growing und linking) angewendet, was zu zwei neuen Inhibitoren mit gegenüber den Start-Fragmenten erhöhter Affinität führte.

Zusammengefasst wurden beide Isoformen von 17 β -HSD14, S205 und T205, biochemisch und strukturell charakterisiert, was zu vier neuen Kristallstrukturen führte. Die ersten zwei Klassen von Inhibitoren dieser Enzyme wurden entdeckt und gründlich charakterisiert. Zusätzlich wurden zum ersten Mal für diese Familie die Strukturen von 12 nicht-steroidalen Inhibitoren im Komplex mit dem Protein ermittelt. Das Fragment-Screening durch die Bestimmung der Struktur von 96 mit Fragmenten getränkten Kristallen führte zu zwei Fragment Hits, die erfolgreich optimiert und zu zwei Inhibitoren mit gegenüber den Vorgänger-Fragmenten erhöhter Aktivität entwickelt werden konnten.

Contents

Summary.....	V
Zusammenfassung.....	IV
Contents.....	XIII
Abbreviations	XVII
1 Introduction.....	1
1.1 Sex steroid hormones	2
1.2 17 β -hydroxysteroid dehydrogenases family	2
1.2.1 Cofactor preference	6
1.2.2 Reducing 17 β -HSDs enzymes	7
1.2.3 Oxidizing 17 β -HSDs enzymes	8
1.2.4 17 β -HSD14	9
1.3 Tools for the characterization of enzymes and their planned application in the current study.....	11
1.4 Aim of the research project and thesis outline	15
2 New Insights into Human β-Hydroxysteroid Dehydrogenase Type 14: First Crystal Structures in Complex with a Steroidal Ligand.....	19
2.1 Introduction	20
2.2 Results and discussion.....	21
2.2.1 Protein expression and purification	21
2.2.2 Protein stability and Thermal Shift Assay (TSA) experiment	21
2.2.3 Activity assay and biochemical characterization of both S205 and T205	23
2.2.4 Crystallization of 17 β -HSD14	24
2.2.5 Description of the NAD ⁺ , estrone binding modes	30
2.3 Conclusion.....	32
2.4 Experimental section.....	32
2.4.1 Site directed mutagenesis.....	32
2.4.2 Expression of the 17 β -HSD14 protein (S205 and T205 variants) and purification.....	33

2.4.3	Thermal shift Assay (TSA)	34
2.4.4	Fluorimetric assay.....	34
2.4.5	Determination of kinetic constants.....	34
2.4.6	Protein crystallization	35
2.4.7	Data collection and processing	35
2.4.8	Structure determination and refinement.....	36
3	First Structure-Activity Relationship of 17β-Hydroxysteroid Dehydrogenase Type 14: Nonsteroidal Inhibitors and Crystal Structures in Complex with the Enzyme.....	37
3.1	Introduction	38
3.2	Results.....	39
3.2.1	Design of 17 β -HSD14 inhibitor candidates	39
3.2.2	Calculation of physicochemical parameters.....	41
3.2.3	Inhibition of 17 β -HSD14 determined with a fluorimetric assay.....	44
3.2.4	Aggregation	44
3.2.5	17 β -HSD14 inhibitory activity.....	44
3.2.6	Substituent variations on the C-ring.....	45
3.2.7	Substituent variations on the A-ring.....	46
3.2.8	Variation of the A-ring	47
3.2.9	Variations on the B-ring.....	48
3.2.10	Trisubstituted pyridines.....	49
3.2.11	Pan Assay Interference Compounds [168].....	50
3.2.12	Crystal structure determination.....	50
3.2.13	Description of the inhibitor binding site.....	51
3.2.14	Description of the binding mode of inhibitors in complex with 17 β -HSD14.....	55
3.2.15	MOE models.....	58
3.2.16	Thermal shift assay	60
3.2.17	Comparison of the 17 β -HSD1, 17 β -HSD2 and 17 β -HSD14 structures.....	60
3.2.18	Selectivity	62
3.3	Discussion	63
3.3.1	Focus on the C-ring part.....	63
3.3.2	Focus on the A-ring part.....	65
3.3.3	Focus on the B-ring part.....	66
3.3.4	Second binding site for compound 3.9	66
3.3.5	Comparison of the 17 β -HSD1, 17 β -HSD2 and 17 β -HSD14 structures.....	67
3.3.6	Basis for structure-based drug design	67
3.4	Conclusion.....	67
3.5	Experimental section.....	68
3.5.1	17 β -HSD14 inhibition assay.....	68

3.5.2	Enzyme expression	68
3.5.3	Radioactive assay using Procedure A.....	69
3.5.4	Enzyme Purification.....	69
3.5.5	Fluorimetric assay using Procedure B.....	70
3.5.6	Protein co-crystallization with inhibitors 3.1, 3.6, 3.9, 3.10, 3.12.....	70
3.5.7	Data collection and processing	71
3.5.8	Structure determination and refinement.....	71
3.5.9	Thermal shift Assay (TSA)	72
4	Structure-Based Design of 17β-HSD14 Inhibitors.....	73
4.1	Introduction	74
4.2	Results.....	75
4.2.1	Structure design of the new inhibitors.....	75
4.2.2	Pan Assay Interference Compounds [168].....	77
4.2.3	Physicochemical Parameters.....	77
4.2.4	Biological Evaluation.....	78
4.2.5	17 β -HSD14 Inhibitory Activity	79
4.2.6	Crystal structure determination.....	81
4.2.7	Description of the binding mode of the pyridine-based inhibitors in complex with 17 β -HSD14	81
4.2.8	Description of the binding mode of three quinoline-based inhibitors in complex with 17 β -HSD14	85
4.2.9	Comparison of the structures of 17 β -HSD14, and 17 β -HSD10.....	87
4.2.10	Selectivity	87
4.2.11	Cytotoxicity evaluation	89
4.2.12	Pgp ATPase Activity Assays	89
4.3	Discussion and conclusion	91
4.3.1	SAR of pyridine derivatives	91
4.3.2	Selectivity of pyridine derivatives	92
4.3.3	SAR and selectivity of the quinoline/naphthalene derivatives	92
4.4	Experimental section.....	96
4.4.1	Enzyme expression and purification.....	96
4.4.2	Inhibition of 17 β -HSD14.....	97
4.4.3	Inhibition of 17 β -HSD1 and 17 β -HSD2.....	97
4.4.4	Inhibition of 17 β -HSD10.....	97
4.4.5	Co-crystallization of the protein with inhibitors.....	98
4.4.6	Crystallography	98
4.4.7	MOE models.....	99
4.4.8	Cytotoxicity Assay	99

4.4.9	Pgp ATPase Activity Assays	99
5	Structural Comparison between 17β-HSD Enzymes and Virtual Screening of Inhibitors	101
5.1	Introduction	102
5.2	Comparison of the crystal structures of 17 β -HSD1 and 17 β -HSD14.....	103
5.3	Comparison of the structures of 17 β -HSD8, 17 β -HSD10 and 17 β -HSD14	108
5.4	Docking studies with 17 β -HSD14	110
6	X-ray Crystallographic Fragment Screening and Hit Optimization	113
6.1	Introduction	114
6.2	Results and Discussion.....	115
6.2.1	Crystallization and Soaking experiments	115
6.2.2	Binding mode of the fragment hits.....	115
6.2.3	Fragment optimization applying fragment growing.....	117
6.2.4	Fragment optimization applying fragment linking.....	119
6.2.5	Inhibitory Activity validation.....	120
6.2.6	Binding mode confirmation of the optimized compounds	122
6.3	Conclusion and Outlook.....	123
6.4	Experimental session.....	124
6.4.1	Enzyme expression and purification.....	124
6.4.2	Protein crystallization and soaking	124
6.4.3	Co-crystallization of the protein with inhibitors.....	125
6.4.4	Data collection and processing	125
6.4.5	Structure determination and refinement.....	125
6.4.6	Inhibition of 17 β -HSD14.....	126
6.4.7	MOE models.....	126
7	Discussion and Conclusions.....	127
	Bibliography	133
	Acknowledgements.....	149
	Curriculum Vitae	151
	Erklärung.....	155

Abbreviations

11 β -HSD	11 β -hydroxysteroid dehydrogenases
17 β -HSD	17 β -hydroxysteroid dehydrogenases
17 β -HSD1	17 β -hydroxysteroid dehydrogenases type 1
17 β -HSD2	17 β -hydroxysteroid dehydrogenases type 2
17 β -HSD8	17 β -hydroxysteroid dehydrogenases type 8
17 β -HSD10	17 β -hydroxysteroid dehydrogenases type 10
17 β -HSD14	17 β -hydroxysteroid dehydrogenases type 15
4-dione	4-androstene-3,17-dione
5-diol	5-androstene-3 β , 17 β -diol
λ	wavelength
Å	Ångström (1 Å = 10 ⁻¹⁰ m)
AKR	aldo-keto reductase
CHES	N-Cyclohexyl-2-aminoethanesulfonic acid
<i>clogP</i>	calculated logarithm of the n-octanol/water partition coefficient
CW	capping water
DHEA	dihydroepiandrosterone
DMSO	dimethyl sulfoxide
DNA	deoxyribonucleic acid
<i>e</i> ⁻	electron
E1	estrone
E2	estradiol
FBLD	fragment-based lead discovery
ER	Estrogen receptor
GOL	glycerol
H-bond	hydrogen bond
HEPES	4-(2-hydroxyethyl)-1-piperazineethanesulfonic acid
HTS	high throughput screening
<i>IC</i> ₅₀	half maximal inhibitory concentration
<i>IG</i> ₅₀	concentration resulting in 50% inhibition of growth

K_d	dissociation constant at equilibrium
K_i	dissociation constant at equilibrium for an inhibitor
K_m	substrate concentration at which the reaction rate is half of V_{max}
kDa	kilodalton
LE	ligand efficiency
Me	Methyl
MPD	2-methyl-2,4-pentanediol
MW	molecular weight
MX	macromolecular X-ray crystallography
NAD(H) ⁺	nicotinamide adenine dinucleotide
NADP(H) ⁺	nicotinamide adenine dinucleotide phosphate
PDB	protein data bank
PEG	polyethylene glycol
RMSD	root-mean-square deviation
SAR	structure-activity relationship
SDR	short-chain dehydrogenase/reductase
T	testosterone
T_m	melting temperature
TLC	thin-layer chromatography
tris	tris(hydroxymethyl)aminomethane
TSA	thermal shift assay
UV light	Ultraviolet
vdW	van der Waals
V_{max}	maximum velocity at saturating substrate concentration
W	water molecule

Chapter 1

Introduction

1.1 Sex steroid hormones

Hormones are signaling molecules that are produced and subsequently released by an endocrine gland into the circulatory system. Thereby, they are able to address distant organs and thus regulate physiology and behavior. Hormones can be categorized into four main chemical classes: amino acid derivatives, polypeptides, eicosanoids, and steroids [1]. Sex hormones are lipophilic compounds derived from cholesterol that belong to the chemical class of steroids [1]. They can be divided into two main classes: Androgens, considered as “male sex hormones” mainly constituted by 4-androstene-3,17-dione (4-dione), as well as testosterone (T) and dihydrotestosterone (DHT). Furthermore, the most important representatives of the estrogens (or so-called “female sex hormones”) are estradiol (E2) and estrone (E1). One crucial role of androgens and estrogens is the induction of body changes, known as primary and secondary sex characteristics. However, both, androgens as well as estrogens, have a variety of effects on various organs and tissues. In fact, estrogens play an important role in maintaining the bone mass by keeping the equilibrium between bone formation and resorption, in vasoprotection and in the immune system [2–5]. In addition, several studies have proven that estrogens are fundamental for the development and maintenance of the brain function. Furthermore, they have shown that an increase in the concentration of E2 is beneficial for the treatment of neuronal diseases [6, 7]. Estrogens and androgens can also be produced by the intracrine system that activates the steroids directly in the local tissue from their inactive precursors, without being released into the blood stream [8, 9].

Due to the many different enzymes that are involved in the biosynthesis of androgen and estrogen starting from cholesterol (Figure 1.1), the cholesterol metabolism pathway is a very attractive but also challenging pathway for the discovery of new potential targets for the treatment of different diseases [10].

1.2 17 β -hydroxysteroid dehydrogenases family

The interest in 17 β -hydroxysteroid dehydrogenases (17 β -HSDs) enzymes started over 40 years ago when their function in eukaryotic and prokaryotic species was characterized [8, 11, 12]. At present, 14 different mammalian 17 β -HSDs have been characterized. Of these, 12 occur in humans, whereas 17 β -HSD6 and 17 β -HSD9 were only identified in rodents [11]. With the exception of 17 β -HSD5, that belongs to the aldo-keto reductase (AKR) superfamily, they all belong to the short-chain dehydrogenase/reductase (SDR) super family [12, 13]. SDR constitutes a large protein family of oxidoreductases (over 160,000 members in the *Uniprot* database), mainly present as oligomeric enzymes. The SDR enzymes share an overall residue identity of 15-30%, mainly resulting from the conserved cofactor binding site and the

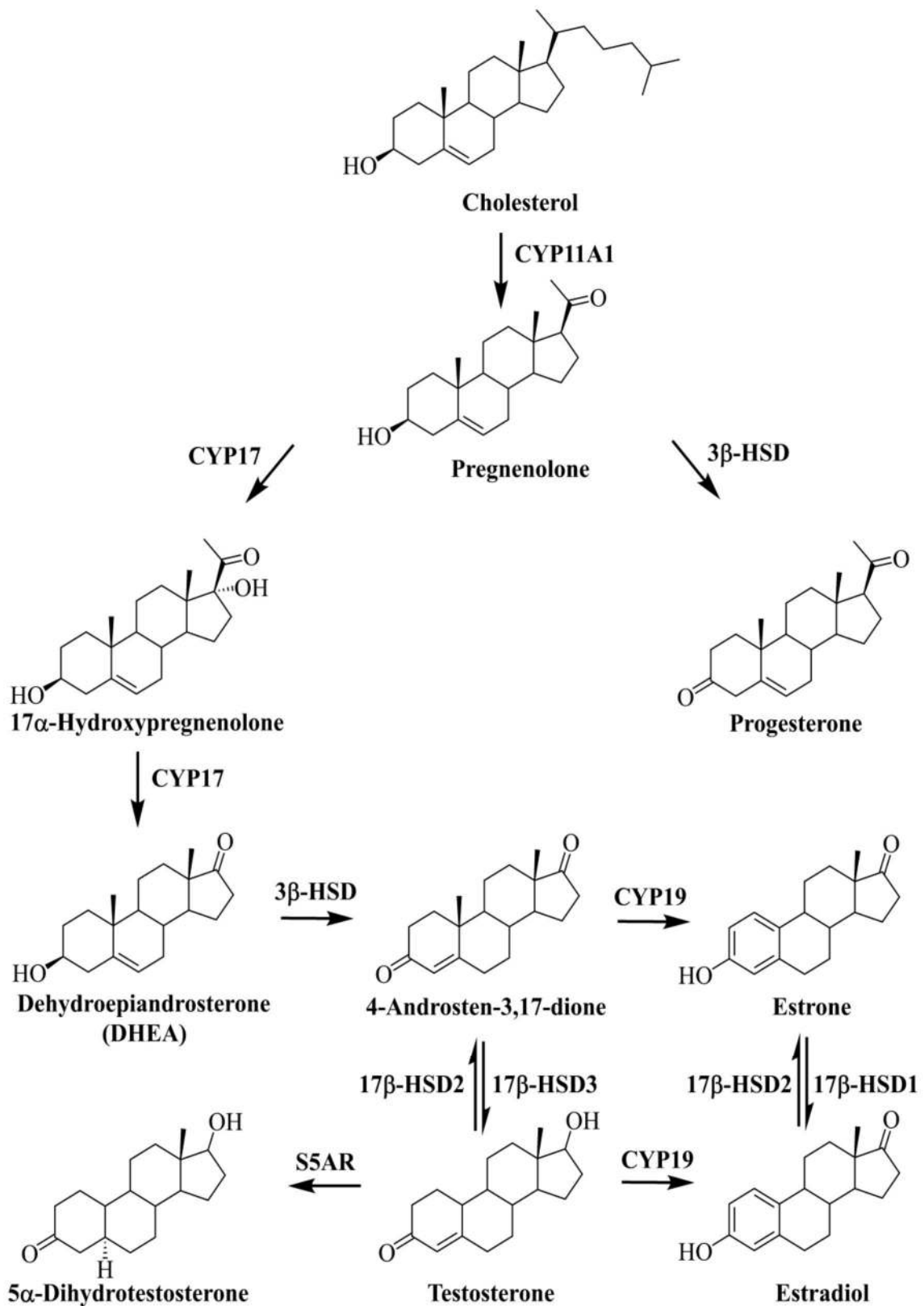


Figure 1.1: Schematic summary of the biosynthesis pathway of the sex steroid hormones (Taken from Gargano M. [14]).

catalytic residues. All members of this family have a conserved Rossmann-fold domain established by an α/β sandwich folding pattern that is arranged in 6 to 7 central β -sheets, and flanked by 3 α -helices at both sides (Figure 1.2) [15–17]. The sequence of the SDR enzymes typically comprises about 250-350 amino acids. The SDR enzymes are NAD(H)/NADP(H) dependent and the cofactor-binding site is located at the N-terminal region [17, 18]. A further characteristic is that they contain a highly conserved Tyr-X-X-X-Lys motif that functions as catalytic domain [19]. The catalytic Tyr residue functions as general acid/base catalyst. The pK_a value of the OH group of the Tyr group is lowered by a neighboring conserved Lys residue, and the substrate binding is achieved through the sidechain of a conserved serine (Figure 1.3) [20, 21]. In many SDRs, a proton relay system appears to involve the 2' OH of the nicotinamide ribose in addition to a conserved water molecule, whereas no metal ion is required for catalysis [16, 17, 21–24].

17 β -HSDs are characterized by the ability to activate or inactivate the sex steroid hormones by stereospecific reduction or oxidation of the keto/alcohol group in position 17 (Figure 1.4). Besides, these enzymes are also involved in the metabolism of different nonsteroidal compounds like retinoid acid, fatty acid and hydroxyacyl CoAs [11, 25–32]. The 17 β -HSD enzymes are bidirectional *in vitro*, whereas *in vivo* they show a preference for the oxidative or

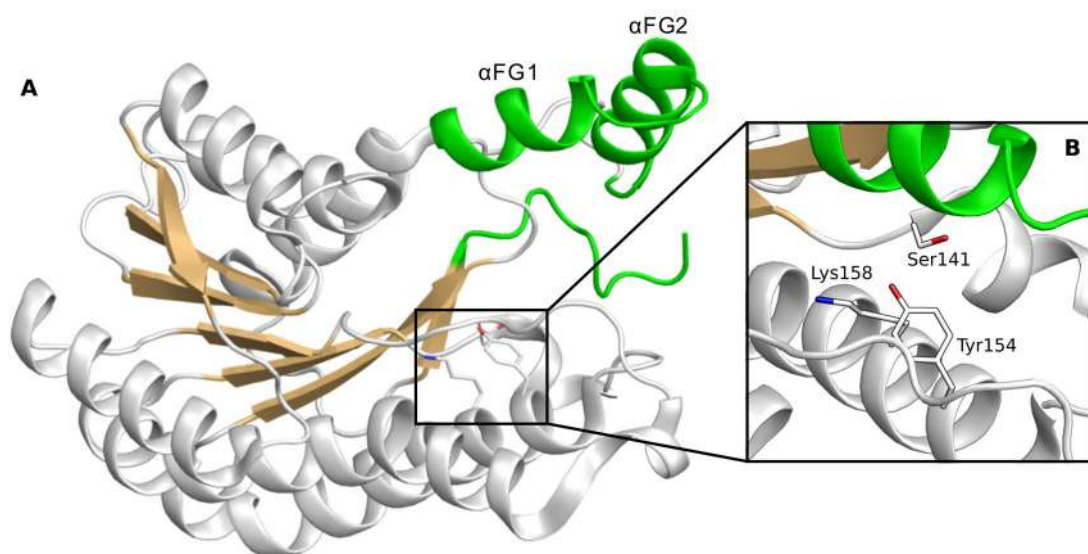


Figure 1.2: (A) Ribbon representation of the 17 β -HSD14 apoenzyme. The conserved Rossmann-fold domain is established by α -helices (white) and β -sheets (beige). The loops giving special shape to the binding pocket and the variable C-terminal tail are colored in green. (B) Close-up view of the substrate binding pocket. The catalytic amino acids are shown as stick model. All structural representations were prepared with PyMOL [33].

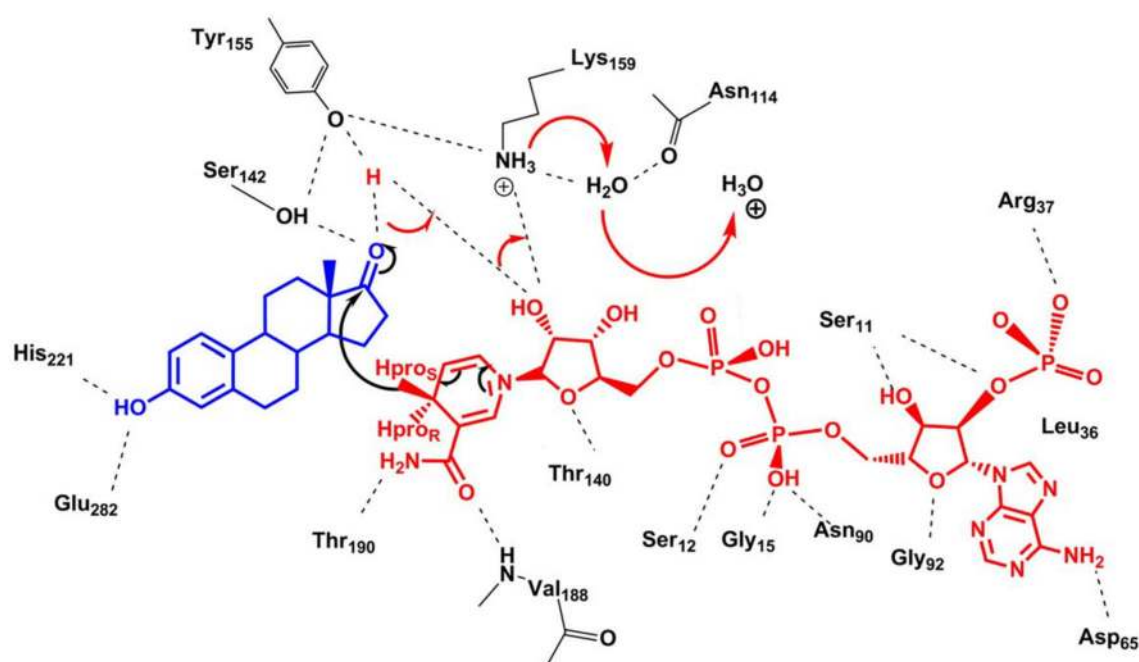


Figure 1.3 Scheme of the postulated reduction mechanism of E1 to E2 by the 17 β -HSD1 enzyme [20, 21, 24]. The cofactor NADPH is colored in red and the substrate E1 in blue. The involved amino acids are displayed in black. Hydrogen bonds are represented as dashed lines, the proton transfer reactions are indicated by arrows (Figure taken and modified from Negri M. *et al.* [24]).

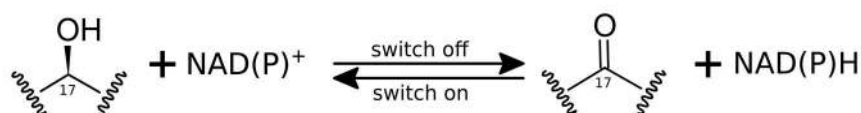


Figure 1.4 Schematic representation of the general catalytic reaction of 17 β -HSDs.

reductive reaction, which is mainly associated by the enzyme localization, the cofactor preference and the availability of substrate [11]. The large substrate variability observed in this protein family is dictated by the C-terminal tail that equips the different enzymes with a special substrate/inhibitor binding site [15, 16]. This back portion is usually folded into three large loops that capture the substrate and undergo a structural rearrangement after binding of cofactor and substrate [26]. The nomenclature of 17 β -HSD enzymes is following the historical description order established by the Human Genome Organization (HUGO). Homology model studies are difficult to perform due to the low similarity of the substrate binding sites between these enzymes. A further reason is the structural flexibility of the C-terminal tail. Thus, it is necessary to structurally characterize every single subtype member of this family in order to understand its function. The following seven human enzymes have

already been structurally characterized: 17 β -HSD1, 17 β -HSD4, 17 β -HSD5, 17 β -HSD8, 17 β -HSD10, 17 β -HSD11 and 17 β -HSD14 [27, 34].

The 17 β -hydroxysteroid dehydrogenases (17 β -HSDs) are essential for the last step of the formation and degradation of steroid hormones. They regulate the intracellular availability of steroid hormones and their potential activation of the nuclear receptors [11, 34]. In addition, these enzymes are specifically expressed in certain tissues. Consequently, this enzyme family is of high interest as therapeutic targets for several steroid hormone dependent diseases [34], and for several types of 17 β -HSDs a correlation with some human diseases has already been found. In addition, the expression level of some of these enzymes can be used as prognostic marker in breast and prostate cancer [35, 36].

1.2.1 Cofactor preference

As mentioned above, 17 β -HSDs drive the redox reactions unidirectional *in vivo*. Inside the cells, the concentration of NADPH is about 500 times higher than of its oxidized form NADP⁺. The NAD⁺ form is about 700 times higher than its reduced NADH form [37–39]. Beside the concentration difference, kinetic studies revealed that 17 β -HSDs are able to discriminate between the non-phosphorylated and the phosphorylated form of the cofactor [40]. These results are in accordance with the crystal structures: an arginine is present in the Rossmann-fold motif of the reductive HSD enzymes that stabilizes the 2'-phosphate moiety of NADPH via a salt bridge. In contrast, in the oxidative enzyme a negative charged amino acid, often aspartate, is present in the same region repulsing the 2'-phosphate group and stabilizing instead the ribose (Figure 1.5) [41–44]. Furthermore, these observations have been confirmed by mutagenesis studies [45, 46].

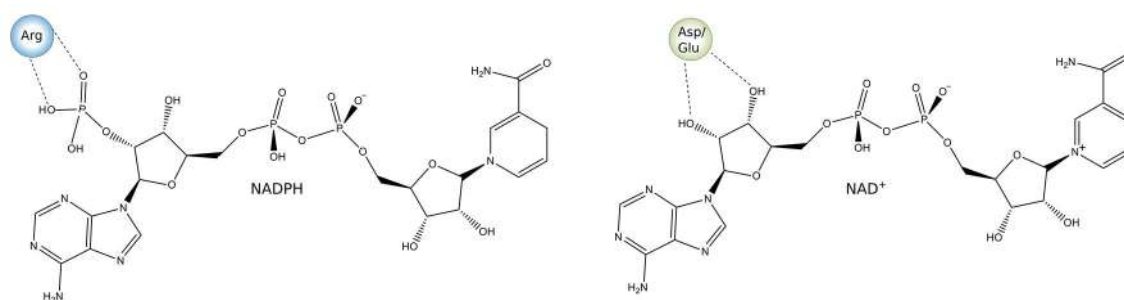


Figure 1.5 Scheme of the binding preferences for NADPH vs. NAD⁺ for reductive/oxidative HSDs.

1.2.2 Reducing 17β -HSDs enzymes

Six reductive 17β -HSDs enzymes are described in the literature [11, 24, 34]. They are activating enzymes and responsible for the high level of active sex steroids in target tissues.

17β -HSD1 was the first enzyme in this family to be cloned and structurally characterized. This enzyme, which is active as a homodimer [47], is one of the most important enzymes involved in the last step of the activation of estradiol starting from estrone, resulting in a high concentration of the sex hormone in the target tissue. This enzyme is estrogen specific. A minor effect on the reduction of androgen was also identified [48–50]. 17β -HSD1 is a cytosolic enzyme that is mainly expressed in breast, endometrium, ovary and placenta. In minor concentration it is expressed in adipose tissue and skin. During the last decades, an increasing number of inhibitors targeting 17β -HSD1 were discovered. The first inhibitors are based on a steroidal scaffold, some are mixed inhibitors combining both, cofactor and steroid, whereas the latter inhibitors show a nonsteroidal core [34, 51–54]. At present, several crystal structures of the apoenzyme, the cofactor-enzyme complex and the ternary complexes with substrate or steroidal inhibitors are already resolved. However, no crystal structure of the enzyme in complex with a nonsteroidal inhibitor has been reported so far. 17β -HSD1 has been proven to play a crucial role in several estrogen-dependent diseases such as breast cancer, ovarian tumor, endometriosis, and uterine leiomyoma [55–63] and it is a validated drug target for estrogen dependent breast cancer.

17β -HSD3 is a microsomal membrane-bound enzyme that is mainly present in the testis that it is bound to the endoplasmic reticulum through its N-terminal domain [11, 64]. 17β -HSD3 has 310 amino acids and it catalyzes the reductive reaction of 4-dione and 5α -androstenedione to testosterone (T) and dihydrotestosterone (DHT), respectively [65, 66]. This enzyme is overexpressed in prostate cancer and, due its catalytic action, its inhibitions would reduce the concentration of T and therefore it could be beneficial against tumor growth [67, 68]. The determination of the structure of this enzyme was unsuccessful due its hydrophobic nature.

17β -HSD5 is located in the cytosol. This enzyme is prevalently expressed in breast, liver and prostate. 17β -HSD5 shows a broad substrate specificity [69, 70]. As it is member of the aldo-ketoreductase (AKR) protein superfamily, it will not be further discussion.

17β -HSD7 is a microsomal enzyme bound to the endoplasmic reticulum. It is present in breast, liver, testis, ovary, kidney, placenta as well as in neuronal tissue and lung [11, 71, 72]. The enzyme is involved in the production of E2. Furthermore, it has been proven that it fulfills a main role in the synthesis of cholesterol [73]. No crystal structure is available so far.

17β -HSD12 is present in microsomes of especially kidney, liver, heart and skeletal muscle and in minor level in placenta, breast and ovary. This enzyme is involved mainly in the

regulation of the lipid biosynthesis and plays only a marginal role in the metabolism of E2 [74–76].

17 β -HSD13 is present in the liver but is also detected in ovary, bone marrow, kidney, brain, lung, skeletal muscle, bladder and testis. It is a cytosolic enzyme and it may be involved in the lipid metabolic pathways [77, 78].

1.2.3 Oxidizing 17 β -HSDs enzymes

Characteristic for these enzymes is that they catalyze oxidation reactions and that they are found ubiquitously in the body also in non-steroidogenic tissues. As they inactivate the sex hormones (oxidation of the potent estradiol and testosterone in estrone and 4-dione, respectively) and thus lower the concentration of the latter in the target tissues, it is assumed that these enzymes play a protective role *in vivo* [11].

17 β -HSD2 is widely expressed in tissues such as placenta, uterus, liver, bone, gastrointestinal and urinary tracts [79–82]. This enzyme is found to be bound to membranes of the microsomal fraction. It catalyzes the conversion of E2, T and DHT to their less potent forms E1, 4-dione and 5 α -androstenedione, respectively [29]. Due to the unspecific localization of 17 β -HSD2 and its physiological role in inactivating the sex hormones, it has been suggested that it plays a role in protecting tissues from excessive steroid concentrations [12]. Several steroidal and non-steroidal inhibitors have already been identified for this enzyme [34, 83, 84]. The estrogen replacement therapy for the treatment of osteoporosis is proven to be beneficial; however, this therapy is no longer recommended due the many side effects [34, 85, 86]. 17 β -HSD2 oxidizes E2 into E1, resulting in a decreased concentration of E2 in bone cells. Therefore, inhibition of this enzyme is a promising approach for the treatment of osteoporosis [34, 87–92]. Unfortunately, the three-dimensional structure of this enzyme is still unknown due to its hydrophobic nature that has proven to be a huge obstacle for the structural elucidation.

17 β -HSD4 is ubiquitously distributed and it is mainly involved in the inactivation of sex steroids. The enzyme 17 β -HSD4 is a much larger enzyme compared to the other 17 β -HSDs and its tertiary structure can be divided into three domains [11, 18, 34].

17 β -HSD8 is located in liver, placenta, gonads and kidney. 17 β -HSD8 can catalyzes a wide range of substrates including estrogen, androgen and fatty acids and its three-dimensional structure is known [11, 34].

17 β -HSD10 is a mitochondrial enzyme that is located in the central nervous system (CNS). It is overexpressed in the amyloid plaques of patients suffering of Alzheimer's disease. The enzyme is involved in several substrate pathways, for instance in the inactivation of sex

steroids and the catabolism of short hydroxyacyl CoAs [93–97]. One class of inhibitors described for this enzyme forms a covalent bond to the cofactor (NAD⁺) and typically has a peculiar chemical structure [94]. Few crystal structures of this protein are available as apoenzyme or in inhibitor-enzyme complexes.

17 β -HSD11 is expressed in liver, lung, placenta and kidney. Its physiological role is not disclosed yet; however, recent studies suggest that the enzyme might be involved in the metabolism of fatty acids rather than in the metabolism of sex steroids [98, 99].

1.2.4 17 β -HSD14

Human 17 β -hydroxysteroid dehydrogenase type 14 (17 β -HSD14) — also called retSDR3, DHRS10 or SDR47C19 — is the latest enzyme identified that belongs to the 17 β -HSD family [11, 16, 32, 34]. Initially, its gene was isolated from the retina by Haeseleer and Palczewski [100]. Subsequently, a second version of the gene was isolated from a melanotic melanoma cell in the framework of a genome sequencing campaign [101, 102]. Both genes are identical with the exception of a single point mutation of the amino acid at position 205: The gene isolated from the retina encodes at this position for a serine (17 β -HSD14 S205), whereas the gene isolated from a melanotic melanoma encodes for a threonine (17 β -HSD14 T205). Since only the S205 variant was characterized so far, the reason for this protein polymorphism is not yet clear. However, it is hard to believe that the single point mutation could give rise to a significant difference in activity, as the structural difference is limited to a single methyl group. Furthermore, it cannot be excluded that a spontaneous mutation occurred during the isolation of the second gene from the cancer tissue. Nevertheless, it would be of high interest to characterize also the T205 protein variant.

As the gene was first isolated from a retina cDNA library, it was hypothesized that this enzyme would be involved in the retinoid metabolism. However, this function could not be proven [100]. Northern blot analyses has revealed that the S205 *hHSD17B14* gene is mainly expressed in brain, liver, placenta [32], and in the kidneys [100]. However, Sivik *et al* [103] applied immunochemical based methods to demonstrate that the protein is also expressed in adrenals and testis as well as in the eyes, heart, kidney, esophagus, liver, rectum, salivary glands, skeletal muscles and in breast cancer tissue [35]. The striking discrepancy between the enzyme-containing tissues reported in the two studies can be explained by the differences in the specificity of the applied antibodies. Thus, further investigation is required before a conclusion can be drawn [104].

Although the *in vitro* reaction of 17 β -HSD14 was investigated, its physiological role *in vivo* is still unclear. About 50 ligands binding to SDR enzymes were tested on 17 β -HSD14, but only some sex steroids showed significant affinity to the enzyme. These results suggest that the

enzyme is potentially involved in the sex steroid metabolic pathway [32]. 17 β -HSD14 catalyzes the oxidation of the alcohol function at position 17 of E2, 5-androstene-3 β , 17 β -diol (5-diol), and T — using NAD⁺ as a cofactor — and transforms them into their less active forms E1, dihydroepiandrosterone (DHEA), and 4-dione, respectively [32]. However, the low turnover rate for these steroids and the not saturatable kinetics of T suggest the hypothesis that *in vivo* the enzyme might play a role also in other metabolic pathways (K_m = 5.6 μ M \pm 1.7 for E2; K_m = 13.6 μ M \pm 1.6 for 5-diol) [32].

Prior to the studies conducted in the framework of this thesis, only a single crystal structure of the 17 β -HSD14 apoenzyme exhibiting a resolution of 2.4 Å was available (PDB ID 1YDE) [32]. The assembly of the enzyme is homotetrameric, and the asymmetric unit of the crystal structure contains four tetramers giving rise to a total of 16 monomers (Figure 1.6). The protein comprises 270 amino acids, whereas only 250 of them could be clearly assigned to the electron density. Beside the typical, conserved Rossmann-fold region (consisting of seven parallel β -sheets and an array of α -helices at both ends) and the catalytic triad — consisting of Ser141, Tyr154 and Lys158 — the structure shows the distinctive flexible loops formed by the segments α FG1 and α FG2 (Figure 1.2). Unfortunately, several pieces of the flexible loops are not visible in the electron density of some of the chains, and none of the chains' C-termini are detectable. The binding cleft of 17 β -HSD14 appears widely open and rather lipophilic. No information about a potential substrate can be derived from this crystal structure and due the scatter over various conformations of the flexible loops, it is difficult to use the structure for docking studies.

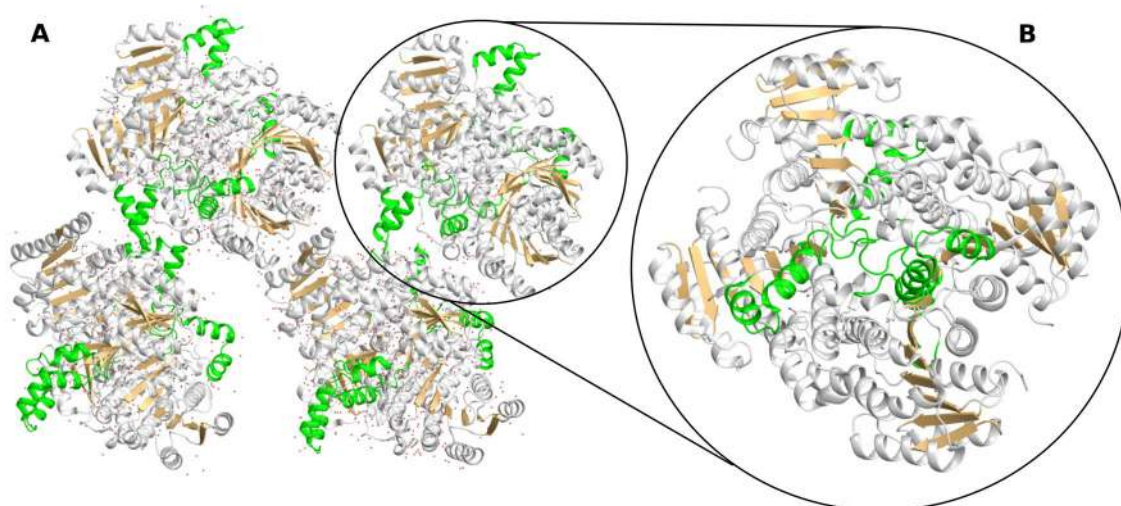


Figure 1.6 (A) Ribbon representation of the four homotetramers in the asymmetric unit of 17 β -HSD14 (PDB ID: 1YDE). (B) Single homotetramer. The conserved Rossmann-fold domain is colored in white and beige. The flexible parts are colored in green.

1.3 Tools for the characterization of enzymes and their planned application in the current study

Different techniques are available for the characterization of enzymes and for studying ligand-protein interactions. The different methods are often complementary to each other, resulting in a more complete and reliable picture of the studied effects in operation. However, during the planning of the experiment to characterize the enzyme structure it is important to take the limitations especially into account. For example, for well-characterized enzymes *in silico* approaches can successfully identify compounds during drug development [104]; however, as mention earlier, it can be rather challenging to identify binders based on homology models derived from of sequence data showing low identity and for proteins exhibiting highly flexible parts. Several attempts to dock ligands into 17 β -HSD14 were performed in the course of some preliminary studies of this project. However, the subsequently determined crystal structures revealed that the predicted binding modes were incorrect.

One of the techniques on which the current thesis is strongly based is **macromolecular X-ray crystallography**. This technique is a diffraction method for the determination of structural information up to the atomic level [105–108]. Since the 17 β -HSD enzyme family does not share a high sequence homology, especially across the binding-site region, crystal structures can provide important insights into the peculiarities of the binding sites. As mention above, one crystals structure for 17 β -HSD14 had already been described in literature prior to this study [32]. Even though this crystal structure already revealed some details about the architecture of this protein, there still remained many open questions. The electron density of highly variable regions of the protein were ill-defined (flexible loops and the C-terminal tail), however they are of utmost importance because they contribute to ligand binding. This deficiency could resulted from several effects, for instance the relative low resolution of the dataset (2.4 Å) could have prevented to properly resolve these mobile regions. Another aspect that makes this structure not ideal as a starting point for a rational drug discovery endeavor is that 16 monomeric units (four tetramers) form the asymmetric unit. These chains of the 16 units all differ in the arrangement of the flexible loops resulting in binding pockets of deviating shape and volume. It is therefore difficult to predict which of the chains represents the relevant conformation of the active binding site competent to accommodate a ligand. Furthermore, the question remains whether the observed flexibility of the protein also occurs while the protein is in complex with a ligand and/or the cofactor. It is obvious that a higher quality of the apoenzyme crystal structure and the availability of multiple crystal structures of the protein in complex with cofactor and ligand would be tremendously beneficial for the intended drug design studies.

Even though the X-ray diffraction technology underwent an immense improvement within the last decades, for instance the development of more powerful light sources at synchrotrons that are equipped with faster detectors, one important factor limiting the quality of the crystal structure is the quality of the protein crystal itself [106, 108]. In this study, in order to produce well-diffracting three dimensional crystals, extensive crystallization screenings were performed.

Crystal structures are also essential for the rational design of ligands. Crystals of protein-ligand complexes can be prepared following two different strategies: Soaking or cocrystallization [109, 110]. The strength of the crystal soaking approach is that it can be performed very fast, since protein-ligand complexes are simply prepared by exposing premanufactured crystals with known diffraction quality to the ligand of interest. Usually soaking of fragments or small ligands is unproblematic; however, more bulky ligands can be incompatible with the crystal packing. Due to their high affinity, they can forcibly squeeze into the pre-shaped active site and thereby adopting themselves unrealistic conformation or inducing conformational changes of protein sidechains/loops, or even interfere with the packing in the crystal. This frequently results in a decrease in crystal quality (increased mosaicity) or even a complete destruction of the exposed crystal. Furthermore, cases have been reported where soaking seemingly results in a different binding mode than cocrystallization [106, 110, 111]. This observation suggests that conformational changes of the protein upon ligand binding are already established in solution prior crystallization — as reflected by the co-crystallized structures — will prevented false conclusions that might occur if premanufactured crystals are subjected to soaking experiments [110, 111]. Cocrystallization is a viable alternative to soaking protocols. In this case, a solution of protein and ligand is prepared that is subsequently used to grow crystals. Thereby, crystals are formed in periodic arrangements of the pre-assembled protein-ligand complexes of interest. Since the ligands bind to the protein already in solution, this induces protein rearrangements and thus reflects better the conformation of the protein-ligand complex in solution and hopefully the biologically relevant conditions — and thus will be less biased by putative imposed crystal packing effects of the apoenzyme. In addition, co-crystallization could even result in a qualitatively better crystal structure. The downside of this technique is that it is more demanding with respect to protein material and can potentially result in a new crystal form that requires new crystallization conditions [109–111].

Through an extensive examination of the protein-ligand complex crystal structure ligand portions that do not achieve interactions to the protein can be identified. This knowledge can be used to rationally improve the chemical structure of the ligand in the next design cycle [112].

If it is intended to study especially the function of the protein, one limitation of macromolecular X-ray crystallography is that hydrogen atoms are usually not detected. Consequently, it is not possible to directly determine the protonation state of ligands and amino acids. Thus, the protonation state can only be rationalized on the basis of consensus interaction patterns and distance and angle between atoms.

Another technique used in this work is the **thermal shift assay (TSA)** also called differential scanning fluorimetry (DSF). The stability of a protein is temperature-dependent [113, 114], and this method detects the differences of the melting temperature of a protein under various conditions. Stable, correctly folded protein tends to have the hydrophilic amino acids exposed to the surface and the hydrophobic ones are buried within the core. At a defined temperature — specific for each macromolecule and dependent on the buffer composition — the protein will partially or completely unfold and, as a consequence, the hydrophobic amino acids will get exposed to the solvent. This assay detects at which temperature this unfolding event occurs. It is usually performed using a real-time PCR device [115], and is dependent on a special dye (SYPRO orange) that begins to fluorescent upon binding to exposed hydrophobic portions of the protein. No or very low fluorescence is detected while the globular protein is correctly folded. However, with increasing temperature the protein will start to unfold and thus expose hydrophobic residues to the solvent phase, thereby getting in contact with the dye, that in consequence starts to fluorescent. Recording the intensity of the fluorescence signal over a temperature range results in a sigmoidal curve, where the melting temperature T_m of the protein is described by the inflection point (Figure 1.7). When the protein is surrounded by molecules that help to stabilize its tertiary structure, a shift to a higher melting point will occur. The TSA is extremely useful for the screening of different additives, for instance different salts and buffers at different pH values, in order to find a buffer composition that shows an optimal stabilizing effect on the protein. The application of buffers that optimally stabilize the protein has the advantage that the yield during protein expression as well as the success rate during crystallization screenings can drastically increase [116]. This assay also allows fast and efficient screening for binding ligands. The principle is that upon binding of a ligand to the protein, the ligand stabilizes or destabilizes through binding the protein architecture and the observed shift of the melting temperature is proportional to the strength of the formed complex (i.e. in close series even to the affinity of the ligand) as well as proportional to the concentration of the ligand. The amount of stabilization due to the complexation with different ligands results in shifts of varying extend of the melting temperature T_m compared to the melting point of the uncomplexed enzyme [116–119]. However, the magnitude of the shift is not reflecting the affinity of the ligand but it is primarily proportional to the change in the entropy of binding upon formation of the complex [119]. Thus, the TSA can be used to discriminate binders from non-binders, but not for the determination and comparison of compound affinities.

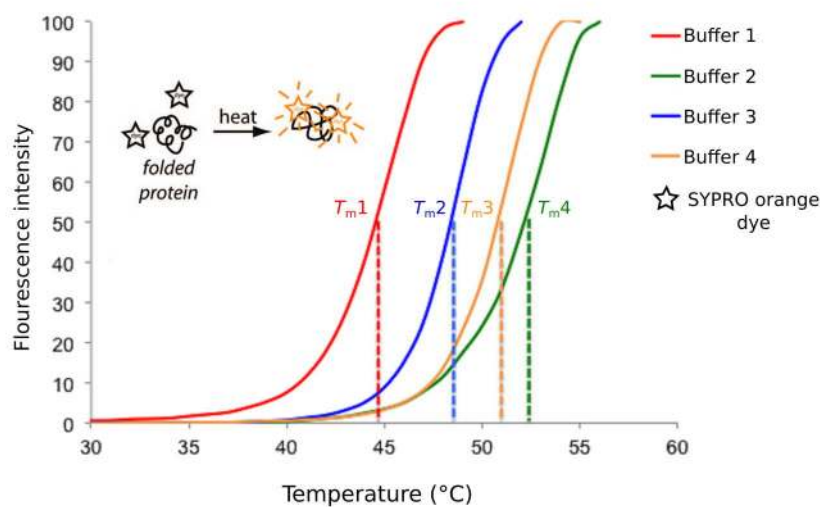


Figure 1.7 Example of TSA curves obtained in the presence of different buffers (taken and modified from [120, 121]).

Biochemical assays are necessary for the characterization of the enzyme activity. As we had no access to a radio-detector for the analysis of the conversion of radiolabeled E2 into E1 as described by Lukacik *et al.* [32], we used instead two different enzymatic assays that were established in our laboratory at different stages of the project. The **thin-layer chromatography (TLC) assay** was only used during the establishment of the protein purification procedure for the detection of the enzyme in the different fractions after column chromatography. The selective transformation of E2 into E1 was visualized by UV light, indicating the presence of the active protein in the studied fractions. However, the assay does not allow the quantification of the conversion of E1 into E2.

For the kinetic characterization, the quantification of the enzymatic turnover of E2 into E1 was determined using a **fluorescence-based assay**. The 96-well plate format used in our fluorescence assay is rather convenient, as it requires only low quantities of the protein, it is fast and can easily be adapted for the evaluation of the inhibitors. The fluorescence-based assay is monitoring the increase of NADH formed by the catalytic reaction by measuring the increase in fluorescence (excitation at 340 nm and emission at 496 nm). As the catalytic reaction has a stoichiometry of one — one molecule of NAD⁺ is converted into one molecule of NADH for each E2 that is converted into E1 — it is trivial to derive the E2 turnover from the NADH formation. However, it has to be considered that if the concentration of the total molecules in the well is too high, the fluorescence signal will get partially quenched and the detected fluorescence will report a lower concentration than actually present (inner filter effect). Furthermore, also other molecules than E2, acting as substrate of the enzyme, could principally participate in the catalytic reaction leading to the formation of NADH. In this

case, the increasing fluorescence would not exclusively represent the formation of E1. Therefore, it is important to perform a negative control of the reaction in parallel, for example containing the enzyme and NAD^+ , but without the substrate E2. One of the largest limitations of this assay are intrinsically self-fluorescent inhibitors. If an inhibitor is fluorescent at a similar wavelength (λ) as NADH, the read out of the fluorescence signal becomes inaccurate and the interpretation of the results is rather difficult or even impossible.

1.4 Aim of the research project and thesis outline

Although the sequencing of the human genome has been solved and all genes are accessible, the physiological role of more than half of all SDR members remains unknown or poorly examined. It is of utmost importance to deorphanize and characterize these enzymes as a basis to explore their physiological functions and thereby identify new potential drug targets for the treatment of human diseases [122].

17β -HSD14 has been suggested to play a role in neuromodulation [32] and in inflammation processes [123]. The availability of a potent and selective enzyme inhibitor would foster research in this direction and potentially support the collection of data to proof the involvement of this enzyme in neuronal diseases. Furthermore, such an inhibitor is also prerequisite for the conduction of proteomic or metabolic studies *in vivo*. In addition, potent and selective enzyme inhibitors are also useful tool compounds to study the consequence of full enzyme inhibition, comparable to the change of the phenotype of a knockout mouse. Having access to such a potent inhibitor allowing the detailed characterization *in vivo*, this protein could prove to be an attractive drug target as it is already the case for 17β -HSD1 [34, 124, 125] and 17β -HSD2 [87, 90–92]. Potent and selective enzyme inhibitors are also needed to address the selectivity issues of inhibitors with respect to other 17β -HSDs.

Taking all these considerations into account, the main research objective of this thesis is to structurally characterize the active site of 17β -HSD14 in order to facilitate the development of highly active inhibitors. Newly discovered and optimized inhibitors can then be applied as tools to further elucidate the structure and function of the enzyme, and to gain insights into the possible functional roles of this enzyme *in vivo*.

Chapter 2 of this thesis (publication [126]) describes the chemical and biological characterization of both S205 and T205 isoforms of 17β -HSD14. To obtain both variants of the recombinant protein in high yield, an expression and purification protocol had to be established. As it turned out that the protein was quite challenging to handle, special attention was attributed to on the different approaches followed to overcome issues during the purification procedure to obtain the protein in crystallization and assay-pure quality, in particular protein stability. An extensive crystallization screening enabled the determination

of four novel crystal structures of the human 17 β -HSD14, as apoenzyme, in binary complex with NAD⁺ and in ternary complex with NAD⁺ and the catalytic product of the enzyme reaction (E1). These crystal structures were the basis to obtain new insights into the enzyme's properties. Since we had access to the S205 as well as to the T205 isoform of the protein, we performed the biochemical characterization of both.

Chapter 3 (publications [126] and [127]) describes our first ligand-based drug discovery approach. The goal of this chapter was to identify and to optimize the first class of 17 β -HSD14 inhibitors. In a preliminary study a library of 17 β -HSD1 and 17 β -HSD2 inhibitors — selected to guarantee scaffold diversity — was tested on potential inhibitory activity for 17 β -HSD14. The most interesting hit was taken as a starting point for further chemical optimization. As matter of fact, this investigation was performed before the first structure of the ternary complex (protein-cofactor-ligand) could be determined. Therefore, the optimization of the inhibitor was performed at the beginning following a ligand-based approach. The newly designed compounds were synthesized and tested for 17 β -HSD14 inhibitory activity. The best inhibitors identified in this study showed a very high affinity toward the enzyme with a K_i of about 10 nM. In this chapter, the first five crystal structures of the protein in its ternary complex with the cofactor and highly potent nonsteroidal inhibitors were further elucidated. It is striking that until now no human SDR 17 β -HSD enzyme structure has ever been reported in complex with a nonsteroidal compound. It is known that several attempts have been conducted with 17 β -HSD1; however, they all failed, possibly owing to the lipophilicity of the active site or the flexibility of the compounds.

Chapter 4 (manuscript in preparation) describes our strategies to optimize the previously reported class of 2,6-pyridine ketone inhibitors (Chapter 3). The availability of the crystal structures of the enzyme in complex with an inhibitor enabled us to pursue a rational structure-based approach. A special focus was placed on scaffold diversity with the aim to further characterize the binding pocket of the target protein and thereby to create inhibitors with different pharmacokinetic properties. Seven new crystal structures of inhibitors in complex with the protein were determined. This was necessary to understand the inhibitors' structure-activity relationship (SAR) as a basis for their further optimization. In fact, these systematic studies revealed how small structural changes of the substituents on the inhibitors can lead to surprising variation of their binding mode. Furthermore, this chapter describes considerations regarding the selectivity profile of the inhibitors toward the different closely related 17 β -HSD enzymes as well as *in silico* determined physicochemical properties of the new inhibitors.

In **Chapter 5** the structural differences between different HSD enzymes are address. X-ray crystal structure models of proteins provide unvaluable structural information about binding sites and therefore enable to chemically tailor ligands to bind to the target. Crystal structures

also allow the comparison between the three-dimensional arrangements of the amino acids determining the active sites of different crystallized members of the family. This information can be useful for modelling of the three-dimensional structural arrangement of other noncrystallizable 17β -HSDs. Structural differences between 17β -HSD14 and three related 17β -HSDs (h 17β -HSD1, h 17β -HSD8, and 17β -HSD10) are discussed, with a focus on each enzyme's active site.

As the starting point for the design of the ligands was taken from an already existing library of 17β -HSD1/2 inhibitors, it was the aim to discover also a new scaffold in order to possibly overcome the selectivity issue toward other HSDs. Thus, in **Chapter 6** (manuscript in preparation), we initiated a fragment-based lead discovery (FBLD) campaign with the goal to discover new inhibitor scaffolds. Therefore, a 96-entry fragment library assembled applying selection criteria following a slightly extended "Rule of 3" was screened. The crystallographic fragment screening approach comprises the promising perspective that more novel hits are identified and structurally characterized than by any other biophysical screening technique, especially for ligands that show a low binding affinity. Nevertheless, such ligands can exhibit high ligand efficiency and the structural information about their binding modes is of utmost importance for further optimization.

Chapter 2

New Insights into Human β -Hydroxysteroid Dehydrogenase Type 14: First Crystal Structures in Complex with a Steroidal Ligand

Introductory remarks

Parts of the following chapter have been published in the *Journal of Medicinal Chemistry* in 2016. The cloning of the plasmid for the 17 β -HSD14 T205 variant was done by Dr. Gabriele Möller. TLC and fluorescence based assay were designed and performed by Dr. Sandrine Marchais-Oberwinkler in collaboration with the author of the thesis. The expression and the purification of the 17 β -HSD14, the crystallization study, the elucidation of the crystal structures and the TSA assay were established and performed by the author of this thesis. Furthermore, the author significantly contributed to the writing of the manuscript in collaboration with Dr. Sandrine Marchais-Oberwinkler and Florian Braun.

2.1 Introduction

17 β -Hydroxysteroid dehydrogenase type 14 (17 β -HSD14), also called retSDR3, DHRS10 or SDR47C19, is the latest 17 β -HSD which has been identified [11, 32, 34]. It belongs to the short-chain dehydrogenase-reductase (SDR) family and its physiological role is yet unknown. Estradiol (E2), 5-androstene-3 β ,17 β -diol (5-diol) and testosterone (T) have been identified as substrates *in vitro* [32]. 17 β -HSD14 catalyzes the alcohol oxidation, NAD⁺ dependent, of the aforementioned estrogens and androgens at their position 17 giving rise to estrone (E1), dehydroepiandrosterone (DHEA), and 4-androstene-3,17-dione (4-dione), respectively [32]. A library of 50 ligands of SDR enzymes were tested at 17 β -HSD14 but only the aforementioned steroids showed significant enzyme affinity, indicating that this enzyme might be involved in steroid metabolism [32].

The gene coding for 17 β -HSD14 was first isolated from the human retinal epithelium by Haeseleer *et al.* [100] and contains a serine at position 205 (S205). An alternate version of the gene was subsequently isolated from a melanotic melanoma cell during a genome sequencing campaign [101]. This allelic variant, termed T205, carries a threonine at position 205. The meaning of the observed polymorphism has not been analyzed until now and the T205 variant has also never been characterized to date. In this study, the structural and the biochemical characterization of the T205 will be addressed as well as its comparison to the S205 enzyme.

Concerning its localization, northern blot analyses have shown that the human HSD17B14 gene is dominantly expressed in the brain, liver, placenta [32], and in the kidney [100]. In another study, using an immunochemical based method Sivik *et al.* [103] demonstrated that the protein is also expressed in adrenals and testis as well as in eye, heart, kidney, esophagus, liver, rectum, salivary glands and skeletal muscle. 17 β -HSD14 has also been identified in breast cancer tissue [35, 103]. 17 β -HSD14 is a cytosolic enzyme [32].

The S205 variant of 17 β -HSD14 has been previously crystallized and the 3D-structure of the apoenzyme determined was by Lukacik *et al.* [32]. Crystal structures of a target protein provide important structural insights into binding sites. However, from the existing structure, no information about the protein/ligand interaction, either with the cofactor or with the substrate, can be extracted.

In this study, the characterization of the new T205 variant and four new crystal structures of the protein as apoenzyme (S205), holoenzyme (T205 and S205) and as inhibitor-enzyme complex (T205) are presented. These results provided further insights for the characterization of this enzyme.

2.2 Results and discussion

2.2.1 Protein expression and purification

Both recombinant 17 β -HSD14 protein variants (S205 and T205) were overexpressed in *E.coli* BL21 *pLysS* via transformation with the corresponding N-6His-tag plasmid, following Lukacik's procedure [32], applying minor modifications. Pure enzyme was obtained with a yield between 8-15 mg of protein per liter of bacterial culture. During the expression and purification process, protein content was followed either by a TLC plate activity assay or by a fluorimetric assay, based on the detection of the formed NADH.

During the establishment of the expression protocol several *E.coli* bacteria lines were tested. It turned out that only the *E.coli* BL21 (DE3) *pLysS* cells were able to overexpress the enzyme in satisfactory amount. The enzyme showed a particular tendency to aggregate and to precipitate with the pellet during the first centrifugation step of the purification of the bacteria homogenate suspension. The problem was resolved by resuspending the pellet deriving from four liters of culture with more buffer (about 400 mL vs 120 mL used by Lukacik *et al.* [32]) and by the addition of 0.5% of Triton X-100, a detergent that helped to keep the protein in solution. To avoid protein precipitation, it was beneficial to lower centrifugation (from 30000g to 17700g). Another issue was the constant contamination with DNA in the fraction containing the recombinant enzyme. DNA contamination could be avoided by using a DE-52 column. As such column is rather expensive, we directly applied the supernatant to a 5 mL Ni-NTA column and we removed DNA with a first washing step using a buffer composed of 50 mM Tris and 1.5 M NaCl. Such high salt concentration removed any nonspecific bound DNA. Unfortunately, the enzyme was still fairly unstable in solution. It was necessary to discover additives to add to the different buffers during purification having the capacity to keep the enzyme in solution. This issue is discussed in the following paragraph.

2.2.2 Protein stability and Thermal Shift Assay (TSA) experiment

The main challenge encountered during protein purification was the low stability of 17 β -HSD14. In the absence of any buffer additives, no or only minor amounts of protein could be isolated. Glycerol is known to stabilize proteins by compacting their structures to a globular shape [128, 129] and its addition substantially increased the efficiency of protein purification. However, it must be emphasized that glycerol in presence of NAD⁺ and the enzyme, without substrate, induces the production of a fluorescent substance which, after investigation, turned out to have the same fluorescence fingerprint as NADH. We concluded that glycerol is recognized as a substrate by 17 β -HSD14, thereby transforming NAD⁺ into NADH. Ethylene

glycol, MPD and PEG₄₀₀ caused the same effect as observed with glycerol. Glucose, which is commonly used as a cryo protectant and is also known to stabilize proteins [130, 131], was identified not to be a substrate and was therefore added during purification. The protein was further stabilized by adding NAD⁺ (0.5 mM) during the purification steps and for storage (0.25 mM).

Glycerol is often used as protein stabilizer during activity assays. To the extent of our knowledge, it is not systematically investigated whether or not glycerol can be accepted as a substrate during enzymatic assays, and whether it interferes with substrate binding. The presence of glycerol might therefore lead to some discrepancies in the interpretation of biological results.

The search for sufficient stabilization conditions, compatible with our fluorimetric activity assay, was supported by TSA. The TSA can be used to quantify the stabilization of a protein upon addition of different buffer additives (Figure 2.1). The reference curve was obtained in the absence of any additive and revealed two inflection points ($T_{m1}= 35.5\text{ }^{\circ}\text{C}$, $T_{m2}= 59\text{ }^{\circ}\text{C}$, Table 2.1). Conversely, in the presence of glycerol, a curve with a single melting point can be observed ($T_m= 57.5\text{ }^{\circ}\text{C}$), indicating that it effectively stabilizes the protein. Similar curves were obtained with MPD, PEG400 and ethylene glycol, but at lower melting temperatures than observed with glycerol (Table 2.1). This indicates a weaker stabilizing effect on the protein [116, 118].

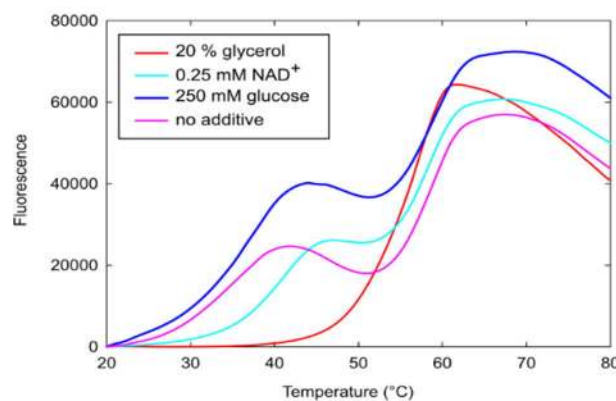


Figure 2.1: TSA curves of 17 β -HSD14 obtained in presence of glycerol (red), NAD⁺ (cyan), glucose (blue) or without any additive (magenta).

Remarkably, adding glucose or NAD⁺ resulted in TSA curves with two maxima. Both molecules independently induced a slight shift in the T_{m1} of the protein but did not greatly affect the T_{m2} . The combination of glucose and NAD⁺ has a greater influence on T_{m1} ($\Delta T_{m1}= +13\text{ }^{\circ}\text{C}$, compared to the measurement without any additive) while T_{m2} remains unchanged.

This result suggests that the first maximum corresponding to T_{m1} might represent a fraction of the protein in a less-stable conformation or the tetramer/dimer disruption, while the second maximum T_{m2} represents the true melting point of the protein in its most stable conformation.

Table 2.1: Effect of different buffer additives on the T_m of 17 β -HSD14

	T_{m1} in °C	T_{m2} in °C
No additive	35.5	59.0
Glycerol 20%		57.5
MPD 10%		47.0
PEG400 10%		53.0
Ethylene glycol 10%		53.0
Glucose 250 mM	37.5	59.5
NAD ⁺ 0.2 mM	41.5	59.0
Glucose 250 mM, NAD ⁺ 0.25 mM	48.5	59.0

The influence of different ligands on 17 β -HSD14 stability was also tested. Pure DMSO was used as control and a T_m of 56 °C was obtained (Table 2.2). No second maximum was identified. However, in the presence of excess of E1 and E2, only a slight shift could be observed ($\Delta T_m = 1.5$ -2 °C).

Table 2.2: Effect of different ligands on the T_m of 17 β -HSD14

	T_m in °C
DMSO 2.5%	56.0
Estradiol 0.25 mM	58.0
Estrone 0.25 mM	57.5

2.2.3 Activity assay and biochemical characterization of both S205 and T205

The activity of 17 β -HSD14 was determined by fluorescence intensity measurement of NADH formed during the catalytic reaction. The reaction was carried out using the purified enzyme, E2 as substrate and NAD⁺ as cofactor. High substrate concentration (32 μ M) had to be applied because of the low sensitivity of the method. All the other 17 β -HSDs have the characteristic ability to perform both oxidative and reductive reactions *in vitro* depending on the oxido-reduction state of the cofactor. Therefore, the activity of 17 β -HSD14 in the presence of E1 and NADH (corresponding to the back reaction) was also tested. However, no conversion to NAD⁺ could be detected after 15 min. *In vivo*, the cytoplasmic NAD⁺

concentration is about 500 times higher than NADH. This indicates that *in vivo* this enzyme should be a pure dehydrogenase.

In order to carry out a biochemical comparison of S205 and T205 variants, kinetic experiments were performed with the substrates E2, 5-diol and T. With all substrates, the enzyme follows Michaelis-Menten kinetics. However, with testosterone, no saturation curve could be observed, and consequently the kinetic parameters could not be determined. For 5-diol and E2 the Michaelis-Menten constants (K_m), the maximum velocities (V_{max}) and the turnover rate values (k_{cat}) were determined (Table 2.3). For the S205 variant, the K_m values obtained are in the same range as those published by Lukacik *et al.* [32]. The kinetic data of the T205 variant are very similar to those of the S205 protein, indicating that the T205 mutation does not influence the catalytic efficiency of the enzyme. This result appears reasonable as the amino acid 205 is not located in the proximity of the catalytic triad. The rather high K_m and low turnover of 17 β -HSD14 for both, 5-diol and E2, had already been pointed out by Lukacik *et al.*[32] and might indicate that the enzyme could bind other types of substrates. The specific activity, in presence of E2, is 1.35 and 1.21 nmol.min⁻¹.mg⁻¹ for S205 and T205, respectively.

Table 2.3: Kinetic analysis of 17 β -HSD14

Substrate	S205			T205		
	K_m (μ M)	V_{max} (nM·min ⁻¹)	k_{cat} (min ⁻¹)	K_m (μ M)	V_{max} (nM·min ⁻¹)	k_{cat} (min ⁻¹)
5-diol	6.6 \pm 1.5	58 \pm 0.4	0.017	7.8 \pm 1.2	68 \pm 0.3	0.019
E2	6.2 \pm 1.4	82 \pm 0.1	0.024	7.9 \pm 1.7	114 \pm 0.3	0.033

Mean values and given standard deviations were calculated based on 5 - 7 measurements

2.2.4 Crystallization of 17 β -HSD14

One crystal structure for 17 β -HSD14 had already been published as apoenzyme before this study was conducted [32]. As described in Chapter 1, this structure showed various limitations that made conclusive structure-based drug design hardly possible. Accordingly, we embarked onto a broad screening for alternative crystallization conditions.

After screening of more than 1200 conditions, our crystallization trials led to four different crystal structures: 17 β -HSD14 as apoenzyme (S205), as binary complexes with NAD⁺ (with both variants S205 and T205), as a complex with the product E1 (T205). All crystal structures of the protein complexes were obtained by co-crystallization. The data processing and the refinement statistics are summarized in Table 2.4.

Table 2.4: Data collection and refinement statistic for the crystal structures.

PDB code ^a	Apo structure (5ICS)	Holo structure S205 (5JSF)	Holo structure T205 (5JS6)	E1 complex (5HS6)
(A) Data collection and processing				
space group	<i>P</i> 12 ₁ 1	<i>I</i> 23	<i>I</i> 23	<i>I</i> 422
unit cell parameters <i>a</i> , <i>b</i> , <i>c</i> (Å)	77.0, 92.2, 87.3	130.2, 130.2, 130.2	130.2, 130.2, 130.2	91.0, 91.0, 131.9
Matthews coefficient ^b (Å ³ /Da)	2.5	3.2	3.2	2.4
solvent content ^b (%)	49.9	61.7	61.7	49.0
(B) Diffraction data				
resolution range (Å)	50-1.52 (1.61-1.52)	50-1.84 (1.95-1.84)	50-2.00 (2.12-2.00)	50-2.02 (2.14-2.02)
unique reflections	169468 (27103)	31827 (5106)	24734 (3933)	18613 (2930)
<i>R</i> (<i>I</i>) _{sym} (%)	5.8 (48.1)	4.7 (49.1)	4.2 (48.3)	9.1 (48.6)
Wilson <i>B</i> factor (Å ²)	13.7	35.06	44.6	26.1
completeness (%)	99.5 (98.8)	99.9 (99.6)	99.4 (98.5)	99.7 (98.7)
redundancy	3.8 (3.8)	6.6 (6.8)	6.6 (6.5)	7.5 (7.6)
<1/ <i>σ</i> (<i>I</i>)>	15.2 (2.7)	21.3 (4.2)	22.7 (3.9)	15.9 (4.3)
(C) Refinement				
resolution range (Å)	43.95-1.52	46.05-1.84	46.03-2.00	46.11-2.02
reflections used in refinement (work/free)	169468 (160994/8474)	31827 (30235/1592)	24734 (23497/1237)	18793 (17682/931)
final <i>R</i> value for all reflections (work/free) (%)	0.13/0.16	0.16/0.19	0.17/0.19	0.16/0.19
protein residues	1033	268	268	257
water molecules	735	86	64	136
RMSD from ideality: bond lengths (Å)	0.008	0.007	0.007	0.007
RMSD from ideality: bond angles (°)	0.937	0.817	0.817	0.868
Ramachandran plot: ^c				
residues in most favored regions (%)	92.5	92.2	92.2	93.3
residues in additionally allowed regions (%)	7.5	7.8	7.8	6.7
residues in generously allowed regions (%)	0.0	0.0	0.0	0.0
residues in disallowed regions (%)	0.0	0.0	0.0	0.0
Mean <i>B</i> factor protein (Å ²) ^d	18.4	45.8	56.3	29.1
Mean <i>B</i> factor ligand (Å ²) ^d	-	-	-	44.9
Mean <i>B</i> factor water molecules (Å ²) ^d	32.2	49.7	56.0	35.6

^a Values in parenthesis describe the highest resolution shell. ^b Calculated with Matthews_coef program from CCP4 suite version 6.4.0 [132]. ^c Calculated with PROCHECK [133]. ^d Mean B factors were calculated with MOLEMAN [134]

The **apo structure** was reproduced using different crystallization conditions than those described by Lukacik *et al.* [32], leading to a structure of 1.52 Å resolution. In the apo form a homotetramer is present in the asymmetric unit of the monoclinic space group $P 2_1$ (Figure 2.2 A). It exhibits the A2B2 symmetry as described by Lukacik *et al.* [32], however, in this new structure the C-terminalus segment is visible. The tetramer is built-up by the interaction of two identical dimers (A2 and B2) each composed of two monomers. The two dimers A2 and B2 differ in the conformation of the flexible loop, formed by the α -helices α FG1 and α FG2 (residues 189–212), which is open in A2 and closed in B2. A maximum shift of about 7 Å is observed between the two conformations of the flexible loop, which adjusts the size of the active site (Figure 2.2). In the dimer A2, the C-terminus of each monomer is inserted into the wide-open active site of the opposite monomer.

The structure highlights a major hydrophobic area at the interface between two monomers (Figure 2.3 A). This information, together with the interacting C-terminal tail, raises the hypothesis that the tetrameric form of this protein is quite stable and might have some functional meaning. The binding pocket constitutes a second rather hydrophobic region (Figure 2.3 B). It is not surprising as this protein catalyzes the oxidation of hydrophobic molecules like E2 and 5-diol.

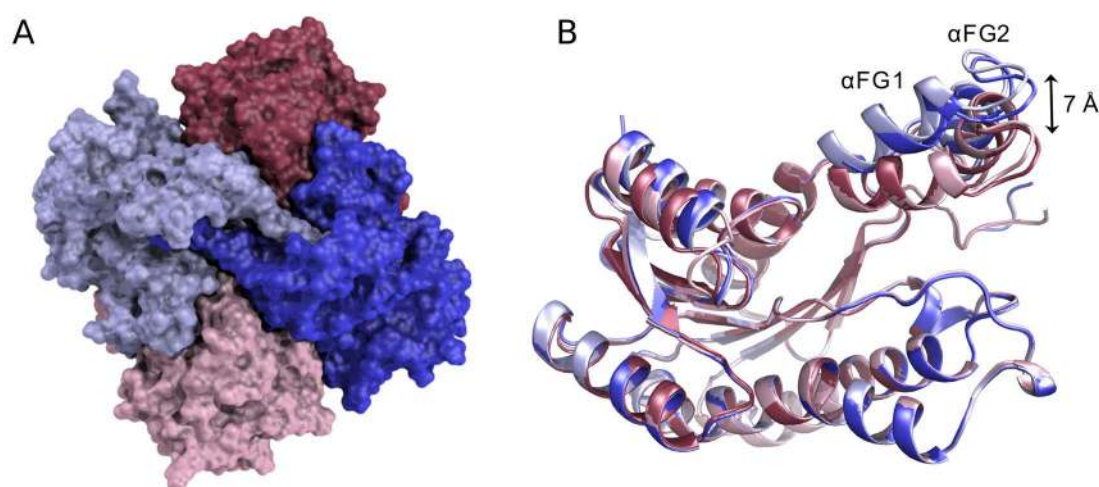


Figure 2.2: (A) Surface representation of the apoenzyme homo-tetramer (PDB code: 5ICS). (B) Ribbon representation of the superimposition of the four chains in the apo structure. The two chains forming dimer B2 are shown in pink shades and the two chains forming dimer A2 are shown in blue shades. All structural representations were prepared with PyMOL [33].

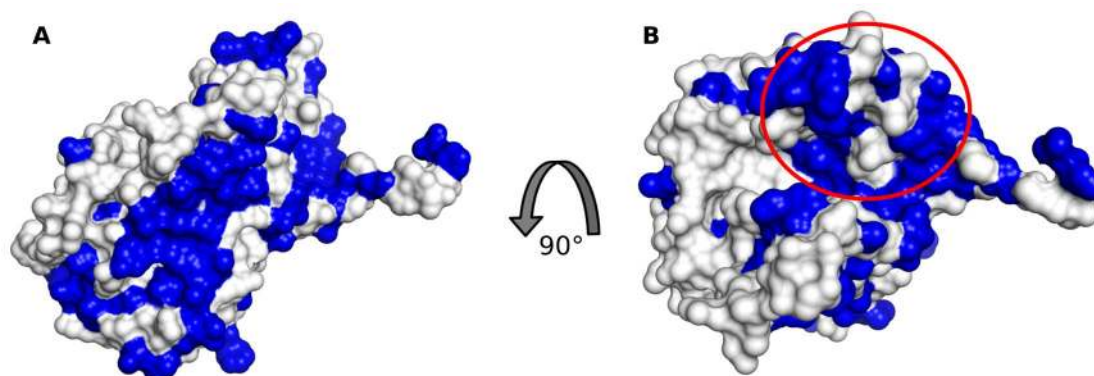


Figure 2.3: Surface representation of one monomer of the apoenzyme (PDB code: 5ICS). Hydrophobic amino acids are colored in blue and hydrophilic in white. **(A)** View on the interface between two monomers. **(B)** The binding site area is circled in red.

Concerning the structural determination of the two C-terminal tails of the dimer A2 of the apoenzyme the electron density map revealed a quite complicated scenario: It was not clear which density belonged to which monomer (Figure 2.4 A). Two possible scenarios were modeled and refined, but both possibilities presented some issues. The first construct was modeled in a way that the C-terminus of the first monomer interacts with the binding site of the second monomer and vice versa (Figure 2.4 B). Thereby, the model fits well to the electron density map and it was possible to explain most of the density. However, it was not possible to build the side chains for Cys255 and Lys256 because they would clash with the backbone of the C-terminus of the other monomer. Furthermore, there is no evidence of a second conformation of the C-terminal tail. The second construct was modeled in a way that the C-terminal tail of a monomer reverts back to its own binding pocket. However, after

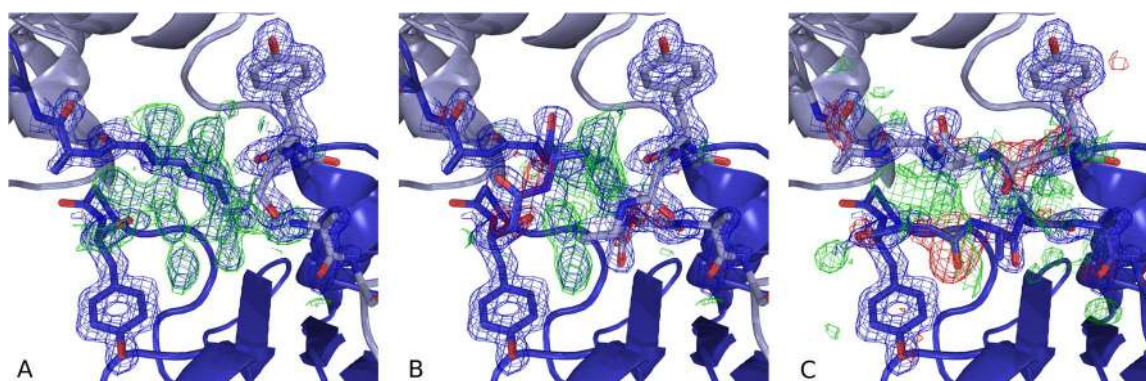


Figure 2.4: Crystal structures of apo 17 β -HSD14 without **(A)**, PDB code: 5ICS) and with two different models of the C-terminus **(B and C)**, see main text). The two monomers of the protein are shown in light blue and dark blue, respectively. The amino acids from Gly252 to Ser258 are shown as sticks. The $2F_o-F_c$ electron density is shown as blue mesh at a contour level of 1σ . The F_o-F_c difference electron density is shown as green and red mesh at contour levels of 3σ and -3σ , respectively.

refinement, the model did not fit well to the electron density, and also showed the clash of the sidechain of Lys256 with the C-terminus of the other monomer (Figure 2.4 C). In addition, to achieve the second construct, the geometries of some amino acids were unfavorable. Therefore, we decided that the first motif, where one C-terminus enters into the binding site of the other monomer, is the most likely conformation and consequently we decided to model this construct. However, we could not model Cys255 and Lys256 for one of the monomers and Gly254 and Cys255 for the other monomer.

In the case of the **holo structure**, both variants of the protein S205 and T205 were co-crystallized in complex with NAD⁺. Both variants contain only one monomer in the asymmetric unit in the cubic space group I23. Here, the tetramer is formed by four identical molecules. The PISA calculation [135] with a total buried area of 6610 Å² for each monomer and the analysis by native ESI mass spectrometry (result not shown) support that the tetrameric form is the assembly present in solution. Unfortunately, due to the high solvent content (61.5%, calculated with the Matthews Probability Calculator[136]·[137]), these crystals are characterized by a lower resolution (1.84 – 2.00 Å). No structural differences between the S205 and the T205 holoenzymes were evident from their 3D-structures as both isoforms were identical, with the mutated amino acid being the only exception (Figure 2.5 B). The flexible loop (α FG1 and α FG2) is fixed in a closed conformation, which reduces the volume of the binding pocket (Figure 2.5 A). The active site cleft is also downsized by the presence of Tyr253' belonging to the C-terminus from the adjacent crystal mate (Figure 2.6 A). The C-terminal part of the monomer is completely defined in the density and reveals a different conformation compared to the dimer A2 of the apo structure: It is not entering the binding pocket of the monomer but it is arranged around the surface of the bordering monomer (Figure 2.6 B). No further major conformational changes are observed.

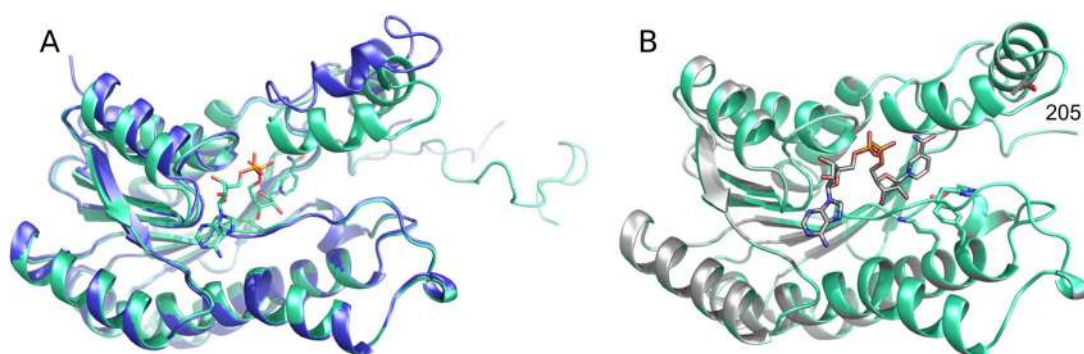


Figure 2.5: (A) Ribbon representation of the superimposed full length binary complexes of variant S205 (green) and a chain of the apoenzyme in the open conformation (blue). (B) Ribbon representation of the superimposed binary complexes of variant S205 (green) and T205 (gray) together with bound NAD⁺; the catalytic triad and the residues 205 are shown as stick model. The C-terminal tail is hidden for an easier comparison (S205 PDB code: 5JSF, T205 PDB code: 5JS6).

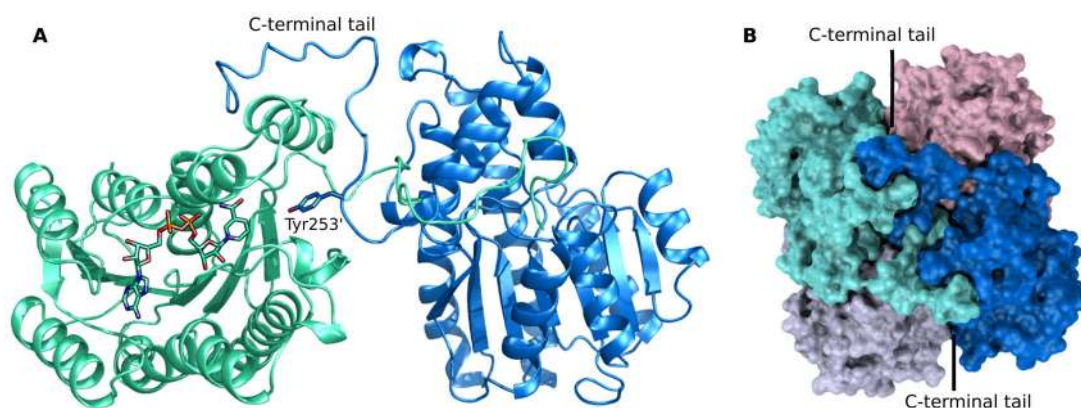


Figure 2.6: (A) Ribbon representation of the 17 β -HSD14 holoenzyme and cofactor NAD⁺. The symmetry equivalent molecule containing Tyr253' is shown in blue on the right hand side. The cofactor and Tyr253' are shown as thin lines. (B) Surface representation of the holoenzyme homotetramer.

In the structure of the E1-protein-NAD⁺ ternary complex a single monomer is present in the asymmetric unit. However, the generation of the symmetry equivalent molecules reveals that, also for this structure, the protein monomers interact with each other in a similar way as for the holo form, generating a tetramer via crystal symmetry. The C-terminal tail of the complex with E1 is very flexible and the amino acids from Ser258 to Ile268 are not defined by the electron density map. Only Pro269, Ser270 and Gly271, which are stabilized by a contact with the asymmetrical equivalent molecule, can be seen. A backbone comparison between the holo form and the ternary complexes does not reveal any differences between the structures. E1 is located in the steroid binding pocket (Figure 2.7 A) that is still downsized by the presence of Tyr253'. The substrate binding site has a conical shape, with the catalytic triad being at the apex of the cone and a wide solvent-exposed opening at the other side.

In all the structures the catalytic triad, composed of Ser141, Tyr154 and Lys158, maintains an identical geometry. A special attention should be paid to His93, which is stabilized by Gln148, located in the substrate binding site and close to the catalytic triad because it is not present in other human SDR 17 β -HSDs (Figure 2.7 B). This fact might be exploited to optimize inhibitor structures in order to achieve specific interactions with 17 β -HSD14 and thereby increasing selectivity toward other human SDR 17 β -HSDs.

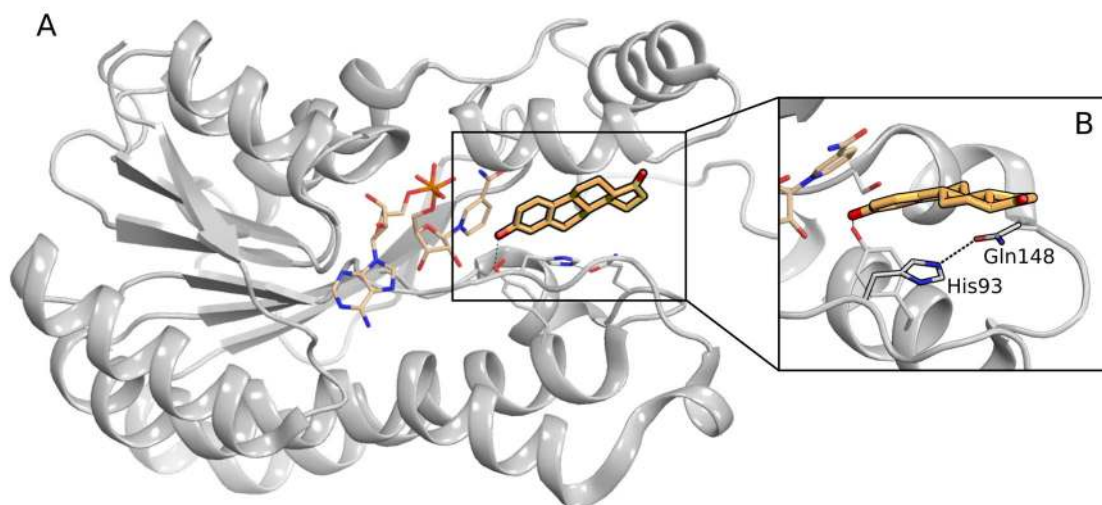


Figure 2.7: (A) Ribbon representation of the 17β-HSD14 (gray) structure as ternary complex. (B) Close-up view of the substrate binding pocket. The E1 is shown as stick model. The amino acids and the cofactor are shown as thin lines. The carbon atoms of E1 are colored in light orange. H-bonds are depicted as black dotted lines.

2.2.5 Description of the NAD⁺, estrone binding modes

Interactions stabilizing the cofactor in 17β-HSD14 are identified for the first time as the previously described structure did not contain NAD⁺. The cofactor NAD⁺ is buried inside the cofactor binding pocket and is coordinated via H-bond contacts to several amino acids and a number of crystallographically observed water molecules (Figure 2.8). These interactions are similar to those previously observed in other 17β-HSDs, for example in 17β-HSD10 [138].

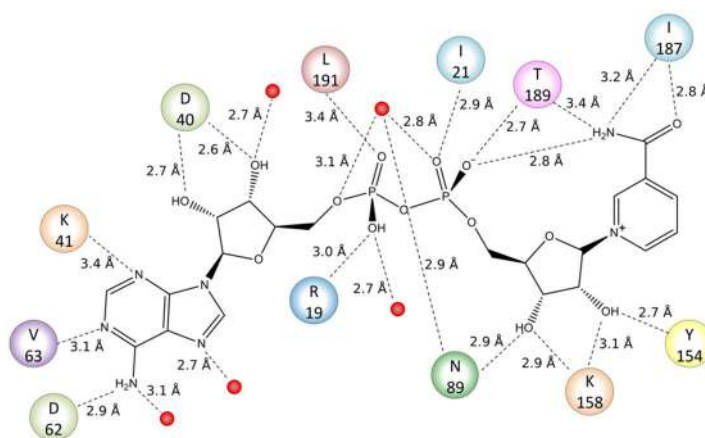


Figure 2.8: Interaction scheme between NAD⁺ and 17β-HSD14 (PDB code: 5ICM). Water molecules are represented in red spheres. H-bond contacts are shown as dotted lines.

E1, the product of the catalytic reaction, is found to be bound to the active site in an atypical fashion with its A-ring positioned in van der Waal's interaction distance to the nicotinamide portion of the cofactor (Figure 2.9) thus placing the actual 17-reaction center in remote position relative to the cofactor. No apparent π -stacking interaction of the steroidal A-ring can be observed with any amino acid. The only H-bond interaction established is between the A-ring's hydroxyl group and the hydroxyl of Tyr154 of the catalytic triad ($d = 2.5 \text{ \AA}$). The carbonyl group in position 17 does not form any interactions, neither with any amino acid nor with the solvent. The steroidal C-ring is placed in the hydrophobic cleft formed by Leu191, Trp192 and Leu195. The methyl group of the E1 is not detectable in the electron density of the ligand and therefore it was not included in the model. The orientation we do observe is, however, not unlikely due to the pseudo symmetry of E1 [139], and this also allows for the possibility that both orientations occur (with the 17 position of E1 binding to the catalytic triad or pointing away from it). No back reaction of the enzyme was observable by fluorescence assay. This result could be explained by the slow transformation rate of E1 to E2 or by the binding of E1 in a non-productive way or by both at the same time. E1 is not stabilized by many interactions. This is comparable to the binding mode of 3 β -hydroxy-5-androsten-17-dione (PDB code: 1HXX) described by Benach *et al.* [22] also with the A-ring close to the catalytic triad. Our structures confirm that the interactions achieved by the cofactor in 17 β -HSD14 are very similar to those established by NAD⁺ in other SDR enzymes [22]. Until now it was not possible to obtain a structure in complex with estradiol, however, it

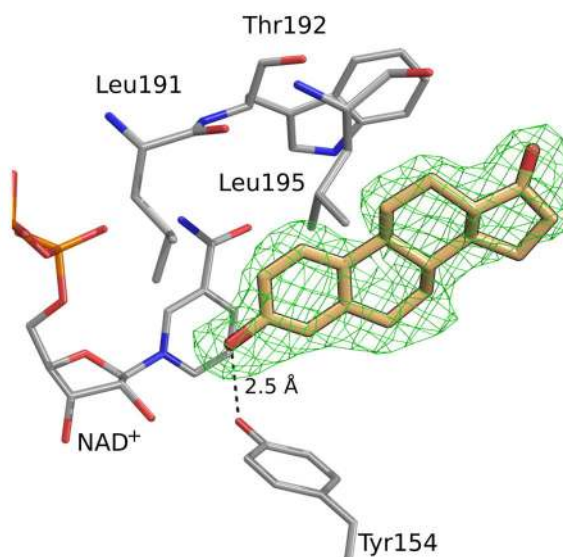


Figure 2.9: Crystal structures of 17 β -HSD14 in complex with E1 (PDB code: 5HS6). Estrone is shown as stick model, the amino acids within a distance of 4.6 \AA and cofactor are shown as thin lines. H-bond distances are depicted as dotted lines. The methyl group of the E1 is not detectable in the electron density of the ligand and therefore it was not included in the model. Fo-Fc difference electron density is shown as green mesh at a contour level of 2 σ .

is predictable that E2, like E1, may not bind so tight in the active site. Together with the weak binding affinities and low-turnovers measured for E2 and 5-diol, it is questionable if the preferred substrates of this enzyme are steroids.

2.3 Conclusion

In this work, we have elucidated the first crystal structures of 17 β -HSD14 in complex with ligands. The structure of the binary complex with the cofactor NAD⁺ differs from the apoenzyme with respect to the flexible loop (α FG1 and α FG2 segment) which adopts a unique closed conformation in the presence of NAD⁺: It is found in either open (A2 dimer) or closed (B2 dimer) conformation without cofactor. His93 and Gln148, that stabilized each other in the substrate binding site close to the catalytic triad, are not present in other human 17 β -HSDs and might be involved to achieve specific interactions with 17 β -HSD14. Binding of the cofactor appears to induce a shift of the flexible loop, which reduces the size of the active site and thereby produces the active conformation of the enzyme. The overall structure and the active site geometry in the ternary complexes with E1 is very similar to those of the binary complex, with the flexible loop in the same closed state delimiting an elongated and conical active site. However, further studies are still necessary to investigate the endogenous substrate and the physiological role of the enzyme *in vivo*.

2.4 Experimental section

2.4.1 Site directed mutagenesis

The plasmid p11-HSD17B14 coding for the S205 variant of human 17 β -HSD14 (sequence according to NCBI data bank entry Q9BPX1) was obtained from Udo Oppermann, Structural Genomics Consortium (SGC) Oxford.

The point mutation in order to gain the T205 variant was introduced into the plasmid by using the QuikChange Lightning Site-Directed Mutagenesis Kit (Agilent Technologies) with the forward primer 5'-CGGACCCGCGTGCGACCATTCGTGAAGGTATGC-3' and the reverse primer 5'-GCATACCTTCACGAATGGTCGCACGCGGGTCCG-3' and following the manufacturer's instructions. Sanger sequencing confirmed the correct mutation.

2.4.2 Expression of the 17 β -HSD14 protein (S205 and T205 variants) and purification

The pET-based vector, p11-Toronto1 (SGC), containing the coding sequences of the human gene HSD17B14 variants S205 and T205 with a *N*-terminal 6His-tag and a TEV (tobacco etch virus) protease cleavage site between the NdeI and BamHI enzyme restriction sites, was used for the transfection of the competent cells BL21 (DE3) pLysS strain of *E. coli*. The transformed cells were grown in 100 mL Terrific Broth medium containing 100 μ g/mL of ampicillin overnight at 37°C. The bacteria were transferred to bigger volume of Terrific Broth (4 L) and let growing at 37°C until they reached an OD₆₀₀ of 0.5. Then the temperature was lowered to 15°C. When the OD₆₀₀ reached the value of 1.0, the expression was induced with 0.5 mM of IPTG and the cells were incubated for further 20 hours at 15°C. The cells were harvested by centrifugation and conserved at -80°C one night before proceeding with the purification. The pellet resulting of 4 L of culture was resuspended in 400 mL of lysing buffer containing 50 mM Tris, 500 mM NaCl, 0.5 mM TCEP, 5 mM imidazole, 250 mM glucose, 1 mM NAD⁺, 0.5% (v/v) Triton X-100 and cOmplet Protease Inhibitor Cocktail Tablet[®] (Roche, Germany) with a set pH of 8. The cells were lysed with a high pressure homogenizer instrument (EmulsiFlex-C5[™], AVESTIN, Mannheim, Germany) and then centrifuged at 17700 *g* for 2h at 4°C.

For the protein purification, the supernatant was applied to a 5 mL Ni-NTA column (HisTrap FF, GE Healthcare Life Sciences, Freiburg, Germany), which was washed in two steps. The first washing step was performed with a buffer composed of 50 mM Tris and 1.5 M NaCl to remove the DNA. The second washing step was performed with a buffer containing 50 mM Tris, 500 mM NaCl, 0.5 mM TCEP, 250 mM glucose, 0.25 mM NAD⁺ and 21 mM imidazole to remove the unspecific binding proteins. For the target protein elution, the buffer of the second washing step was used with an imidazole concentration of 300 mM. The *N*-6His-tag was cleaved off by incubation with the TEV protease while the protein mixture was dialyzed overnight against 4 L of buffer (50 mM Tris, 500 mM NaCl, 0.5 mM TCEP, 250 mM glucose and 0.25 mM NAD⁺) at 4°C. For separation of the TEV protease from the 17 β -HSD14, the sample was again run over the 5 mL Ni-NTA column and the flow through containing the target protein was collected. As additional purification step, a size exclusion column (Superdex 75 26/60, GE Healthcare Life Sciences, Freiburg, Germany) was used with a running buffer comprising 50 mM Tris, 500 mM NaCl, 0.5 mM TCEP and 250 mM glucose. A NAD⁺ solution 0.25 mM (batch for enzymatic assay) or 0.6 mM (batch for crystallization studies) was added. The protein solution was flash frozen in liquid nitrogen and stored at -80°C. The molecular weight of each variant was verified by mass spectrometry in denaturation condition using a LTQ-FT Ultra mass spectrometer (ThermoFisher, Dreieich, Germany) equipped with an ESI source (MW S205 = 28641 Da, MW T205= 28655 Da).

2.4.3 Thermal shift Assay (TSA)

The thermal shift assay was conducted in a 96 well PCR plate (Bio-Rad, Munich, Germany) using a real-time PCR instrument (iCycler5, Bio-Rad, Munich, Germany). The running buffer was obtained by the dilution (1:1000) of SYPRO orange dye (Invitrogen, ThermoFisher Life Technologies, Darmstadt, Germany) in a buffer composed of 50 mM Tris, 0.5 M NaCl and 0.5 mM TCEP, pH 8.0. For the protein stability study, the running buffer was mixed with different additives (20% glycerol, 10% MPD, 10% PEG 400, 10% ethylene glycol, 250 mM glucose or 0.25 mM NAD⁺). For the protein complexes, a concentration of 2.5% of DMSO (reference measurement) or a stock solution in pure DMSO of compound **2**, estrone, or estradiol was added to the running buffer containing 250 mM glucose and 0.25 mM NAD⁺ (final ligand concentration of 0.25 mM and final DMSO concentration of 2.5%). A protein concentration of 2.6 μ M was used (3 μ L) and the different solutions were added to a final volume of 40 μ L.

2.4.4 Fluorimetric assay

The activity assay was based on measuring the fluorescence of the NADH formed. The oxidation of E2 into E1 in presence of NAD⁺ and purified 17 β -HSD14 was followed. Fluorescence spectra were recorded on a Tecan Saphir 2. NADH fluorescence emission was measured at 496 nm following excitation at 340 nm. The slit width for excitation was 7 nm while that for emission was 15 nm. The assay was performed in 100 mM phosphate buffer at pH 8.0, mixed with estradiol in DMSO (32 μ M) and NAD⁺ (1.5 mM) to reach a final DMSO concentration of 0.05%. The enzymatic reaction was started by addition of the pure protein (1 mg/mL, 3.0 μ M) and measured continuously for 15 min at 25°C. Reactions were performed in 200 μ L volumes. The assay was run in 96 well-plates in duplicate in three independent experiments. A linear relationship between product formation and reaction time was established. The slope of the reaction, representing the velocity of the NADH formation, was quantified. For each new batch of protein, a control experiment was run without E2 to assess the absence of activity in absence of substrate.

2.4.5 Determination of kinetic constants

For the determination of the kinetic parameters the substrate concentration was varied at least between 12% and 250% of the estimated K_m value. Kinetic constants were calculated from the initial velocity data by direct fitting curves as Hanes Woolf plot.

2.4.6 Protein crystallization

The activity of the protein was proven before use in each crystallization study. The crystallization of the apo form as well as the cocrystallization of the holoenzyme and of 17-HSD14 in complex with E1 were performed by sitting drop vapor diffusion technique. Initially, an automatized crystallization screening of 1248 conditions was performed (*MarXtal*, University of Marburg).

For the apo structure (S205), 0.1 μ L of protein solution (10 mg/mL) were combined with an equal volume of mother liquor having the composition: 0.1 M sodium acetate, 30% (w/v) PEG 4000, 0.2 M ammonium acetate, 20% glycerol, pH 4.60. After growing for 5 weeks at 18°C, crystals were harvested, exposed to the mother liquor solution with the addition of 20% glycerol for 30 seconds and finally flash frozen with liquid nitrogen.

The two isoforms (S205 and T205) of the holoenzyme were crystallized by combining 2 μ L of a solution containing protein (9.5 mg/mL) and 0.6 mM NAD⁺ with 2 μ L of a buffer composed of 0.1 M HEPES and 3.3 M sodium formate, pH 7.00. Over a time period of two weeks at 18°C, the crystals were grown, harvested and flash frozen using a cryo buffer made of mother liquor with 20% (w/v) PEG400.

A solution containing 0.1 M CHES, 1 M tri-sodium citrate, 0.4 mM E1 and 1% DMSO, pH 9.5, was mixed with the protein solution (9.5 mg/mL, T205), containing 0.6 mM NAD⁺, in a ratio 1:1 to obtain the protein-estrone complex. After growing for 4 weeks at 18°C, the crystals were exposed to a cryo buffer for 3 sec composed of 0.1 M CHES, 1 M tri-sodium citrate, 1% DMSO, 20% (w/v) glucose, pH 9.5, containing 0.4 mM of estrone, and subsequently flash frozen in liquid nitrogen.

2.4.7 Data collection and processing

The data collection of protein-estrone (PDB code: 5HS6) was achieved at Elettra beamline XRD1 in Trieste, Italy at a wavelength of 1Å and a temperature of 100 K on a silicon Pilatus 2M pixel detector. For the holo structure of both variants (S205 PDB code: 5JSF; T205 PDB code: 5JS6), the data collection was performed at beamline ID23-1 of the European Synchrotron Radiation Facility (ESRF) [140] in Grenoble, France at a wavelength of 0.97242 Å and a temperature of 100K on a silicon Pilatus 6M pixel detector. The diffraction data of apo form dataset (PDB code: 5ICS) was collected on BL 14.1 operated by the Helmholtz-Zentrum Berlin (HZB) at the BESSY II electron storage ring (Berlin-Adlershof, Germany) [141] at a wavelength of 0.9184 Å and a temperature of 100 K on a silicon Pilatus 6M pixel detector. All datasets were indexed, processed and scaled with XDS [142].

2.4.8 Structure determination and refinement

All structures were determined by molecular replacement with the program PHASER MR [143] from the CCP4 suite [132]. The structure 5EN4 was used as a search model. In the refinement, a subset corresponding to 5% of all reflections were omitted during refinement and used for the calculation of R_{free} . Model building was achieved in COOT [144] and refinement using PHENIX.refine version 1.10.1-2155 [145]. Ligands SMILE codes were created with *Molinspiration* v2014.11[146] and built with the Grade Web Server [147], which was also used for energetically minimization and restraint generation. Cartesian simulated annealing, applying default parameters, was used as a first refinement step. Subsequently, refinement of XYZ coordinates, occupancies and individual B-factors were alternated with structural adaption in COOT [144] until the model was readily built and gave the best possible explanation of the electron density. For the apo structure (PDB code: 5ICS), the temperature factors of all atoms, except hydrogen atoms, were refined anisotropically with additional NCS restraints. TLS refinement was performed for the protein-complex structures (estrone complex PDB code: 5HS6) and the both variants of the holoenzyme (S205 PDB code: 5JSF, T205 PDB code: 5JS6) with appropriate TLS groups from the TLSMD web server[148][149]. The model of the apo- and holo structure a were refined with hydrogens automatically added by PHENIX.refine.

Chapter 3

First Structure-Activity Relationship of 17 β -Hydroxysteroid Dehydrogenase Type 14: Nonsteroidal Inhibitors and Crystal Structures in Complex with the Enzyme

Introductory remarks

Parts of the following chapter have been published in the *Journal of Medicinal Chemistry* in 2016. The preliminary inhibition assay was done by Dr. Gabriele Möller. Fluorescence-based assays were designed and performed by Dr. Sandrine Marchais-Oberwinkler in collaboration with Florian Braun. The synthesis of the compounds and their characterization was carried out by Florian Braun. The expression and the purification of the 17 β -HSD14, the computational modeling studies, the TSA assay and the crystallization studies and the elucidation of the first crystal structures of the protein-inhibitor complexes were established and performed by the author of this thesis. Furthermore, the author significantly contributed to the discussion and to the writing of the manuscript in collaboration with Florian Braun and Dr. Sandrine Marchais-Oberwinkler.

3.1 Introduction

Human 17β -hydroxysteroid dehydrogenase type 14 (17β -HSD14), also called DHRS10 and retSDR3, is an oxido-reductase belonging to the SDR (Short-chain Dehydrogenase-Reductase) family [11, 32]. *In vitro*, the enzyme oxidizes the hydroxyl group at position 17 of estradiol (E2) and 5-androsten- $3\beta,17\beta$ -diol (5-diol) in presence of the cofactor NAD^+ , however, *in vivo*, its natural substrate is still unknown.

While Sivik *et al.* [103] described a broad distribution pattern of 17β -HSD14 across various tissues based on immunohistochemistry studies, Northern blotting experiments showed that the enzyme is predominantly expressed in the brain, liver and placenta [32] as well as in the kidney [100]. Furthermore, immunofluorescence studies revealed a cytosolic localization [32].

In order to understand the function of 17β -HSD14, the enzyme needs to be further characterized. Inhibitors are useful chemical tools, which can be used not only to characterize the binding site of an enzyme but also to get insight into the physiological role of the latter upon *in vivo* administration. No inhibitor has been reported for this enzyme.

The crystal structure of the human 17β -HSD14 has been determined recently as holoenzyme (PDB code: 5JS6 and 5JSF) and as ternary complex with estrone (E1) (PDB code: 5HS6). In solution, 17β -HSD14 is a tetramer.[126] The binding cavity was shown to be rather lipophilic with a conical shape. The substrate active site is narrow in the vicinity of the catalytic triad and is solvent exposed at the other end. Tyr253' from the C-terminal chain of the adjacent unit in the tetramer reduces the size of the active site.

Up to now 14 different 17β -HSD subtypes have been reported [34]. 17β -HSD1 and 17β -HSD2, the two best characterized subtypes, predominantly catalyze the oxidation and reduction of estrogens and androgens. Inhibitors of these two enzymes have already been reported [10, 52, 124, 150–160]. While 17β -HSD1 is a cytosolic enzyme and shows a reductive activity *in vivo* (activation of estrogens), 17β -HSD2 is membrane-bound and catalyzes the oxidation of estrogens and androgens to their less potent analogues similarly to 17β -HSD14. However, 17β -HSD2 and 17β -HSD14 differ in their tissue distribution pattern since in contrary to 17β -HSD14, 17β -HSD2 is not present in the human brain temporal lobe [161]. The presence of 17β -HSD14 in the brain might indicate that this enzyme is involved in the regulation of active estrogens and androgens in this organ [32].

The goal of this work was to identify the first 17β -HSD14 nonsteroidal inhibitors and to optimize their structures, which led to highly active compounds. The inhibitor optimization was performed following a ligand-based approach. The synthesis and biological evaluation of highly active compounds with a nonsteroidal scaffold together with five new crystal structures of the ternary complexes are reported. Analysis of the crystal structures of the

ternary complexes revealed the location of the inhibitor binding sites as well as the resulting protein-inhibitor interactions and a complex pattern of hydrogen bonds (H-bonds) contributing to the strong affinity of these compounds to the enzyme. The physicochemical properties of the new inhibitors as well as selectivity considerations were also addressed.

3.2 Results

3.2.1 Design of 17 β -HSD14 inhibitor candidates

Although 17 β -HSDs belong to the same superfamily they share a low overall sequence identity (between 15 and 30 %). Nonetheless, considering the fact that 17 β -HSD1 and 17 β -HSD2 catalyze the same reaction as 17 β -HSD14, the substrate binding site of the three enzymes should exhibit a high structural similarity. Based on this idea, it was assumed that some inhibitors developed for 17 β -HSD1 and 17 β -HSD2 should also bind to 17 β -HSD14 and that a common scaffold could be used as starting point, to optimize them for 17 β -HSD14 binding. In a first screen, a small library of 34 17 β -HSD1 and 17 β -HSD2 inhibitors, chosen on the basis of structural diversity (Figure 3.1), was tested for 17 β -HSD14 inhibitory activity using a radioactive displacement assay. This assay was performed with the recombinantly

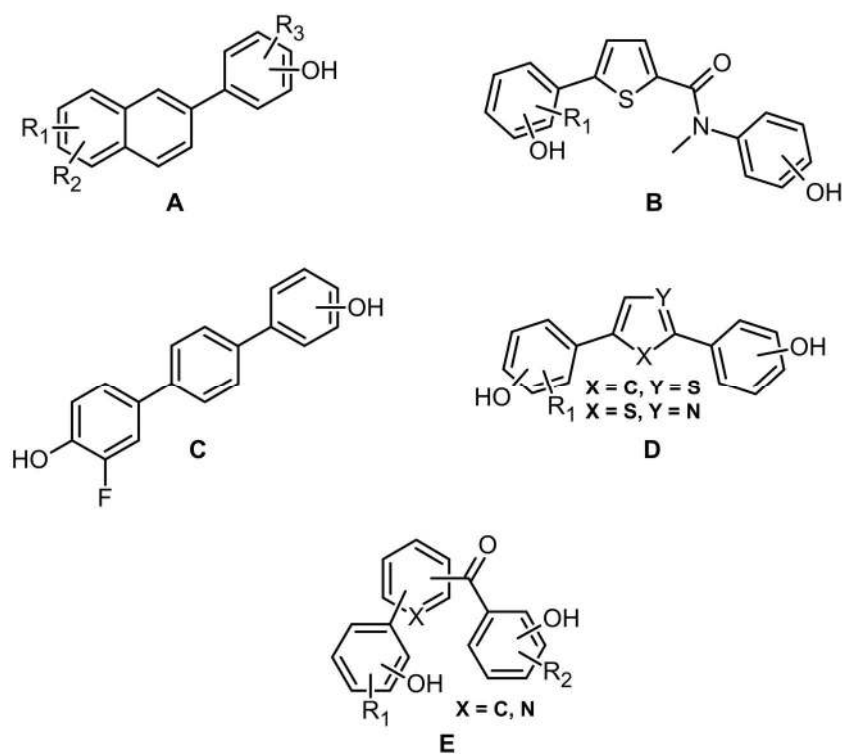
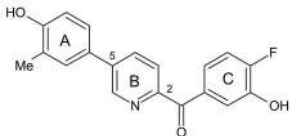
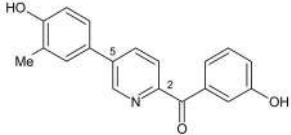
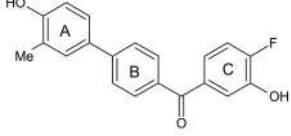
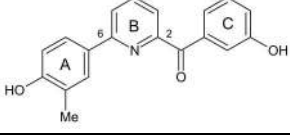


Figure 3.1: Scaffold of inhibitors from a 17 β -HSD1 and 17 β -HSD2 library tested for 17 β -HSD14 inhibitory activity.

expressed enzyme in a bacterial suspension since the pure protein was not available at that time. Thereby sets of active and inactive compounds were identified.

While the series of tested naphthalenes **A** and thiophene amides **B** contained mostly inactive compounds, the dihydroxyphenylbenzenes **C**, -thiophenes and -thiazoles **D** showed examples of low to moderate inhibitory activity against 17 β -HSD14 (between 10% and 45% inhibition at 1 μ M). In addition, some of the latter derivatives were also reported to possess very high potency for 17 β -HSD1 and/or 17 β -HSD2 (IC₅₀ in the low nM range), which might lead to difficulties achieving high selectivity for 17 β -HSD14. These parent scaffolds were therefore not considered for further optimization. Some members of the pyridine ketone class **E** also showed remarkable inhibitory activity for 17 β -HSD14, paralleled by rather low or moderate activity against 17 β -HSD1 (Table 3.1, compound **3.2**), which rendered this class as promising scaffold for further investigations. They were therefore chosen as a starting point for the development of new 17 β -HSD14 inhibitors.

Table 3.1: Most interesting compounds identified in the first screen.

Cmpd	Structure	Inhibition of 17 β -HSD14 % Inh. @ 1 μ M ^a	Inhibition of 17 β -HSD1 IC ₅₀ (μ M) ^b	Inhibition of 17 β -HSD2 IC ₅₀ (μ M) ^c
3.2		62%	1.27	0.10
3.3		0%	5.48	0.26
3.4		19%	0.29	0.04
3.5		32%	19.65	0.26

^a Recombinant 17 β -HSD14 enzyme, bacterial suspension, substrate [³H]-E2 [18.3 nM], NAD⁺ [7.5 mM], mean value of 3 determinations; standard deviation < 10 %.

^b Placental 17 β -HSD1 enzyme, cytosolic fraction, substrate [³H]-E1 + E1 [500 nM], NADH [0.5 mM], mean value of at least 3 determinations; standard deviation < 20 %.

^c Placental 17 β -HSD2 enzyme, microsomal fraction, substrate [³H]-E2 + E2 [500 nM], NAD⁺ [1.5 mM], mean value of at least 3 determinations; standard deviation < 20 %

The most interesting hits identified in the preliminary screen are listed in Table 3.1. The compounds can be categorized into 2,5- (**3.2**, **3.3**) and 2,6-substituted (**3.5**) pyridine ketones and the 1,4-substituted phenyl (**3.4**). In the 2,5-compound class, **3.2** and **3.3** (62% inhibition at 1 μ M vs 0%) differ by the presence/absence of a fluorine atom in *ortho* position to the OH group of the C-ring, suggesting the importance of this atom for inhibitory activity. Furthermore, comparison of **3.2** with **3.4** (62% inhibition at 1 μ M vs 19%) shows that the pyridine core B is more potent than the phenyl analog, pointing toward the importance of the nitrogen atom in the B-ring for activity. Concerning the 2,6-compound class, comparison of **3.5** with 2,5-substituted **3.3** (32% inhibition at 1 μ M vs 0%) shows that moving the A-ring from 5- to 6-position leads to a gain in activity.

Furthermore, considering the selectivity aspect, the poor inhibitory activity of the 2,6-substituted **3.5** toward 17 β -HSD1 (IC_{50} = 19.65 μ M), compared to the 2,5-substituted analog **3.3** (IC_{50} = 5.48 μ M) suggests that the 2,6-substitution pattern might improve selectivity for 17 β -HSD14 toward 17 β -HSD1. Selectivity against 17 β -HSD2 does not become obvious with the set of studied test compounds. Consequently, the 2,6-pyridine ketone class was selected for optimization and the derivatives, with modification at the A-ring as well as at the C-ring by substituents with different properties. Overall, 35 compounds were synthesized and their synthesis pathways are described in the thesis of Florian Braun. The obtained compounds are listed in Table 3.2. Special attention was paid to the physicochemical properties of the designed compounds in order to focus on compounds which should have a promising bioavailability profile according to the Veber rules [162] and the Lipinski rule of 5 [163].

3.2.2 Calculation of physicochemical parameters

For each synthesized compound (Table 3.2), the molecular weight (MW) was calculated to be in the range of 300 to 400 g/mol, aside from the trisubstituted compounds **3.31-3.33** with a slightly higher MW. The $clogP$ was calculated *in silico* (using Molinspiration [146]) and turned out to be below 5 except for **3.31-3.33**. The total polar surface area (tPSA), the number of rotational bonds as well as the number of H-bond donors and acceptors fulfill the Veber rules [162] and the Lipinski rule of 5 [163]. In addition, considering the potential role of the enzyme in the brain, the capability of the inhibitors to cross the blood–brain barrier (BBB) should also be taken into account. The physicochemical properties to be met by compounds showing a good BBB penetration are described by Pajouhesh and Lenz [164]. These criteria are matched for most of the synthesized compounds especially for **3.17** and **3.28** as examples. The solubility range of most of the compounds was also determined by mixing several concentrations of the studied inhibitors in 100 mM phosphate buffer at pH 7.4 and analyzing its precipitation status at different time points (0, 1, 2 and 24 h). The pK_a

values of the OH groups at the A- and at the C-ring were determined *in silico* for all compounds (using Marvin Sketch), showing that the introduction of a fluorine group in *ortho* position to a OH group decreases the pKa value by about one unit (e.g. pKa OH/C-ring: 8.8 for **3.7** and 7.8 for **3.8**). The physicochemical parameters are summarized in Table 3.2. The chemical formulas of the listed derivatives are given in the following Table 3.3-3.7.

Table 3.2: Physicochemical property of the synthesized inhibitors.

Cmpd	MW ^a	clogP ^a	cpKa ^b	tPSA ^a	solubility	Rotat. bonds ^a	HD ^a	HA ^a
3.1	325	3.02	1.85 (N) 7.71 (O/C-ring) 12.19 (4-O/A-ring) 8.74 (3-O/A-ring)	90.65	≥ 200 μM	3	3	5
3.6	323	4.35	1.94 (N) 7.76 (O/C-ring) 9.92 (O/A-ring)	70.42	100-200 μM	3	2	4
3.8	327	3.86	1.82 (N) 7.58 (O/C-ring) 8.23 (O/A-ring)	70.42	100-200 μM	3	2	4
3.9	327	3.83	0.78 (N) 7.46 (O/C-ring) 8.07 (O/A-ring)	70.42	≥ 200 μM	3	2	4
3.10	343	3.54	0.69 (N) 6.30 (2-O/C-ring) 10.83 (3-O/C-ring) 7.76 (O/A-ring)	90.65	≥ 200 μM	3	3	5
3.11	345	3.93	0.67 (N) 6.95 (O/C-ring) 7.84 (O/A-ring)	70.42	-	3	2	4
3.12	325	3.20	0.69 (N) 7.12 (2-O/C-ring) 11.84 (3-O/C-ring) 7.88 (O/A-ring)	90.65	≥ 200 μM	3	3	5
3.13	309	3.90	0.70 (N) 6.95 (O/C-ring) 7.84 (O/A-ring)	70.42	25-50 μM	3	2	4
3.14	341	2.93	0.70 (N) 7.09 (2-O/C-ring) 12.94 (3-O/C-ring) 8.81 (4-O/C-ring) 7.83 (O/A-ring)	110.88	≥ 200 μM	3	4	6
3.15	341	3.14	0.60 (N) 7.06 (2-O/C-ring) 13.57 (3-O/C-ring) 8.52 (4-O/C-ring) 7.78 (O/A-ring)	110.88	≥ 200 μM	3	6	4
3.16a	307	4.26	1.82 (N)	39.20	< 3.13 μM	4	0	3
3.16	293	3.99	1.82 (N) 7.76 (O/C-ring)	50.19	25-50 μM	3	1	3
3.17	336	4.06	1.41 (N) 7.76 (O/C-ring) 4.85 (N/A-ring)	53.43	25-50 μM	4	1	4

Table 3.2 (continued)

3.18	309	3.48	1.73 (N) 7.75(O/C-ring) 9.24(O/A-ring)	70.42	100-200 μ M	3	2	4
3.19	307	2.85	1.64 (N) 7.22(2-O/C-ring) 11.84(3-O/C-ring) 9.23(O/A-ring)	90.65	\geq 200 μ M	3	3	5
3.20	323	4.35	1.81 (N) 7.75(O/C-ring) 9.59(O/A-ring)	70.42	50-100 μ M	3	2	4
3.21	311	4.15	1.88 (N) 7.76(O/C-ring)	50.19	< 3.13 μ M	3	1	3
3.22	346	4.75	1.82 (N) 7.76(O/C-ring)	50.19	< 3.13 μ M	3	1	3
3.23a	335	4.48	2.03(N)	48.43	< 3.13 μ M	5	0	4
3.23	327	3.93	2.04(N) 7.48 (O/C-ring) 8.08 (O/A-ring)	70.42	100-200 μ M	3	2	4
3.24	217	2.10	2.46(N) 7.76 (O/C-ring)	50,19	\geq 200 μ M	2	1	3
3.25	299	3.57	1.54 (N) 7.76(O/C-ring)	50.19	6.25-12.5 μ M	3	1	3
3.26	300	3.45	3.82 (N) 7.76(O/C-ring)	53.43	100-200 μ M	3	1	4
3.27	315	2.43	2.54 (N) 6.72(O/C-ring) 7.80(O/A-ring)	56.67	25-50 μ M	3	1	5
3.28	309	4.19	7.76(O/C-ring)	59.42	100-200 μ M	4	1	4
3.29	324	4.25	7.26(2-O/C-ring) 11.88(3-O/C-ring) 8.05(O/A-ring)	77.75	50-100 μ M	3	3	4
3.30	341	1.57	6.95(2-O/C-ring) 11.77(3-O/C-ring) 7.71(O/A-ring)	103.2	\geq 200 μ M	3	3	6
3.31	429	6.46	1.68 (N) 7.75(O/C-ring) 10.08(O/A-ring) 9.45(O/D-ring)	90.65	100-200 μ M	4	3	5
3.32	433	5.95	1.52 (N) 7.65(O/C-ring) 9.87(O/A-ring) 8.39(O/D-ring)	90.65	\geq 200 μ M	4	3	5
3.33	357	3.51	0.69 (N) 7.46(O/C-ring) 8.06(O/A-ring) 14.60(O-CH ₂ -)	90.65	\geq 200 μ M	4	3	5

^acalculated with Molinspiration [146]^bcalculated with Marvin Sketch 15.9.14

3.2.3 Inhibition of 17 β -HSD14 determined with a fluorimetric assay

A fluorimetric assay, quantifying the NADH fluorescence formed during the catalytic reaction, was used to evaluate the inhibitory activity of the synthesized compounds. In the assay, the purified recombinant human enzyme, E2 as substrate, NAD⁺ as cofactor and the inhibitors were used. Due to the low sensitivity of the assay, a high enzyme concentration (between 3.0 μ M and 3.5 μ M) and a high concentration of substrate E2 (32 μ M) was necessary. The results are expressed as percent of inhibition measured at an inhibitor concentration of 2 μ M. The inhibition constant K_i was experimentally determined using an inhibitor concentration ranging from 2.6 μ M to 100 μ M or 260 nM to 10 μ M, depending on the inhibitor potency and solubility. As the inhibitor and protein concentrations were in the same range, no classical kinetic analysis could be applied [165]·[166]. The results were analyzed applying the quadratic Morrison equation for tight binding [167]. When the inhibitor was not sufficiently soluble at the required concentration, no K_i could be determined and the results were expressed as percent inhibition at the highest soluble concentration of the inhibitor. The results are shown in Tables 3.3-3.6. Compounds showing less than 10% inhibition at a concentration of 100 μ M were considered to be inactive.

3.2.4 Aggregation

It was verified that the compounds did not aggregate or induce aggregation of the protein by testing the compounds with and without detergent (0.5% v/v Tween 20). No significant changes in the inhibitor activity could be noticed at the different conditions.

3.2.5 17 β -HSD14 inhibitory activity

Starting from the hit 2,6-pyridine ketone **3.5**, modifications were undertaken at the C-ring and A-ring by introduction of different substituents (R, R', Chart 3.1). These substituents were selected to represent different electronic properties: Electron donating or electron withdrawing, H-bond donor, H-bond acceptor, lipophilic and hydrophilic. Changes were

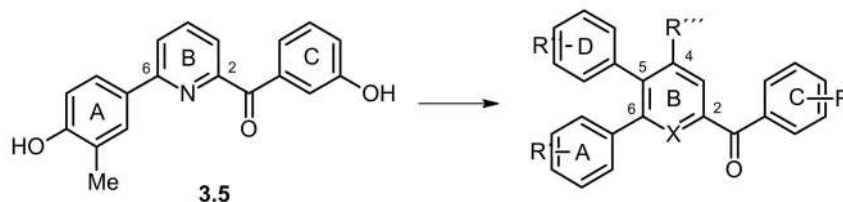


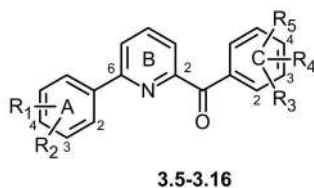
Chart 3.1: Modifications undertaken on the hit compound **3.5**.

also performed at the central B-ring by replacement of the nitrogen by a carbon or a *N*-oxide moiety. An additional phenyl ring (D) with various substituents (R'') was introduced in 5-position or a hydroxymethyl group (R''') in 4-position leading to trisubstituted derivatives.

3.2.6 Substituent variations on the C-ring

In the first inhibitor screen it could be shown, that in the 2,5-pyridine class (Table 3.1) the addition of a fluorine atom in *ortho* position to the hydroxyl group at the C-ring (**3.2** compared to **3.3**) resulted in a notable increase in potency of the inhibitor. The analogous fluorinated compound **3.6** (2,6-substituted pyridine) was therefore synthesized and proved to bind 10 times stronger compared to the reference compound **3.5** ($K_i = 245$ nM for **6** vs 26 nM for **5**, Table 3.3). The affinity enhancement caused by the 4-F substituent at the C-ring could

Table 3.3: 17 β -HSD14 inhibitory activity and binding constant (K_i) of 2,6-pyridine derivatives with different substituents at the C-ring.



Compound	R ₁	R ₂	R ₃	R ₄	R ₅	17 β -HSD14 % inhibition @ 2 μ M ^a	K_i (nM) ^a
3.5	3-Me	4-OH	H	3-OH	H	34	245 \pm 21
3.6	3-Me	4-OH	H	3-OH	4-F	60	26 \pm 3
3.7	3-F	4-OH	H	3-OH	H	16	467 \pm 91
3.8	3-F	4-OH	H	3-OH	4-F	67	36 \pm 5
3.9	2-F	3-OH	H	3-OH	4-F	72	13 \pm 5
3.10	2-F	3-OH	2-OH	3-OH	4-F	76	11 \pm 3
3.11	2-F	3-OH	2-F	3-OH	4-F	72	9 \pm 3
3.12	2-F	3-OH	2-OH	3-OH	H	65	64 \pm 4
3.13	2-F	3-OH	2-OH	H	H	66	135 \pm 2
3.14	2-F	3-OH	2-OH	3-OH	4-OH	25	405 \pm 177
3.15	2-F	3-OH	2-OH	3-OH	6-OH	11	796 \pm 122
3.16a	H	H	H	3-OMe	4-F	ni	nd
3.16	H	H	H	3-OH	4-F	57	63 \pm 3

^a Recombinantly expressed and purified 17 β -HSD14 enzyme, fluorimetric assay, substrate E2 [32 μ M], NAD⁺ [1.2 mM], 25°C, mean value of at least two independent experiments each with three technical repeats; ni: no inhibition (<10% inhibition at 100 μ M), nd: not determined.

also be observed using another substitution pattern at the A-ring: 3-F/4-OH ($K_i = 467$ nM for **7** vs 36 nM for **8**, Table 3.3).

The influence of the substituent pattern used for the C-ring was subsequently studied in more detail with compounds containing a 2-F/3-OH phenyl A-ring motif (compounds **3.9-3.15**, Table 3.3). Addition of a 2-OH or a 2-F to the 3-OH/4-F at the C-ring resulted in equipotent compounds ($K_i = 13$ nM; 11 nM and 9 nM, respectively for **3.9**, **3.10** and **3.11**). Replacing the 3-OH/4-F at the C-ring (**3.9**) by a 2-OH/3-OH motif (**12**; $K_i = 64$ nM) led to a slight decrease in affinity. Addition of a 4-OH group (**3.14**, $K_i = 405$ nM) or of a 6-OH group at the C-ring (**3.15**, $K_i = 796$ nM) resulted in a strong decrease in activity.

The presence of the 3-OMe group at the C-ring (**3.16a**, inactive at a concentration of 100 μ M) was detrimental for the inhibitory activity compared to the 3-OH analogue (**3.16**, $K_i = 63$ nM).

3.2.7 Substituent variations on the A-ring

2,6-Pyridine derivatives containing the C-ring motif (3-OH/4-F or 2-OH/3-OH) were synthesized with different substituents at varying positions of the A-ring (Table 3.4).

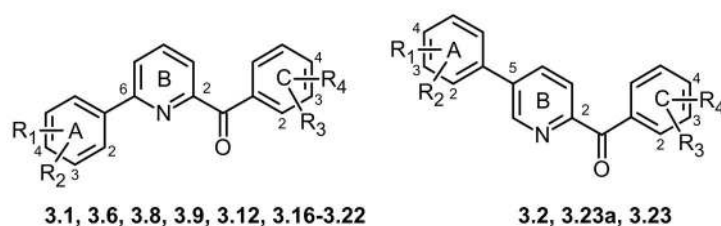
Compounds with one substituent in the 3- or 4-position (**3.17**: 3-NMe₂, $K_i = 7$ nM; **3.18**: 3-OH, $K_i = 7$ nM; **3.19**: 3-OH, $K_i = 44$ nM and **3.21**: 4-F, $K_i = 221$ nM) showed that their substitution with a polar moiety at 3-position (**3.17**, **3.18**, **3.19**) led to stronger binding compared to the one with a lipophilic group at 4-position (**3.21**). This effect is confirmed in case the A-ring is disubstituted (**3.22**) with the 3-Cl and 4-F substituents, which led to a compound with a similar binding constant as the mono 4-F derivative **3.21** ($K_i = 190$ nM and 221 nM for **3.22** and **3.21**, respectively). These lipophilic groups exerted a detrimental effect on the binding affinity, which was lower compared to the unsubstituted phenyl (**3.16**, $K_i = 63$ nM).

The compounds with two substituents in 2/3- or in 3/4-positions of the A-ring (**3.1**: 3-OH/4-OH, $K_i = 7$ nM; **3.6**: 3-Me/4-OH, $K_i = 26$ nM; **3.8**: 3-F/4-OH, $K_i = 36$ nM; **3.9**: 2-F/3-OH, $K_i = 13$ nM) had similar binding constants with the exception of **3.20** (3-OH/4-Me, $K_i = 47$ nM) with a slightly decreased affinity. No significant difference in activity could be observed between mono- and disubstituted compounds at the A-ring as long as a 3-OH or a 4-OH moiety was present. In summary, the best affinities were achieved in the presence of a 3-OH or a 3-NMe₂ moiety at the A-ring.

In the 2,5-pyridine class, the affinity of **3.23** ($K_i = 17$ nM) with a 3-F/4-OH substitution pattern at the A-ring was similar to that of compound **3.2** ($K_i = 24$ nM) with a 3-Me/4-OH

substitution pattern at the A-ring and fell into the same range of compounds in the 2,6-class. Furthermore, the methoxy derivative **3.23a** was less active compared to the hydroxylated analogue **3.23** as similarly observed for compound **16a**.

Table 3.4: 17 β -HSD14 inhibitory activity and binding constant (K_i) of pyridine derivatives with different substituents at the A-ring.



Compound	Position A-ring	R ₁	R ₂	R ₃	R ₄	17 β -HSD14	
						% inhibition @ 2 μ M ^a	K_i (nM) ^a
3.1	6	3-OH	4-OH	3-OH	4-F	69	7 \pm 1
3.2	5	3-Me	4-OH	3-OH	4-F	60	24 \pm 9
3.6	6	3-Me	4-OH	3-OH	4-F	60	26 \pm 3
3.8	6	3-F	4-OH	3-OH	4-F	67	36 \pm 5
3.9	6	2-F	3-OH	3-OH	4-F	72	13 \pm 5
3.12	6	2-F	3-OH	2-OH	3-OH	65	64 \pm 4
3.16a	6	H	H	3-OMe	4-F	ni	nd
3.16	6	H	H	3-OH	4-F	57	63 \pm 3
3.17	6	3-NMe ₂	H	3-OH	4-F	57	7 \pm 1
3.18	6	3-OH	H	3-OH	4-F	65	7 \pm 2
3.19	6	H	3-OH	2-OH	3-OH	51	44 \pm 3
3.20	6	3-OH	4-Me	3-OH	4-F	64	47 \pm 7
3.21	6	H	4-F	3-OH	4-F	37	221 \pm 46
3.22	6	3-Cl	4-F	3-OH	4-F	44	190 \pm 45
3.23a	5	3-F	4-OMe	3-OMe	4-F	12	57% \pm 6 ^b
3.23	5	3-F	4-OH	3-OH	4-F	61	17 \pm 5

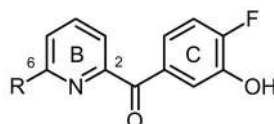
^a Recombinantly and expressed purified 17 β -HSD14 enzyme, fluorimetric assay, substrate E2 [32 μ M], NAD⁺ [1.2 mM], 25 $^{\circ}$ C mean value of at least two independent experiments each with three technical repeats; ^b% inhibition @ 22,2 μ M

3.2.8 Variation of the A-ring

In order to investigate the role of the phenyl A-ring, pyridine derivatives lacking the A-ring (**3.24**) or derivatives decorated with different heterocycles in 6-position of the B-ring (**3.25-3.28**) were designed (Table 3.5). Comparison of compound **3.24** (K_i = 1541 nM) with **3.16** (K_i = 63 nM) showed a decrease in activity. The nonaromatic piperidine **3.26** (K_i = 407 nM)

was also a weaker binder, while the 4-methylpiperazine **27** ($K_i = 190$ nM) showed a similar inhibitory activity, when compared to **3.16**.

Table 3.5: 17β -HSD14 inhibitory activity and binding constant (K_i) of 2,6-pyridine derivatives with different substituents in 6-position of the pyridine ring (different A-rings).



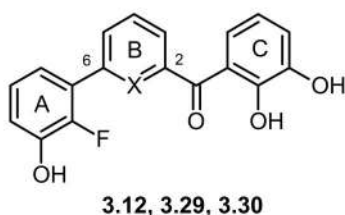
3.16, 3.24-3.28

Compound	R	17β -HSD14 % inhibition @ $2 \mu\text{M}^a$	K_i (nM) ^a
3.16	phenyl	57	63 ± 3
3.24	H	13	1541 ± 146
3.25	thiophen-3-yl	50	97 ± 28
3.26	piperidin-1-yl	43	407 ± 16
3.27	4-methylpiperazin-1-yl	31	190 ± 21
3.28	-O-phenyl	55	50 ± 0

^a Recombinantly expressed purified 17β -HSD14 enzyme, fluorimetric assay, substrate E2 [$32 \mu\text{M}$], NAD^+ [1.2 mM], 25°C mean value of at least two independent experiments each with three technical repeats

3.2.9 Variations on the B-ring

In the design section it was reported that in the 2,5-pyridine class the central ring played a crucial role in affinity. This aspect was also investigated in the 2,6-class by the synthesis of the phenyl analogue **3.29** and the corresponding *N*-oxide **3.30** (Table 3.6). Comparison of the biological data of these compounds with the pyridine analogue **3.12** ($K_i = 64$ nM) showed that both, the phenyl derivative **3.29** ($K_i = 21$ nM) and the *N*-oxide derivative **3.30** ($K_i = 132$ nM) had a similar affinity as the pyridine **3.12**.

Table 3.6: 17 β -HSD14 inhibitory activity and binding constant (K_i) for compounds with different B-rings.

Compound	X	17 β -HSD14	
		% inhibition @ 2 μ M ^a	K_i (nM) ^a
12	N	77	64 \pm 4
29	C	60	21 \pm 2
30	N ⁺ -O ⁻	47	132 \pm 13

^a Recombinantly expressed and purified 17 β -HSD14 enzyme, fluorimetric assay, substrate E2 [32 μ M], NAD⁺ [1.2 mM], mean value of at least two independent experiments each with three technical repeats

3.2.10 Trisubstituted pyridines

Based on the hypothesis that the C-ring and the carbonyl group of both the 2,5- and 2,6-pyridines achieve the same interaction as a consequence of binding in the same area, the similarity in affinity of the 2,5-derivative **3.23** (K_i = 17 nM) and the 2,6-derivative **3.8** (K_i = 36 nM, Table 3) suggested that the available space for binding the additional ring must be large, even tolerating an A-ring attached to the 5- or 6-position. Trisubstituted pyridines combining substitutions at the 5- and 6-positions were therefore synthesized (**3.31** and **3.32**, Table 3.7). These trisubstituted compounds turned out to be equipotent (**3.31**, K_i = 9 nM; **3.32**, K_i = 15 nM) with a similar affinity compared to the disubstituted derivatives **3.6** and **3.23**.

Introducing a hydroxymethyl group at the 4-position of the B-ring led to a slight decrease in activity (**3.33** K_i = 86 nM compared to **3.9** K_i = 13 nM, Table 3.7).

Table 3.7: 17 β -HSD14 inhibitory activity and binding constant (K_i) of pyridine derivatives with an additional D-ring or a substituent in 4-position.

Compound	R ₁	R ₂	17 β -HSD14 % inhibition @ 2 μ M ^a	K_i (nM) ^a
3.6			60	26 \pm 3
3.23			61	17 \pm 5
3.31	3-Me	4-OH	71	9 \pm 4
3.32	2-F	3-OH	63	15 \pm 4
3.33	-	-	47	86 \pm 7

^a Recombinantly and expressed purified 17 β -HSD14 enzyme, fluorimetric assay, substrate E2 [32 μ M], NAD⁺ [1.2 mM], mean value of at least two independent experiments each with three technical repeats

3.2.11 Pan Assay Interference Compounds [168]

All the biologically evaluated compounds were tested *in silico* for nonspecific binding in order to identify false positives using the Pains-remover computer tool [169]. From the compounds analyzed, seven did not pass the filter, including **3.10**, **3.12**, **3.14**, **3.19**, **3.20**, **3.29**, **3.30** suggested as nonspecific binders. They all share as common characteristic a catechol moiety. It is known that catechols can be toxic [170], however, the inhibitory data of these compounds are presented as they are useful to establish a better structure-activity relationship comprehension. In case these compounds turn out to be highly interesting, further assays should be performed to characterize their toxicity.

3.2.12 Crystal structure determination

The inhibitors with the highest binding affinity were selected for crystal structure determination in order to get insight into their binding mode. Crystal structures could be obtained for five different inhibitors by cocrystallization of the protein in complex with cofactor and ligands (**3.1**, PDB code: 5ICM; **3.6**, PDB code: 5L7T; **3.9**, PDB code: 5L7Y; **3.10**, PDB code: 5L7W; **3.12**, PDB code: 5EN4). The data collection, processing, and refinement statistics are reported in Table 3.8. The crystals were obtained by two different conditions, however, all crystal structures show the same tetragonal space group (I422) with only one

monomer present in the asymmetric unit. The crystal structures disclosed, that the protein is a homotetramer, in accordance with a previous study [126]. The structures obtained have a resolution ranging from 1.52 Å to 2.02 Å. The C-terminal tail of the complexes is very flexible and the amino acids from Ser258 to Ile268 remain undefined in the electron density map with the exception of Pro269, Ser270 and Gly271, which are stabilized by contact to a crystal mate, like already observed for the structure of the E1-protein complex. A backbone comparison between the structure of the holoenzyme and the ternary complexes does not reveal any differences between the structures.

3.2.13 Description of the inhibitor binding site

The superimposition of all five ternary complexes reveals that binding of the different ligands does not induce conformational changes of the overall geometry of the protein (Figure 3.2), showing a mean RMSD of 0.15 ± 0.04 Å between the alignment based on the coordinates of the C α atoms of the structures, as calculated with COOT [171]. The cofactor interacts with the Rossmann fold region and experiences similar interactions as already observed for the 17 β -HSD14 holo structure and in complex with E1 [126]. The inhibitor binds into the substrate binding site (Figure 3.3), which is restricted by two α -helices from the flexible loop (α FG1 and α FG2, residues 189-212, in orange), a portion of the α F helix (containing the catalytic Tyr154, Lys158, in yellow), the short α EF helix (residue 142-146, in cyan), the segment that connects α E with β D (from Asn89 to Arg98, in green), and the C-terminal tail (in red, Figure 3.4). Furthermore, Tyr253' from the adjacent monomer (in gray on the right hand side, Figure 3.4) is pointing toward the inhibitor binding site, reducing the volume of the active site cleft. The annotation of the different helices and β -sheets follows the nomenclature described by Lukacik *et al.* [32]. The flexible loop is in a conformation that closes the binding pocket, reducing the size of the substrate binding site. Furthermore, the inhibitor binding site is predominantly hydrophobic, with two main hydrophilic regions: The first one corresponds to the two residues of the catalytic triad Tyr154 and Ser141, and the second one is formed by His93 and Gln148 (Figure 3.5). This second region shapes the binding site in a peculiar form and could be relevant for the achievement of selectivity considering that no other human SDR 17 β -HSDs present a histidine at this position.

Table 3.8: Data collection and refinement statistic for the crystal structures.

PDB code ^a	Complex with 3.6 , 5L7T	Complex with 3.9 , 5L7Y	Complex with 3.10 , 5L7W	Complex with 3.12 , 5EN4	Complex with 3.1 , 5ICM
(A) Data collection and processing					
space group	I422	I422	I422	I422	I422
unit cell parameters <i>a</i> , <i>b</i> , <i>c</i> (Å)	91.2, 91.2, 131.4	91.6, 91.6, 132.5	91.0, 91.0, 132.2	91.7, 91.7, 135.0	91.7, 91.7, 133.8
Matthews coefficient ^b (Å ³ /Da)	2.4	2.4	2.4	2.5	2.4
solvent content ^b (%)	48.5	49.3	48.5	50.4	49.9
(B) Diffraction data					
resolution range (Å)	50-1.98 (2.10-1.98)	50-1.91 (2.03-1.91)	50-1.76 (1.86-1.76)	50-1.52 (1.61-1.52)	50-1.68 (1.78-1.68)
unique reflections	19413 (3002)	21943 (3336)	27439 (4039)	44532 (7097)	32511 (5122)
<i>R</i> (<i>I</i>) _{sym} (%)	8.2 (48.4)	8.8 (49.7)	8.4 (49.8)	5.3 (47.3)	8.1 (49.3)
Wilson <i>B</i> factor (Å ²)	26.0	21.7	20.6	19.5	19.96
completeness (%)	98.9 (97.1)	98.9 (94.8)	97.6 (90.3)	99.9 (99.6)	99.1 (98.3)
redundancy	7.2 (6.7)	7.2 (6.6)	9.3 (8.5)	14.6 (14.6)	6.9 (6.7)
< <i>I</i> /σ(<i>I</i>)>	17.8 (3.5)	16.8 (3.7)	17.1 (3.7)	28.4 (6.6)	14.1 (2.9)
(C) Refinement					
resolution range (Å)	46.05-1.98	46.31-1.91	39.7-1.76	46.8-1.52	37.82-1.68
reflections used in refinement (work/free)	19413 (18442/971)	21943 (20845/1098)	27439 (26067/1372)	44532 (42305/2227)	32511 (30885/1626)
final <i>R</i> value for all reflections (work/free) (%)	0.15/0.19	0.14/0.16	0.15/0.19	0.11/0.13	0.16/0.19
protein residues	256	256	254	251	255
water molecules	172	188	204	99	189
RMSD from ideality: bond lengths (Å)	0.007	0.009	0.009	0.008	0.009
RMSD from ideality: bond angles (°)	0.850	0.993	1.066	1.062	1.004
<i>Ramachandran plot</i> : ^c					
residues in most favored regions (%)	92.3	93.3	91.8	93.2	92.8
residues in additionally allowed regions (%)	7.7	6.7	8.2	6.8	7.2
residues in generously allowed regions (%)	0	0	0	0	0.0
residues in disallowed regions (%)	0	0	0	0	0.0
Mean <i>B</i> factor protein (Å ²) ^d	22.2	20.3	24.6	22.9	23.0
Mean <i>B</i> factor ligand (Å ²) ^d	31.3	27.3 (interface) 35.1 (binding pocket)	26.9	31.6	26.1
Mean <i>B</i> factor water molecules (Å ²) ^d	29.9	27.9	34.8	33.7	32.9

^a Values in parenthesis describe the highest resolution shell. ^b Calculated with Matthews_coef program from CCP4 suite version 6.4.0.[132] ^c Calculated with PROCHECK.[133] ^d Mean B factors were calculated with MOLEMAN.[134]

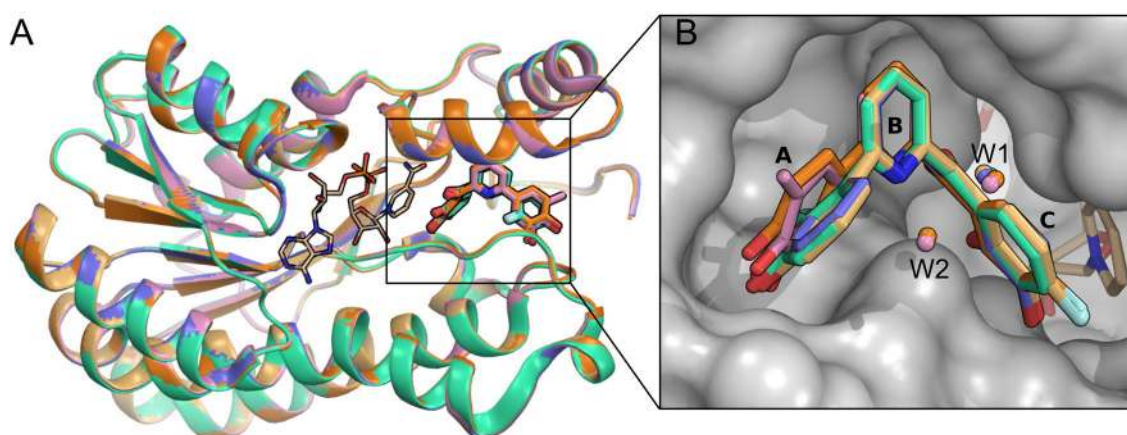


Figure 3.2: Superimposition of the crystal structures of 17 β -HSD14 obtained in ternary complexes with five inhibitors: **3.1**, **3.6**, **3.9**, **3.10**, **3.12**. **(A)** The enzyme 17 β -HSD14 is shown as ribbon model (5ICM in orange, 5L7T in pink, 5L7Y in purple-blue, 5L7W in ocher and 5EN4 in green); inhibitors are shown as stick models. The cofactor NAD⁺ is shown as thin line. **(B)** Close-up view on the binding pocket. The protein 17 β -HSD14 is displayed by use of the solvent accessible surface. The carbon atoms of the inhibitors are shown for **3.1** in orange, **3.6** in pink, **3.9** in purple blue, **3.10** in ocher and **3.12** in green. Inhibitors are shown as stick models and cofactor as thin line. The water molecules W1 and W2 are represented in the same color as the corresponding inhibitor of the individual structures. W1 corresponds to water molecule 472 in 5ICM, 518 in 5L7T, 508 in 5L7Y, 496 in 5L7W, 450 in 5EN4; W2 corresponds to water molecule 530 in 5ICM and 502 in 5L7T, in the respective crystal structure. All structural representations were prepared with PyMOL [33].

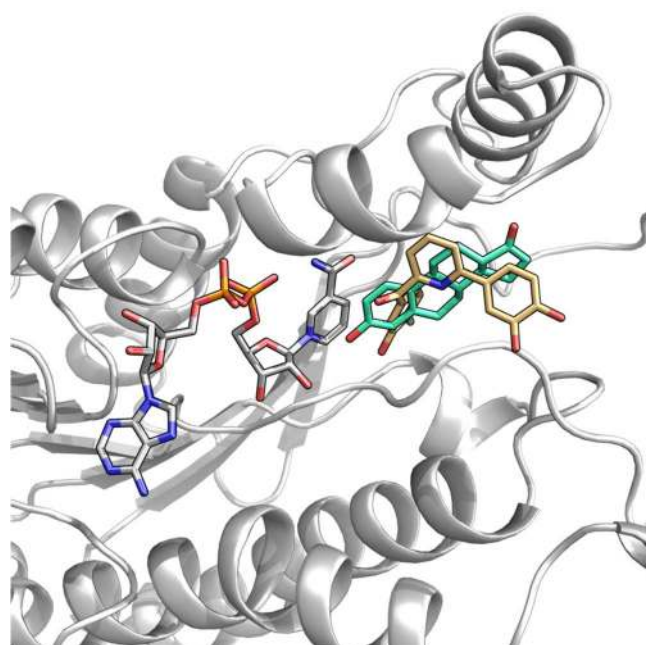


Figure 3.3: Superimposition of the crystal structures of 17 β -HSD14 obtained in ternary complexes with E1 and an inhibitor. The enzyme 17 β -HSD14 is shown in gray as ribbon model; E1, cofactor NAD⁺ and inhibitor are shown as stick models. The carbon atoms of E1 are shown in light green, in beige for the inhibitor and in gray for NAD⁺.

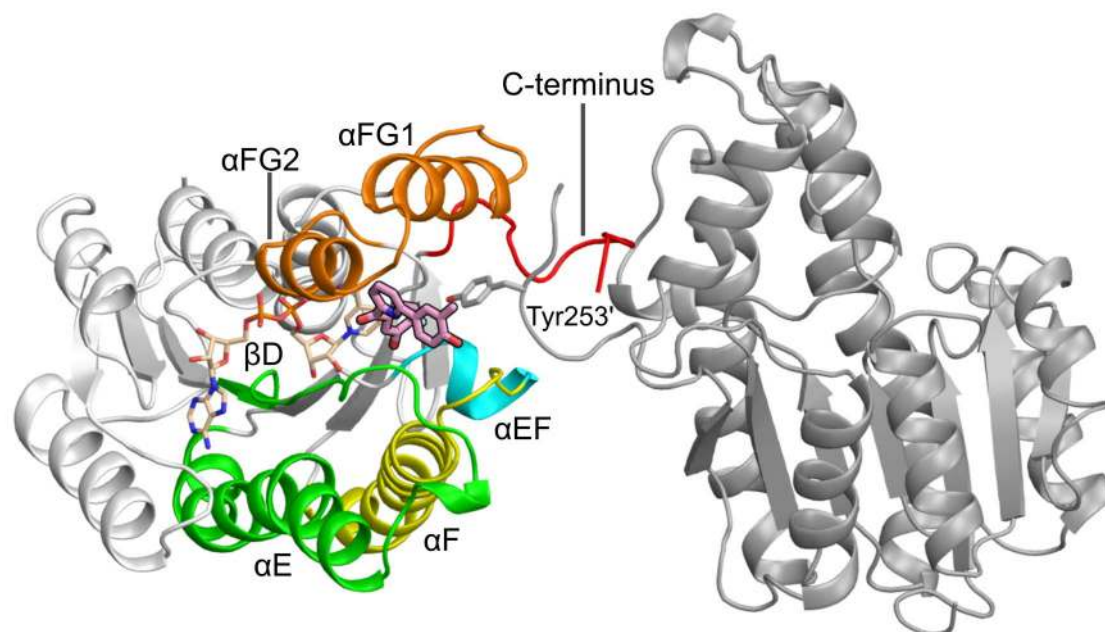


Figure 3.4: Ribbon representation of inhibitor **6** in complex with the protein 17 β -HSD14 and cofactor NAD⁺. The inhibitor binding site is delimited by α FG1 and α FG2 (orange), α F (the helix containing the catalytic Tyr154 and Lys158, yellow), α EF (cyan), α E and β D (green) and C-terminal tail (red). Inhibitor **3.6** is shown as stick model and its carbon atoms are colored in pink. The symmetry equivalent molecule containing Tyr253' is shown in gray on the right hand side. The cofactor and Tyr253' are shown as thin lines.

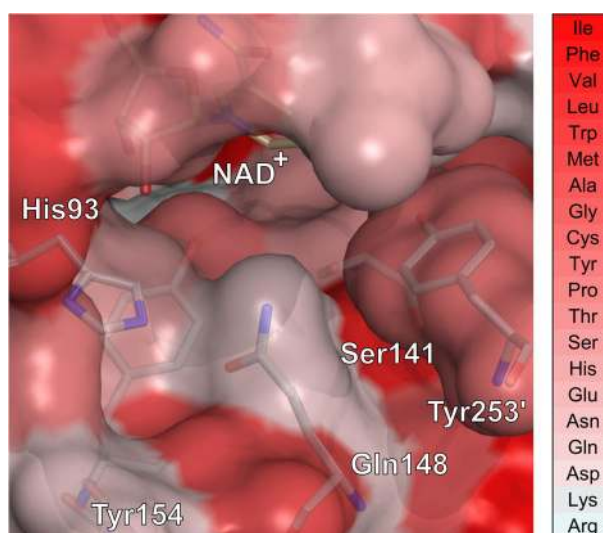


Figure 3.5: Surface representation of 17 β -HSD14; color coded according to the Eisenberg hydrophobicity scale (from dark red for highly hydrophobic amino acids to white for highly hydrophilic amino acids) [172]. The cofactor NAD⁺ and amino acids are shown as stick models. The amino acid of the symmetry equivalent molecule is referred as prime (').

3.2.14 Description of the binding mode of inhibitors in complex with 17 β -HSD14

In the surface representation, it is obvious that the V-shape of the inhibitor scaffold matches well with the geometry of the active site (Figure 3.2 B). For all five crystallized inhibitors, additional water molecules are observed in the binding pockets: Water W1 is found for all inhibitors in the same position. W1 is localized between the B- and C-ring, at an approximate 4 Å distance from the B-ring. W1 establishes an H-bond interaction with the side-chain of Asn186 ($d \approx 2.7$ Å). Water W2 is only observed for **3.1** and **3.6** (Figure 3.2 B) and is located above the plane of the A-ring. W2 interacts with W1 (H-bond contact $d \approx 2.6$ Å). In case of the other three inhibitors, the orientation of the A-ring plane is shifted, inducing the displacement of W2.

The structures and details of the interactions of all inhibitors are shown in Figure 3.6 (A: **3.1**, B: **3.6**; C: **3.12**; D: **3.9**; E: **3.10**). All the inhibitors have the same B-ring scaffold (2,6-pyridine) differing in the nature of their A- and C-ring substituents. The C-ring is located in vdW distance to the nicotinamide moiety of NAD⁺. The 3-OH group at the C-ring interacts via remarkably short H-bond interactions with the side chain of Tyr154 ($d = 2.3$ - 2.5 Å) and the side chain of Ser141 ($d = 2.5$ - 2.6 Å), the latter two amino acids belonging to the catalytic triad. The 4-F group at the C-ring of **3.6** is not involved in any specific interaction. The angle between the keto group and the phenyl C-ring is identical in all the inhibitors independent of the presence or absence of the 2-OH group at the C-ring. The keto group and the pyridine ring bind exactly at the same position for all of them. Interestingly, the keto group between the pyridine and the C-ring does not form any interactions but seems to be important for the inhibitor to adopt the correct geometry.

The central pyridine B-ring is anchored by van der Waals contacts with Trp192 and Leu195, which wrap around the top part of the pyridine ring. No close contacts are observed with His93. For **6**, the 3-Me group at the A-ring is not involved in any interaction. An H-bond interaction is formed between the 4-OH at the A-ring of **3.1** and **3.6** with the carbonyl backbone of Ala149 ($d = 2.7$ - 3.1 Å). The two 3-OH groups of the catechol ring of **3.1** form a polar interaction with the carbonyl backbone oxygen of Ala149 ($d = 2.8$ Å).

The aromatic A-ring is not stabilized by any π -stacking interactions, however, it is in van der Waals distance with Pro96. No water mediated H-bond interactions are observed; nonetheless, it is remarkable that W1 remains present in this lipophilic environment. In total for **3.1** and **3.6**, circa 90 van der Waals contacts are achieved by the ligand and its surface is buried to about 94.0 % (considering only one monomer of the protein, the number of van der Waals contacts achieved are summed up to 86 and the buried surface is 87.4 %). In **3.9**, **3.10** and **3.12**, a rotation of the A-ring plane is observed. Nevertheless, the altered orientation still allows the 3-OH group at the A-ring to be at H-bond distance to Ala149-CO ($d = 2.8$ - 3.0 Å, as observed with **3.6**). The aromatic A-ring can also establish a van der Waals interaction with

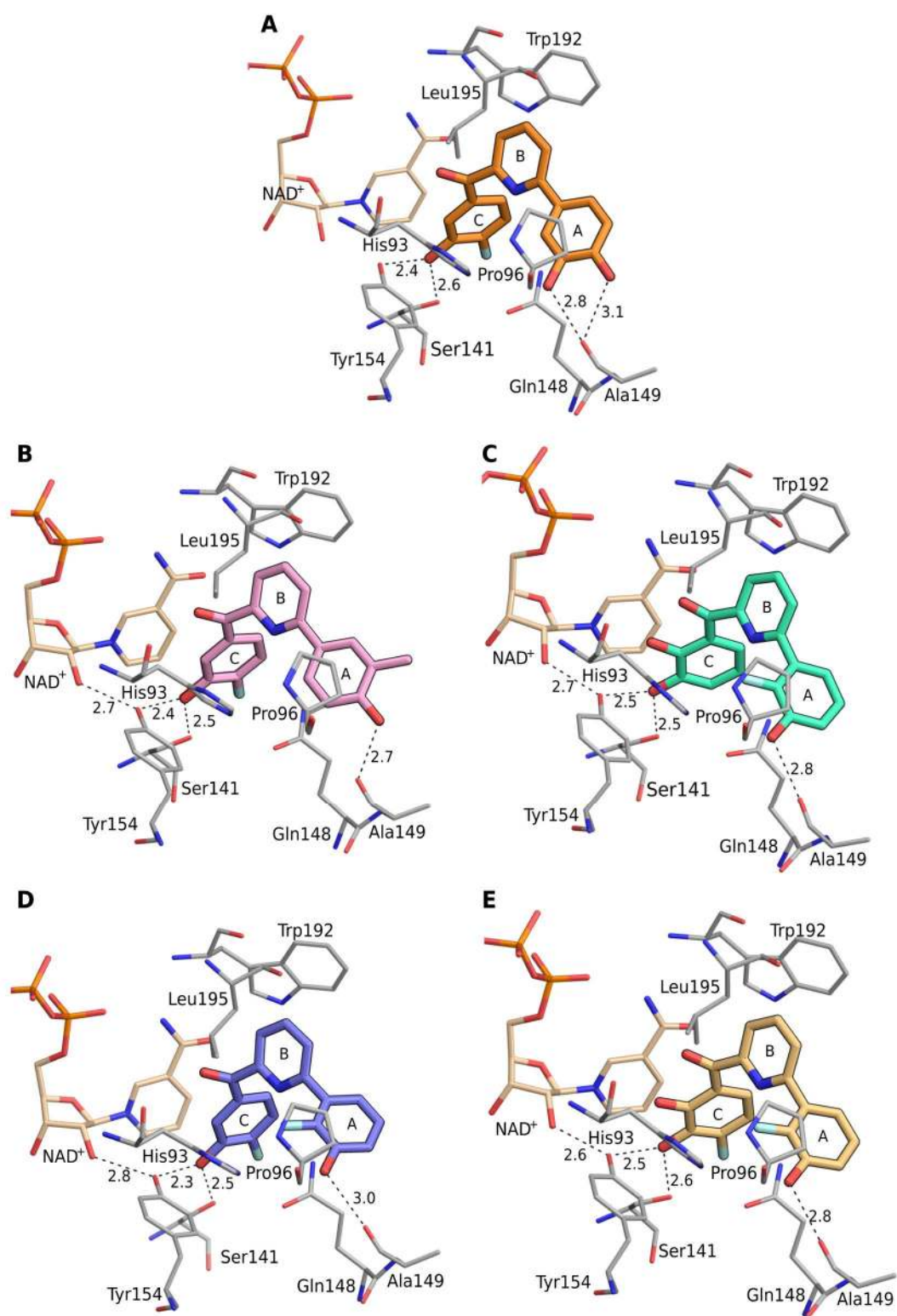


Figure 3.6: Crystal structures of 17 β -HSD14 in complex with cofactor NAD⁺, and inhibitors **3.1** (in orange, **A**), **3.6** (in pink, **B**), **3.12** (in green, **C**), **3.9** (in purple blue, **D**) and **3.10** (in ocher, **E**). The inhibitors are shown as stick models. The amino acids, within a distance of 5 Å, and the cofactor are shown as thin lines. H-bonds are depicted as dotted lines. Distances are given in Å.

the amino acid Pro96. In summary for the inhibitor with this A-ring orientation, circa 80 van der Waals contacts are observed with about 93.0 % of its surface buried in the protein binding pocket (considering only one protein monomer, the ligand achieves 80 van der Waals contacts and its surface is buried to 88.2 %).

Interestingly, the crystal structure of **3.9** in ternary complex with 17 β -HSD14 shows the presence of a second inhibitor molecule at the interface between two tetramers (Figure 3.7 A). Close inspection of this interface binding site (Figure 3.7 B) highlights that the inhibitor is stabilized through an H-bond interaction between the 3-OH group at the A-ring to the hydroxyl group of the Ser44 side chain ($d= 3.2$ Å) and with a water molecule W405 ($d= 2.6$ Å), which is stabilized by Arg19 ($d= 3.0$ Å). The keto group interacts with the other tetramer through a water molecule W434 ($d= 2.7$ Å), which is also bound to the NH from the backbone of Leu83' ($d= 3.0$ Å) and the carbonyl group of the backbone of Tyr128' ($d= 2.9$ Å). The copy of **3.9** binding to the interface is placed in a rather hydrophilic environment. The overall geometry of the interface ligand differs from that of the active site ligand: The dihedral angles, for the ligand in the active site and for the ligand binding at the interface, between the keto group and C-ring are -29° and 4° respectively, and between the keto group and the B-ring are 129° and -133° respectively (considering the plane through the keto group as 0°). The dihedral angle between C_2 at the A-ring and the nitrogen at the B-ring is 131° for the ligand in the binding pocket and -60° for the ligand present at the interface. A superimposition of the interface and active site compounds can be seen on Figure 3.8.

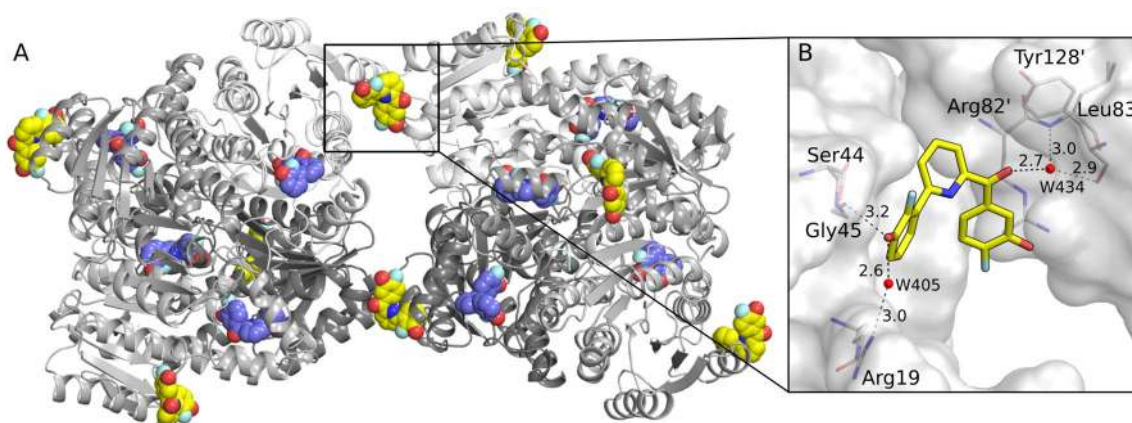


Figure 3.7: (A) Overall view of the crystal structure of two 17 β -HSD14 tetramers in complex with **3.9**. The protein monomers are shown as ribbon models and colored in gray. The inhibitors are shown as sphere models. The inhibitors located in the substrate binding site are colored in purple blue while the inhibitors located between the interfaces of the tetramers are shown in yellow. (B) Close-up view of the second ligand binding site of **3.9** located at the interface between two tetramers. The enzyme is displayed by use of the solvent accessible surface. Inhibitor **3.9** is shown as stick model. The amino acids are shown as thin lines. The amino acids of the symmetry equivalent molecule are referred to prime ('). H-bonds are depicted as black dotted lines. Distances are given in Å.

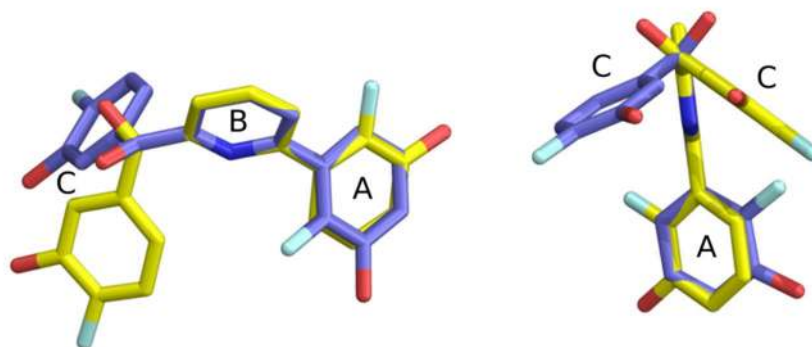


Figure 3.8: Superimposition of compound **3.9** based on the pyridine B-rings of the ligand at the interface (in yellow) and active site (in purple blue).

3.2.15 MOE models

The inhibitors **3.16a**, **3.17**, **3.23**, **3.30** and **3.31** were modeled inside the crystal structure of **3.12** and minimized with MOE [173]. During the minimization, the protein and the C-ring of the ligands were fixed with the exception of **3.16a** where the full ligand was set free to move. The resulting modeled compounds are shown in Figure 3.9.

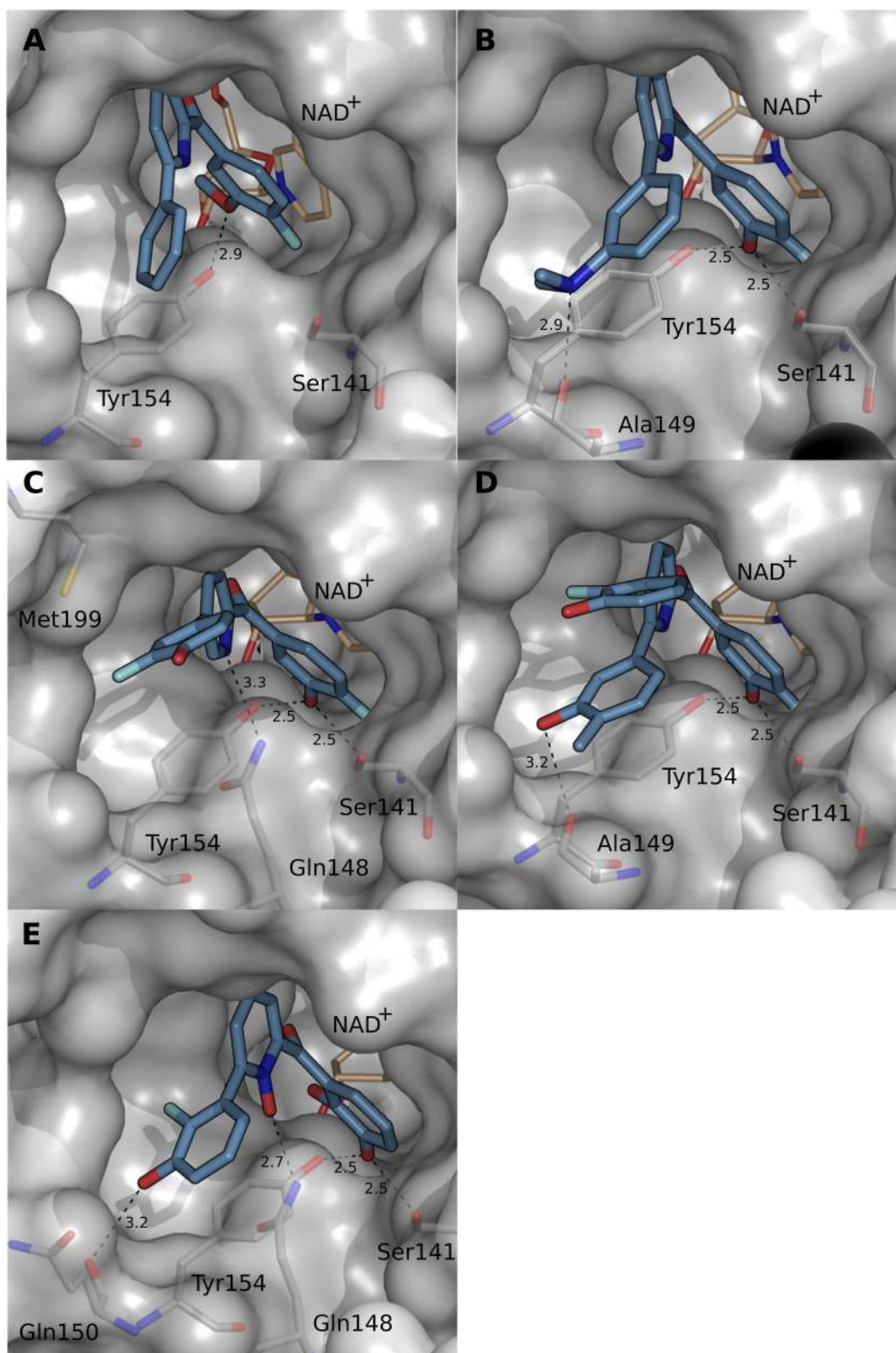


Figure 3.9: Modeled structures of 17 β -HSD14 in complex with inhibitor **3.16a** (A), **3.17** (B), **3.23** (C), **3.31** (D) and **3.30** (E). The protein is displayed by use of the solvent accessible surface. The inhibitors are shown as stick models and their C atoms are colored in light blue. The amino acids, within a distance of 3.5 Å, and cofactor are shown as thin lines. H-bonds are depicted as black dotted lines. Distances are given in Å.

3.2.16 Thermal shift assay

The influence of different ligands on 17 β -HSD14 stability was also tested. 2.5% DMSO solution in the buffer was used as control and a T_m of 56 °C was obtained (Table 3.9). A strong positive shift was recorded upon addition of our inhibitors ($\Delta T_m=11.5-15.0^\circ\text{C}$), indicating that the inhibitors have a strong affinity for the protein resulting in a strong stabilizing effect [116, 118].

Table 3.9: Effect of different ligands on the T_m of 17 β -HSD14 (2.6 μM).

	T_m in °C
DMSO 2.5%	56.0
Compound 3.1 0.25 mM	70.5
Compound 3.6 0.25 mM	67.5
Compound 3.9 0.25 mM	71.0
Compound 3.12 0.25 mM	70.5

3.2.17 Comparison of the 17 β -HSD1, 17 β -HSD2 and 17 β -HSD14 structures

The existing crystal structure of 17 β -HSD1 in ternary complex with the cofactor NADP⁺ and E2 (PDB code: 1FDT) allows the direct comparison with the 17 β -HSD14 structure in complex with the cofactor NAD⁺ and estrone (E1, PDB code: 5HS6). The superimposition reveals a structural conservation of the enzymes only in some regions (22% of sequence identity calculated with COOT [171], Figure 3.10). Small differences in the NAD⁺/NADP⁺ binding site can be observed between type 14 and type 1 (RMSD of 1.6 Å calculated with COOT [171] based on Ca alignment). This result was expected since both enzymes bind a different cofactor (NAD⁺ for 17 β -HSD14 vs NADP⁺ for 17 β -HSD1). The flexible loop in 17 β -HSD1 restricts the end of the binding cavity, while the corresponding loop in 17 β -HSD14 is shifted upwards leaving the binding site widely open. This results in a smaller binding pocket for the type 1 enzyme. Furthermore, while the catalytic triad is conserved in both enzymes, the steroids accommodate in the binding sites with different orientations and achieve distinct interactions.

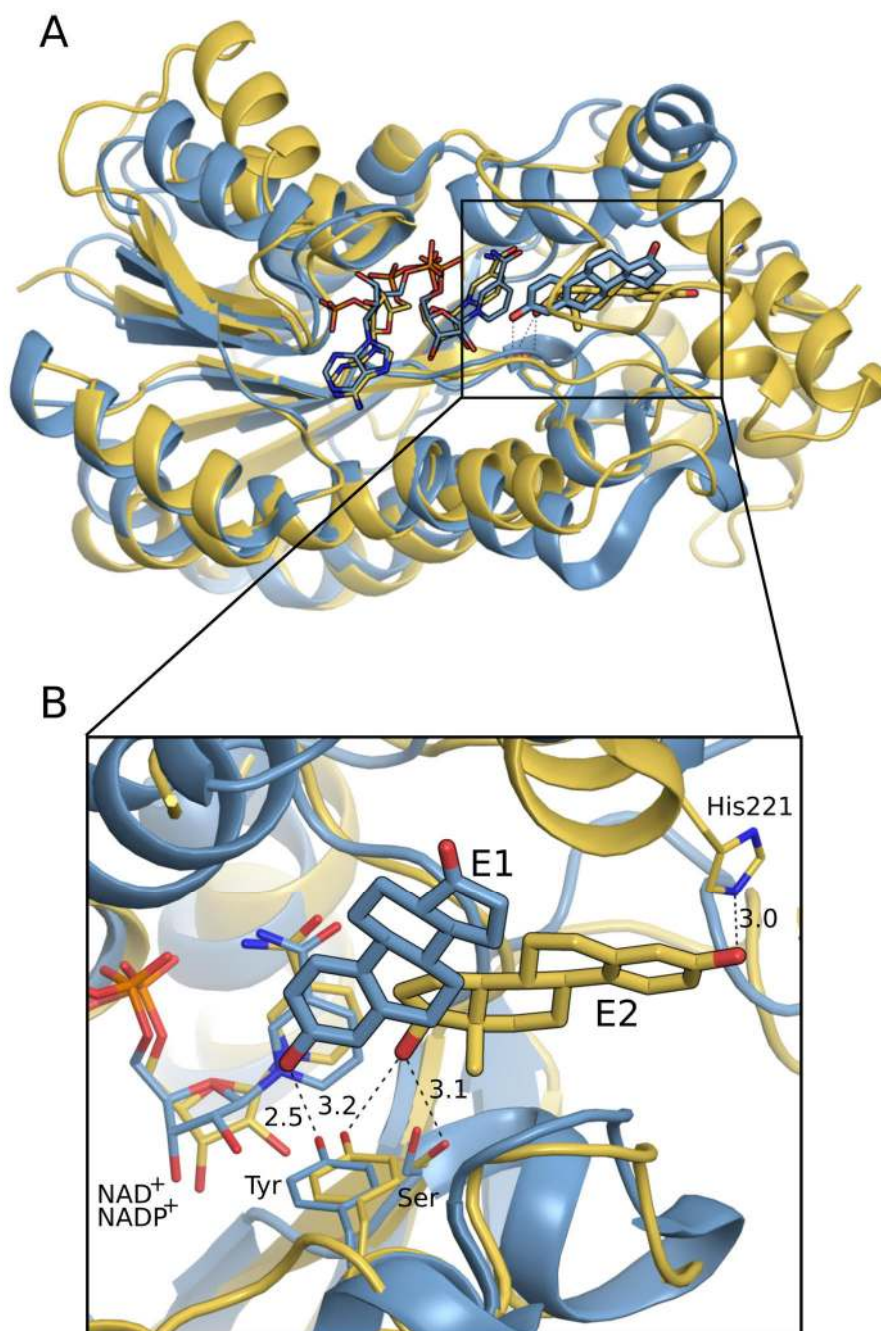


Figure 3.10: (A) Superimposition of 17 β -HSD1 (yellow, PDB code: 1FDT) and 17 β -HSD14 (light blue, PDB code: 5HS6) structures as ternary complexes. (B) Close-up view of the superimposed substrate binding pocket. The proteins are shown as ribbon model. The steroids are shown as stick models. The amino acids, involved in binding of the steroids (Tyr154 for 17 β -HSD14; Tyr155, Ser142 and His 221 for 17 β -HSD1), and the cofactors are shown as thin lines. The carbon atoms of E1 in complex with 17 β -HSD14 are colored in light blue and the carbon atoms of (E2) in complex with 17 β -HSD1 are colored in yellow. H-bonds are depicted as black dotted lines. Distances are given in Å.

3.2.18 Selectivity

Taking into account that the parent scaffold of the new 17 β -HSD14 inhibitors was derived from 17 β -HSD1 and 17 β -HSD2 inhibitors, it was of utmost importance to study their selectivity profile with respect to 17 β -HSD1 and 17 β -HSD2 binding.

The 17 β -HSD1 and 17 β -HSD2 inhibition assay was performed using a radioactive assay, quantifying the amount of [³H]-labeled E2 (for type 1) and [³H]-labeled E1 (for type 2) formed after incubation with protein, cofactor and the inhibitor as previously described [174]. The results are shown in Table 3.10, expressed as percent inhibition when tested at an inhibitor concentration of 1 μ M.

As expected the 2,5-pyridine **3.23** showed the highest affinity for 17 β -HSD1 (47% inhibition) compared to the 2,6-pyridines (**3.6-3.20**, 9-23% inhibition), which were all nearly inactive in 17 β -HSD1.

Inhibition of 17 β -HSD2 was slightly higher than that of 17 β -HSD1 for the compounds with a 2,6-substitution pattern (between 30% and 62% inhibition at 1 μ M concentration for **3.6-3.20**) and much higher for the 2,5-pyridine ketones (64% and 85% when tested at 1 μ M concentration for **3.23** and **3.2**, respectively).

A direct comparison of the 17 β -HSD1 and 17 β -HSD2 inhibitory activities with those of 17 β -HSD14 is however problematic as different conditions were used in the assays.

However, under the applied condition in the 17 β -HSD2 inhibition assay, using the Cheng-Prusoff equation for competitive inhibition, a calculated K_i (cK_i) could be estimated: For a compound with an IC_{50} of around 1 μ M (50% inhibition at 1 μ M) a cK_i of about 450 nM was expected (with K_m 17 β -HSD2 = 400 nM in this assay [175] and $[S] = 500$ nM).

With 48% and 43% inhibition of 17 β -HSD2, compounds **3.9** and **3.10** showed a $cK_i \geq 450$ nM. Comparison of their K_i values for 17 β -HSD2 and 17 β -HSD14 binding allowed to calculate a selectivity factor (ratio of $K_{i(HSD2)}/K_{i(HSD14)}$), which could be estimated to be around 35 for **9** and ≥ 41 for **3.10**. Compounds **3.9** and **3.10** are relatively selective 17 β -HSD14 inhibitors. The selectivity profile of **3.12** toward 17 β -HSD2 (with only 30% inhibition at 1 μ M) should be even better.

Table 3.10: 17 β -HSD14 binding constant (K_i) and 17 β -HSD1/ 17 β -HSD2 inhibitory activities (% inhibition) of the most interesting compounds.

Compound	17 β -HSD14 K_i (nM) ^a	17 β -HSD1 % inhibition @ 1 μ M ^b	17 β -HSD2 % inhibition @ 1 μ M ^c
3.2	24 \pm 9	47%	85%
3.5	245 \pm 21	6%	85%
3.6	26 \pm 3	9%	62%
3.9	13 \pm 5	23%	43%
3.10	11 \pm 3	12%	48%
3.12	64 \pm 4	13%	30%
3.18	7 \pm 2	13%	34%
3.20	47 \pm 7	14%	37%
3.23	17 \pm 5	47%	64%

^a Recombinant purified 17 β -HSD14 enzyme, fluorimetric assay, substrate E2 [32 μ M], NAD⁺ [1.2 mM], 25°C, mean value of at least two independent experiments each with three technical repeats.

^b Placental 17 β -HSD1 enzyme, cytosolic fraction, substrate [³H]-E1 + E1 [500 nM], NADH [0.5 mM], mean value of 2 determinations; standard deviation < 20 %.

^c Placental 17 β -HSD2 enzyme, microsomal fraction, substrate [³H]-E2 + E2 [500 nM], NAD⁺ [1.5 mM], mean value of 2 determinations; standard deviation < 20 %

As steroidomimetics, the synthesized compounds might show undesired binding affinity to the estrogen receptors (ERs) α and β . Wetzl *et al.* reported that the most interesting compounds 3.2-3.5, identified in the first screen, showed very low affinities to both ER subtypes (< 0.1 %, taking E2 as 100% reference) [176]. It is therefore to expect, that the synthesized compounds, which bear the same scaffold, do not bind tightly to the ERs.

3.3 Discussion

The combination of the biological results, the crystal structures of the five ligands in ternary complex with the protein and the physicochemical properties provide the basis for the understanding of the structure-activity relationship of the 2,5- and 2,6-substituted pyridine derivatives.

3.3.1 Focus on the C-ring part

The 3-OH group at the C-ring achieves important H-bond interactions with Tyr154 and Ser141, which stabilizes the inhibitor in the enzyme binding site. The increase in acidity of this OH moiety, enhanced by the addition of a fluorine atom in *ortho* position to the OH group, correlates with a gain in binding affinity. The crystal structures indicate that the H-bond length between the 3-OH group at the C-ring and Tyr154 is rather short ($d = 2.3 - 2.5$

Å). This result supports the hypothesis of Hwang *et al.* [177] which describes that in SDR enzymes, the pKa of the OH group from the catalytic tyrosine is decreased (through electrostatic interaction with the protonated catalytic Lys-NH₃⁺ and NAD⁺) and that this Tyr-OH is present as deprotonated species in the active site. In our structures, the negatively charged (or at least highly polarized) Tyr154-O⁻ can interact via H-bond interactions with 3-OH groups at the C-ring of the inhibitors, leading to a strong contact between the inhibitor and the protein. This interaction becomes even more stable in presence of an increasingly acidic OH group at 3-position, once it is more strongly polarized O(δ⁻)-H(δ⁺).

In addition, it can be seen in the crystal structures that the inhibitors are involved in a more complex H-bonding network via the interaction with Tyr154, also including the ribose-OH groups of the cofactor, Lys158, Asn88, Asn89 and two to three water molecules (Figure 3.11). The highlighted H-bonding network reinforces the strength of the interaction between Tyr154 and the OH group at the C-ring of the inhibitor,[178] thereby strongly stabilizing the ligand in the binding pocket.

The H-bond donor/acceptor profile involved in the interaction between the 3-OH group at the C-ring and Tyr154/Ser141 can be interpreted in more details: A deprotonated Tyr154 implies that the 3-OH group at the C-ring of the inhibitor interacts with Tyr154-O⁻ as H-bond donor and with the hydroxyl group of Ser141 as H-bond acceptor. For the inhibitors

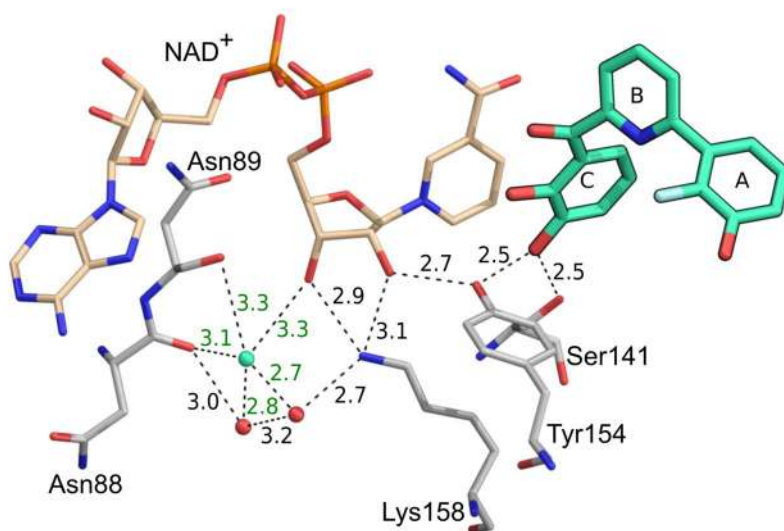


Figure 3.11: H-bonding network stabilizing the inhibitor **3.12** in the 17β-HSD14 binding site. The carbon atoms of **3.12** are colored in green and shown as stick model. The amino acids, involved in the H-bonding network, and the cofactor NAD⁺ (beige) are shown as thin lines. H-bond interactions are depicted as dotted lines. Distances are given in Å. Water molecules are shown as spheres. The water molecules present in all protein-inhibitor complex structures are colored in red, an additional water molecule is visible in the case of the complexes with **3.1** and **3.12** (higher resolution crystal structures) and is colored in green.

also bearing a 2-OH group at the C-ring moiety, an intramolecular H-bond with their keto groups can be formed and no interaction with Tyr154 is expected (the OH group of Tyr 154 is already involved in a contact with the ribose-OH and the 3-OH group at the C-ring inhibitor, and is not available for an additional interaction). In addition, it can be remarked that the rigidification induced by the intramolecular H-bond does not correlate with an increase in binding affinity (comparison of compounds **3.9** and **3.10**).

Replacing the 3-OH group at the C-ring by a 3-OMe moiety was shown to be detrimental for inhibitory activity (**3.16a**: no inhibition @100 μ M compared to **3.16**: K_i = 63 nM). When compound **16a** was modeled into the crystal structure of 17 β -HSD14 (Figure 3.9 A), it resulted in a shift of the binding pose (compared to the compounds observed in the crystal structures, see Figure 3.6), which could allow an H-bond interaction between the oxygen of the 3-OMe group and the OH group of Tyr154 of the catalytic triad, however, the H-bond contact is only possible when the 3-OMe group acts as an acceptor (Figure 3.9 A). The inactivity of this compound confirms the hypothesis that an H-bond donor in 3-position of the C-ring is necessary for the inhibitory activity of the compound. In addition, no interaction with Ser141 could be observed in the presence of the 3-OMe group in the model structure.

3.3.2 Focus on the A-ring part

Based on the biological results, it is evident that the removal of the A-ring leads to a strong decrease in activity (**3.16**, K_i = 63 nM compared to **3.24** K_i = 1541 nM), indicating an important interaction of the A-ring with the protein. The crystal structures show that no amino acid is able to achieve a π -stacking interaction in the vicinity of the aromatic A-ring. This result suggests that the aromatic A-ring must be stabilized by hydrophobic interactions with Pro96.

Furthermore, it can be observed that the introduction of a 3-OH or 4-OH group on the A-ring induces a slight increase in affinity compared to the unsubstituted A-ring. Either these hydroxyl moieties interact with the carbonyl backbone of Ala149 via a weak H-bond interaction or the benefit of a strong interaction with Ala149 is decreased by the desolvation cost. It is also striking that neither an electron donating nor an electron withdrawing group has an influence on the potency.

The significant affinity enhancement of the dimethylamino derivative **3.17** was investigated using the modeled structure (Figure 3.9 B). Here, the NMe₂ moiety comes into close contact with the carbonyl group of Ala149. A strong interaction would only be possible between the NMe₂ group and the carbonyl oxygen when the tertiary amine is protonated. However, taking into account the pK_a value of the NMe₂ group it is unlikely that this group is charged.

The gain in affinity might come from additional hydrophobic interactions between the latter group and Pro96.

In the complex structure with **3.6** the 3-Me group at the A-ring interacts neither with the protein nor with the solvent. Instead, it is pointing toward an empty cavity, while the 3-OH group of **3.12** is oriented in the opposite direction interacting with Ala149. The swapped orientation of the 3-Me group at the A-ring of **3.6** might result from electrostatic repulsions between the methyl group and the carbonyl moiety of Ala149.

Regarding the almost equipotent 2,5-substituted (**3.23**, $K_i = 17$ nM) and the 2,6-substituted derivative (**3.8**, $K_i = 36$ nM), it was previously suggested, that the C-rings of both compounds achieve the same interaction and that the space available for accommodating the A-ring at either 5- or 6-position must be large to host a ring at both positions. From the modeled structure of **3.23** (Figure 3.9 C), it can be assumed that the A-ring in 5-position fits well into the binding pocket, interacting through hydrophobic contacts with Met199. Furthermore, the modeled 2,5,6-trisubstituted derivative **3.31** ($K_i = 9$ nM) also suggests that compounds bearing rings at 5- and 6-position can fit in the cavity and may achieve an intramolecular π -stacking interaction ($d = 4$ Å, Figure 3.9 D).

3.3.3 Focus on the B-ring part

Investigating the importance of the nitrogen at the B-ring indicates that inhibitor **3.12** ($K_i = 64$ nM) and its phenyl analogue **3.29** ($K_i = 21$ nM) show similar affinities. Obviously, the nitrogen does not achieve any specific interaction with the protein, as confirmed by the crystal structure. However, the pyridine moiety enhances the solubility for the compounds of this inhibitor class. Concerning the *N*-oxide derivative **3.30** ($K_i = 132$ nM), the previously observed interaction between the 3-OH group at the A-ring of compound **3.12** with Ala149 can no longer be accomplished, however, this OH-group can now address the backbone carbonyl group of Gln150, as suggested by the modeled structure (Figure 3.9 E). An additional H-bond interaction of N^+-O^- with Gln148 could be gained, but the high desolvation penalty induced by the introduction of the charges might not be compensated, overall resulting in no increase in affinity.

3.3.4 Second binding site for compound 3.9

For compound **3.9**, a second binding pose at the tetramer interface was observed. The inhibitor was refined to occupancy of 80% at this additional binding site, suggesting that this ligand exhibits a lower affinity for this region compared to the active site. The binding of the inhibitor in this position might be irrelevant for the inhibitory process, while it might be an

artefact resulting from crystal packing as the binding at the interface does not induce any conformational changes of the ternary structure and of the ligand binding site. However, it is striking that Michiels *et al.* [179] reported in their NMR studies that phytoestrogens might also bind at the dimer interface of 17 β -HSD1.

3.3.5 Comparison of the 17 β -HSD1, 17 β -HSD2 and 17 β -HSD14 structures

A positive influence of a fluorine atom in ortho position to a phenolic hydroxyl group was already reported during the development of 17 β -HSD1 dihydroxyphenylthiophenes inhibitors [150] and 17 β -HSD2 hydroxyphenyl-*N*-methylsulfonamide thiophenes inhibitors [89]. As no crystal structures of 17 β -HSD1 and 17 β -HSD2 in complex with these nonsteroidal compounds are available, their binding modes remain unclear. As 17 β -HSD type 1, type 2 and type 14 belong to the SDR superfamily, they share similarities in the region in the vicinity of the catalytic triad. The presence of the complex H-bonding network was also identified in the type 1 enzyme after analysis of its crystal structure (PDB code: 1FDT). It could be expected that the 17 β -HSD1 and 17 β -HSD2 inhibitors with an acidic OH-phenyl group have a similar binding mode, interacting with the catalytic triad as observed in the crystal structure of type 14. Therefore, these new 17 β -HSD14 structures in complex with nonsteroidal inhibitors can represent a useful comparative data for 17 β -HSD1 docking studies and 17 β -HSD2 homology modelling.

3.3.6 Basis for structure-based drug design

Based on these results, it should be possible to optimize the current ligands using structure-based drug design. In this compound class the interactions with the catalytic Tyr154 and Ser141, as well as with Ala149 are very important to anchor the ligand scaffold in the correct position. Specific interactions involving His93 and Gln148 in inhibitor binding should result in an improved activity and selectivity, particularly as His93 is not present in other human SDR 17 β -HSDs. Addressing the water molecule W1 should also lead to an additional interaction with the protein. As the active site is open and solvent exposed, the polar amino acids which are in close neighborhood to the active site next to the surface could also be targeted by specific interactions.

3.4 Conclusion

Nonsteroidal 17 β -HSD14 inhibitors have been identified. The initial hits identified in a preliminary screen in the 2,6-substituted pyridine class showed a K_i around 250 nM/300 nM

which was optimized to result in six highly active compounds with $K_i < 15$ nM and two with a K_i of 7 nM. The considerations of substituent effects applied during optimization were successful. It appears that at the C-ring, an acidic 3-OH group is essential to achieve high potency, interacting via strong H-bond contacts to Tyr154 and Ser141 thereby stabilizing the interaction through an extensive H-bonding network. The structure-activity relationship found for the A-ring shows, that a 3-OH or a 4-OH group increases the potency of the inhibition by interacting with Ala149. The crystal structures in complex with the inhibitors confirm the rather large active site, reduced by the C-terminal chain from an adjacent monomer. The new 17 β -HSD14 inhibitors show good physicochemical properties, which should be associated with a good bioavailability profile. They also present a good selectivity profile toward both closely related subtypes 17 β -HSD1 and 17 β -HSD2. The determined crystal structures give important insights not only to characterize the novel protein target but also to understand the binding poses of these nonsteroidal inhibitors and provide the basis for their further structure-based optimization.

3.5 Experimental section

3.5.1 17 β -HSD14 inhibition assay

In a preliminary study compounds 3.1-3.5 were tested using a radioactive displacement assay (Procedure A, % of inhibition at a concentration of 1 μ M). The newly synthesized compounds were tested using a fluorimetric assay (Procedure B, as percent inhibition at 2 μ M, percent inhibition at the concentration of highest solubility of the compound and K_i). Procedure A and B use the same enzyme source, obtained from a bacterial culture. In procedure A, the assay is performed with a bacterial suspension, and in procedure B with the purified form of the enzyme. Due to differences in assay conditions only results within the same assay can be compared.

3.5.2 Enzyme expression

The pET based plasmid containing the coding sequences of the human gene HSD17B14 (using the T205 variant), with a *N*-terminal 6His-tag and a TEV (Tobacco Etch Virus) protease cleavage site was used for the transfection of *E. coli* BL21 (DE3) pLysS competent cells. The transformed bacteria cells were grown overnight in 100 mL of Terrific Broth medium containing 100 μ g/mL of ampicillin at 37°C. Subsequently, 25 mL of the overnight culture were transferred in 1 L of the aforementioned medium and allowed to grow at 37 °C until an OD₆₀₀ of 0.4 was reached. Then the temperature was lowered to 15° C. When the culture reached the OD₆₀₀ of 1.0 the cells were induced with 0.5 mM of IPTG. The bacteria

cells were harvested by centrifugation and conserved at -80° C overnight before proceeding with the purification.

3.5.3 Radioactive assay using Procedure A

The bacterial pellet obtained was resuspended in 100 mM phosphate buffer pH 7.7. The bacterial suspension was incubated with [³H]-E2 (final concentration: 18.3 nM) in the presence of the potential inhibitor in DMSO (final concentration in assay: 1 μ M, final DMSO concentration: 1%) at 37°C. The enzymatic reaction was started by addition of NAD⁺ (7.5 mM) and incubated for 2 h. The reaction was stopped by addition of 0.21 M ascorbic acid in a methanol/acetic acid mixture (99:1, v/v). Substrate and product were extracted from the reaction mixture by SPE (Strata C18-E columns from Phenomenex on a vacuum device). Separation and quantification of the radioactive steroids was performed with HPLC (Luna 5 μ m C18(2), 125 x 4.00 mm from Phenomenex, with an acetonitrile/water mixture (43:57, v.v), flow rate 1mL/min). Substrate conversion in % was calculated after integration of the product and substrate peaks. Inhibition was calculated based on conversion without potential inhibitor (DMSO only) which was set to 0% inhibition.

3.5.4 Enzyme Purification

The cell pellet, previously obtained after IPTG induction, was resuspended in a buffer containing 50 mM Tris, 500 mM NaCl, 0.5 mM TCEP, 250 mM glucose, 1 mM NAD⁺, 0.5% (v/v) Triton X-100 and cOmplet Protease Inhibitor Cocktail Tablet (Roche, Germany) adjusted at a pH of 8. The cells were disrupted with a high pressure homogenizer (EmulsiFlex-C5™, AVESTIN, Mannheim, Germany) and the obtained homogenate was centrifuged at 17700 g for 2h at 4°C. The supernatant was applied to a Ni-NTA column (5 mL HisTrap FF, GE Healthcare Life Sciences, Freiburg, Germany). Two washing steps were applied: in the first, to remove the DNA, a buffer composed of 50 mM Tris and 1.5 M NaCl was run against the Ni-column. The second washing step was then performed with a buffer containing 50 mM Tris, 500 mM NaCl, 0.5 mM TCEP, 250 mM glucose, 0.25 mM NAD⁺ and 21 mM imidazole to remove the unspecific binding proteins. The target protein was eluted by increasing the imidazole concentration in the buffer to 300 mM. TEV protease was added to the protein mixture to cleave the N-6His-tag and the product solution was dialyzed overnight at 4°C to reduce the imidazole concentration in the sample (50 mM Tris, 500 mM NaCl, 0.5 mM TCEP, 250 mM glucose and 0.25 mM NAD⁺). A second Ni-NTA column was used for separation of the TEV protease from the 17 β -HSD14. In this step the protein was collected from the flow through of the column, while the TEV protease remained on the column. With the goal to increase the purity of the protein, an additional purification step, using a size

exclusion chromatography (Superdex 75 26/60, GE Healthcare Life Sciences, Freiburg, Germany) was performed with a running buffer comprising 50 mM Tris, 500 mM NaCl, 0.5 mM TCEP and 250 mM glucose. To the isolated target protein, an NAD⁺ solution 0.25 mM (batch for enzymatic assay) or 0.6 mM (batch for crystallization studies) was added. The protein solution was flash-frozen in liquid nitrogen and stored at -80°C.

3.5.5 Fluorimetric assay using Procedure B

The potential inhibitor (in DMSO, final DMSO concentration in assay: 1%) was added to a mixture of NAD⁺ (1.2 mM) and E2 (32 μM) in 100 mM phosphate buffer pH 8. The enzymatic reaction was started by addition of the purified enzyme (1 mg/ml) and the production of the fluorescent NADH formed was measured continuously for 15 min at 25°C. The fluorimetric assays were recorded on a Tecan Sapphire 2 (λ_{ex} at 340 nm and λ_{em} at 496 nm). The slit width for excitation was 7 nm and for emission 15 nm. Reactions were performed in 200 μL volumes. The assay was run in 96 well-plates in duplicate, each experiment resulting from three technical repeats. A linear relationship between product formation and reaction time was obtained. The slope of the progress curves was calculated by linear regression. The inhibitors do not show fluorescence at the concentrations used in the assay.

The K_i values were calculated using the Morrison equation [167]. For calculation, three constants were necessary: the substrate concentration (32 μM), the K_m for 17β-HSD14 with this substrate E2 (6.18 μM [126]) and the concentration in active protein, which was determined experimentally for each experiment (3.2 or 3.3 μM), using the procedure detailed by Copeland [167]. The fitting and data analysis was performed using GraphPad Prism 7.

3.5.6 Protein co-crystallization with inhibitors 3.1, 3.6, 3.9, 3.10, 3.12

Protein activity was verified before performing the crystallization studies for each inhibitor. The co-crystallization of 17β-HSD14 in complex with the four inhibitors 3.1, 3.6, 3.9, 3.10 and 3.12 was performed by sitting drop vapor diffusion technique.

For the crystallization of inhibitors 3.6 and 3.9 in complex with the protein an inhibitor stock solution in pure DMSO was added to the protein solution (9.5 mg/mL) containing 0.6 mM NAD⁺ with a final inhibitor concentration of 0.8 mM and a DMSO concentration of 1%. 2 μL of the mother liquor containing 0.1 M CHES, 1 M tri-sodium citrate, pH 9.5, was mixed with 2 μL of the protein solution. After growing for 4 weeks at 18°C, the crystals were exposed to a cryo buffer composed of the mother liquor with the addition of 20% (w/v) glucose and 0.4 mM of either 3.6 or 3.9, and subsequently flash-frozen in liquid nitrogen.

The inhibitors **3.1**, **3.10** and **3.12** were crystallized under different conditions. The same concentration of the protein containing 0.6 mM of NAD⁺, was mixed with inhibitor and DMSO, to the final concentration of 4 mM of inhibitor and 5% DMSO. Afterwards, 2 μ L of this protein-inhibitor solution were mixed with 2 μ L of mother liquor composed of 0.1 M HEPES, 20% (w/v) PEG6000 and 5% (v/v) DMSO, adjusted to pH 7.0. Crystals were grown at a temperature of 18°C for four weeks. The crystals obtained with **3.10** were exposed to a cryo buffer obtained by the combination of mother liquor with the addition of 20% glucose and successively flash-frozen with liquid nitrogen. The crystals resulting from the complex with **3.12** were kept at room temperature.

3.5.7 Data collection and processing

The data for the protein-inhibitor complex structure containing **3.1** (PDB code: 5ICM) and **3.10** (PDB code: 5L7W) were collected at Elettra Sincrotrone at beamline XRD1 in Trieste, Italy. The data collection was achieved at a wavelength of 1Å and a temperature of 100 K on a DECTRIS Pilatus 2M pixel detector. The diffraction data of **3.6** and **3.9**, were obtained at beamline P13 at a wavelength of 0.8 Å and a temperature of 100 K (PDB code: 5L7T and PDB code: 5L7Y, respectively) and **3.12** at beamline P14 at a wavelength of 0.9763 Å and a temperature of 291 K (PDB code: 5EN4) at PETRA III (EMBL/DESY) in Hamburg, Germany, on a silicon Pilatus 6M pixel detector. All datasets were indexed, processed and scaled with XDS [142].

3.5.8 Structure determination and refinement

The structures were determined by molecular replacement with the program PHASER MR [143] from the CCP4 suite [132]. The structure 5EN4 was determined using 1YDE [32] as starting point for the molecular replacement search. For the remaining structures, 5EN4 was used as a search model. A subset that corresponds to 5% of the reflections was used for the calculation of R_{free} and consequently was omitted from the refinement. The model was built in Coot [171] and refined using PHENIX.refine version 1.10.1-2155 [145]. The ligands were energetically minimized and their restraints were generated using Grade Web Server [147] and eLBOW [145] based on the SMILES codes obtained with Molinspiration v2014.11 [146]. As first refinement step, for all the structures, a Cartesian simulated annealing was performed using default parameters. The final models were built in Coot with alternating structural modification and refinement of XYZ coordinates, occupancies and individual B-factors in Phenix. With exception of 5L7T, hydrogens were included in the models of the structures. For 5EN4, the temperature factors of all atoms, except hydrogen atoms and solvent

molecules, were refined anisotropically. For 5L7W and 5ICM, TLS refinement was performed with TLS groups selected from the TLSMD web server [148, 149]. For 5L7T and 5L7Y, the temperature factors were refined isotropically.

Hydrogen bonds and van der Waals contacts between the protein 17 β -HSD14 and the inhibitors were assigned with the aid of the program CONTACTSYM [180, 181]. The buried surfaces of the inhibitors in the binding pocket were calculated using the program MS [182, 183].

3.5.9 Thermal shift Assay (TSA)

The thermal shift assay was conducted in a 96 wells PCR plate (Bio-Rad, Munich, Germany) using a real-time PCR instrument (iCycler5, Bio-Rad, Munich, Germany). The running buffer was obtained by the dilution (1:1000) of SYPRO orange dye (Invitrogen, ThermoFisher Life Technologies, Darmstadt, Germany) in a buffer composed of 50 mM Tris, 0.5 M NaCl and 0.5 mM TCEP, pH 8.0. For the protein complexes, a concentration of 2.5% of DMSO (reference measurement) or a stock solution in pure DMSO of compound **3.2**, estrone, or estradiol was added to the running buffer containing 250 mM glucose and 0.25 mM NAD⁺ (final ligand concentration of 0.25 mM and final DMSO concentration of 2.5%). A protein concentration of 2.6 μ M was used (3 μ L) and the different solutions were added to a final volume of 40 μ L.

Chapter 4

Structure-Based Design of 17 β -HSD14 Inhibitors

Introductory remarks

The following chapter is part of a manuscript in preparation. Fluorescence-based assays were designed and performed by Dr. Sandrine Marchais-Oberwinkler in collaboration with Florian Braun. The synthesis of the compounds, their characterization and the Pgp efflux pumps assay were carried out by Florian Braun. The expression and the purification of the 17 β -HSD14, the crystallization studies and the elucidation of the crystal structures of the protein-inhibitor complexes were established and performed by the author of this thesis. The selectivity assay was done by Dr. Gabriele Möller (Helmholtz Zentrum Munich) and Dr. Martin Frotscher (Saarland University). The cytotoxicity study was performed by Nathalie Guragossian and Prof. Dr. Marc Le Borgne (University of Lyon, France). Furthermore, the author significantly contributed to the discussion and to the writing of the manuscript in collaboration with Florian Braun and Dr. Sandrine Marchais-Oberwinkler.

4.1 Introduction

17 β -hydroxysteroid dehydrogenase type 14 (17 β -HSD14), also known as DHRS10 and retSDR3, is the latest 17 β -HSD enzyme identified and belongs to the Short-chain Dehydrogenase-Reductase (SDR) superfamily [11, 32]. *In vitro*, the enzyme catalyzes the oxidation at the 17 position of two prominent steroid hormones, estradiol (E2) and 5-androsten-3 β ,17 β -diol (5-diol), in presence of the cofactor NAD⁺ thus converting them into their less active analogs, estrone (E1) and dehydroepiandrosterone (DHEA) [32]. However, considering the low turnover of the enzyme for E2 and 5-diol (0.02 and 0.033 min⁻¹, respectively [126]) and their low binding affinity as substrates (about 6 μ M [126]), it is not really clear whether the enzyme is also involved in the steroid regulation *in vivo*.

The enzyme was described by Sivik *et al.* [103] to show a broad distribution across various tissues as evaluated by immunohistochemistry studies, while northern blot analyses demonstrated that the enzyme is predominantly expressed in brain, liver, placenta [32] and kidney [100]. 17 β -HSD14 is a cytosolic enzyme, as highlighted by immunofluorescence studies, and its quaternary structure consists of a homotetramer [32, 126].

The crystal structures of 17 β -HSD14 in complex with NAD⁺ were determined (PDB codes: 5JS6 and 5JSF) and they revealed that the enzyme has a rather lipophilic conical active site, narrow in the proximity of the catalytic triad and is solvent exposed at the other end [126]. In addition, the binding pocket is reduced in size by Tyr253' from an adjacent enzyme monomer in the tetrameric assembly.

The first class of nonsteroidal inhibitors for this enzyme were recently described by us [127]. One of the most promising inhibitor is the compound **3.9** (Figure 4.1) [127]. It is a member of the (6-phenyl)pyridin-2-yl methanone class and it exhibits a high binding affinity to the enzyme ($K_i = 13$ nM). The crystal structure of this inhibitor with the enzyme was elucidated and showed that the inhibitor adopts a conformation with a complementary shape to the substrate binding pocket [127]. It is bound to in the active site via different interactions: The most relevant interactions that the inhibitor achieves are strong H-bond contacts between 3-OH group on the C-ring and the catalytic residues Tyr154 and Ser141. An additional H-bond interaction between the 3-OH group on the A-ring and the Ala149 is also observed. The carbonyl group and the pyridine ring of the inhibitor addresses the hydrophobic pocket formed by Leu191, Trp192 and Leu195 (Figure 4.1).

Goal of this study was the optimization the structure of **3.9** in order to develop an optimal tool compound that could be used to investigate the physiological role of the enzyme *in vivo*. To reach this goal, a structure-based optimization of **3.9** was undertaken to extensively exploit potentially new interactions provided by the enzyme and to therefore improve the binding affinity of the compounds. The newly designed compounds were synthesized, tested

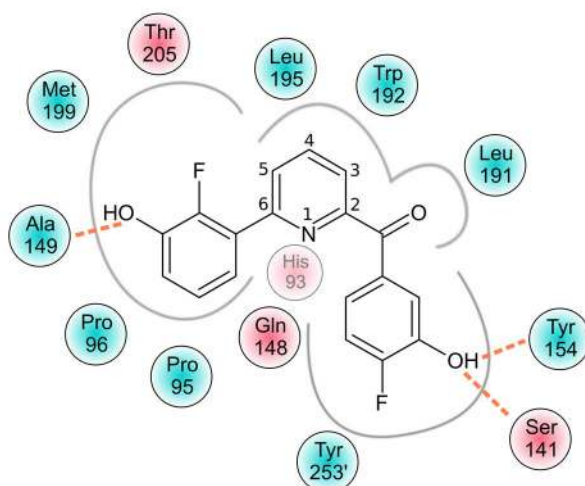


Figure 4.1: Schematic representation of the binding mode of **3.9** in the binding pocket of 17 β -HSD14. Amino acids with polar functional groups are colored in red. Prevalent hydrophobic amino acids are colored in blue. The different pockets formed by the amino acids are highlighted with gray lines. H-bonds are depicted as orange dotted lines.

for 17 β -HSD14 inhibition and for seven of them the crystal structures of the corresponding inhibitor-enzyme complex were determined. The crystal structures were crucial for the better understanding of the structure-activity relationship (SAR) additionally disclosing a shifted binding mode in case of one inhibitor. The profiling of the most potent inhibitors of the series was subsequently initiated. The selectivity towards different 17 β -HSD enzymes along with cytotoxicity and ligand solubility were tested and their *in silico* physicochemical properties were calculated. As 17 β -HSD14 is also present in the brain, it is important that the tool compound is also capable of crossing the blood brain barrier (BBB). The most interesting 17 β -HSD14 inhibitors of our series (selective, no cytotoxic and with promising physicochemical properties) were tested for their ability to pass the BBB. As, Pgp efflux pumps are the most important transporters involved in multiple drug resistance and present in the BBB and liver [184], the behavior of the tool compounds toward these efflux pumps was also investigated and taken into account in order to choose the best tool compounds for follow-up *in vivo* studies.

4.2 Results

4.2.1 Structure design of the new inhibitors

The scaffold of **3.9** was used as a starting point for structure-based modification in order to optimize the geometry of the inhibitor toward higher affinity for 17 β -HSD14 with the intention to identify the key interactions between the individual inhibitors and the protein.

In the (6-phenyl)pyridin-2-yl methanone class, the interaction of the 3-OH group of the C-ring with Tyr154 from the catalytic triad is essential to achieve high inhibitory activity. The increased acidity of the 3-OH function is boosted by the substitution with an adjacent fluorine atom (in *ortho* position to the OH group). This correlates with a significant gain in binding affinity [127], thus, the 3-OH/4-F pattern at the C-ring was maintained during the development process.

In the first optimization strategy (A) we focused on the replacement of the linking carbonyl group of **3.9** (Chart 4.1), acting as a bridge between the B- and C-ring. The crystal structure disclosed that the carbonyl group is important to induce the overall V-shape of the inhibitor scaffold to perfectly match the architecture of the protein's active site (Figure 4.2). Nevertheless, the carbonyl group does not form any direct interaction with any neighboring amino acid of the protein. Therefore, our idea was to investigate the role of this linker by replacing the carbonyl group with polar linker groups such as an ether oxygen, a secondary amine or apolar groups such as a tertiary amine and an ethenyl group. The geometry of the modified scaffold (angle between the B- and C-rings) had to be kept similar to that of **3.9** also leaving the positions of the B- and C-rings virtually unchanged. Furthermore, amide groups were introduced to grow the distance between B- and C-ring and to evaluate the consequences of pushing the pyridine B-ring deeper into the substrate binding site.

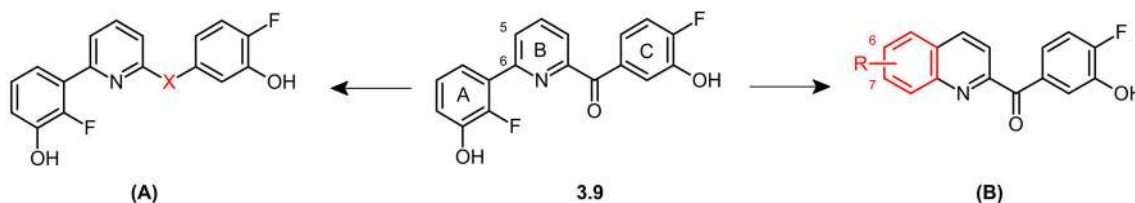


Chart 4.1: Synthetic modifications starting from the 2,6-pyridine ketone **3.9**.

Additionally, a relatively large hydrophobic pocket next to the B-ring in the direction of the exit vectors at the 5 and 6 position of the pyridine core is observed in the crystal structure of **3.9** (Figure 4.2). Therefore, another optimization strategy (B) was selected to address this hydrophobic pocket by extending the pyridine core and fusing the A- with the B-rings, which will result in a quinoline-based scaffold. In addition, the rigidity of the quinoline scaffold compared to that of the pyridine-based inhibitors [127] may also be beneficial for inhibitory activity [185]. Furthermore, the possible establishment of another scaffold may give access to compounds with modified pharmacokinetic properties. Hydrophilic and hydrophobic substituents can be introduced in 6- and 7-position of the quinoline moiety to explore chemical space in this region of the binding pocket (Chart 4.1).

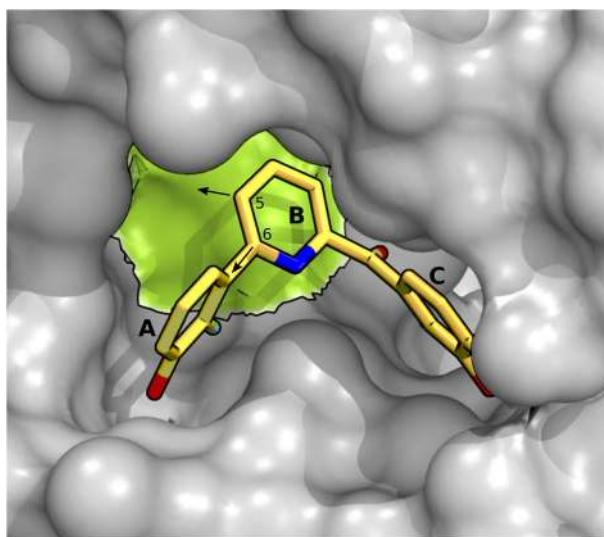


Figure 4.2: Close-up view of the binding pocket as formed in the crystal structure of 17 β -HSD14 obtained as ternary complex with **3.9** (PDB code: 5L7Y). The protein is represented in gray by the solvent accessible surface. The inhibitor is shown as stick model. Carbon atoms of the ligand **3.9** are shown in yellow. The relatively large hydrophobic pocket adjacent to the B-ring is highlighted in green. All structural representations were prepared with PyMOL [33].

4.2.2 Pan Assay Interference Compounds [168]

In order to identify undesired compounds, which might bind unspecifically to numerous biological targets, all designed compounds were validated *in silico* using the PAINS-remover computer tool [169]. As none of them was signed as unspecific binder, all were synthesized.

4.2.3 Physicochemical Parameters

Prior to synthesis, the physicochemical properties of all designed compounds were computed to only consider compounds which match with a good predicted bioavailability profile. The molecular weight was selected to fall into a range of 250-400 g/mol. The *clogP*, the total polar surface area (tPSA), the number of rotational bonds and H-bond donors and acceptors were calculated *in silico* using ACD/Percepta (14.0.0) and adhere to the Veber Rule [162] and the Lipinski Rule of five [163].

The potential of the designed compounds to cross the BBB was also taken into account, as 17 β -HSD14 has been reported to be also present in the brain [32]. Therefore, the tool compounds to be studied *in vivo* should be able to permeate the BBB. Especially for the pyridine compounds **3.9**, **4.1**, **4.2**, **4.3** and **4.4** as well as for the quinolines **4.8**, **4.10**, **4.12** and **4.16** the physicochemical properties fit well with the profile defined by Pajouhesh and Lenz [164] for compounds showing a good BBB penetration. The solubility range of most of the

compounds was also determined by mixing the studied inhibitors at several concentrations in 100 mM phosphate buffer at pH 7.4 and analyzing the precipitation status at different time points (0, 1, 2 and 24 h). The calculated physicochemical parameters and experimental determined solubilities are summarized in Table 4.1.

Table 4.1: Physicochemical property table of the designed inhibitors.

compd	MW ^a	clogP ^a	rotatable bonds ^a	H-bond donor ^a	H-bond acceptor ^a	tPSA ^a	Solubility ^b
3.9	327.28	2.98	3	2	4	70.42	> 200 μ M
4.1	315.27	3.32	3	2	4	62.58	> 200 μ M
4.2	314.19	3.49	3	3	4	65.38	> 200 μ M
4.3	328.31	3.73	3	2	4	56.59	> 200 μ M
4.4	325.31	4.06	3	2	3	53.35	> 200 μ M
4.8	267.25	3.08	2	1	3	50.19	100-200 μ M
4.9	266.27	4.45	2	1	2	37.30	25-50 μ M
4.10	281.28	3.43	2	1	3	50.19	25-50 μ M
4.11	284.15	2.59	2	2	4	70.42	> 200 μ M
4.12	292.26	2.86	3	1	4	73.98	25-50 μ M
4.14	282.27	2.24	2	3	4	76.21	50-100 μ M
4.15	339.32	1.03	4	4	6	105.31	> 200 μ M
4.13	335.29	2.22	3	2	7	104.65	> 200 μ M
4.16	373.38	4.19	3	2	4	70.42	12.5-25 μ M

^aCalculated with ACD/Percepta 14.0.0

^bSolubility tested in Phosphate-Buffered Saline (PBS, pH 7.4) at various inhibitor concentrations (3.13-200 μ M, final DMSO concentration 2%). Clarity of the solutions was evaluated optically.

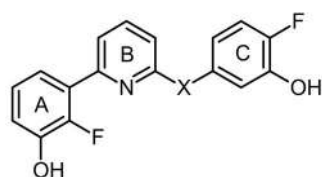
4.2.4 Biological Evaluation

The inhibitory activity of the synthesized compounds was evaluated by means of a fluorescence-based assay, quantifying the fluorescence of NADH produced during the catalytic reaction. The assay was carried out using the purified, recombinantly expressed enzyme, E2 as substrate, NAD⁺ as cofactor, and the inhibitors, as already reported [126]. A high enzyme concentration (between 2.2 μ M and 3.4 μ M) and substrate concentration of E2 (32 μ M) had to be used because the sensitivity of the assay was low. As no classical kinetic analysis could be applied for the determination of K_i [165, 166] (as the inhibitor concentration studied was in the same range as the enzyme concentration used) the results were analyzed using the quadratic Morrison equation for tight binding inhibitors [167]. This procedure was recently described by us for the inhibitors in the (6-phenyl)pyridin-2-yl methanone class [127]. For **4.8a**, no K_i could be determined due to its limited solubility and its inhibitory activity was expressed as percentage at the highest soluble concentration of the inhibitor (100 μ M).

4.2.5 17 β -HSD14 Inhibitory Activity

Starting from the (6-phenyl)pyridin-2-yl methanone **3.9**, the linker between the B- and the C-ring was investigated following our first optimization strategy concept by replacing the carbonyl group with different functional groups. Ether **4.1** ($K_i = 58$ nM), amine **4.2** ($K_i = 47$ nM), and methylamine **4.3** ($K_i = 42$ nM) were shown to be equipotent ligands with slightly decreased affinity compared to **3.9** ($K_i = 13$ nM). The introduction of an ethenyl group resulted in a ten times more potent inhibitor **4.4** ($K_i = 1.5$ nM), whereas the presence of an amide linker led to a decrease in inhibitory activity (**4.5**, 686 nM, **4.7**, 336 nM) and a methylated amide (**4.6**, 2030 nM) was even detrimental for 17 β -HSD14 inhibition compared to **3.9** (Table 4.2).

Table 4.2: 17 β -HSD14 binding constant (K_i) of 2,6-pyridine derivatives with different linkers between the B- and C-ring.



3.9, 4.1-4.7

compd	X	17 β -HSD14 K_i (nM) ^a
3.9	C=O	13 \pm 5
4.1	O	58 \pm 12
4.2	NH	47 \pm 7
4.3	NMe	42 \pm 8
4.4	C=CH ₂	1.5 \pm 0.4
4.5	-NHCO-	686 \pm 54
4.6	-NMeCO-	2030 \pm 180
4.7	-CONH-	336 \pm 54

^a Recombinantly expressed, purified 17 β -HSD14 enzyme, fluorimetric assay, substrate E2 [32 μ M], NAD⁺ [1.2 mM], 25°C, mean value of at least three independent experiments each with three technical repeats.

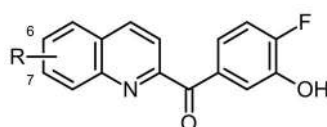
In a second approach to modify the basic scaffold, the pyridine B-ring of compound **3.9** ($K_i = 13$ nM) was expanded and led to the equipotent quinoline-based inhibitor **4.8** ($K_i = 12$ nM). The presence of the 3-OMe group at the C-ring (**4.8a**, no inhibition @ 2 μ M; 21% inhibition @ 100 μ M) was detrimental for the inhibitory activity compared to the 3-OH analogue **4.8** (69% inhibition @ 2 μ M). The role of the nitrogen atom of the quinoline moiety with respect to the inhibitory activity was further investigated by the synthesis of naphthalene **4.9** ($K_i = 6$ nM), which was shown to have a similar binding affinity as the quinoline derivative **4.8** (Table 4.3).

Table 4.3: 17 β -HSD14 binding constant (K_i) of quinoline and naphthalene derivatives.

Compd	X	R	17 β -HSD14 K_i (nM) ^a
3.9			13 \pm 5
4.8a	N	OMe	21% @ 100 μ M
4.8	N	OH	12 \pm 3
4.9	CH	OH	6 \pm 2

^a Recombinantly expressed, purified 17 β -HSD14 enzyme, fluorimetric assay, substrate E2 [32 μ M], NAD⁺ [1.2 mM], 25°C, mean value of at least three independent experiments each with three technical repeats.

Furthermore, compound **4.8** ($K_i = 12$ nM) was decorated with different substituents in 6- and 7-position to investigate their role regarding inhibitory activity. A methyl group in 6-position (**4.10**, $K_i = 6$ nM) did not influence notably the binding affinity, whereas a hydrophilic OH-group reduced potency ten times as indicated by inhibitor **4.11** ($K_i = 119$ nM) compared to **4.8**. In 7-position, the introduction of non-hydrophilic substituents (**4.12**, $K_i = 9$ nM; **4.16**, $K_i = 6$ nM) as well as of polar substituents (**4.13**, $K_i = 10$ nM; **4.14**, $K_i = 34$ nM; **4.15**, $K_i = 23$ nM) resulted in inhibitors with virtually unchanged affinities compared to **4.8** (Table 4.4).

Table 4.4: 17 β -HSD14 binding constant (K_i) of 6- and 7-substituted quinoline derivatives.**4.8, 4.10-4.16**

compd	R	17 β -HSD14 K_i (nM) ^a
4.8	H	12 \pm 3
4.10	6-Me	6 \pm 2
4.11	6-OH	119 \pm 7
4.12	7-CN	9 \pm 1
4.13	7-(tetrazole-5-yl)	10 \pm 2
4.14	7-NH ₂	34 \pm 7
4.15	7-NHGly	23 \pm 2
4.16	3-Me,4-OH-C ₆ H ₃	6 \pm 2

^a Recombinantly expressed, purified 17 β -HSD14 enzyme, fluorimetric assay, substrate E2 [32 μ M], NAD⁺ [1.2 mM], 25°C, mean value of at least three independent experiments each with three technical repeats.

4.2.6 Crystal structure determination

Inhibitors of both, the pyridine and the quinoline series, showing the best binding affinity for 17 β -HSD14 were selected for crystallization study. Seven inhibitors could be co-crystallized in complex with the protein resulting in crystals of sufficient quality for structure determination (**4.1**, PDB code: 5O6O; **4.3**, PDB code: 5O43; **4.4**, PDB code: 5O42; **4.8**, PDB code: 5O6Z; **4.10**, PDB code: 5O6X; **4.12**, PDB code: 5O7C and **4.15**, PDB code: 5O72). All the crystals exhibited tetragonal symmetry in space group (*I422*) with only one monomer forming the asymmetric unit of the homotetramer formed with other symmetry equivalent molecules in accordance with the previous study [126]. The structures obtained have a resolution ranging between 1.35 Å to 1.91 Å. The crystal structures disclosed that only small changes of the inhibitor's substituent pattern can induce important variations of their binding modes. Data collection, processing and refinement statistics can be found in the Table 4.5 A and B.

4.2.7 Description of the binding mode of the pyridine-based inhibitors in complex with 17 β -HSD14

The superimposition of the crystal structures of the enzyme in ternary complexes with **4.1**, **4.3** and **4.4** revealed that these three inhibitors, despite a chemically varied linker between the C- and the B-ring, adopted a similar binding mode compared to **3.9** (Figure 4.3 A). For all three crystallized inhibitors, the same conserved water molecule (**W1**) is founded at unchanged position as described for the others known pyridine-based inhibitors [127]. All inhibitors with the different linkers adopted the same V-shaped conformation as observed for **3.9**. As expected, the ether oxygen (**4.1**, Figure 4.3 B) is not involved in any direct interaction with the protein, whereas the methyl amine (**4.3**, Figure 4.3 C) and ethylene moiety (**4.4**, Figure 4.3 D) accommodate well in the hydrophobic pocket formed by Leu191, Trp192 and Leu195. The enhanced flexibility of the ligand with the ether linker is reflected in the split conformation of the A- and B-ring of **4.1**. Compared to **3.9**, remarkably the slightly different valence angle between the B- and C-ring ($\sim 1^\circ$) of the ethylene linker pushes the B-ring of **4.4** into the direction of Leu195 leading to about 180°-flip of the A-ring plane and resulting in an orientation of the OH- and F- substituents in opposing direction. The 4-OH group at the A-ring of all the inhibitors is within H-bond distance with the carbonyl backbone of Ala149 ($d = 2.7\text{-}2.9$ Å).

Table 4.5 A. Data collection and refinement statistic for the crystal structures.

PDB ID code ^a	Complex with 4.1 , 5O6O	Complex with 4.3 , 5O43	Complex with 4.4 , 5O42
(A) Data collection and processing			
space group	I422	I422	I422
unit cell parameters <i>a</i> , <i>b</i> , <i>c</i> (Å)	91.4, 91.4, 133.3	91.6, 91.6, 133.1	91.5, 91.5, 133.1
Matthews coefficient ^b (Å ³ /Da)	2.4	2.4	2.4
solvent content ^b (%)	49.4	49.5	49.4
(B) Diffraction data			
resolution range (Å)	50-1.45 (1.54–1.45)	50-1.50 (1.59-1.50)	50-1.76 (1.86-1.76)
unique reflections	50086 (7930)	45487 (7233)	28404(4435)
<i>R</i> (<i>I</i>) _{sym} (%)	7.3 (49.2)	9.0 (50.4)	9.8 (52.0)
Wilson <i>B</i> factor (Å ²)	12.6	13.9	18.1
completeness (%)	99.8 (99.3)	99.9 (100.0)	99.6 (98.1)
redundancy	8.6 (8.2)	8.6 (8.8)	7.9 (8.1)
<I/σ(I)>	18.1 (3.9)	13.7 (3.3)	15.3 (3.4)
(C) Refinement			
resolution range (Å)	45.69-1.45	46.41-1.50	46.38-1.76
reflections used in refinement (work/free)	50086(47581/2505)	45487 (43212/2275)	28404 (26983/1421)
final <i>R</i> value for all reflections (work/free) (%)	0.15/0.17	0.15/0.17	0.15/0.19
protein residues	256	253	256
water molecules	206	220	208
RMSD from ideality: bond lengths (Å)	0.008	0.007	0.008
RMSD from ideality: bond angles (°)	1.039	0.981	0.986
<i>Ramachandran plot</i> : ^c			
residues in most favored regions (%)	91.8	91.3	91.3
residues in additionally allowed regions (%)	8.2	8.7	8.2
residues in generously allowed regions (%)	0	0	0.5
residues in disallowed regions (%)	0	0	0
Mean <i>B</i> factor protein (Å ²) ^d	17.7	18.2	21.6
Mean <i>B</i> factor ligand (Å ²) ^d	25.0	23.1	20.5
Mean <i>B</i> factor water molecules (Å ²) ^d	28.2	30.7	32.0

^a Values in parenthesis describe the highest resolution shell. ^b Calculated with Matthews_coef program from CCP4 suite version 6.4.0.[132] ^c Calculated with PROCHECK.[133] ^d Mean B factors were calculated with MOLEMAN.[134]

Table 4.5 B. Data collection and refinement statistic for the crystal structures.

PDB code ^a	Complex with 4.8 , 5O6Z	Complex with 4.12 , 5O7C	Complex with 4.15 , 5O72	Complex with 4.10 , 5O6X
(A) Data collection and processing				
space group	I422	I422	I422	I422
unit cell parameters <i>a</i> , <i>b</i> , <i>c</i> (Å)	91.3, 91.3, 132.6	91.2, 91.2, 131.8	92.2, 92.2, 134.1	91.1, 91.1, 133.4
Matthews coefficient ^b (Å ³ /Da)	2.4	2.4	2.5	2.4
solvent content ^b (%)	49.0	48.7	50.2	49.1
(B) Diffraction data				
resolution range (Å)	50-1.57 (1.67-1.57)	50-1.60 (1.70-1.60)	50-1.91 (2.03-1.91)	50-1.35 (1.43-1.35)
unique reflections	39289 (6231)	36906 (5872)	22541 (3581)	117838 (19085)
<i>R</i> (<i>I</i>) _{sym} (%)	5.1 (50.6)	7.5 (47.5)	8.3 (4.3)	5.9 (51.9)
Wilson <i>B</i> factor (Å ²)	16.4	15.3	22.3	11.8
completeness (%)	99.8 (99.9)	99.5 (99.8)	99.7 (99.7)	99.9 (99.9)
redundancy	8.6 (8.6)	8.5 (8.2)	8.3 (8.6)	6.8 (6.6)
< <i>I</i> /σ(<i>I</i>)>	26.5 (3.9)	17.4 (3.5)	18.1 (4.0)	19.1 (3.7)
(C) Refinement				
resolution range (Å)	45.7-1.57	46.1-1.60	46.6-1.91	46.4-1.35
reflections used in refinement (work/free)	39289 (37324/1965)	36906 (35060/1846)	22541 (21414/1127)	117838 (111952/5886)
final <i>R</i> value for all reflections (work/free) (%)	0.14/0.16	0.16/0.19	0.17/0.21	0.12/0.14
protein residues	257	257	255	253
water molecules	222	218	203	246
RMSD from ideality: bond lengths (Å)	0.008	0.008	0.010	0.006
RMSD from ideality: bond angles (°)	0.996	0.993	1.045	0.947
<i>Ramachandran plot</i> : ^c				
residues in most favored regions (%)	91.4	91.4	91.3	91.7
residues in additionally allowed regions (%)	8.1	8.1	8.2	7.8
residues in generously allowed regions (%)	0.5	0.5	0.5	0.5
residues in disallowed regions (%)	0	0	0	0
Mean <i>B</i> factor protein (Å ²) ^d	19.0	19.7	23.8	13.9
Mean <i>B</i> factor ligand (Å ²) ^d	27.6	31.7	35.7	18.5
Mean <i>B</i> factor water molecules (Å ²) ^d	30.7	30.7	31.7	27.8

^a Values in parenthesis describe the highest resolution shell. ^b Calculated with Matthews_coef program from CCP4 suite version 6.4.0.[132] ^c Calculated with PROCHECK.[133] ^d Mean B factors were calculated with MOLEMAN.[134]

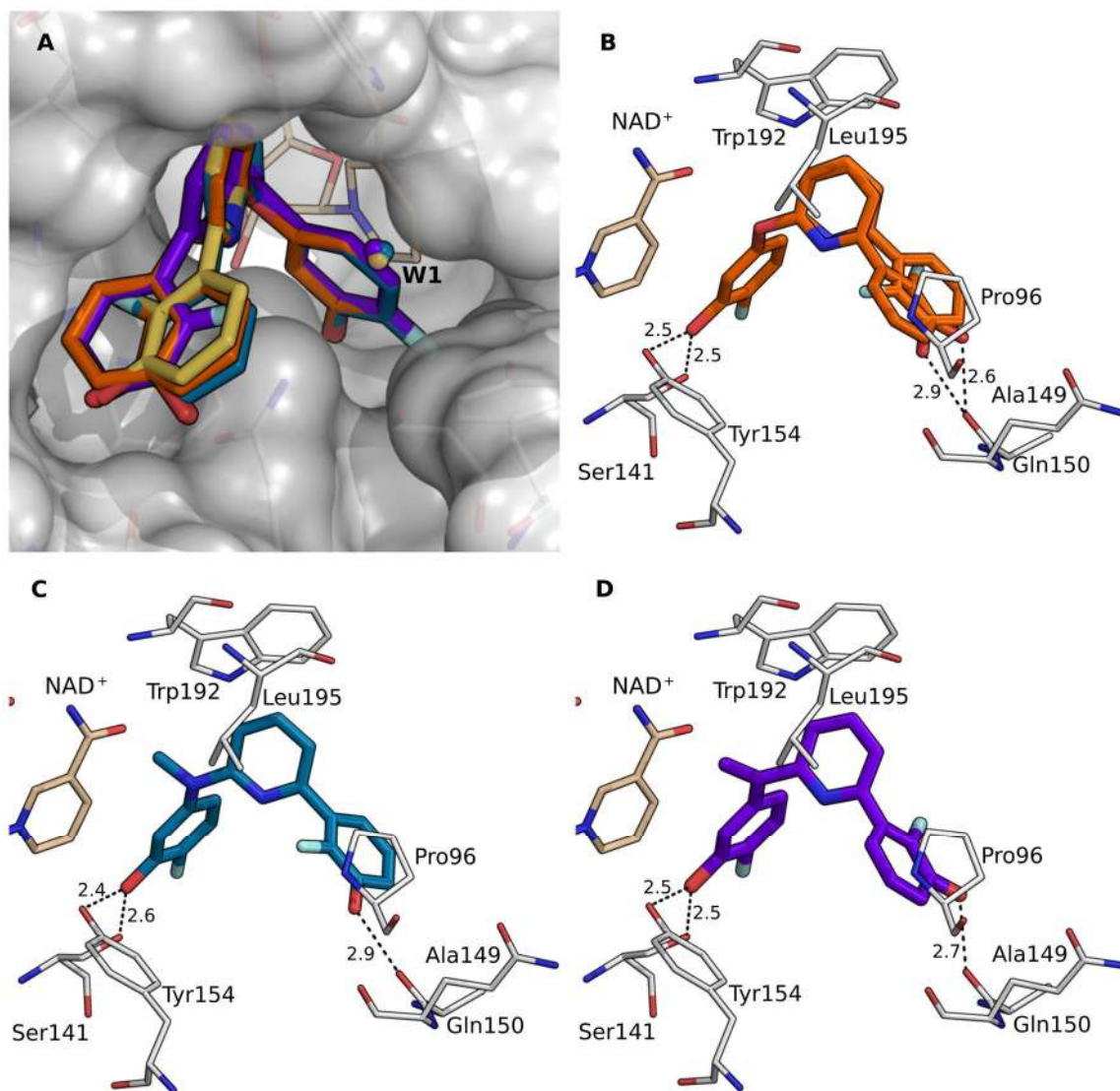


Figure 4.3: Close-up view on the binding pocket after superimposition of the four crystal structures of 17 β -HSD14 obtained as ternary complexes with the pyridine-based inhibitors: **3.9** (PDB code: 5L7Y, **A**) [127], **4.1** (PDB code: 5O6O, **A** and **B**), **4.3** (PDB code: 5O43, **A** and **C**), and **4.4** (PDB code: 5O42, **A** and **D**). The carbon atoms of the ligands are shown for **3.9** in yellow, **4.1** in orange (two conformers), **4.3** in blue, **4.4** in purple and NAD⁺ in light beige. (**A**) The protein is displayed in gray as solvent accessible surface. Inhibitors and cofactor are shown as stick models. The individual sites of the water molecule W1 are represented in the same color as the corresponding inhibitor in the various structures. W1 corresponds to water molecule 472 in 5ICM, 501 in 5O6O, 472 in 5O43 and 488 in 5O42 in the respective crystal structures. The amino acids within a distance of 4.6 Å are shown as thin lines. In panel **B**, **C** and **D**, the carbon atoms of the amino acids are shown in white, H-bond distances are depicted as dotted lines. Distances are given in Å.

4.2.8 Description of the binding mode of three quinoline-based inhibitors in complex with 17 β -HSD14

The C-ring of the three quinoline-based inhibitors **4.8**, **4.12** and **4.15** is located in the same region as in the 2,6-pyridine inhibitor class. The 3-OH group of the C-ring experiences the same H-bond interactions with Tyr154 ($d = 2.4\text{--}2.5$ Å) and Ser141 ($d = 2.4\text{--}2.5$ Å) as described for the previous inhibitor class (Figure 4.4 A and B and Figure 4.5). The quinoline core addresses the hydrophobic region formed by Pro95, Pro96, Leu191, Trp192 and Leu195 (amino acids shown in Figure 4.1). The amine substituent of **4.15** is in H-bond distance with the carbonyl group of the side chain of Gln150 ($d = 2.9$ Å), while no additional interaction can be observed for the nitrile substituent of **4.12** (Figure 4.5).

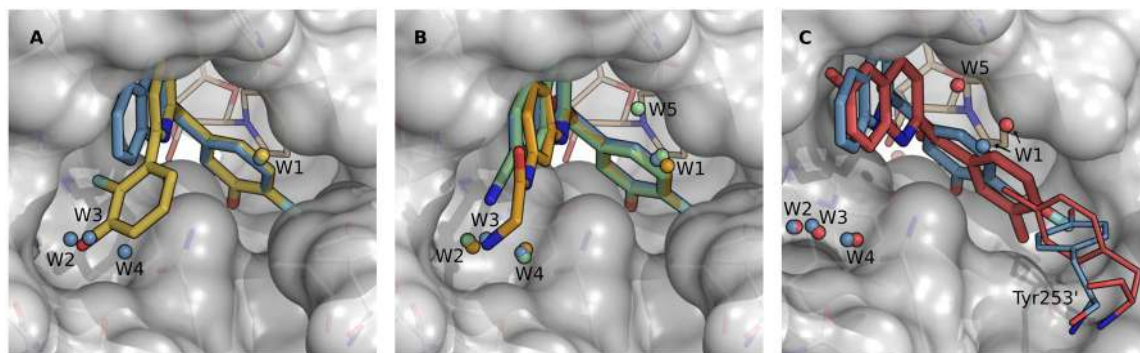


Figure 4.4: Close-up view of the binding pocket of the superimposed crystal structures of 17 β -HSD14 obtained in ternary complexes with different inhibitors. The protein is displayed in gray as solvent accessible surface. Inhibitors and cofactor are shown as stick models. The carbon atoms of the NAD⁺ are shown in light beige. The water molecules W1, W2, W3, W4 and W5 are represented in the same color as the corresponding inhibitor of the individual structures. **(A)** The carbon atoms of the ligands are shown for **3.9** (PDB code: 5L7Y) [127] in yellow and **4.8** (PDB code: 5O6Z) in blue. **(B)** The carbon atoms of the ligands are shown for **4.8** in blue, **4.12** (PDB code: 5O7C) in green and **4.15** (PDB code: 5O72) in light orange. **(C)** The carbon atoms of the ligands are shown for **4.8** in blue and **4.10** (PDB code: 5O6X) in red.

Compound **4.10** displays a slightly deviating binding mode when compared to the other inhibitors described so far. The entire compound is pushed deeper into the active site and it is the only inhibitor that induces an altered conformation of the sidechain of Tyr253' of the neighboring monomer in the functional tetramer (Figure 4.4 C). The C-ring of **4.10** is now stacked behind Tyr253'. The 3-OH group of this phenyl ring succeed to remain within H-bond distance of the side chain hydroxy group of Ser141 ($d = 2.4$ Å) which is part of the catalytic triad. Furthermore, it involves the carbonyl group of the backbone of Pro184 in an H-bond contact ($d = 3.4$ Å). However, the direct H-bond interaction between the 3-OH group and the side chain of Tyr154, found in all other structures with 17 β -HSD14 inhibitors, is no longer present. Instead, the carbonyl group of the ligand interacts with Tyr154 mediated

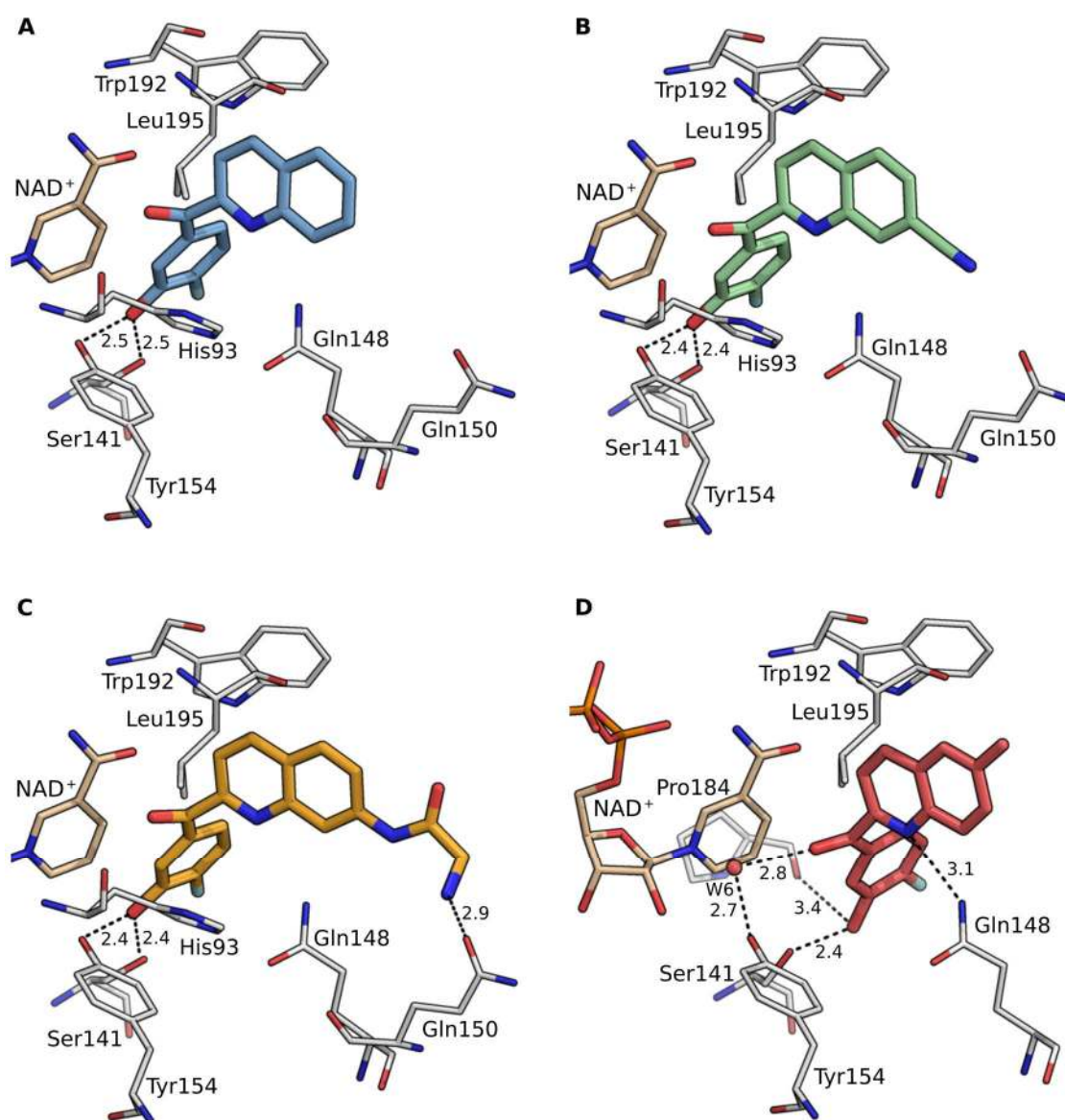


Figure 4.5: Crystal structures of 17β-HSD14 in complex with cofactor NAD⁺ and inhibitors. The carbon atoms of **4.8** are shown in blue (**A**), **4.12** in green (**B**), **4.15** in light orange (**C**) and **4.10** in red (**D**). The inhibitors and cofactor NAD⁺ are shown as stick models. The amino acids are shown as thin lines with carbon atom in white. The water molecule **W6** is represented as red sphere. H-bonds are depicted as dotted lines. Distances are given in Å.

via a water molecule **W6** ($d = 2.7$ and 2.8 Å). The methylquinoline moiety is completely buried in the hydrophobic pocket composed by Pro95, Pro96, Leu191, Trp192 and Leu195 and, in addition, the quinoline nitrogen is within H-bond distance to the sidechain of Gln148 ($d = 3.1$ Å, Figure 4.5 D). The conserved water molecule **W1** is also present as described for the pyridine-based inhibitor (Figure 4.4). It is found in conserved position as for all the quinoline-based inhibitors. However, in the case of the protein complex with **4.10**, the water

molecule is shifted upward due to the different conformation of this inhibitor. Overall three additional conserved water molecules can be observed in the four structures, located in the pocket usually occupied by the A-ring of the pyridine-based inhibitors (Figure 4.4). In case of the complex with **4.15**, one water molecule (**W3**) is displaced by the amino group of the glycine moiety of the inhibitor.

4.2.9 Comparison of the structures of 17 β -HSD14, and 17 β -HSD10.

Structural comparison between the cofactor binding site of human 17 β -HSD14 (PDB code: 5L7Y [127]) and 17 β -HSD10 (PDB code: 1U7T [94]) reveals how the overall geometry of the enzymes is conserved. The structure of 17 β -HSD14 can be divided into two distinct regions. The first region contains the Rossmann-fold scaffold where the cofactor binds, while the second region is responsible for substrate recognition [32, 126, 127]. Structural comparison between the two enzymes revealed that the cofactor is found with nearly identical geometry in the pocket, with an RMSD value of 0.6 Å (calculated with fconv [186]). The second region deviates among the protein residues in both cases, although the position of the catalytic triad and Asp114 (number referred to 17 β -HSD14) is preserved. The flexible loop of 17 β -HSD10 is slightly shorter compare to the one of 17 β -HSD14. Nevertheless, the resulting binding pockets are of similar volume and shape. However, 17 β -HSD10 has an additional solvent-exposed loop (residues 141–146, Figure 4.6). For both example of 17 β -HSD10 and 17 β -HSD14, the C-terminal tail is completely unstructured. In case of 17 β -HSD14, it is involved in the interactions between both monomers. The position of Gln165 in 17 β -HSD10 enzyme is occupied by His93 and Gln148 in the case of 17 β -HSD14. The different arrangement of the amino acids results in a shallower binding pocket for 17 β -HSD10 compare the one of 17 β -HSD14. The inhibitors occupy a similar region in types 14 and 10, However, the inhibitor for 17 β -HSD10 adopts a rather planar geometry, reinforced by Leu206 that orients toward the center of the pocket, suggesting that a more kink-shaped inhibitor such as **3.9** would not fit in to the binding pocket (Figure 4.6). As there is no other structures of the human 17 β -HSD10 enzyme, it is hard to tell if the conformation of the flexible loop is ligand induce.

4.2.10 Selectivity

We initially derived the class of 2,6-pyridine ketone inhibitors taking **3.9** as reference compound retrieved from a library of known 17 β -HSD1 and 17 β -HSD2 inhibitors [127]. It was therefore important to validate whether a preference of binding toward 17 β -HSD1 and 17 β -HSD2 was maintained or whether the optimized compounds showed already a good

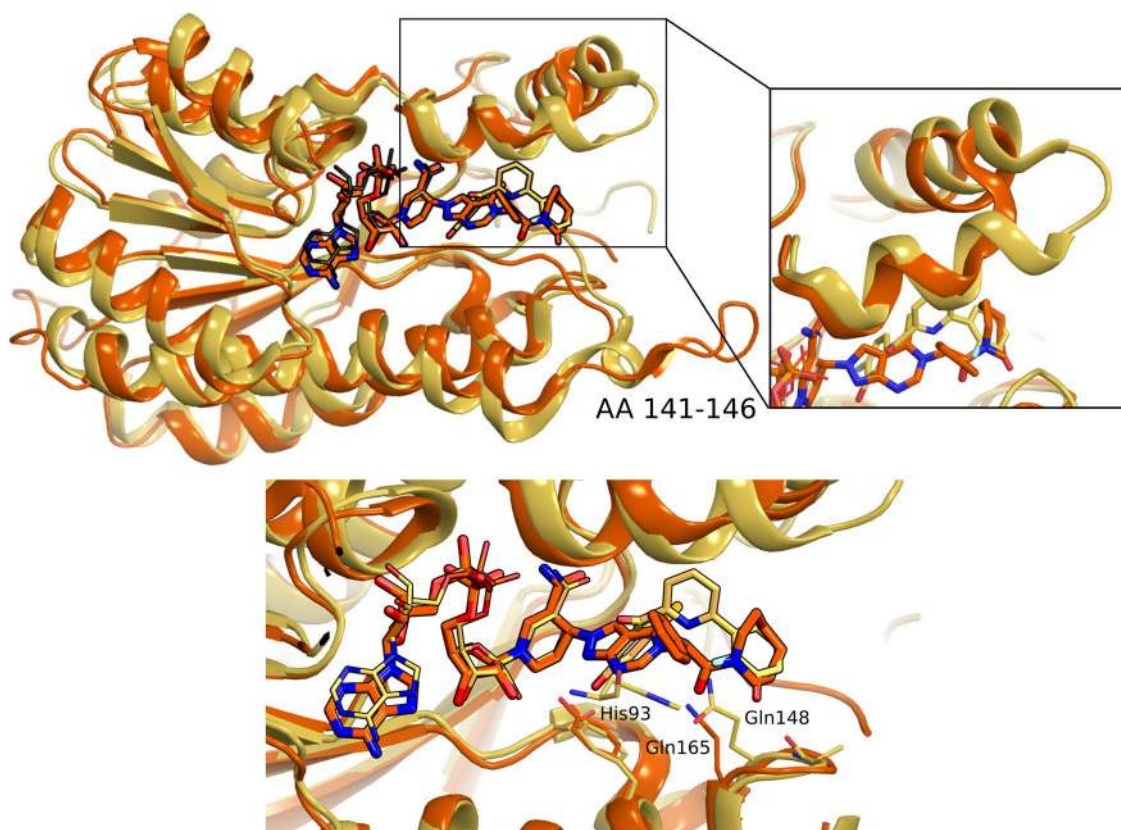


Figure 4.6: Superimposition of 17 β -HSD14 (yellow, PDB code: 5L7Y) and 17 β -HSD10 (orange, PDB code: 1U7T) structures. The proteins are shown as ribbon model. The ligands and cofactors are shown as stick models and their carbon atoms are colored as the corresponding protein structure.

selectivity profile toward 17 β -HSD14. In addition, as mentioned previously, the investigation of the selectivity profile with respect to binding toward 17 β -HSD10 is of high concern considering the given high similarity of 17 β -HSD14 with the latter enzyme.

We selected inhibitors that showed good inhibition of 17 β -HSD14 ($K_i < 100$ nM) to validate the selectivity profile towards 17 β -HSD1, 17 β -HSD2 and 17 β -HSD10. The potential of the selected 14 inhibitors to inhibit 17 β -HSD1, 17 β -HSD2 and 17 β -HSD10 was studied using a competitive radioactive assay, by quantifying the formation of of [3 H]-labeled E2 (for 17 β -HSD type 1) and [3 H]-labeled estrone (E1, for 17 β -HSD type 2 and 10) after incubation of the protein with the cofactor and the inhibitor [174]. The results of the assay are shown in Table 4.6 and expressed as percentage of inhibition.

The first approach to modify the scaffold of the pyridine derivatives resulted in the production of less selective compounds (4.1, 4.2, 4.3 and 4.4), which showed even higher affinity for 17 β -HSD1 and 17 β -HSD2, (57-99% 17 β -HSD1 inhibition @ 1 μ M and 82-100%

17 β -HSD2 inhibition @ 1 μ M) compared to the initial compound **3.9** (8% 17 β -HSD1 inhibition and 56% 17 β -HSD2 inhibition @ 1 μ M).

The second strategy to optimize the scaffold, which led to the quinoline-based compounds **4.8-4.16**, resulted in inhibitors which showed no significant inhibitory activity toward 17 β -HSD1, only the naphthalene derivative **4.9** falls out of this profile and exhibits high 17 β -HSD1 inhibitory activity (64% inhibition @ 1 μ M).

In our previous study [127], we could show that **3.9** shows a 17 β -HSD2 inhibition of 50% at 1 μ M, corresponding to an IC₅₀ of 1 μ M. Taking into account the kinetic constant of the assay (K_m = 400 nM, substrate concentration = 500 nM), a K_i for **3.9** can be estimated to be about 450 nM. The determined K_i for **3.9** in the 17 β -HSD14 assay was 13 nM. **3.9** is therefore about 35 fold more selective on 17 β -HSD14 compared to 17 β -HSD2. As compounds **4.12**, **4.13** and **4.15** exhibit a 17 β -HSD2 inhibition in the same range as **3.9** (52-63% inhibition @ 1 μ M), it can be expected that they will be as selective as **3.9** toward 17 β -HSD2, thus underlining the satisfactory selectivity discrimination of the quinoline-based inhibitors against 17 β -HSD1 and 17 β -HSD2.

With respect to 17 β -HSD10, only compounds **4.1** and **4.3** showed a weak inhibitory activity (17% and 19% inhibition @ 1 μ M, respectively) while all the other synthesized derivatives are inactive suggesting an overall very convincing selectivity profile toward 17 β -HSD10 (Table 4.6).

4.2.11 Cytotoxicity evaluation

Seven compounds, selected on the basis of their 17 β -HSD14 inhibition profile and selectivity were evaluated for their cytotoxicity using an MTT assay based on the HEK293 cell line. All tested compounds, **3.9**, **4.4**, **4.11**, **4.13** and **4.15** displayed a very low cytotoxicity (IG₅₀ > 100 μ M). Due to insufficient solubility, **4.11** and **4.12** could not be tested at 100 μ M, however, the cells showed 80% survival at a concentration of 20 μ M, the maximally possible concentration tested.

4.2.12 Pgp ATPase Activity Assays

Pgp, also termed MDR1 and ABCB1, is an integral plasma membrane protein expressed at the luminal surface of the BBB [187]. The enzyme is an ATP-dependent drug efflux pump, which plays an important role in multi-drug resistance [184]. As mentioned, 17 β -HSD14 was described to be also expressed in the brain and liver [100]. Goal of the project is the development of tool compounds to study the physiological role of 17 β -HSD14 *in vivo*, it was

Table 4.6: 17 β -HSD type 1, 2 and 10 inhibitory activities (% inhibition) of the most interesting compounds.

compd	17 β -HSD1 % Inh. @ 1 μ M ^a	17 β -HSD2 % Inh. @ 1 μ M ^b	17 β -HSD10 % Inh. @ 1 μ M ^c
3.9	8	56	n.i.
4.1	69	100	17
4.2	57	82	n.i.
4.3	99	100	19
4.4	88	100	n.i.
4.8	6	76	n.i.
4.9	64	96	n.i.
4.10	12	78	n.i.
4.11	20	71	n.i.
4.12	n.i.	56	n.i.
4.13	n.i.	52	n.i.
4.14	21	83	n.i.
4.15	3	63	n.i.
4.16	11	80	n.i.

^a Placental 17 β -HSD1 enzyme, cytosolic fraction, substrate [³H]-E1 + E1 [500 nM], NADH [0.5 mM], mean value of 2 determinations; standard deviation < 10 %.

^b Placental 17 β -HSD2 enzyme, microsomal fraction, substrate [³H]-E2 + E2 [500 nM], NAD⁺ [1.5 mM], mean value of 2 determinations; standard deviation < 10 %.

^c Recombinantly expressed 17 β -HSD10 enzyme, bacterial suspension, substrate [³H]-E2 [25 nM], NAD⁺ [0.75 mM], mean value of 3 determinations; standard deviation < 10 %.

important to validate whether the most promising compounds in both the pyridine and the quinoline class, affect Pgp either as substrate or as inhibitor or leave this transporter unaffected [164]. The following four compounds from the two classes were selected to test for Pgp interaction: **3.9**, **4.12**, **4.13** and **4.15**. They combine good 17 β -HSD14 inhibitory potency with convincing selectivity profile.

The assay was performed in successive manner. At first the tested inhibitor and ATP were incubated simultaneously with the Pgp protein present in a cell membrane fraction. After quenching of the reaction, unmetabolized ATP was detected by means of an ATP-dependent luminescence signal which was generated after addition of firefly luciferase. The impact of the tested compounds **3.9**, **4.12**, **4.13** and **4.15** on the efflux pump was examined in comparison to untreated samples (control) and samples treated with the selective Pgp inhibitor sodium orthovanadate (Na₃VO₄) and verapamil, a known substrate of the Pgp. The results can be seen on Figure 4.7.

The untreated sample (**a**) showed some luminescence indicating the production of some ATP originating from other sources than Pgp as cell fraction membranes were used and no purified Pgp. The ATP consumption for samples exposed to the Pgp inhibitor (Na₃VO₄, **b**)

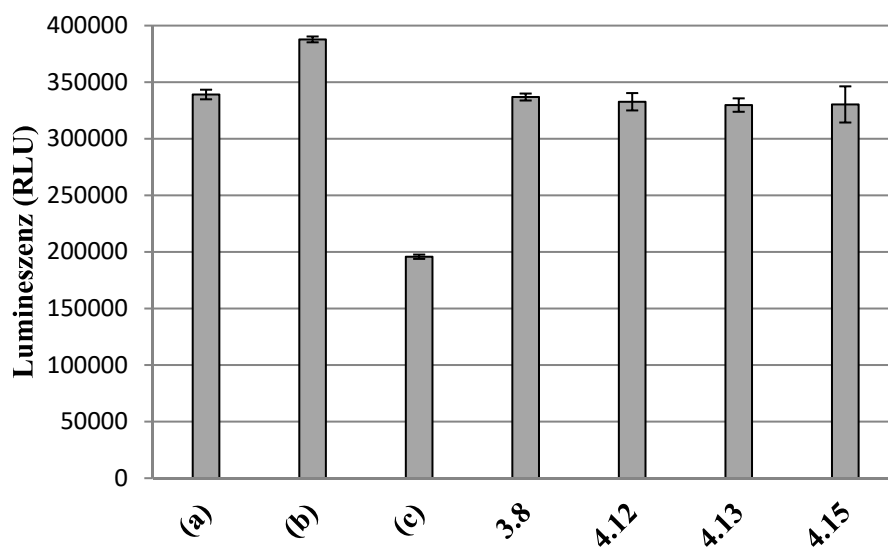


Figure 4.7: Effect of the four 17 β -HSD14 inhibitors **3.9**, **4.12**, **4.13** and **4.15** on Pgp ATPase activity. **(a)**, untreated sample, **(b)** Pgp inhibitor Na₃VO₄ and **(c)** Pgp substrate verapamil. Data were analyzed in term of relative light units (RLU) from two independent experiments with three technical repeats.

was blocked resulting in luminescence increase compared to the untreated samples. The difference in the luminescence signal of these samples represented the basal activity of the tested protein Pgp. Verapamil **(c)** stimulated the Pgp ATPase activity as it is a substrate of the protein. A decrease in ATP was observed correlating with a significant drop in luminescence compared to untreated samples. For samples containing **3.9**, **4.12**, **4.13** and **4.15** no significant change in luminescence compared to untreated samples could be observed. In consequence our compounds can be classified as neither substrates nor inhibitors of the efflux pump Pgp (Figure 4.7).

4.3 Discussion and conclusion

4.3.1 SAR of pyridine derivatives

Our first structure-based modifications of the initial pyridine-based scaffold led to the ten-fold more potent compound **4.4** ($K_i = 1.5$ nM) compared to **3.9** ($K_i = 13$ nM). The crystal structure with this ligand revealed that its ethylene linker is more deeply buried in the hydrophobic pocket defined by Leu191, Leu195 and Trp192. Obviously this hydrophobic linker maintains the conformational properties but is beneficial for binding due to its lower desolvation penalty compared to the carbonyl analog (**3.9**) which does not use its polar oxygen for any interaction. The flipped A-ring (compared to **3.9**) led to an improved

geometry where this ring comes in proximity of the hydrophobic region build up by Pro95, Pro96 and Leu195. In addition, the 3-OH group attached to the A-ring is moved to a more favorable H-bond distance ($d = 2.7 \text{ \AA}$) toward the carbonyl group of the Ala149 backbone. Taken together these aspects might be responsible for the gain in affinity. Using an ether- (4.1), amine- (4.2) or methylamine linker (4.3) does not enhance activity over 3.9. Compounds 4.5, 4.6 and 4.7 lose in affinity possibly owing to the introduced polar amide linkers which are exposed to a predominantly hydrophobic environment. In addition, the A-rings of these inhibitors remain partly solvent exposed, likely as the compounds appear rather long for the binding site.

4.3.2 Selectivity of pyridine derivatives

All the newly synthesized pyridine-based inhibitors showed a high selectivity toward 17 β -HSD10. However, a less satisfactory selectivity profile toward 17 β -HSD1 and 17 β -HSD2 was caused by all the pyridine which do not bear a carbonyl linker including 4.1, 4.2, 4.3 and 4.4. A rational explanation of the observed selectivity profile of the inhibitors toward 17 β -HSD1, 17 β -HSD2 and 17 β -HSD10 in structural terms appears rather difficult to elucidate. Due to the conformational properties of the 17 β -HSD1 binding pocket — with the flexible loop restricting the remote part, opposite to the catalytic triad, and its several adapted conformations — it is extremely challenging to perform reliable docking studies. The lack of a crystal structure of 17 β -HSD2, the rather flat binding site and the completely different mechanism of action of the 17 β -HSD10 inhibitor **AG18051** [94] (covalently attached to the cofactor, PDB code: 1U7T) do not allow a detailed conclusive comparison. Taken together the activity profile and the selectivity profile of the pyridines, it appeared reasonable to maintain the carbonyl linker for further investigation in the quinoline class.

4.3.3 SAR and selectivity of the quinoline/naphthalene derivatives

According to the second optimization step, the goal was to extend the central pyridine core to address the empty lipophilic pocket adjacent to the A- and B-ring (Figure 4.2). The designed quinoline-based inhibitor 4.8 was modelled into the crystal structure and the simulation suggested a good fit into the active site of the protein (Figure 4.8). The binding mode of 4.8 was verified by the co-crystal structure and allowed the understanding of its very high potency ($K_i = 12 \text{ nM}$) as anticipated (Figure 4.8). As already remarked by Braun *et al.* [127], replacing the 3-OH group at the C-ring by a 3-OMe moiety resulted in a strong drop of binding affinity (4.8a, 21% inhibition @ 100 μM). The naphthalene compound 4.9 was synthesized to investigate the importance of the pyridine nitrogen in the core ring system of

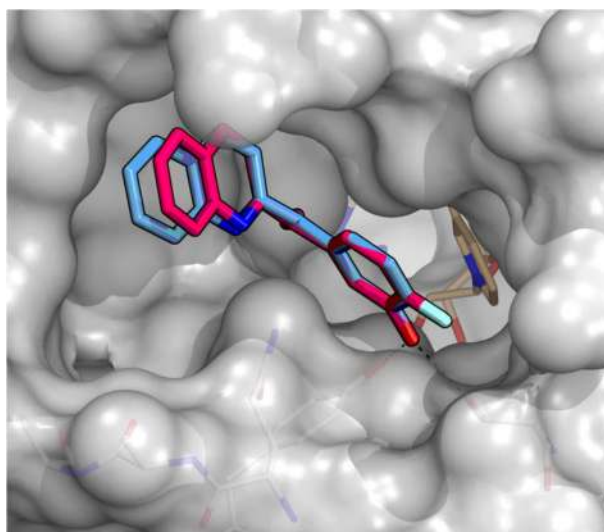


Figure 4.8: Superimposition of the modeled structure of 17 β -HSD14 in complex with inhibitor **4.8** and its crystal structure (PDB code: 5O6Z). The protein is displayed in gray by use of the solvent accessible surface. The ligands are shown as stick models. The C atoms of the modeled ligand are colored in pink and in blue for the crystalized compound. Amino acids and cofactor are shown as thin lines. H-bonds are depicted as black dotted lines.

4.8. The derivative **4.9** ($K_i = 6$ nM) showed a similar binding affinity compared to the quinoline analogue **4.8**. However, the nitrogen of the quinoline core enhances the solubility over its naphthalene analogue. In addition, it was shown that the selectivity profile toward 17 β -HSD types 1 and 2 was less favorable for naphthyl analog **4.9** and therefore not further developed.

The decoration of the quinoline core with substituents showing different hydrophobicity profiles resulted in highly active inhibitors (**4.10-4.16**). From the crystal structures of **4.12** and **4.15** (Figure 4.5), it became apparent that all ligands adopted the same binding mode as **4.8**, interacting with Tyr154 and Ser141 from the catalytic triad. The additional hydrophobic interactions of the extended core motif with the pocket built-up by Leu191, Trp192, Leu195 and Met199 may have compensated the loss of the A-ring and of the H-bond interaction with Ala149 which were observed for compound **3.9** [127] (e.g. **4.8**, $K_i = 12$ nM vs. **3.9** $K_i = 13$ nM). The nitrile group of **4.12**, pointing off from the active site without performing any additional interactions with the protein, resulted in no significant change in the binding affinity ($K_i = 9$ nM). For **4.15**, an additional H-bond interaction of the exocyclic amino group was experienced. However, no increase in affinity compared to compound **4.8** was observed ($K_i = 23$ nM). A similar experience with respect to the inhibitory potency was made for **4.13** bearing a rather hydrophilic tetrazole moiety ($K_i = 10$ nM). As no crystal structure could be obtained for **4.13**, the ligand was modeled as a complex with 17 β -HSD14 and an

H-bond interaction of the quinoline core with the side chain of Gln148 could be identified (Figure 4.9 C).

The analog modeling of the binding mode of the 7-aminoquinoline derivative **4.14** ($K_i = 34$ nM) also did not revealed any additional interactions of the amino group (Figure 4.9 B). The introduction of a 6-OH group at the quinoline core led to a loss in affinity by a factor of ten as observed for **4.11** ($K_i = 119$ nM). The modeled complex structure of **4.11** predicted a similar binding mode as the one adopted by the other quinoline-based inhibitors (Figure 4.9 A). However, the polar 6-OH group is pointing into the rather hydrophobic region formed

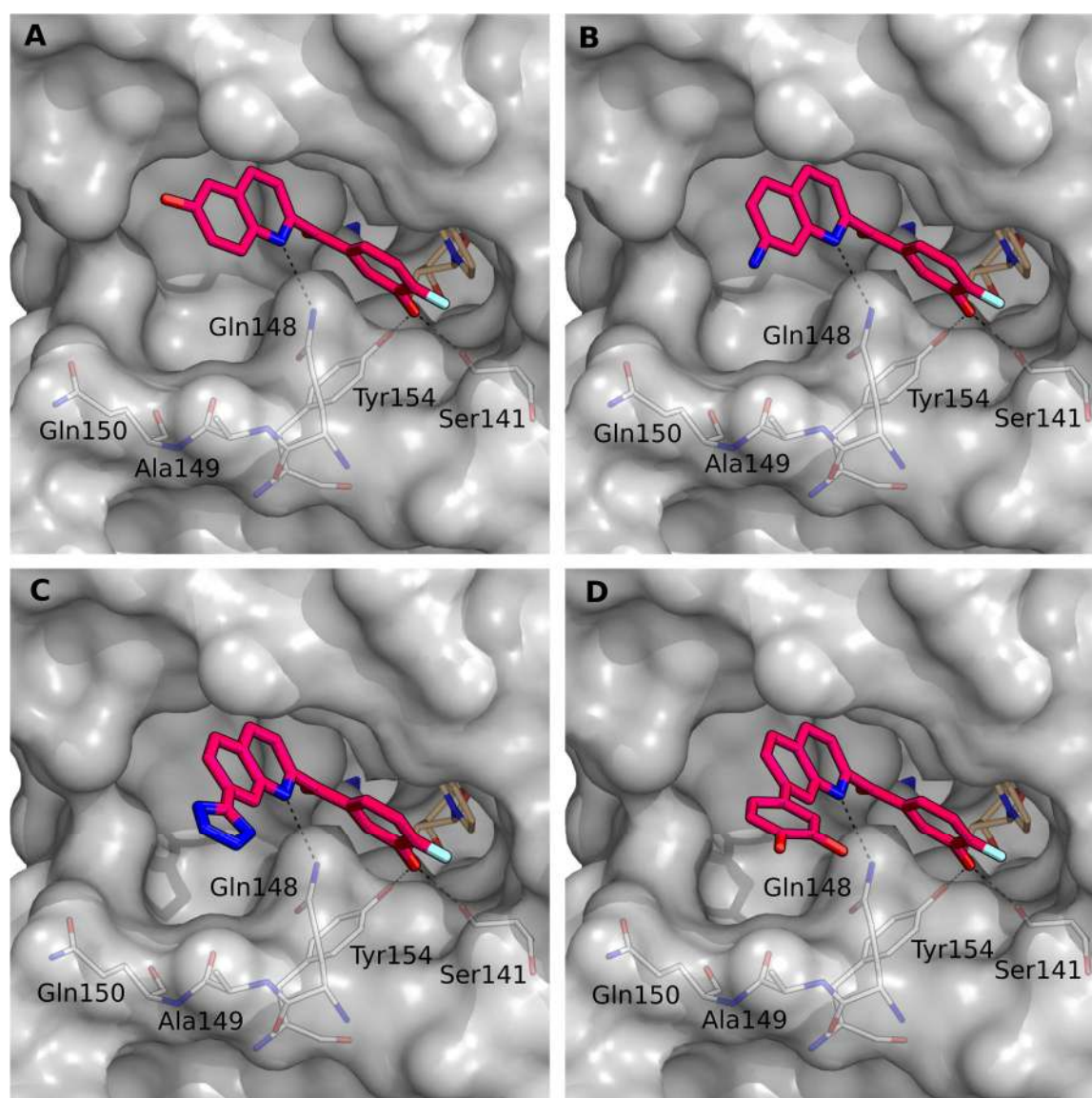


Figure 4.9: Modeled structures of 17β-HSD14 in complex with inhibitors **4.11** (A), **4.13** (C), **4.14** (B) and **4.16** (D). The protein is displayed in gray by use of the solvent accessible surface. The inhibitors are shown as stick models. The C atoms of the modeled ligand are colored in pink. Amino acids and cofactor are shown as thin lines. H-bonds are depicted as black dotted lines.

by Met199 and Thr205 which might explain the observed loss in activity. The structurally increased ligand **4.16** showed a high affinity to the protein ($K_i = 6$ nM). The modelled complex suggests an enhanced contact surface between ligand and protein resulting in improved potency (Figure 4.9 D).

The deviating binding mode of the 6-methylquinoline derivative **4.10** did not parallel a significant change in binding affinity compared to **4.8** ($K_i = 6$ nM vs $K_i = 13$ nM, respectively). Surprisingly, the 3-OH group of the C-ring did not form an H-bond interaction with Tyr154 of the catalytic triad, which was reported to be essential to achieve high potency [127], but it is in H-bond distance with Ser141. Instead, Tyr154 forms an H-bond network via a water molecule (**W6**) with the ligand's carbonyl linker. In addition, an H-bond interaction between Gln148 and the central quinoline nitrogen was formed. The quinoline core along with the 6-methyl group are deeply buried in the hydrophobic pocket flanked by Leu191, Tpr192, Leu195, Met199 and Thr205 (Figure 4.5). Taken together, these effects seem to compensate the loss in the direct interaction to Tyr154.

Interestingly, a water molecule (**W6**) is entrapped to mediate a contact between ligand and protein. This water is also found at the same position in the complex structures with **4.10**, **4.12** and for the holoenzyme (PDB code: 5JSF and 5JS6). The fact that this water molecule is in close proximity to the catalytic triad and overall present in four structures, raises the question about its possible involvement in the catalytic mechanism (Figure 4.10).

Regarding the selectivity of the synthesized quinoline-based inhibitors, the affinity toward 17 β -HSD1 and 17 β -HSD10 was minor rendering these compounds prominent as quite selective binders. Adding the selectivity profile toward 17 β -HSD2 to this comparison, **4.12**, **4.13** and **4.15** can be highlighted to exhibit signatures comparable to that of **3.9**. Considering the potency and selectivity profiles, the initial compound **3.9** and the newly synthesized quinoline-based inhibitors **4.12**, **4.13** and **4.15** exhibit the best profiles. Furthermore, these four compounds displayed very low cytotoxicity ($IG_{50} > 100$ μ M) and disqualify them as neither substrates nor inhibitors of the multi-drug resistance protein Pgp ATPase, suggesting them as potent tool compounds for the further investigations regarding putative *in vivo* administration to reveal insights into the physiological role of 17 β -HSD14.

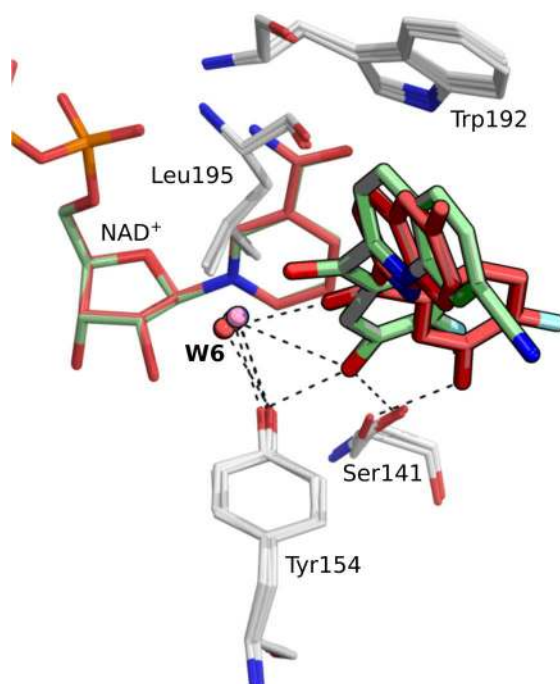


Figure 4.10: Superimposition of the crystal structures of 17 β -HSD14 holoenzyme (PDB code: 5JSF and 5JS6) and in complex with cofactor NAD⁺ and inhibitors. The carbon atoms of **4.12** are colored in green (PDB code: 5O7C) and **4.10** in red (PDB code: 5O72). The inhibitors and cofactor NAD⁺ are shown as stick models. The amino acids are shown as thin lines with carbon atom in white. H-bonds are depicted as dotted lines. The water molecules **W6** are represented in the same color as the corresponding inhibitor of the individual structures and are colored in blue for 5JSF and in pink 5JS6.

4.4 Experimental section

4.4.1 Enzyme expression and purification

The pure recombinant 17 β -HSD14 enzyme was obtained via heterologous expression using p11-Toronto1 vector and the competent cells BL21 *pLysS* strain of *E.coli* as previously described [126, 127]. The protein purification was performed applying two steps of affinity chromatography (Ni-NTA column) followed by size-exclusion chromatography. The stability of the protein was increased by the addition of the cofactor (NAD⁺) and of 250 mM of glucose to the buffer during the purification and storage. Purity was confirmed by SDS page and mass spectrometry (result not shown).

4.4.2 Inhibition of 17 β -HSD14

Inhibitory activities were evaluated with a fluorimetric assay as previously described.[127] Briefly, to a mixture of NAD⁺ (1.2 mM) and E2 (32 μ M) in 100 mM phosphate buffer pH 8, the potential inhibitor was added in DMSO (final DMSO concentration in assay: 1%) and the enzymatic reaction was started by addition of the purified enzyme (1 mg/ml). The production of the fluorescent NADH formed was measured continuously for 15 min on a Saphir Tecan2. A linear relationship between product formation and reaction time was obtained and the slope of the progress curves was calculated by linear regression. The K_i values were calculated by means of the Morrison equation using the procedure detailed by Copeland [167] as previously described.[127] The fitting and data analysis were performed using GraphPad Prism 7.

4.4.3 Inhibition of 17 β -HSD1 and 17 β -HSD2

17 β -HSD1 and 17 β -HSD2 were partially purified from human placenta according to previously described procedures [174, 188]. For the 17 β -HSD1 inhibition assay the cytosolic fraction was incubated with NADH [500 μ M], and the potential inhibitor was added in DMSO (final concentration in assay: 1 μ M, final DMSO concentration: 1%) at 37°C in a phosphate buffer (50 mM). The enzymatic reaction was started by addition of radioactive [2,4,6,7-³H]-E1 in a mixture with the unlabeled substrate E1 (final concentration: 500 nM) and stopped with HgCl₂ after 10 min. Separation and quantification of the extracted radioactive steroids were performed by HPLC coupled to a radioflow detector. The 17 β -HSD2 inhibition assay was performed similarly incubating the microsomal fraction in the presence of NAD⁺ [1500 μ M] and [2,4,6,7-³H]-E2 in a mixture with the unlabeled substrate E2 (final concentration: 500 nM).

4.4.4 Inhibition of 17 β -HSD10

A suspension of the bacterial pellet in 100 mM phosphate buffer pH 7.7 was incubated with [6,7-³H]-E2 (final concentration: 25 nM) in presence of the potential inhibitor in DMSO (final concentration in assay: 1 μ M, final DMSO concentration: 1%) at 37°C. The enzymatic reaction was started by addition of NAD⁺ (0.75 mM) and stopped by means of 0.21 M ascorbic acid in a methanol/acetic acid mixture (99:1, v/v) after an incubation time of 30 min. Substrate and product were extracted from the reaction mixture by SPE (Strata C18-E columns from Phenomenex on a vacuum device). Separation and quantification of the radioactive labeled steroids was performed with HPLC (Luna 5 μ m C18(2), 125 x 4.00 mm from Phenomenex, with an acetonitrile/water mixture (43:57, v.v), flow rate 1 mL/min).

Substrate conversion is given in % as calculated after integration of the product and substrate peaks. Inhibition was calculated based on conversion without potential inhibitor (DMSO only) which was set to 0% inhibition.

4.4.5 Co-crystallization of the protein with inhibitors

The co-crystallization of 17 β -HSD14 in complex with the different classes of inhibitors was performed following the already described slightly optimized protocols [126, 127].

The final inhibitor concentration of 4 mM was incubated with the protein solution (9.5 mg/mL) containing 0.6 mM NAD⁺ and 5% DMSO for 30 minutes. The mixture was then centrifuged at 10000 g for 20 minutes in order to separate the precipitated. Afterwards, 2 μ L of the supernatant was mixed with 2 μ L of mother liquor composed of 0.1 M HEPES, 20% (w/v) PEG6000 and 5% (v/v) DMSO, adjusted to pH 7.0. Crystals of sufficient quality for data collection were grown at a temperature of 18°C for 10 days and then exposed for a few seconds to a cryo buffer obtained by the combination of mother liquor with the addition of 20% glucose. Finally the specimen were successively flash-frozen in liquid nitrogen.

4.4.6 Crystallography

Data collection and processing

All the datasets of the structures of the protein-inhibitor complexes were collected at beamline 14.1 at BESSY II in Berlin, Germany. The data collection was achieved with a wavelength of 0.9184 Å and a temperature of 100 K on a DECTRIS Pilatus 6M pixel detector. All datasets were indexed, processed and scaled with XDS [142].

Structure determination and refinement

The structures were determined by molecular replacement with the program PHASER MR[143] from the CCP4 suit.[132] In all cases, coordinates of the PDB entry 5EN4 were used as a search model. A subset, corresponding to 5% of the reflections, was used for the calculation of R_{free} and consequently was omitted from the refinement. The model was built in COOT [171] and refined using PHENIX.refine version 1.10.1-2155 [145]. The ligands were energetically minimized and their restraints were generated using Grade Web Server [147] and eLBOW [145] based on the SMILES codes obtained with Molinspiration v2013.91 [146]. As first refinement step for all structures, a Cartesian simulated annealing was performed using default parameters. The final models were built in COOT with alternating structural

modification and refinement of XYZ coordinates, occupancies and individual B-factors in *PHENIX*. Hydrogens were included in the models of the structures. For 5O6X, the temperature factors of all atoms, except hydrogen atoms and solvent molecules, were refined anisotropically. For 5O72, the temperature factors were refined isotropically. For the other five structures, TLS refinement was performed with nine TLS groups selected from the TLSMD web server [148, 149].

4.4.7 MOE models

The inhibitor **4.8**, **4.11**, **4.13**, **4.14** and **4.16** were model inside the crystal structure PDB code: 5L7Y [126] and minimized with MOE [173]. During minimization, the AMBER12 force field was applied. The heavy atoms of the protein and the 3-OH group at the C-ring of the inhibitors were fixed. In order to give to the ligand sufficient freedom to move also the residues His93, Gln148 and Met199 where allowed unrestricted to move during minimization.

4.4.8 Cytotoxicity Assay

Potential cytotoxicity of inhibitors **3.9**, **5.12**, **5.13** and **5.15** toward HEK293 cells was determined by an MTT assay [189] as previously described [190]. The cells were seeded into 96-well plates overnight at a 1×10^4 cells/well density. Series of inhibitor concentrations (from 0 to 100 μ M) were added to the well and incubated for 72 h, at 37 °C under 5% CO₂. The cell viability was subsequent evaluated by the MTT colorimetric assay.

4.4.9 Pgp ATPase Activity Assays

The effect of inhibitors **3.9**, **5.12**, **5.13** and **5.15** on Pgp ATPase activity was evaluated by means of the Pgp-Glo™ assay system (Promega, Madison, WI, USA). In a white 96-well plate, the inhibitors **3.9**, **5.12**, **5.13** and **5.15** were incubated in DMSO (final concentration in assay: 10 μ M) with 25 μ g of recombinant human Pgp membrane. The Pgp-glo assay buffer was used as the untreated sample control. The positive control of drug induced Pgp ATPase activity was obtained by addition of 200 μ M verapamil to the assay buffer. As selective inhibitor of Pgp ATPase activity, 100 μ M sodium orthovanadate in the assay buffer was used. All the samples contained a final DMSO concentration of 1%. The Pgp ATPase activity was initiated by the addition of 5 mM MgATP and incubated at 37 °C for 60 min. Luminescence was recorded after adding 50 μ L of ATP detection reagent. After 25 min of incubation at room temperature, the total luminescence signal was detected on a Tecan Sapphire 2.

Chapter 5

Structural Comparison between 17 β -HSD Enzymes and Virtual Screening of Inhibitors

Introductory remarks

This chapter is based on the results preliminary addressed in Chapters 2 and 3. In the following a detailed discussion of the structural differences between 17 β -HSD14 and the other 17 β -HSD proteins will be provided. Furthermore, docking studies performed during the early stage of this project will be discussed.

5.1 Introduction

Crystal structures of proteins provide valuable structural information on how a ligand binds to a target protein. Additionally, mechanistic insights can be obtained by comparing the three-dimensional arrangement of amino acids that determine the active site of different enzymes of the 17 β -HSD family.

In the following, a structural comparison is performed between 17 β -HSD14 and other 17 β -HSDs that have been deposited as crystal structures in the publicly available Protein Databank (PDB). The structures of 17 β -HSDs used for comparison were selected based on the catalyzed reaction, the formed complex and the quality of the respective crystal structures. The information obtained from this comparison will assist in the modelling of the three-dimensional structures of other not yet crystallized 17 β -HSDs. In the following, structural differences between 17 β -HSD14 and three related 17 β -HSDs (h17 β -HSD1, h17 β -HSD8, and 17 β -HSD10) are discussed. A focus is put on the enzymes' active sites. 17 β -HSD5 is the only 17 β -HSD protein that belongs to the AKR superfamily. However, a direct comparison to 17 β -HSD14 is difficult due to its low structural similarity (Figure 5.1), and thus will not be considered in the following. 17 β -HSD2 catalyzes the same reaction as 17 β -HSD14. Unfortunately, no crystal structure of 17 β -HSD2 is available to date and thus a structural comparison between type 2 and type 14 is not possible.

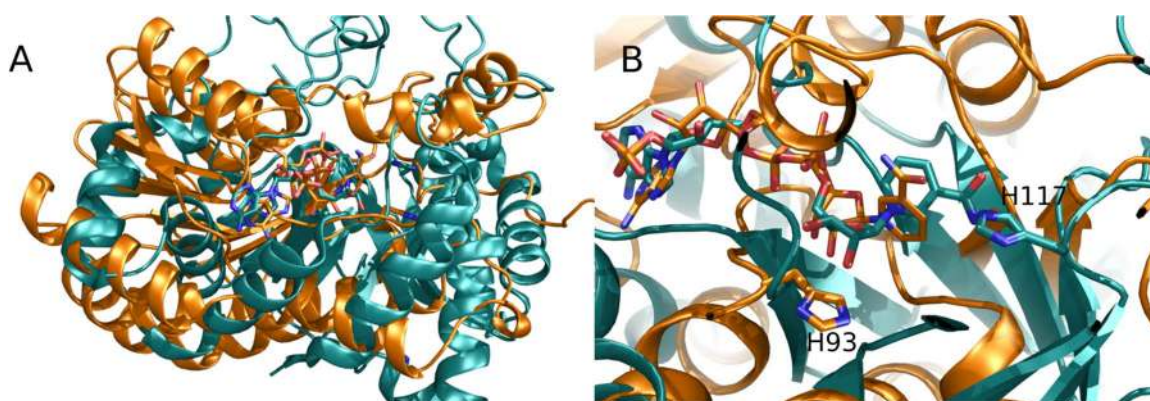


Figure 5.1: Superimposition based on the coordinates of the cofactor of the crystal structures of the 17 β -HSD14 variant T205 (orange) and 17 β -HSD5 (green) displayed as ribbon models; the bound cofactor is shown as stick model. **(A)** Overview of the superimposed tertiary structures. **(B)** Close up view of the cofactor binding pockets. His93 of 17 β -HSD14 and His117 of 17 β -HSD5 are shown as stick models (PDB code for 17 β -HSD14: 5JS6; 17 β -HSD5: 1S1P). Structural representations were prepared with PyMOL [33].

5.2 Comparison of the crystal structures of 17 β -HSD1 and 17 β -HSD14

Until now, 22 crystal structures of 17 β -HSD1 as apoenzyme or in complex with a substrate/product or inhibitor have been deposited in the PDB. Five of these structures with a resolution between 1.60 to 2.24 Å have been selected for the structural comparison with 17 β -HSD14. Ten of the aforementioned 22 17 β -HSD1 crystal structures had to be excluded from the comparison since they showed differences between R_{free} and R_{work} larger or equal to 10%. The large difference in the R values possibly indicates inaccuracies in the crystal structure models (severe overfitting) that would consequently lead to an erroneous discussion. Additional seven structures had to be excluded since the flexible loop of 17 β -HSD1 (residues 190-201), that contributes structurally to the binding pocket, was not resolved in their electron density maps. The superimposition based on the Ca coordinates of the five selected crystal structures of 17 β -HSD1 reveals how the adopted conformation of the flexible loop drastically deviates depending on the bound state of the enzyme (apoenzyme, PDB code:1BHS; complex with steroid, PDB code: 1DHT; ternary complex with cofactor and estradiol, PDB code: 1FDT; inhibitor complexes, PDB code: 1I5R and 3HB5), whereas the remaining part of the enzyme stays conformationally virtually unchanged (Figure 5.2).

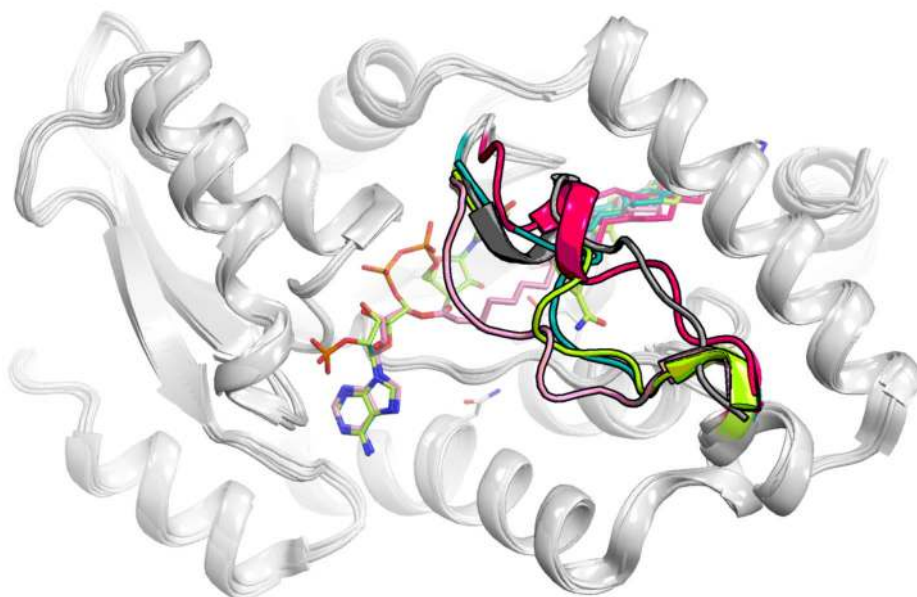


Figure 5.2: Superimposition of the five 17 β -HSD1 crystal structures selected for geometrical comparison. The residues 190-201 that comprise the flexible loop are displayed in gray for 1BHS, magenta for 1DHT, dark green for 1FDT, pink for 1I5R and in light green for 3HB5. The structurally conserved parts of the protein are colored in white. Ligands are displayed as stick models.

An analysis of the superimposition of the 17β -HSD1 apoenzyme (PDB code 1BHS [21]) with the DHT-enzyme complex in absence of the cofactor (PDB code 1DHT [50]) highlights that the hormone alone does not induce a large structural rearrangement of the flexible loop (Figure 5.3 A). However, it cannot be excluded that this conformational transition does not occur because DHT is not the preferred substrate of the enzyme. In fact, 17β -HSD1 prefers the oxidized form of estrogen as substrate. The comparison between the apoenzyme and the ternary E2-NADP⁺-enzyme complex (PDB code 1FDT [20]) reveals that, in the case of the latter complex, the flexible loop restricts the available space of the binding pocket due to a shift of maximally about 10 Å in distance (Figure 5.3 B). An analysis of the steroid binding pose reveals that the DHT molecule is slightly displaced and thus — in contrast to E2 — it does not establish interactions with Tyr155, a residue being part of the catalytic triad (Figure 5.3 A and C).

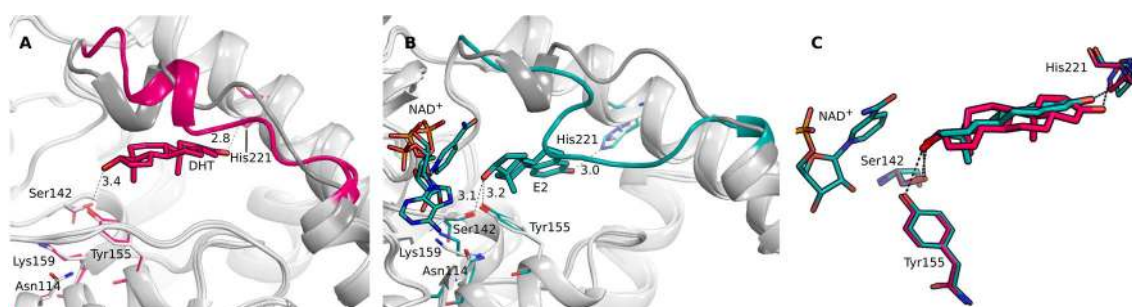


Figure 5.3: Superimposition of the 17β -HSD1 crystal structures. Cofactor, steroidal ligands and amino acids that are part of the catalytic tetrad (Asn114, Ser142, Tyr155 and Lys159) and that bind the steroids are shown as stick models. Portions of the enzymes that do not undergo significant conformational changes are colored in white. Distances are given in Å. **(A)** The flexible loop in the crystal structures of the apoenzyme (1BHS) is colored in gray and for 1DHT in magenta. The carbon atoms of DHT and of relevant amino acids of 1DHT are colored in dark pink. **(B)** The flexible loop in the crystal structures of the apoenzyme (1BHS) is colored in gray and for the complex with NADP⁺ and E2 (1FDT) in dark green. Carbon atoms of E2, NADP⁺ and of relevant amino acids in the structure of 1FDT are colored in dark green. **(C)** Close up view of the binding pocket of 17β -HSD1. The carbon atoms for 1DHT are colored in magenta and for 1FDT in dark green.

The finding that the loop undergoes a larger conformational rearrangement upon cofactor binding to the enzyme 17β -HSD1 is in accordance with our observations of similar properties of 17β -HSD14 (as discussed in Chapter 2). It seems unlikely that the deviating conformations of the flexible loop are caused by differences in crystal packing, since all three crystal structures occur in identical space group with very similar unit cell parameters.

As already mention earlier, no crystal structures of 17β -HSD1 in complex with a nonsteroidal inhibitor have been reported yet. In contrast, crystal structures of the enzyme in complex with steroidal inhibitors do exist. It is remarkable how chemically different inhibitors can

induce deviating conformational changes of the flexible loop. The enzyme-NADP⁺-steroidal inhibitor (E₂B) complex (PDB code 3HB5 [191], Figure 5.4) does not show significant differences compared to the enzyme-NADP⁺-E2 complex structure (PDB code 1FDT). Only a slight inhibitor-induced adaptation of the flexible loop is observed for the latter structure (Figure 5.5 A). In fact, the main steroidal part of the inhibitor is placed in an area where usually the steroids are bound (interacting with Ser142 and Tyr155 on the one side and with His 221 on the other side). However, the benzamide moiety induces a slight structural adjustment of the binding mode of the inhibitor; as a consequence, the interactions with His221 and Tyr155 are no longer established (Figure 5.5 C). In the crystal structure of the enzyme in complex with a chemically merged estradiol-adenosine hybrid inhibitor (EM1745) (PDB code 1I5R [192], Figure 5.4), the flexible loop is displaced by the aliphatic chain of the hybrid inhibitor and thus adopts a different geometry compared to the crystal structure of the enzyme-NADP⁺-E2 complex, 1FDT (Figure 5.5 B). However, the binding mode of the steroid core of the inhibitor is closely matching the one of E2 (Figure 5.5 D). This induced-fit behavior triggered by the inhibitor, at least with the presently studied ligands, is not observed for the 17 β -HSD14 enzyme, where a significant transition of the conformation of the flexible loop was only observed between the apo- and holoenzyme. The flexibility of the binding pocket observed for these enzymes is a clear obstacle for *in silico* studies, for instance ligand docking or selectivity studies following a correlation of the three-dimensional shape of the binding pocket and the bound potential ligand. It seems impossible to predict which ligand does and which one does not induce a structural rearrangement of the loop.

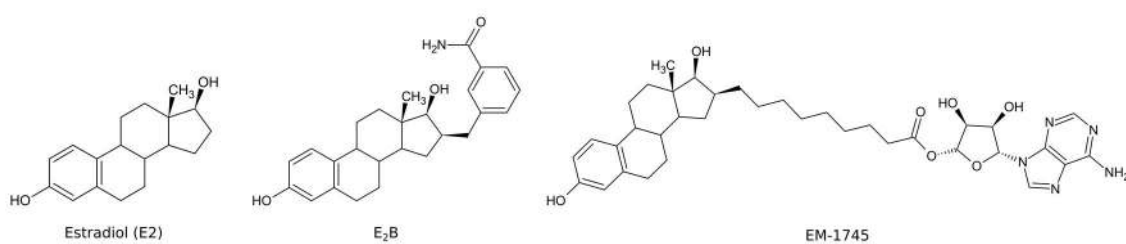


Figure 5.4: Structure of the ligands in complex of the 17 β -HSD1 enzyme.

The determined crystal structure of 17 β -HSD1 in complex with the cofactor NADP⁺ and E2 (PDB code 1FDT) allows a direct comparison with the crystal structure of 17 β -HSD14 in complex with the cofactor NAD⁺ and estrone (E1, PDB code 5HS6). The superimposition reveals a spatial conservation between the structures only in some regions (Figure 5.6 A). The calculated overall sequence identity is about 20% as determined by the program *Clustal Omega* [193–195].

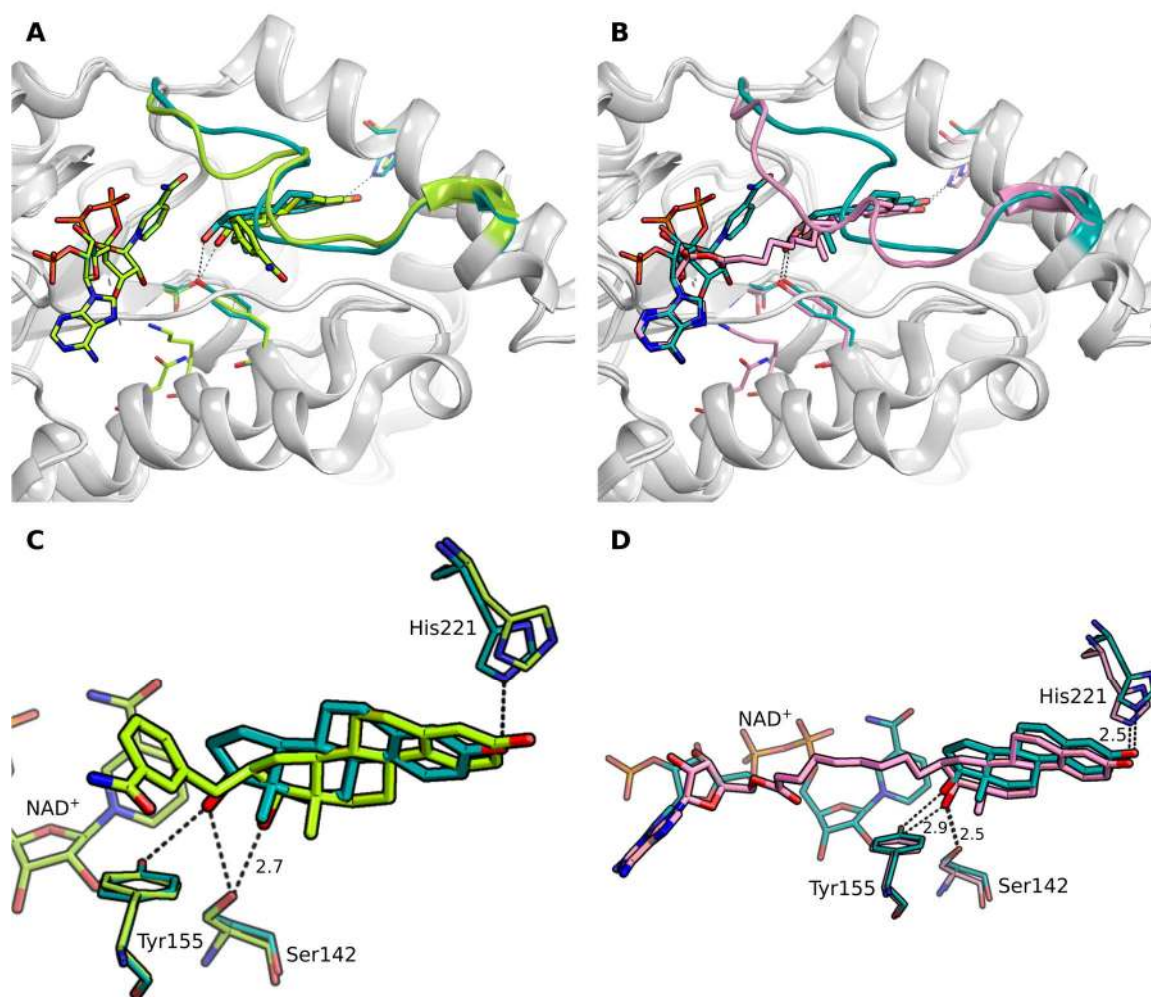


Figure 5.5: Superimposition of the 17β-HSD1 crystal structures. The macromolecules are shown as ribbon models. Cofactor, inhibitors and amino acids, that are part of the catalytic tetrad (Asn114, Ser142, Tyr155 and Lys159) and that bind the steroids, are shown as stick models. The portions of the enzymes that do not undergo conformational changes are colored in white. Distances are given in Å. **(A-B)** The flexible loop found in the crystal structure of 1FDT is colored in dark green, for that of 115R in light green and for 3HB5 in pink. **(C-D)** Close up view of the binding pocket of 17β-HSD1. The carbon atoms for E2 (PDB code 1FDT) are colored in dark green, for the steroid inhibitor (PDB code 3HB5) in light green and for the hybrid inhibitor (PDB code 115R) in pink.

The structure of 17β-HSD14 can be divided into two distinct regions. The first region consists of a Rossmann-fold motif that contains the cofactor binding site, whereas the second region is responsible for substrate recognition [32, 126, 127]. Small differences in the NAD⁺/NADP⁺ binding site can be experienced between type 14 and type 1 (RMSD of 1.6 Å based on an alignment of all C α atoms as calculated with *COOT* [171] and *fconv* [186]). This result comes not unexpected since both enzymes recognize different cofactors (NAD⁺ for 17β-HSD14 versus NADP⁺ for 17β-HSD1). The flexible loop of 17β-HSD1 restricts the outer

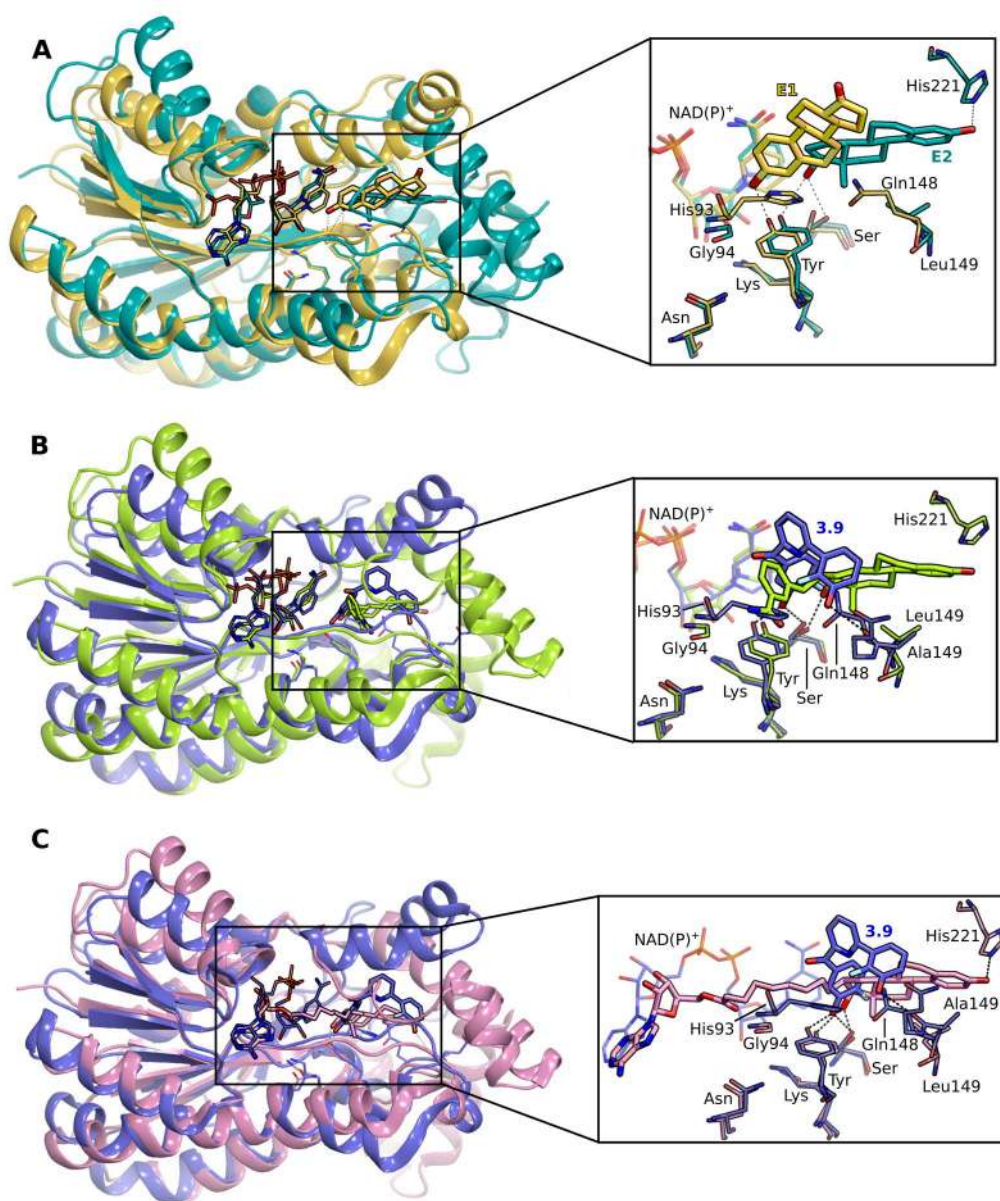


Figure 5.6: Superimposition of the crystal structures of 17 β -HSD14 and 17 β -HSD1. The protein structures are shown as ribbon models. The steroids, cofactors, inhibitors and key amino acids (His93, Asn114, Ser141, Gln148, Ala149, Tyr154 and Lys158 for 17 β -HSD14; Gly94, Asn114, Ser142, Leu149, Tyr155, Lys159 and His 221 for 17 β -HSD1), are shown as stick models. H-bonds are depicted as black dotted lines. Distances are given in Å. **(A)** Superimposition of 17 β -HSD1 (dark green, PDB code 1FDT) and 17 β -HSD14 (yellow, PDB code 5HS6) as ternary complexes and close-up view of the superimposed substrate in the binding pocket. The carbon atoms of E1 in complex with 17 β -HSD14 are colored in yellow and the carbon atoms of E2 in complex with 17 β -HSD1 are colored in dark green. **(B)** Superimposition of 17 β -HSD1 (light green, PDB code 3HB5) and 17 β -HSD14 (purple, PDB code 5L7Y) as ternary complexes with compound **3.9** and close-up view of the superimposed inhibitors in the binding pocket. The carbon atoms of **3.9** in complex with 17 β -HSD14 are colored in purple and the carbon atoms of the steroidal inhibitor in complex with 17 β -HSD1 are colored in light green. **(C)** Superimposition of 17 β -HSD1 (pink, PDB code: 1I5R) and 17 β -HSD14 (purple, PDB code 5L7Y) as ternary complexes with compound **3.9** and close-up view of the superimposed inhibitors in the binding pocket. The carbon atoms of the hybrid steroidal inhibitor in complex with 17 β -HSD1 are colored in pink.

part of the binding pocket resulting in a smaller volume of the latter one, whereas the corresponding loop in 17 β -HSD14 leaves one side of the binding pocket widely open. Furthermore, while the catalytic triad is conserved in both enzymes, the steroids adopt different orientations in the binding sites and thus establish deviating interactions. Another difference is that in E2 is stabilized by the Ser142 and Tyr155 on one side and by His221 on the other side in 17 β -HSD1. This double stabilization could not be seen in the structure of 17 β -HSD14 as the histidine residue is not present in this region of the binding pocket and E1 is interacting only with Tyr154 (Figure 5.6 A). The superimposition of the ternary complex structures of 17 β -HSD14 (PDB code 5L7Y [127]) and 17 β -HSD1 (PDB codes 3HB5 and 1I5R) highlights further differences between the protein structures. For example, the C-terminal portion of 17 β -HSD1 is folded in term of two α -helices that enclose the active cleft. This stands in contrast to the other three enzyme structures (17 β -HSD8, 17 β -HSD10 and 17 β -HSD14), where the C-terminal tail does not adopt any ordered secondary structural element, and in case of 17 β -HSD14 it is involved in interactions between two monomers. While the inhibitors in 17 β -HSD14 adopt a V-like shape in order to properly fit into the binding pocket, inhibitors of 17 β -HSD1 adopt a rather planar binding pose (Figure 5.6 B-C). The V-like shape of the 17 β -HSD14 binding pocket is determined by the two amino acids His93 and Gln148, which are not present in 17 β -HSD1. Instead, in the latter enzyme their positions are occupied by Gly94 and Leu149, respectively. In addition, His93 and Gln148 are also decreasing the hydrophobicity of the binding pocket. It can be expected that designing inhibitors that match with the given three-dimensional requirement of 17 β -HSD14 and that optionally address His93 and/or Gln148 should result in a larger selectivity discriminating with respect to 17 β -HSD1. The superimposition of the enzyme in complex with E1 and with inhibitor 3.9 (Chapter 3) reveals how His93 and Gln148 need to rotate slightly in order to accommodate the different ligands (Figure 5.7). This fact supports the hypothesis that the latter residues are potentially responsible for the substrate selectivity of this enzyme.

5.3 Comparison of the structures of 17 β -HSD8, 17 β -HSD10 and 17 β -HSD14

In contrast to the plethora of structures determined for 17 β -HSD14 and 17 β -HSD1, only few are published for 17 β -HSD8 and 17 β -HSD10. Thus, it is difficult to perform the same analysis of the flexible loop for the latter two enzymes as performed for 17 β -HSD14 and 17 β -HSD1 (*vide supra*). Only one structure where the loop is fully determined is available for either 17 β -HSD8 or 17 β -HSD10.

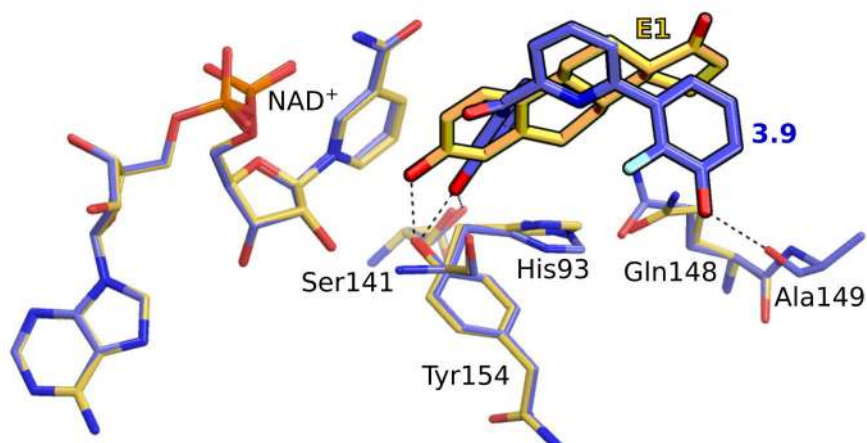


Figure 5.7: Close-up view of the binding mode of the ligands of the superimposed 17 β -HSD14 complexes. The cofactors, inhibitor **3.9** and amino acids are shown as stick models. Carbon atoms of the inhibitor-complex structure (PDB code 5L7Y) are colored in purple and for 5HS6 in yellow. H-bonds are depicted as black dotted lines and labeled with their distances in Å.

A structural comparison between the cofactor binding site of human 17 β -HSD14 (PDB code 5L7Y [127]), 17 β -HSD8 (PDB code 2PD6, unpublished results) and 17 β -HSD10 (PDB code 1U7T [94]) reveals how the overall geometry of the cofactor binding pocket is maintained in the three proteins. In the crystal structures of 17 β -HSD14, 17 β -HSD8 and 17 β -HSD10 the geometry of the bound cofactor within the pocket is almost identical, with RMSD values of 0.5 Å and 0.6 Å, respectively (relative to 17 β -HSD14, calculated with fconv [186]). The substrate binding site is deviating very much in amino acid composition for each protein, in contrast to the cofactor binding site, even though the position of the catalytic triad and Asp114 (number refers to 17 β -HSD14) is preserved in all three enzymes. The flexible loops of 17 β -HSD8 and 17 β -HSD10 have approximately similar size, but are shorter than in 17 β -HSD14 (Figure 5.8). Nevertheless, the resulting substrate binding pockets are of similar volume and shape, narrow in the proximity of the catalytic triad and open and solvent exposed on the other side. Consequently, the inhibitors occupy almost the same area in types 14 and 10. However, 17 β -HSD10 has an additional solvent exposed loop between β D and α E (Figure 5.8 B). A close comparison of the binding pockets reveal that the catalytic tetrad, consisting of Asn-Ser-Tyr-Lys, is perfectly conserved in all three enzymes. However, 17 β -HSD8 and 17 β -HSD10 share a common Gln (166 and 165, respectively), whereas the position of this Gln is occupied by His93 and Gln148 in the case of 17 β -HSD14. The different arrangement of the amino acids results in an overall flatter binding pocket for 17 β -HSD8 and 17 β -HSD10 compared to the one of 17 β -HSD14 (Figure 5.9). In conclusion, in order to achieve a sufficient selectivity toward 17 β -HSD14, spatially demanding inhibitors, potentially

interacting with His93 and Gln148, are probably preferred by the latter enzyme compared to 17 β -HSD8 and 17 β -HSD10.

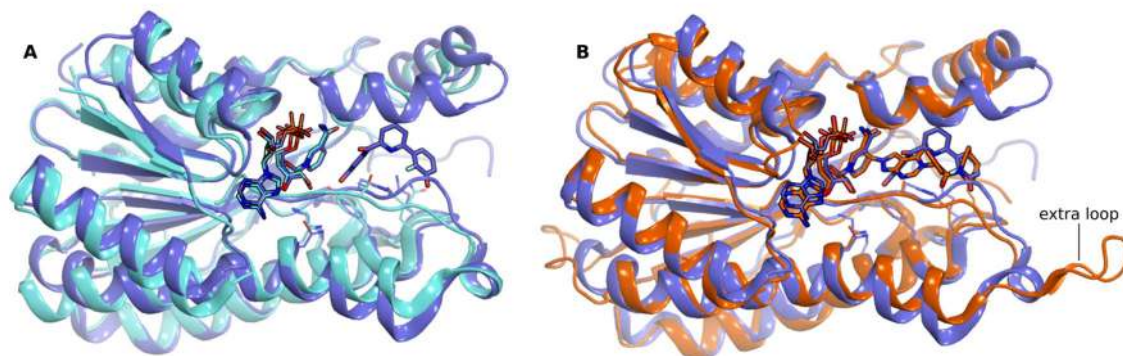


Figure 5.8: Superimposition of 17 β -HSD14 (purple, PDB code 5L7Y), 17 β -HSD8 (cyan, PDB code 2PD6) and 17 β -HSD10 (orange, PDB code 1U7T). The proteins are shown as ribbon models. Ligands and cofactors are shown as stick models, their carbon atoms are colored in the color of the corresponding protein.

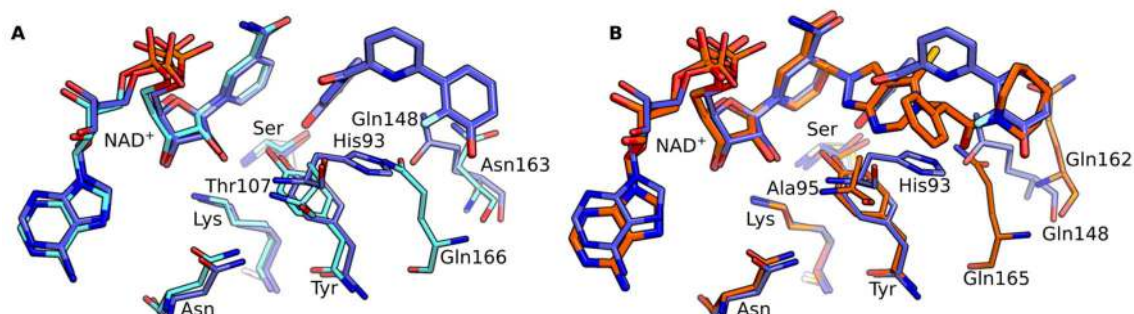


Figure 5.9: Close up view of the binding pocket in the superimposition of 17 β -HSD14 (purple, PDB code 5L7Y), 17 β -HSD8 (cyan, PDB code 2PD6) and 17 β -HSD10 (orange, PDB code 1U7T). The inhibitors, amino acids and cofactors are shown as stick models and their carbon atoms are shown with the same color as the corresponding protein structures (His93, Asn114, Ser141, Gln148, Tyr154 and Lys158 for 17 β -HSD14; Thr107, Asn127, Ser156, Asn163, Gln166, Tyr169 and Lys173 for 17 β -HSD8; Ala95, Asn121, Ser155, Asn163, Gln165, Tyr162 and Lys172 for 17 β -HSD10).

5.4 Docking studies with 17 β -HSD14

At the early stage of this study, a docking study with the program GOLD (Genetic Optimization for Ligand Docking) [196] was performed with the aim to rationally select ligands from a library of about 400 17 β -HSD1 and 17 β -HSD2 compounds for an initial *in vitro* screening. As the docking studies were performed before the crystals structures of 17 β -

HSD14 in complex with ligands had been determined the only reference that could be taken was the already published apo-structure (PDB code 1YDE [32]). Several issues had to be overcome to perform the docking study. For instance, identifying the best performing scoring function for this class of enzyme was not trivial as there were not published structures of 17 β -HSDs in complex with an inhibitor available to validate the docking attempts. Therefore, the docking performance was evaluated using 24 structures of the ternary complex of 11 β -HSD1. This enzyme had been selected due to the availability of the many crystal structures of the protein in complex with nonsteroidal inhibitors and due to its rough similarity with 17 β -HSD14. In fact, these two enzymes share the same tertiary structure (Rossmann-fold motif) and 22% of sequence identity (calculated with *COOT* [144, 171], based on the alignment of the C α atoms of PDB code 1YDE for 17 β -HSD14 and PDB code 1XU9 for 11 β -HSD1 [197]). Furthermore, their catalytic residues are conserved and the flexible loop shaping the binding pocket is approximately similar in size (Figure 5.10).

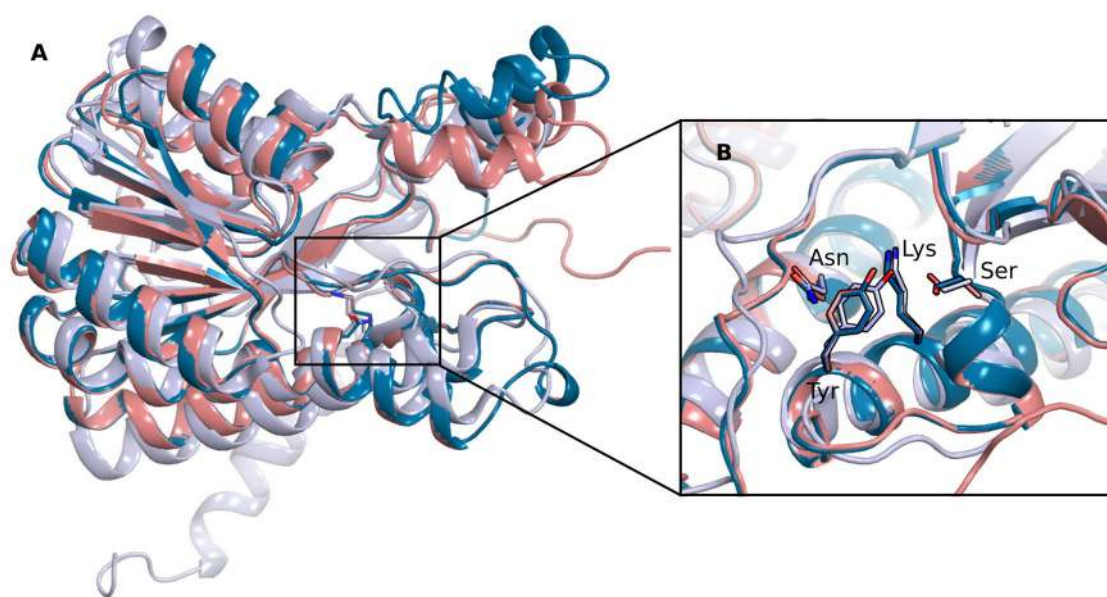


Figure 5.10: Superimposition of 17 β -HSD14 (open loop in blue and closed loop in salmon, PDB code 1YDE) and 11 β -HSD1 (light blue, PDB code 1XU7). The proteins are shown as ribbon model and the catalytic tetrad as stick model (Asn114, Ser141, Tyr154 and Lys158 for 17 β -HSD14; Asn143, Ser170, Tyr183 and Lys187 for 11 β -HSD1). **(A)** Overview of the tertiary structures. **(B)** Close-up view of the catalytic residues.

To evaluate the four scoring functions of *GOLD* (*GoldScore*, *ChemScore*, *ASP* and *CHEMPLP*) and to elucidate which of them performs best with 17 β -HSD14, the inhibitors bound in the crystal structures of 11 β -HSD1 were first removed from the complex and then redocked into the respective binding pocket from where they had been removed.

Subsequently, every inhibitor was docked into the binding pockets of each of the individual 24 crystal structures of 11 β -HSD1 (cross-docking attempt). The docking was set in a way to generate only three poses for each ligand. A visual inspection of the docking results revealed that *ChemScore* and *CHEMPLP* produced the best fit of the ligands into the binding pocket and generated the closest binding pose with respect to the one observed in the crystal structures. Before the validated settings could be applied to 17 β -HSD14, a model of the enzyme in complex with its cofactor had to be generated with *MOE* [173]. The cofactor model was derived from the crystal structure of 17 β -HSD8 (PDB code 2PD6), the most similar enzyme to 17 β -HSD14 of this protein family. The NAD⁺ was manually inserted into the cofactor binding pocket followed by a minimization with *MOE* using the MMFF94X force-field. During minimization, protein atoms except for H atoms were kept rigid. The enzyme-cofactor model was generated using the monomer of the protein with the flexible loop in the open as well as in the closed conformation leading to two final models.

A preliminary study to dock E2 (the substrate of 17 β -HSD14) into the binding pocket was performed using both generated models. However, only the model with the open conformation resulted in a satisfying result. Therefore, the model with the loop in the open conformation was selected to proceed further with the simulation. To additionally refine the docking settings, a set of 15 molecules consisting of 5 active compounds and 10 decoys found by an initial enzymatic testing was docked into the model (Chapter 3). *ChemScore* ranked the 5 active compounds within the top 8 scored molecules and thereby confirmed that this scoring function performs best for this enzyme. Consequently, the model with the open loop conformation and *ChemScore*, as scoring function, were selected to perform the docking of the 400 entries from the 17 β -HSD1 and 17 β -HSD2 nonsteroidal inhibitor library. According to the visual inspection of the top 100 generated poses, 15 molecules were selected to be tested experimentally for their inhibitory activity against the enzyme 17 β -HSD14. Unfortunately, a reliable hit rate for this study could not be determined for two reasons: Firstly, only about half of the selected molecules were available for testing. Secondly, with successful determination of the crystal structure of 17 β -HSD14 it became obvious that only the closed conformation of the flexible loop is adopted upon ligand binding and not, as anticipated in this initial docking runs, the open conformation of the loop. Thus, all binding poses predicted by docking are significantly shifted relative to their binding poses in the crystal structure. This study shows the limitation of a virtual screening attempt for a rather flexible protein in the absence of crystal structures. Even if some of the ligands would be correctly selected, the results would be based, to some extent, on incorrect assumptions.

Chapter 6

X-ray Crystallographic Fragment Screening and Hit Optimization

Introductory remarks

A library of 96 fragments was assembled in the framework of the BMBF project Frag2Xtal. Protein expression and purification, crystallization experiments, soaking experiment and structure determination were designed and carry out by the author of this thesis. Part of the soaking experiments was performed by Lorena Zara under the supervision of the author of this thesis. The optimized ligands were designed by the author of this thesis in collaboration with Florian Braun. The synthesis of the optimized ligands and the determination of their binding affinity were performed by Florian Braun.

6.1 Introduction

Within the last decade, fragment-based lead discovery (FBLD) has become a promising approach for the discovery of new lead structures. Since fragments are significantly smaller (<300 Da) than typical ligands discovered in high-throughput screening (HTS) campaign — which focus on screening candidates usually comprising already drug-like properties particularly in term of size and molecular weight — fragments are smaller and weaker binding with respect to the interaction features provided by a binding pocket. Consequently, fragment screening usually results in a significantly higher hit rate than a HTS screening, and therefore a fragment library usually contain much less entries than HTS libraries to cover a large variety of chemical functional groups to map the properties of a protein binding site (~1000 entries of a fragment library compared to 100,000 up to millions entries for a HTS library) [198]. Hence, the design of a fragment library and its screening on a given target is also feasible in an academic setting which usually cannot afford the resources necessary for an HTS campaign. Fragments usually contain multiple heteroatoms and even though the affinity of fragments is low, the established interactions are usually of high quality and indicate the hot spots of binding. Therefore, fragment hits are good starting points for the further lead optimization [199]. Furthermore, since starting fragments are designed for low lipophilicity, also the resulting drug-like molecule will usually show lower lipophilic than an HTS hit giving rise to superior pharmacokinetic properties of the evolved lead candidates [200]. However, since the fragment can, due to its limited size, establish only a few interactions with the residues of the binding pocket of the target protein, fragments usually have a very low affinity. Thus, their successful identification is very challenging. The detection of fragment binders commonly follows a screening cascade, starting with a biophysical screening assay (e.g. SPR, NMR, thermal shift assay), and subsequently confirmed hits are characterized by X-ray crystallography. However, in a recent comprehensive case study [201, 202], it could be shown that the preselection of a on first sight promising subset of fragments by the biophysical assays followed by a subsequent crystallographic characterization misses a fairly large amount of putative crystallographic hits (nearly 50%), and does not even achieve the expected enrichment rate making the subsequent crystallographic analysis more efficient [198, 203, 204]. We therefore decide to perform the screening of the entire 96-entry *in-house* fragment library directly on protein crystals without application of any pre-filter on the target protein 17 β -HSD14. So far, the reported nonsteroidal 17 β -HSD14 inhibitors all comprise a very similar and highly lipophilic scaffold. Consequently, the discovery of a novel scaffold using a fragment-based lead discovery approach could result in the development of new lead candidates with improved physicochemical properties.

6.2 Results and Discussion

6.2.1 Crystallization and Soaking experiments

Crystals of 17 β -HSD14 as holoenzyme were used to perform the soaking experiments with the 96 fragment library. As described by Bertolotti *et al.* [126], in crystal of the apoenzyme two of the binding pockets of the assembled homotetramer are not available for binding, since they are occupied by the C-terminal tail of an adjacent monomer. Furthermore, due to the high concentration of the cofactor NAD⁺ present under physiological conditions, it is unlikely that the apo form of the enzyme is available in a significant concentration *in vivo*. Consequently, crystals of the enzyme-NAD⁺ complex display the more relevant system for the soaking experiments. In addition, the cubic symmetry space group (*I*23) of these crystals only requires data collection of 45° to achieve completeness, substantially speeding up data collection time and/or closing for collection of highly redundant dataset which will improve the electron density maps and thus facilitating the identification of which are often only bound fragments partially occupied. Since fragment cocktails have been reported to decrease hit rates [199], we decided to soak of the 96 fragments individually. The concentration of the fragment in the soaking solution and the soaking time were adjusted depending on how the exposed crystals tolerated the applied conditions.

High quality datasets of individual crystals exposed to the 96 fragments could be obtained. All datasets exhibit a resolution of at least 2.7 Å and are 99.9-100% complete. All solved crystal structures were initially refined with an automatic refinement pipeline [198] in order to reduce the phase error and thus improve the quality of the *F_o-F_c* difference electron density to facilitate fragment hit identification. After thorough visual inspection, two hits (**J6** and **J15**) were unequivocally identified in the electron density. Data processing and preliminary refinement statistics are found in Table 6.1.

6.2.2 Binding mode of the fragment hits

The superimposition of the crystal structures of the enzyme in complex with fragments **J6** and **J15** (chemical structures in Charts 6.1 and 6.2) reveals that these two ligands occupy different regions of the binding pocket (Figure 6.1). Fragment **J15** is found in close proximity to the catalytic triad with its carboxyl group in H-bonding distance to the sidechains of Tyr154 and Ser141, as well as to the sidechain of Tyr253' contributed by a symmetry related monomer of the functional tetramer (Figure 6.2). The hydroxyl group of **J15** is pointing toward Asn186, however, it is out of interaction distance. Surprisingly, fragment **J6** occupies a position remotely from the catalytic amino acids. The oxygen atoms of the 1,3-benzodioxole moiety of the latter fragment are within H-bonding distance to the sidechain of

Table 6.1. Data collection and refinement statistics.

	Complex with J6	Complex with J15
(A) Data collection and processing^a		
space group	I32	I32
unit cell parameters a, b, c (Å)	129.5, 129.5, 129.5	129.8, 129.8, 129.8
Matthews coefficient ^b (Å ³ /Da)	3.2	3.2
solvent content ^b (%)	61.1	61.3
(B) Diffraction data		
resolution range (Å)	50-2.25 (2.39–2.25)	50-2.47 (2.62–2.47)
unique reflections	17085 (2783)	13260 (2123)
R(<i>I</i>) _{sym} (%)	7.3 (50.1)	7.1 (50.5)
Wilson B factor (Å ²)	38.8	46.5
completeness (%)	98.5 (99.5)	100.0 (99.9)
redundancy	11.3 (11.2)	6.6 (6.6)
<I/σ(I)>	24.4 (4.7)	19.2(3.5)
(C) Refinement*		
resolution range (Å)	45.79-2.25	45.89-2.47
reflections used in refinement (work/free)	17085 (16230/855)	13260 (12597/663)
final R value for all reflections (work/free) (%)	0.16/0.19	0.16/0.21
protein residues	268	268
water molecules	85	13
RMSD from ideality: bond lengths (Å)	0.007	0.007
RMSD from ideality: bond angles (°)	0.840	0.868

^a Values in parenthesis describe the highest resolution shell. ^b Calculated with Matthews_coef program from CCP4 suite version 6.4.0.[132] *Preliminary data.

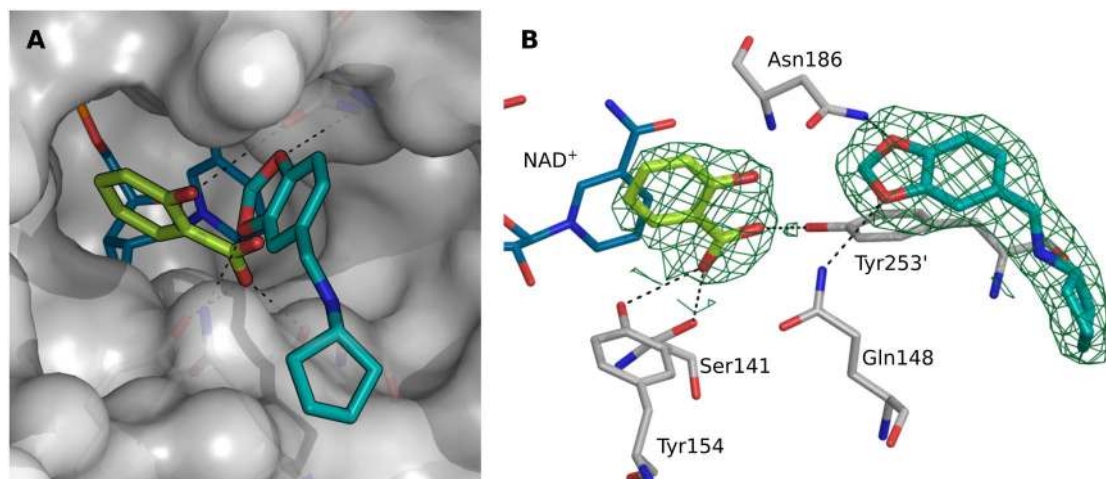


Figure 6.1: Close-up view of the binding pocket of 17β-HSD14. In both panels, the crystal structures of **J6** and **J15** are superimposed for comparison. Carbon atoms of **J6** are displayed in light blue, of **J15** in light green, and of NAD⁺ in dark blue. H-bond contacts are depicted as dashed lines. *F_o-F_c* difference electron density is shown as green mesh at a contour level of 3 σ. **(A)** The solvent-excluded surface of the protein is displayed in light gray. Inhibitors and cofactor are shown as stick models. **(B)** The amino acids involved in the binding of the fragments are shown as thin lines with C atoms in gray (hetero-atoms color coded).

Gln148 and Asn186. Furthermore, the secondary amino group establishes a hydrogen-bond interaction with the backbone carbonyl group of Tyr253' from the symmetry equivalent crystal mate being part of the functional tetramer (Figure 6.2 B).

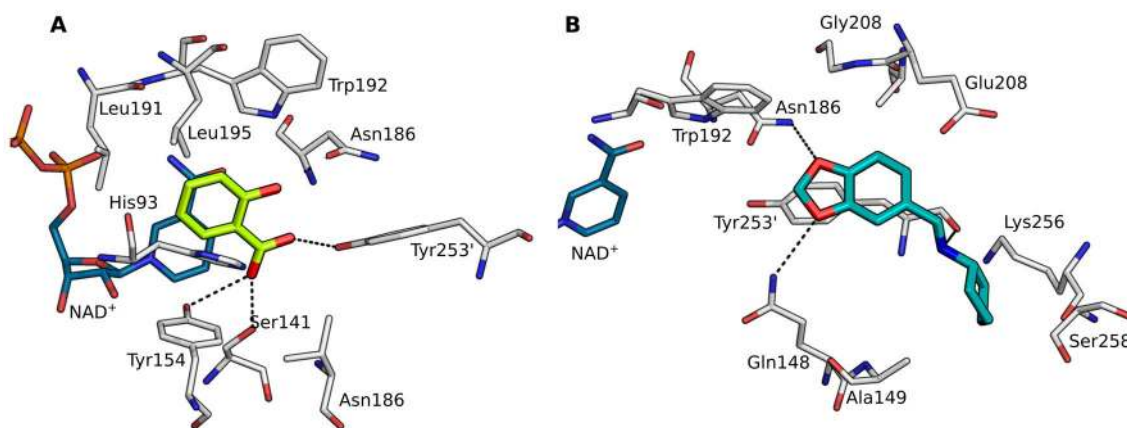


Figure 6.2: Crystal structures of 17 β -HSD14 in complex with cofactor NAD⁺ and (A) fragment **J6** and (B) fragment **J15**. Close-up view of the binding pocket. Carbon atoms of **J6** are shown in light blue, of **J15** in light green and of the cofactor NAD⁺ in blue. The inhibitors and cofactor NAD⁺ are shown as stick models. The amino acids within a distance of 4.6 Å are shown as thin stick models with carbon atom in white. H-bonds are depicted as dashed lines.

6.2.3 Fragment optimization applying fragment growing

After analysis of the crystal structures, we initiated a structure-based optimization of the discovered fragment hits with the goal to design a new lead inhibitor scaffold. The discovered fragments were decorated with different substituents in order to achieve additional interactions with the binding site and thereby increase binding affinity.

As a first step to optimize **J15** (Chart 6.1), we eliminated the hydroxyl group since the crystal structure revealed that this moiety does not establish any interaction to the protein. Furthermore, the hydroxyl group can potentially present a steric impediment for further synthetically optimization of the fragment hit. As a next step, moieties were attached to **6.1** with the aim to address the hydrophobic binding pocket of 17 β -HSD14 that is composed by Leu191, Trp192 and Leu195 (Figure 6.2). Two of the designed inhibitors (the pyridine **6.4** and the quinoline **6.6**) were modeled with MOE [173] into the crystal structure of 17 β -HSD14 applying the crystallographically determined binding mode of the scaffold of **J15** as a starting point. According to the derived models these compounds should theoretically fit nicely into the binding pocket (Figure 6.3). Therefore, **6.4**, **6.6** and the other four compounds (Chart 6.1) were synthesized.

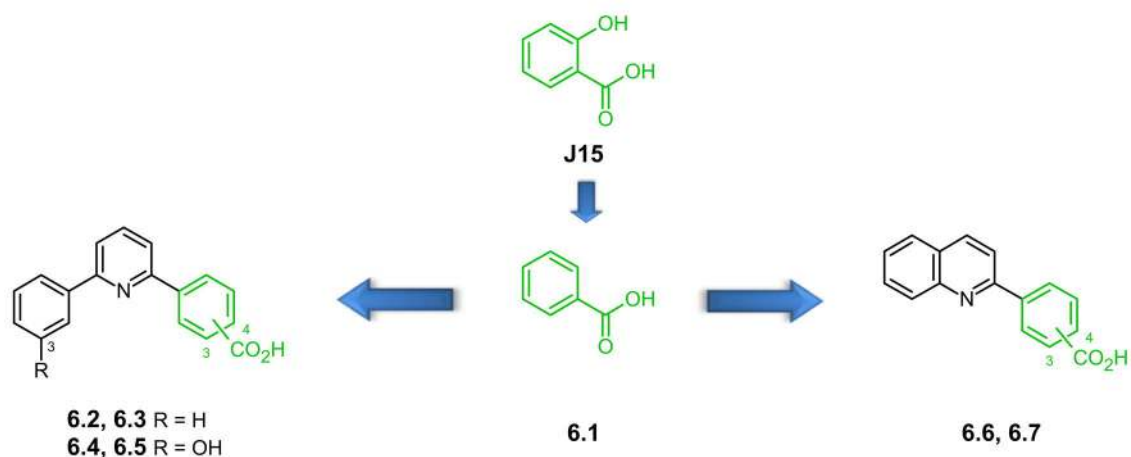


Chart 6.1: Fragment growing strategy for fragment **J15**.

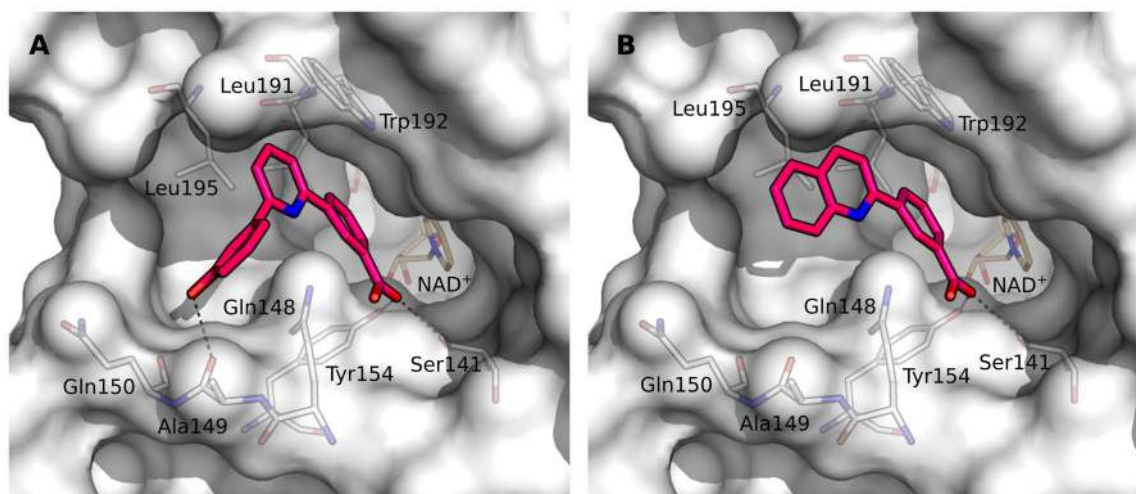


Figure 6.3: Modeled structures of 17 β -HSD14 in complex with compounds **6.4** (A) and **6.6** (B). The surface of the protein is displayed in gray. The inhibitors are shown as magenta stick models (hetero-atoms color-coded). Amino acids (white) and cofactor NAD⁺ (beige) are shown as thin stick models. H-bonds are depicted as black dotted lines.

The strategy for fragment growing of **J6** is displayed in Chart 6.2. The *N*-methylcyclopentanamine tail was removed from the compound since, according to the crystal structure, this moiety should not contribute significantly to the affinity as no pronounced interaction could be identified. Furthermore, removal of the moiety facilitated the synthesis of follow-up derivatives. Similar as in the case of **J15**, the designed inhibitors were first modeled into the crystal structure obtained with **J6** (Figure 6.4), and, since the modeled binding mode looked promising, compound **6.9** was subsequently synthesized.

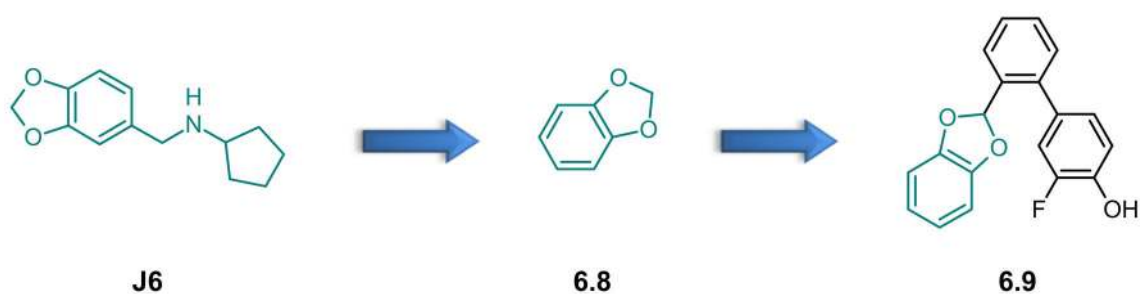


Chart 6.2: Fragment growing strategy for fragment **J6**.

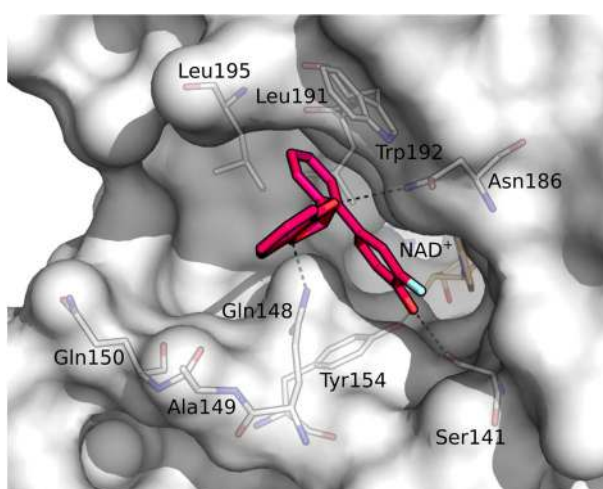


Figure 6.4: Modeled structure of 17 β -HSD14 in complex with compound **6.9**. The surface of the protein is displayed in gray. The inhibitor is shown in magenta as stick model with color-coded heteroatoms. Protein residues (white) and the cofactor NAD⁺ (beige) are shown as thin sticks. H-bonds are depicted as black dotted lines.

6.2.4 Fragment optimization applying fragment linking

Since fragments **J6** and **J15** occupy positions in the binding cleft of 17 β -HSD14 directly adjacent to each other, covalent linking of both fragments appeared as a feasible strategy to generate a new ligand with improved potency. However, covalent linking to two fragments is known to be a non-trivial and risky endeavor, since already small reinforced special changes either of the valence and torsion angles or even distances of the two fragments with respect to each other can partly or entirely diminish affinity of the generated compound. The trimmed fragments **J15** and **J6**, also used in our fragment growing strategy (**6.1** and **6.8**, respectively) were covalently connected via an ethyl linker to give compound **6.10** (Chart 6.3). Prior to synthesis, **6.10** was validated by modelling. Since the original fragment portions of the

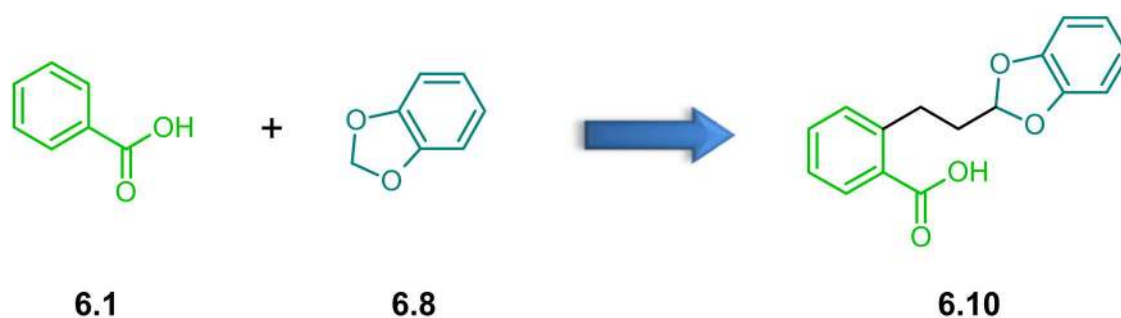


Chart 6.3: Fragment linking strategy for fragment **J6** and **J15**.

generated supermolecule maintained binding modes (Figure 6.5), the ligand was subsequently synthesized.

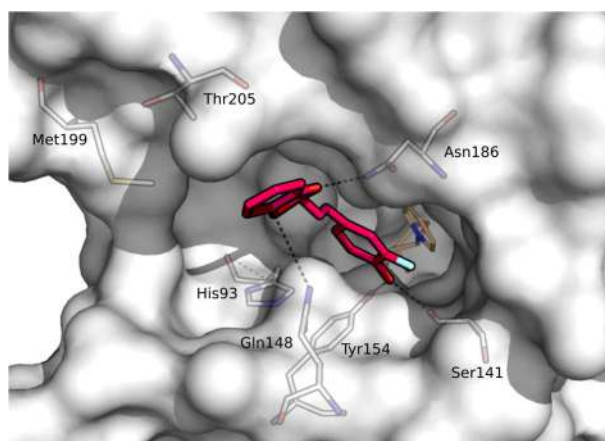
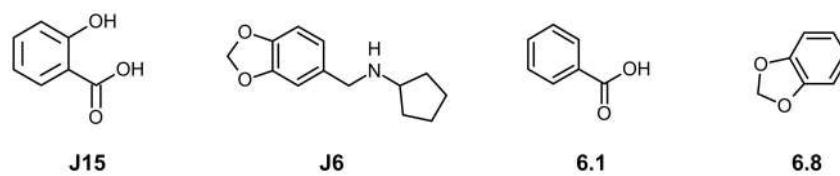


Figure 6.5: Modeled structure of 17 β -HSD14 in complex with compound **6.10**. The surface of the protein is displayed in gray. The inhibitor is shown in magenta as stick model with color-coded heteroatoms. Protein residues (white) and the cofactor NAD⁺ (beige) are shown as thin sticks. H-bonds are depicted as black dotted lines.

6.2.5 Inhibitory Activity validation

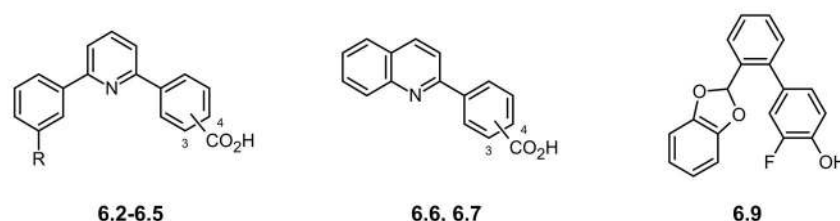
The original fragment hits **J6** and **J15** and the building blocks **6.1** and **6.8** were tested for their inhibitory activity against 17 β -HSD14. Even at high concentration of 250 μ M, all four molecules did not show any significant affinity to block the protein (Table 6.2). Most likely it would have been difficult to identify them in a biophysical screening cascade.

Table 6.2: 17 β -HSD14 binding constant (K_i) of the starting fragments.


Chemical structures of starting fragments: J15 (2-hydroxybenzoic acid), J6 (1-(2-(2,3-dihydrobenzofuran-5-yl)ethyl)pyrrolidine), 6.1 (benzoic acid), and 6.8 (2,3-dihydrobenzofuran).

17 β -HSD14	
compd.	(% Inh. @ 250 μ M) ^a
J15	16
J6	n.i.
6.1	n.i.
6.8	n.i.

Subsequently, also the newly synthesized, size-increased compounds were tested for their inhibitory activity against 17 β -HSD14. All compounds that resulted from fragment growing showed an improved affinity relative to the starting fragments. From the optimized fragments, compound **6.4** (derived from fragment **J15**) showed the highest affinity with a K_i of 1.9 μ M. The optimized compound starting from fragment **J6**, ligand **6.9**, also showed an improved in affinity toward the enzyme with 63% @ 100 μ M (Table 6.3). However, due to its poor solubility, it was impossible to determine its K_i value.

Table 6.3: 17 β -HSD14 binding constants (K_i) of the design compounds.


Chemical structures of design compounds: 6.2-6.5 (2-(4-R-phenyl)pyridin-5-yl)benzoic acid derivatives), 6.6, 6.7 (2-(4-CO₂H-phenyl)quinoline), and 6.9 (2-(2-(2,3-dihydrobenzofuran-5-yl)ethyl)pyrrolidine-1-yl)benzoic acid derivative).

compd.	R	Pos. CO ₂ H	17 β -HSD14	
			(% Inh. @ 250 μ M) ^a	K_i (μ M) ^a
6.2	H	3	76	8.7 \pm 0.8
6.4	OH	3	93	1.9 \pm 0.1
6.3	H	4	80	6.8 \pm 1.2
6.5	OH	4	83	4.8 \pm 1.0
6.6	-	3	86	8.1 \pm 0.8
6.7	-	4	92	7.0 \pm 0.5
6.9	-	-	63 @ 100 μ M	-

The generated compound **6.10** from the fragment linking strategy was identified to have an increased affinity compared to the individual starting fragments (Table 6.4). This is a very encouraging result since there are only a few examples of successful fragment linking in literature.

Table 6.4: 17 β -HSD14 binding constant (K_i) of the ligand designed by employing the fragment linking strategy.

17 β -HSD14		
compd.	(% Inh. @ 250 μ M) ^a	K_i (μ M) ^a
6.10	67%	17.6 \pm 0.5

6.2.6 Binding mode confirmation of the optimized compounds

To further validate the best compounds from each fragment optimization strategies, we co-crystallized them in complex with 17 β -HSD14 in order to confirm the predicted binding mode. Two crystal structures were determined and the data collection and refinement statistic are reported in Table 6.5.

Table 6.5. Data collection and refinement statistics.

^a	Complex with 6.4 ,	Complex with 6.10 ,
(A) Data collection and processing		
space group	I422	I422
unit cell parameters a, b, c (Å)	91.4, 91.4, 133.1	91.0, 91.0, 133.0
Matthews coefficient ^b (Å ³ /Da)	2.4	2.4
solvent content ^b (%)	49.2	49.4
(B) Diffraction data		
resolution range (Å)	50-1.62 (1.72–1.62)	50-2.08 (2.21–2.08)
unique reflections	36077 (5762)	17131 (2714)
R(I) _{sym} (%)	7.1 (49.8)	10.2 (50.9)
completeness (%)	99.9 (99.7)	99.9 (99.9)
redundancy	8.5 (8.5)	8.8 (9.2)
<1/ σ (I)>	18.9 (3.5)	17.0(4.2)
(C) Refinement*		
resolution range (Å)	39.90-1.62	46.22-2.08
reflections used in refinement (work/free)	36077 (34273/1804)	17131 (16274/857)
final R value for all reflections (work/free) (%)	0.13/0.16	0.19/0.21
protein residues	254	251
water molecules	126	48
RMSD from ideality: bond lengths (Å)	0.008	0.007
RMSD from ideality: bond angles (°)	0.994	0.818

^a Values in parenthesis describe the highest resolution shell. ^b Calculated with Matthews_coef program from CCP4 suite version 6.4.0.[132] *Preliminary data.

The superimposition of the crystal structures of the enzyme in complex with fragment **J15** and ligand **6.4** reveals that the benzoic acid moiety of the optimized ligand establishes the same interaction as fragment **J15** (Figure 6.6 A). In addition, the central pyridine moiety addresses the hydrophobic pocket composed by Leu191, Trp192 and Leu195 and its 3-OH

group is in H-bonding contact to the backbone carbonyl oxygens of Ala149 and Gln150. These additional interactions lead to a strong improvement in affinity of **6.4** compared to the starting fragment **J15**. Also the benzoic acid moiety of compound **6.10** (designed by fragment linking) adopts the same binding mode as in the crystal structure of **J15**. However, compared to fragment **J6**, the benzodioxole portion of **6.10** is shifted in space and accommodates the hydrophobic pocket composed of Leu191, Trp192, Leu195, Met199 and Thr205 (Figure 6.6 B).

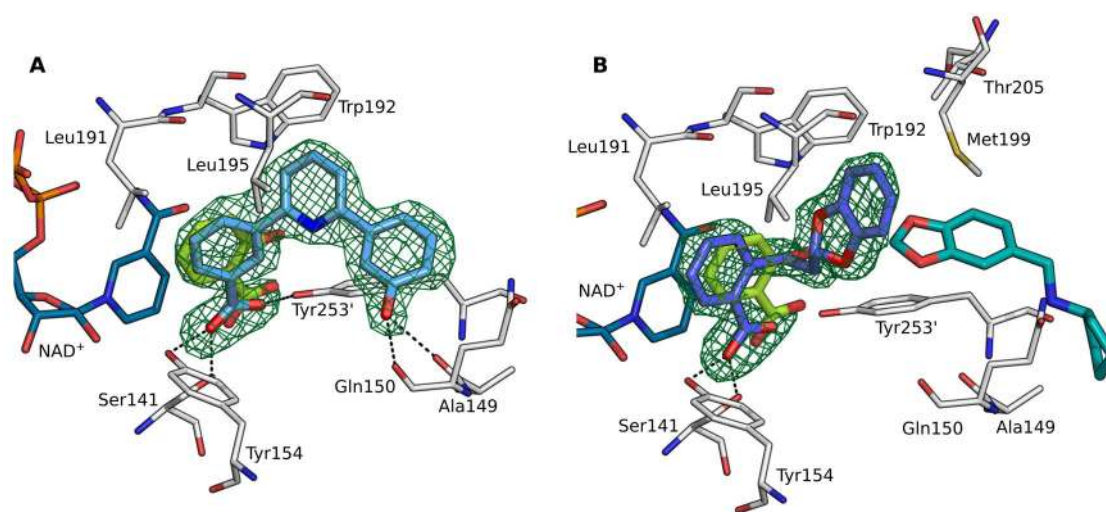


Figure 6.6: Superimposition of the crystal structures of 17 β -HSD14 in complex with cofactor NAD⁺ and fragment **J15** and **6.4** (A) and fragment **J15**, **J6** and **6.10** (B). A close-up view of the binding pocket is depicted. Carbon atoms of **J6** are shown in turquoise, of **J15** in light green, **6.4** in light blue, **6.10** in purple-blue, and of the cofactor NAD⁺ in dark blue. The inhibitors and cofactor NAD⁺ are shown as stick models. The amino acids within a distance of 4.6 Å are shown as thin stick models with carbon atom in white. H-bonds are depicted as dashed lines. *F_o-F_c* difference electron density is shown as green mesh at a contour level of 3 σ .

6.3 Conclusion and Outlook

From the sample of 96 candidate fragments screened against 17 β -HSD14, two fragments could be identified as hits in the electron density maps. Two different optimization strategy strategies (fragment growing and fragment linking) were employed for the development of new size-increased ligands with affinity against the enzyme. After computer-aided design of putative synthesis improved candidates, the most promising ones were synthesized and subsequently tested for their inhibitory activity against the target protein. All compounds that resulted from this fragment optimization proved to have enhanced affinities toward the enzyme compared to the original fragments that have been used as starting material.

Compounds **6.4** and **6.10** could be successfully crystallized in complex with 17 β -HSD14. Whereas the part from the starting fragment of compound **6.4** showed a conserved binding mode, the observed pose of **6.10** was only partially conserved as the benzodioxole moiety occupied a shifted position relative to its position found for the starting fragment **J6**. The shifted position of the benzodioxole moiety is possibly caused by the introduction of the ethyl linker and thus it is worthwhile to test linkers of deviating length and different chemical composition to find one that allows the benzodioxole moiety to adapt an orientation better matching that observed for fragment **J6**. In order to exclude that, besides the two fragments that have been clearly identified, any additional fragments are still bound to 17 β -HSD14 and have been overlooked due to insufficiently defined electron density, the *Fo-Fc* difference electron density maps should be reinspected applying the *PanDDA* program. The latter program enables a sharpening of the electron density features of a bound fragment and thereby facilitates its identification.

6.4 Experimental session

6.4.1 Enzyme expression and purification

The pure recombinant 17 β -HSD14 enzyme was obtained via heterologous expression as previously described [126, 127]. The protein purification was accomplished by two steps of affinity chromatography (Ni-NTA column) followed by size-exclusion chromatography. The stability of the protein was maintained by the addition of 0.6 mM cofactor NAD⁺ prior to our crystallization trials with the soaking technique. The purity was confirmed by SDS page.

6.4.2 Protein crystallization and soaking

The crystallization of 17 β -HSD14 in complex with cofactor NAD⁺ was carry out as already described [126]. In summary, 2 μ L of a solution containing 0.1 M HEPES and 3.3 M sodium formate, pH 7.00, was mixed with 2 μ L of the protein solution (9.5 mg/mL, T205), containing 0.6 mM NAD⁺. After growing for 2 weeks at 18°C, appropriated crystals were exposed for a time span of 1 min up to 20 hours to the soaking solution containing 0.2M NaCl, 0.1M HEPES set at pH 7.00, 17.5% PEG3350, 100-50 mM fragment with a final DMSO concentration of 10% and 25.0% PEG 400 as cryo-protectant. The crystals obtained were subsequently flash frozen in liquid nitrogen.

6.4.3 Co-crystallization of the protein with inhibitors

The co-crystallization of 17 β -HSD14 in complex with the different types of inhibitors was performed following the already described procedure [126, 127]. The final inhibitor concentration of 4 mM was incubated with the protein solution (9.5 mg/mL) containing 0.6 mM NAD⁺ and 5% DMSO for 30 minutes. The mixture was then centrifuged at 10000 g for 20 minutes in order to separate the precipitates. Afterwards, 2 μ L of the supernatant was mixed with 2 μ L of mother liquor composed of 0.1 M HEPES, 20% (w/v) PEG6000 and 5% (v/v) DMSO and adjusted to pH 7.0. Crystals of sufficient quality for data collection were grown at a temperature of 18°C for 10 days and then exposed for a few seconds to a cryo buffer solution obtained by the combination of mother liquor with the addition of 20% glucose and then flash-frozen in liquid nitrogen.

6.4.4 Data collection and processing

The data collection of crystals exposed to soaking trials with the 96 probe fragments and of the two co-crystallized inhibitor complexes was achieved at beamlines , Elettra beamline XRD1 in Trieste, Italy at a wavelength of 1Å and a temperature of 100 K on a Pilatus 2M pixel detector, ID23-1 beamline at the European Synchrotron Radiation Facility (ESRF) [140] in Grenoble, France at a wavelength of 0.97242 Å and a temperature of 100K on a silicon Pilatus 6M pixel detector, BL 14.1 operated by the Helmholtz-Zentrum Berlin (HZB) at the BESSY II electron storage ring (Berlin-Adlershof, Germany) [141] at a wavelength of 0.9184 Å and at a temperature of 100 K on a Pilatus 6M pixel detector and at beamline P13 at PETRA III (EMBL/DESY) in Hamburg, Germany, on a silicon Pilatus 6M pixel detector at a temperature of 100K. All datasets were indexed, processed and scaled with XDS [142].

6.4.5 Structure determination and refinement

All structures were determined by molecular replacement with the program PHASER MR [143] from the CCP4 suite [132]. The structure 5JS6 was used as a search model. In the refinement, a subset corresponding to 5% of all reflections were omitted during refinement and used for the calculation of R_{free} . Model building was achieved in COOT [144] and refinement using the PHENIX.refine version 1.10.1-2829 [145]. Ligand SMILE codes were created with *Molinspiration* v2014.11[146] and built as 3D-models with the Grade Web Server [147], which was also used for energetically minimization and restraint generation. Cartesian simulated annealing, applying default parameters, was used as a first refinement step. Subsequently, refinement of XYZ coordinates, occupancies and individual B-factors

were alternated with structural adaption in COOT [144] until the model was readily built and gave the best possible explanation of the electron density.

6.4.6 Inhibition of 17 β -HSD14

Inhibitory activities were evaluated with a fluorimetric assay as previously described [126, 127]. Briefly, the potential inhibitor was added in DMSO (final DMSO concentration in assay: 1%) to a mixture of NAD⁺ (1.2 mM) and estradiol (32 μ M) in 100 mM phosphate buffer pH 8, and the enzymatic reaction was started with the addition of the purified enzyme (1 mg/ml). The production of the fluorescent NADH formed was measured continuously for 15 min on a Saphir Tecan2. A linear relationship between product formation and reaction time was obtained and the slope of the progress curves was determined by linear regression. The K_i values were calculated by means of the Morrison equation using the procedure detailed by Copeland [167] as previously described.[127] The fitting and data analysis were performed using GraphPad Prism 7.

6.4.7 MOE models

The inhibitors **6.2-6.7** and **6.9-6.10** were modeled inside the crystal structure of the protein in complex with **J15** and minimized with MOE [173]. During minimization, the AMBER12 force field was applied. The heavy atoms of the protein and the oxygen atom of the carboxylic acid group of the inhibitors involved in H-bond to Tyr154 were kept fix. In order to give to the ligand sufficient freedom to move also the residues His93, Gln148 and Met199 were allowed to move unrestrictedly during minimization.

Chapter 7

Discussion and Conclusions

17 β -Hydroxysteroid dehydrogenase type 14 (17 β -HSD14, retSDR3 or SDR47C1) is the latest subtype of 17 β -HSD (belonging to the SDR family) that has been identified [32]. This enzyme oxidizes the hydroxyl group at position 17 of estradiol (E2) and 5-androstenediol (5-diol) under the presence of NAD⁺ as cofactor *in vitro*. The cDNA of the corresponding gene, called DHRS10, was originally isolated from retina epithelium. Two variants of this cytosolic protein exist: S205 and S205T. So far, the protein has not been thoroughly investigated in detail and its physiological role remains unknown.

Prior to this thesis, the 17 β -HSD14 apoenzyme (S205) had already been crystallized by Lukacik *et al.* [32]. The determined structure revealed a very broad and open active site, a cofactor binding domain for NAD⁺, and, characteristic for the SDR family, the conserved catalytic triad and the Rossmann-fold motif. Unfortunately, several amino acids from the flexible loops of some chains were not defined in the electron density, and none of the C-termini of the chains could be detected. It is impossible to derive information regarding a potential substrate from this crystal structure. Furthermore, due to the various conformations of the flexible loops, this crystal structure is poorly suited for docking studies. Therefore, the new structural determination of this protein alone as well as in complex with its cofactor and substrate was of utmost importance.

Chapter 2 reports the successful establishment of the expression and purification protocols to get high yield of pure recombinant 17 β -HSD14 protein. The thermal shift assay (TSA) was critical for the success of the protein purification, since it allowed the identification of a buffer that enhances the stability of the protein. Subsequently, the two enzyme isoforms (S205 and T205) were biochemically characterized. No difference between the catalytic actions of the two isoform could be evidenced. Employing extensive crystallographic screenings, it was possible to reproduce the structure of the apoenzyme with an even improved resolution by 0.9 Å compared to the reported value. The asymmetric unit of the determined apoenzyme structure is a homotetramer (the native form of the enzyme) and exhibits only two conformations of the flexible loops (segments α FG1 and α FG2) found in an either open (A2 dimer) or closed (B2 dimer) conformation. Next, the structures of the binary complexes (in complex with cofactor NAD⁺) of both protein isoforms (S205 and T205) were elucidated. No structural difference between the two isoforms could be recorded. However, these structures are different from the apoenzyme with respect to the flexible loop which adopts a unique closed conformation in the presence of NAD⁺. Binding of the cofactor appears to induce a shift of the flexible loop, which reduces the size of the active site and thereby produces the active conformation of the enzyme. The ternary complex of the enzyme with E1 (estrone) and NAD⁺ was also elucidated. The overall structure and the active-site geometry of the ternary and binary complex are very similar. Both have the flexible loop in the same closed conformation and the size of their active site is reduced by the C-terminal chain of the adjacent monomer (Tyr253'). E1, the product of the catalytic reaction, is found

to be bound to the active site in an atypical fashion with its A-ring positioned within van der Waals interaction distance to the nicotinamide moiety of the cofactor, whereas the carbonyl group of E1 in position 17 does not establish any interactions. In conclusion, a structural characterization of the protein in different binding state could be successfully achieved.

Enzyme inhibitors are useful tool compound to study the consequences of full enzyme inhibition *in vivo*. This could help to clarify whether this enzyme might be interesting as a new drug target for a certain disease. In addition, potent and selective inhibitors are also useful to address the selectivity issue with other 17 β -HSDs. As no inhibitor of 17 β -HSD14 has been reported prior to this study, the goal was to identify and optimize 17 β -HSD14 nonsteroidal inhibitors as well as to disclose their structure-activity relationship (SAR). **Chapter 3** describes the initially performed screen of a 17 β -HSD1 and 17 β -HSD2 inhibitors library against 17 β -HSD14, selected with respect to scaffold diversity. The most promising hit with respect to 17 β -HSD14 activity and selectivity toward 17 β -HSD1 and 17 β -HSD2 was taken as starting point for further chemical modification applying a ligand-based approach. Newly designed compounds were synthesized and subsequently tested for their 17 β -HSD14 inhibitory activity. The two best inhibitors identified in this study (**3.1** and **3.9**) had a very high affinity toward the enzyme with a K_i equal to 7 nM. Prior to this thesis, no human 17 β -HSD structures have been reported in complex with a nonsteroidal compound. Nevertheless, after an extensive crystallographic screening, the crystallization and structure determination of five crystal structures of the protein in ternary complex with its cofactor and different nonsteroidal inhibitors could be accomplished. The 3D-structures confirmed that the inhibitors bind to the substrate binding site. It was possible to rationalize the strong affinity of these inhibitors toward the enzyme by analysis of the molecular interactions stabilizing the inhibitor, especially the H-bond contact with catalytic Tyr154. In addition, the important role of an extended H-bond network in the stabilization process could be highlighted (Figure 7.1). The selectivity of the most potent compounds with respect to 17 β -HSD1 and 17 β -HSD2 could be addressed and **3.9** demonstrated to have also a good selectivity discrimination with respect to both related enzymes 17 β -HSD1 and 17 β -HSD2 (23% and 43% at 1 μ M, respectively). Taken together, the first potent nonsteroidal inhibitors with a good *in vitro* selectivity profile could be identified, and their structures in complex with the protein could be obtained. In the following, these results enabled a strong basis to pursue a structure-based optimization approach for the discovery of new class of 17 β -HSD14 inhibitors.

Chapter 4 describes two different structure-based strategies to optimized ligand **3.9** (Figure 7.2). The first structure-based modifications of the initial pyridine-based scaffold led to the ten-fold more potent compound **4.4** ($K_i = 1.5$ nM) compared to the initial **3.9** ($K_i = 13$ nM). However, even though all the newly synthesized pyridine-based inhibitors showed a high selectivity toward 17 β -HSD10, a less satisfactory selectivity profile toward 17 β -HSD1 and

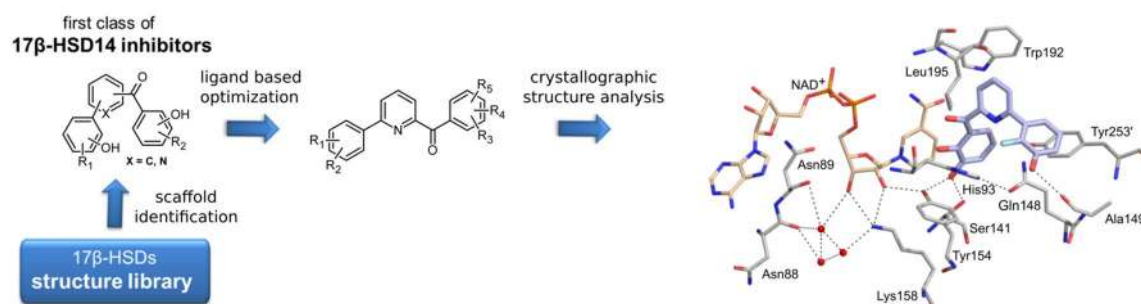


Figure 7.1: Schematic summary of Chapter 3. On the left, the preliminary screening of known 17 β -HSD14 inhibitors is shown leading to the first optimization candidates. On the right, the H-bond network stabilizes the inhibitor bound to the active site of 17 β -HSD14. Carbon atoms of the inhibitor are colored in gray and displayed as sticks. Protein residues involved in establishing the H-bonding network and the cofactor NAD⁺ (beige) are shown as thin sticks. H-bond interactions are depicted as dotted lines. Water molecules are shown as red spheres.

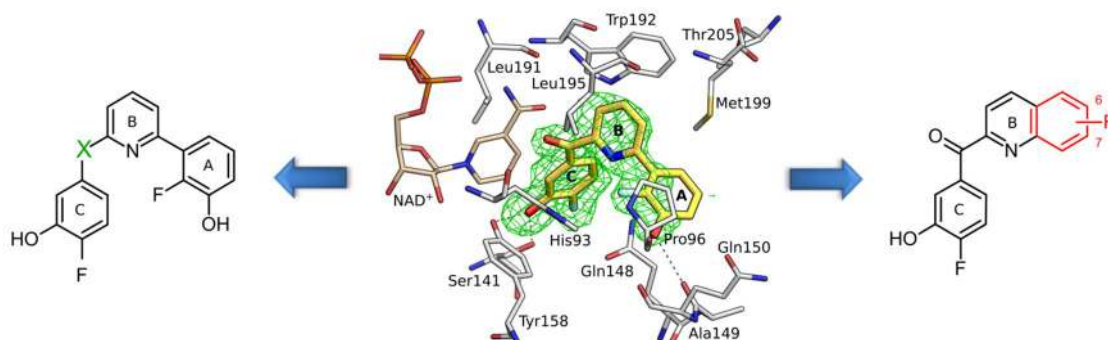


Figure 7.2: Schematic summary of Chapter 4. On the left and on the right, synthetic modifications scheme starting from the 2,6-pyridine ketone **3.9** are indicated. The image in the center shows a close-up view of the binding pocket of 17 β -HSD14 in complex with **3.9**. The inhibitor is shown as stick model with carbon atoms colored in yellow. Protein residues (white) and the cofactor NAD⁺ (beige) are shown as thin sticks. H-bond interactions are depicted as dotted lines. The F_0 - F_c difference electron density is shown as green mesh at a contour level of 3σ .

17 β -HSD2 was observed. The optimization of the cocrystallization conditions resulted in the determination of three new crystal structures of the inhibitor-enzyme complex. The analysis of the crystal structure of **4.4** in complex with the protein revealed how this ligand achieves its high affinity through a complementary geometry with the enzyme.

The goal of the second structure-based optimization strategy was to extend the central pyridine core to interact with the empty binding pocket adjacent to the A and B-ring. The designed quinoline-based inhibitors were first modelled into the crystal structure and, as the simulation suggested a good fit to the active site of the protein, they were subsequently synthesized. The predicted binding mode of **4.8** was confirmed by the co-crystal structure and, as anticipated, the very high potency ($K_i = 12$ nM) was subsequently determined by

biophysical characterization. Four co-crystal structures were obtained of the enzyme in complex with the quinoline-based inhibitors. Crystal structures of the protein-ligand complexes were prerequisite for understanding the inhibitor's SAR and for their further optimization. The determined crystal structures revealed how small chemical modifications of the inhibitor's substituents can affect the adopted binding mode. In fact, the deviating binding mode of **4.10** (that differs from **4.8** by only a single methyl group) did not result in a significant change of the binding affinity compared to **4.8** ($K_i = 6$ nM vs $K_i = 13$ nM, respectively). Surprisingly, the 3-OH group of the C-ring did not form a direct H-bond interaction with Tyr154 of the catalytic triad. Instead, it establishes an H-bond only with Ser141. Nevertheless, Tyr154 establishes an H-bonding contact through a bridging water molecule (**W6**) with the ligand's carbonyl linker. The fact that this water molecule is found in close proximity to the catalytic triad and that so far its position was found conserved in four structures, raises the question about a possible involvement in the catalytic mechanism.

The selectivity profile of three compounds (**4.12**, **4.13** and **4.15**) between 17 β -HSD14 and the three other proteins (17 β -HSD1, 17 β -HSD2, and 17 β -HSD10) was comparable to the selectivity profile of **3.9**. Thus, these four compounds exhibit the most favorable selectivity profile as well as the highest potency. In addition, **3.9**, **4.12**, **4.13** and **4.15** showed a very low cytotoxicity ($IG_{50} > 100$ μ M) and were not appointed either as substrates or as inhibitors of the multi-drug resistance protein Pgp, indicating that these compounds might not be efflux from the brain and at the same time the risk of potential side effects would be reduced. This suggests them as potent tool compounds for the further investigation of a putative *in vivo* administration to get insights into the physiological role of 17 β -HSD14.

In **Chapter 5**, a structural comparison with the aim to rationally explain the selectivity profiles of the ligands between 17 β -HSD14 and other 17 β -HSDs was conducted. The superimposition based on the C α coordinates of the crystal structures of 17 β -HSD1 reveals how the adopted conformation of the flexible loop drastically deviates depending on the bound state of the enzyme. Furthermore, the comparison revealed that different inhibitor classes induce different conformational geometries for this protein region. The variable character of the flexible loop is also observed for 17 β -HSD14. As only one crystal structure for 17 β -HSD8 and 17 β -HSD10 has been published yet, it is difficult to perform the same analysis of the flexible loop for the latter two enzymes. The typical V-like shape of the binding pocket of 17 β -HSD14 is determined by the two amino acids His93 and Gln148, which are not present in 17 β -HSD1, 17 β -HSD8 and 17 β -HSD10. In addition, the latter three enzymes also exhibit a rather flat binding pocket. In conclusion, it has to be expected that the design of inhibitors that match with the characteristically three-dimensional requirements of 17 β -HSD14 (and optionally address His93 and/or Gln148) should increase the selectivity toward the latter target. A docking study with the program GOLD (Genetic Optimization for Ligand Docking) [196] was performed with the aim to rationally select ligands for an initial

in vitro screening from a library of about 400 17 β -HSD1 and 17 β -HSD2 compounds. Despite a properly validated docking protocol and several attempts to dock ligands into 17 β -HSD14, the predicted binding modes of the ligands were in poor agreement with the later crystallographically determined binding modes due to the large flexibility of the binding pocket.

Chapter 6 describes a large fragment screening campaign by X-ray crystallography with the aim to discover new inhibitor scaffolds. The fragment screening library, developed by the Klebe group in collaboration with the structural biology group at the HZB, Berlin and consisting of 96 different fragments was subjected to crystals of 17 β -HSD14. The fragment screening resulted in the identification of two fragments that could be clearly identified in the electron density (**J6** and **J15**). However, no significant inhibitory activity against 17 β -HSD14 could be detected for these two fragments, likely due to very weak binding. Thus, besides examples already reported in literature, this result again proves that crystallographic fragment screening is a superior approach to identify binders compared to other biophysical screening methods. This is especially the case when the binding affinity of the fragment is very low. In addition to hit identification, crystallographic screening provides essential structural information about the binding mode of the ligand, which is an utmost prerequisite for their further structure-based optimization. Furthermore, the possibility of false positives can certainly be excluded when a clear electron density could be obtained. In order to enhance the affinity against the target of the two identified fragment hits, two strategies (fragment growing and fragment linking) have been applied. The new compounds were designed by computational modelling applying the crystallographically determined binding modes of the fragments as a basis, and subsequently synthesized, tested for their 17 β -HSD14 activity, and finally crystallized. This approach resulted in two newly designed ligands exhibiting a better affinity than the starting fragments.

In summary, both isoforms, S205 and T205, of 17 β -HSD14 were biochemically and structurally characterized and it resulted in four new crystal structures. The first two classes of inhibitor for this enzyme were discovered and the ligands were thoroughly profiled. In addition, the structures of 12 nonsteroidal inhibitors in complex with the protein were elucidated for the first time for this protein family. The fragment screening, after the determination of 96 structures, resulted in two fragment hits that were successfully optimized and it culminated in two more active inhibitors compared to their starting point.

Bibliography

- [1] Nussey S, Whitehead S (2001) *Principles of endocrinology. An Integrated Approach*. ed Publishers BS (BIOS Scientific Publishers, Oxford) Available at: <https://www.ncbi.nlm.nih.gov/books/NBK20/#A10>
- [2] Carr MC (2003) The Emergence of the Metabolic Syndrome with Menopause. *J Clin Endocrinol Metab* 88: 2404–2411.
- [3] Husen B, Huhtinen K, Poutanen M, Kangas L, Messinger J, Thole H (2006) Evaluation of inhibitors for 17 β -hydroxysteroid dehydrogenase type 1 in vivo in immunodeficient mice inoculated with MCF-7 cells stably expressing the recombinant human enzyme. *Mol Cell Endocrinol* 248: 109–113.
- [4] Weitzmann MN, Pacifici R, Parslow TG, Katz DR, Fuller K (2006) Estrogen deficiency and bone loss: an inflammatory tale. *J Clin Invest* 116: 1186–94.
- [5] Gunnarsson C, Hellqvist E, Stål O, Group2 and the SSBC (2005) 17beta-Hydroxysteroid dehydrogenases involved in local oestrogen synthesis have prognostic significance in breast cancer. *Br J Cancer* 92: 547–52.
- [6] Birge SJ (1997) The role of estrogen in the treatment of Alzheimer's disease. *Neurology* 48: 36–41.
- [7] Gillies GE, McArthur S (2010) Estrogen Actions in the Brain and the Basis for Differential Action in Men and Women: A Case for Sex-Specific Medicines. *Pharmacol Rev* 62. Available at: <http://pharmrev.aspetjournals.org/content/62/2/155.long>
- [8] Labrie F, Luu-The V, Lin S-XX, Simard J, Labrie C (2000) Role of 17 β -hydroxysteroid dehydrogenases in sex steroid formation in peripheral intracrine tissues. *Trends Endocrinol Metab* 11: 421–7.
- [9] Labrie F (1991) Intracrinology. *Mol Cell Endocrinol* 78: 113–18.
- [10] Poirier D (2003) Inhibitors of 17 β -hydroxysteroid dehydrogenases. *Curr Med Chem* 10: 453–77.
- [11] Lukacik P, Kavanagh KL, Oppermann U (2006) Structure and function of human 17 β -hydroxysteroid dehydrogenases. *Mol Cell Endocrinol* 248: 61–71.
- [12] Peltoketo H, Luu-The V, Simard J, Adamski J (1999) 17beta-hydroxysteroid dehydrogenase (HSD)/17-ketosteroid reductase (KSR) family; nomenclature and main characteristics of the 17HSD/KSR enzymes. *J Mol Endocrinol* 23: 1–11.

- [13] Labrie F, Luu-The V, Lin SX, Simard J, Labrie C, El-Alfy M, Pelletier G, Bélanger A (2000) Intracrinology: role of the family of 17 beta-hydroxysteroid dehydrogenases in human physiology and disease. *J Mol Endocrinol* 25: 1–16.
- [14] Gargano EM (2015) Development of 17 β -Hydroxysteroid Dehydrogenase Type 2 and Type 1 Inhibitors for the Treatment of Osteoporosis and Estrogen Dependent Diseases. Dissertation (Universität des Saarlandes).
- [15] Jörnvall H, Persson B, Krook M, Atrian S, González-Duarte R, Jeffery J, Ghosh D (1995) Short-chain dehydrogenases/reductases (SDR). *Biochemistry* 34: 6003–13.
- [16] Oppermann U, Filling C, Hult M, Shafqat N, Wu X, Lindh M, Shafqat J, Nordling E, Kallberg Y, Persson B, Jörnvall H (2003) Short-chain dehydrogenases/reductases (SDR): the 2002 update. *Chem Biol Interact* 143–144: 247–253.
- [17] Persson B, Kallberg Y (2013) Classification and nomenclature of the superfamily of short-chain dehydrogenases/reductases (SDRs). *Chem Biol Interact* 202: 111–5.
- [18] Moeller G, Adamski J (2006) Multifunctionality of human 17 β -hydroxysteroid dehydrogenases. *Mol Cell Endocrinol* 248: 47–55.
- [19] Puranen TJ, Poutanen MH, Peltoketo HE, Vihko PT, Vihko RK (1994) Site-directed mutagenesis of the putative active site of human 17 β -hydroxysteroid dehydrogenase type 1. *Biochem J* 304: 289–293.
- [20] Breton R, Housset D, Mazza C, Fontecilla-Camps JC (1996) The structure of a complex of human 17 β -hydroxysteroid dehydrogenase with estradiol and NADP⁺ identifies two principal targets for the design of inhibitors. *Structure* 4: 905–915.
- [21] Ghosh D, Pletnev VZ, Zhu DW, Wawrzak Z, Duax WL, Pangborn W, Labrie F, Lin SX (1995) Structure of human estrogenic 17 β -hydroxysteroid dehydrogenase at 2.20 Å resolution. *Structure* 3: 503–13.
- [22] Filling C, Berndt KD, Benach J, Knapp S, Prozorovski T, Nordling E, Ladenstein R, Jörnvall H, Oppermann U (2002) Critical Residues for Structure and Catalysis in Short-chain Dehydrogenases/Reductases. *J Biol Chem* 277: 25677–25684.
- [23] Hedlund J, Jörnvall H, Persson B (2010) Subdivision of the MDR superfamily of medium-chain dehydrogenases/reductases through iterative hidden Markov model refinement. *BMC Bioinformatics* 11: 534.
- [24] Negri M, Recanatini M, Hartmann RW, Kollman P, Case D (2010) Insights in 17 β -HSD1 Enzyme Kinetics and Ligand Binding by Dynamic Motion Investigation. *PLoS One* 5: e12026.
- [25] Penning TM (1996) 17 β -Hydroxysteroid dehydrogenase: inhibitors and inhibitor design. *Endocr Relat Cancer* 3: 41–56.
- [26] Penning TM (2011) Human hydroxysteroid dehydrogenases and pre-receptor regulation: Insights into inhibitor design and evaluation. *J Steroid Biochem Mol Biol* 125: 46–56.
- [27] Moeller G, Adamski J (2009) Integrated view on 17 β -hydroxysteroid dehydrogenases. *Mol Cell Endocrinol* 301: 7–19.
- [28] Meier M, Möller G, Adamski J (2009) Perspectives in Understanding the Role of Human 17 β -Hydroxysteroid Dehydrogenases in Health and Disease. *Ann N Y Acad Sci* 1155: 15–24.

- [29] Luu-The V (2001) Analysis and characteristics of multiple types of human 17 β -hydroxysteroid dehydrogenase. *J Steroid Biochem Mol Biol* 76: 143–151.
- [30] Haller F, Moman E, Hartmann RW, Adamski J, Mindnich R (2010) Molecular Framework of Steroid/Retinoid Discrimination in 17 β -Hydroxysteroid Dehydrogenase Type 1 and Photoreceptor-associated Retinol Dehydrogenase. *J Mol Biol* 399: 255–267.
- [31] Zhongyi S, Rantakari P, Lamminen T, Toppari J, Poutanen M (2007) Transgenic Male Mice Expressing Human Hydroxysteroid Dehydrogenase 2 Indicate a Role for the Enzyme Independent of Its Action on Sex Steroids. *Endocrinology* 148: 3827–3836.
- [32] Lukacik P, Keller B, Bunkoczi G, Kavanagh KL, Hwa Lee W, Adamski J, Oppermann U, Lee WH, Hwa Lee W, Adamski J, Oppermann U (2007) Structural and biochemical characterization of human orphan DHRS10 reveals a novel cytosolic enzyme with steroid dehydrogenase activity. *Biochem J* 402: 419–427.
- [33] The PyMOL Molecular Graphics System, Version 1.7.x Schrödinger, LLC.
- [34] Marchais-Oberwinkler S, Henn C, Möller G, Klein T, Negri M, Oster A, Spadaro A, Werth R, Wetzel M, Xu K, Frotscher M, Hartmann RW, Adamski J (2011) 17 β -Hydroxysteroid dehydrogenases (17 β -HSDs) as therapeutic targets: Protein structures, functions, and recent progress in inhibitor development. *J Steroid Biochem Mol Biol* 125: 66–82.
- [35] Sivik T, Gunnarsson C, Fornander T, Nordenskjöld B, Skoog L, Stål O, Jansson A (2012) 17 β -Hydroxysteroid Dehydrogenase Type 14 Is a Predictive Marker for Tamoxifen Response in Oestrogen Receptor Positive Breast Cancer. *PLoS One* 7: e40568.
- [36] Jansson AK, Gunnarsson C, Cohen M, Sivik T, Stål O (2006) 17 β -Hydroxysteroid Dehydrogenase 14 Affects Estradiol Levels in Breast Cancer Cells and Is a Prognostic Marker in Estrogen Receptor-Positive Breast Cancer. *Cancer Res* 66: 11471–11477.
- [37] Sherbet DP, Papari-Zareei M, Khan N, Sharma KK, Brandmaier A, Rambally S, Chattopadhyay A, Andersson S, Agarwal AK, Auchus RJ (2007) Cofactors, redox state, and directional preferences of hydroxysteroid dehydrogenases. *Mol Cell Endocrinol* 265266: 83–88.
- [38] D Voet and J G Voet (1990) *Biochemistry* (Headington Hill Hall, New York)
- [39] Agarwal AK, Auchus RJ (2005) Minireview: Cellular Redox State Regulates Hydroxysteroid Dehydrogenase Activity and Intracellular Hormone Potency. *Endocrinology* 146: 2531–2538.
- [40] Jin J-Z, Lin S-X (1999) Human Estrogenic 17 β -Hydroxysteroid Dehydrogenase: Predominance of Estrone Reduction and Its Induction by NADPH. *Biochem Biophys Res Commun* 259: 489–493.
- [41] Duax WL, Pletnev V, Addlagatta A, Bruenn J, Weeks CM (2003) Rational Proteomics I. Fingerprint Identification and Cofactor Specificity in the Short-Chain Oxidoreductase (SCOR) Enzyme Family. *Proteins Struct Funct Genet* 53: 931–943.
- [42] Pletnev VZ, Weeks CM, Duax WL (2004) Rational proteomics II: Electrostatic nature of cofactor preference in the short-chain oxidoreductase (SCOR) enzyme family. *Proteins Struct Funct Bioinforma* 57: 294–301.

- [43] Mazza C, Breton R, Housset D, Fontecilla-Camps JC (1998) Unusual charge stabilization of NADP⁺ in 17 β -hydroxysteroid dehydrogenase. *J Biol Chem* 273: 8145–52.
- [44] Shi R, Lin S-X (2004) Cofactor hydrogen bonding onto the protein main chain is conserved in the short chain dehydrogenase/reductase family and contributes to nicotinamide orientation. *J Biol Chem* 279: 16778–16785.
- [45] Chen Z, Tsigelny I, Lee WR, Baker ME, Chang SH (1994) Adding a positive charge at residue 46 of *Drosophila* alcohol dehydrogenase increases cofactor specificity for NADP⁺. *FEBS Lett* 356: 81–85.
- [46] Scrutton NS, Berry A, Perham RN (1990) Redesign of the coenzyme specificity of a dehydrogenase by protein engineering. *Nature* 343: 38–43.
- [47] Lin SX, Yang F, Jin JZ, Breton R, Zhu DW, Luu-The V, Labrie F (1992) Subunit identity of the dimeric 17 β -hydroxysteroid dehydrogenase from human placenta. *J Biol Chem* 267: 16182–16187.
- [48] Luu-The V, Zhang Y, Poirier D, Labrie F (1995) Characteristics of human types 1, 2 and 3 17 β -hydroxysteroid dehydrogenase activities: oxidation/reduction and inhibition. *J Steroid Biochem Mol Biol* 55: 581–587.
- [49] Poutanen M, Miettinen M, Vihko R (1993) Differential estrogen substrate specificities for transiently expressed human placental 17 β -hydroxysteroid dehydrogenase and an endogenous enzyme expressed in cultured COS-m6 cells. *Endocrinology* 133: 2639–2644.
- [50] Han Q, Campbell RL, Gangloff A, Huang YW, Lin SX (2000) Dehydroepiandrosterone and dihydrotestosterone recognition by human estrogenic 17 β -hydroxysteroid dehydrogenase. C-18/c-19 steroid discrimination and enzyme-induced strain. *J Biol Chem* 275: 1105–1111.
- [51] Messinger J, Hirvelä L, Husen B, Kangas L, Koskimies P, Pentikäinen O, Saarenketo P, Thole H (2006) New inhibitors of 17 β -hydroxysteroid dehydrogenase type 1. *Mol Cell Endocrinol* 248: 192–198.
- [52] Brozic P, Lanisnik Risner T, Gobec S (2008) Inhibitors of 17 β -hydroxysteroid dehydrogenase type 1. *Curr Med Chem* 15: 137–150.
- [53] Bey E, Marchais-Oberwinkler S, Werth R, Negri M, Al-Soud YA, Kruchten P, Oster A, Frotscher M, Birk B, Hartmann RW (2008) Design, Synthesis, Biological Evaluation and Pharmacokinetics of Bis(hydroxyphenyl) substituted Azoles, Thiophenes, Benzenes, and Aza-Benzenes as Potent and Selective Nonsteroidal Inhibitors of 17 β -Hydroxysteroid Dehydrogenase Type 1 (17 β -HSD1). *J Med Chem* 51: 6725–6739.
- [54] Oster A, Klein T, Werth R, Kruchten P, Bey E, Negri M, Marchais-Oberwinkler S, Frotscher M, Hartmann RW (2010) Novel estrone mimetics with high 17 β -HSD1 inhibitory activity. *Bioorg Med Chem* 18: 3494–3505.
- [55] Hilborn E, Stål O, Jansson A (2017) Estrogen and androgen-converting enzymes 17 β -hydroxysteroid dehydrogenase and their involvement in cancer: with a special focus on 17 β -hydroxysteroid dehydrogenase type 1, 2, and breast cancer. *Oncotarget* 8: 30552–30562.
- [56] Miyoshi Y, Ando A, Shiba E, Taguchi T, Tamaki Y, Noguchi S (2001) Involvement of up-regulation of 17 β -hydroxysteroid dehydrogenase type 1 in maintenance of intratumoral high estradiol levels in postmenopausal breast cancers. *Int J Cancer* 94: 685–689.

- [57] Jansson A (2009) 17 β -hydroxysteroid dehydrogenase enzymes and breast cancer. *J Steroid Biochem Mol Biol* 114: 64–67.
- [58] Blomquist CH, Bonenfant M, McGinley DM, Posalaky Z, Lakatua DJ, Tuli-Puri S, Bealka DG, Tremblay Y (2002) Androgenic and estrogenic 17 β -hydroxysteroid dehydrogenase/17-ketosteroid reductase in human ovarian epithelial tumors: evidence for the type 1, 2 and 5 isoforms. *J Steroid Biochem Mol Biol* 81: 343–351.
- [59] Šmuc T, Pucelj MR, Šinkovec J, Husen B, Thole H, Rižner TL (2007) Expression analysis of the genes involved in estradiol and progesterone action in human ovarian endometriosis. *Gynecol Endocrinol* 23: 105–111.
- [60] Saloniemi T, Järvensivu P, Koskimies P, Jokela H, Lamminen T, Ghaem-Maghamsi S, Dina R, Damdimopoulou P, Mäkelä S, Perheentupa A, Kujari H, Brosens J, Poutanen M (2010) Novel Hydroxysteroid (17 β) Dehydrogenase 1 Inhibitors Reverse Estrogen-Induced Endometrial Hyperplasia in Transgenic Mice. *Am J Pathol* 176: 1443–1451.
- [61] Kasai T, Shozu M, Murakami K, Segawa T, Shinohara K, Nomura K, Inoue M (2004) Increased Expression of Type I 17 β -Hydroxysteroid Dehydrogenase Enhances *in Situ* Production of Estradiol in Uterine Leiomyoma. *J Clin Endocrinol Metab* 89: 5661–5668.
- [62] Vihko P, Herrala A, Härkönen P, Isomaa V, Kaija H, Kurkela R, Pulkka A (2006) Control of cell proliferation by steroids: The role of 17HSDs. *Mol Cell Endocrinol* 248: 141–148.
- [63] Vihko P, Herrala A, Härkönen P, Isomaa V, Kaija H, Kurkela R, Li Y, Patrikainen L, Pulkka A, Soronen P, Törn S (2005) Enzymes as modulators in malignant transformation. *J Steroid Biochem Mol Biol* 93: 277–283.
- [64] Azzi A, Rehse PH, Zhu D-W, Campbell RL, Labrie F, Lin S-X (1996) Crystal structure of human estrogenic 17 β -hydroxysteroid dehydrogenase complexed with 17 β -estradiol. *Nat Struct Mol Biol* 3: 665–668.
- [65] Laplante Y, Poirier D (2008) Proliferative effect of androst-4-ene-3,17-dione and its metabolites in the androgen-sensitive LNCaP cell line. *Steroids* 73: 266–271.
- [66] Moghrabi, Nabil and Andersson S (1998) 17 β -Hydroxysteroid Dehydrogenases: Physiological Roles in Health and Disease. *TEM* 7: 265–270.
- [67] Vicker N, Sharland CM, Heaton WB, Ramos Gonzalez AM, Bailey H V, Smith A, Springall JS, Day JM, Tutill HJ, Reed MJ, Purohit A, Potter BVL (2009) The design of novel 17 α -hydroxysteroid dehydrogenase type 3 inhibitors. *Mol Cell Endocrinol* 301: 259–265.
- [68] Koh E, Noda T, Kanaya J, Namiki M (2002) Differential expression of 17 β -hydroxysteroid dehydrogenase isozyme genes in prostate cancer and noncancer tissues. *Prostate* 53: 154–159.
- [69] Lin H-K, Jez JM, Schlegel BP, Peehl DM, Pachter JA, Penning TM (1997) Expression and Characterization of Recombinant Type 2 3 α -Hydroxysteroid Dehydrogenase (HSD) from Human Prostate: Demonstration of Bifunctional 3 α /17 β -HSD Activity and Cellular Distribution. *Mol Endocrinol* 11: 1971–1984.
- [70] Matsuura K, Shiraishi H, Hara A, Sato K, Deyashiki Y, Ninomiya M SS (1998) Identification of a Principal mRNA Species for Human 3 α -Hydroxysteroid Dehydrogenase Isoform

- (AKR1C3) That Exhibits High Prostaglandin D2 11-Ketoreductase Activity. *J Biochem* 124: 940–946.
- [71] Song D, Liu G, Luu-The V, Zhao D, Wang L, Zhang H, Xueling G, Li S, Désy L, Labrie F, Pelletier G (2006) Expression of aromatase and 17 β -hydroxysteroid dehydrogenase types 1, 7 and 12 in breast cancer An immunocytochemical study. *J Steroid Biochem Mol Biol* 101: 136–144.
- [72] Liu H, Robert A, Luu-The V (2005) Cloning and characterization of human form 2 type 7 17 β -hydroxysteroid dehydrogenase, a primarily 3 β -keto reductase and estrogen activating and androgen inactivating enzyme. *J Steroid Biochem Mol Biol* 94: 173–179.
- [73] Ohnesorg T, Keller B, Hrabé de Angelis M, Adamski J (2006) Transcriptional regulation of human and murine 17beta-hydroxysteroid dehydrogenase type-7 confers its participation in cholesterol biosynthesis. *J Mol Endocrinol* 37: 185–97.
- [74] Sakurai N, Miki Y, Suzuki T, Watanabe K, Narita T, Ando K, Yung TMCC, Aoki D, Sasano H, Handa H (2006) Systemic distribution and tissue localizations of human 17beta-hydroxysteroid dehydrogenase type 12. *J Steroid Biochem Mol Biol* 99: 174–181.
- [75] Moon Y-A, Horton JD (2003) Identification of two mammalian reductases involved in the two-carbon fatty acyl elongation cascade. *J Biol Chem* 278: 7335–7343.
- [76] Luu-The V, Tremblay P, Labrie F (2006) Characterization of Type 12 17 β -Hydroxysteroid Dehydrogenase, an Isoform of Type 3 17 β -Hydroxysteroid Dehydrogenase Responsible for Estradiol Formation in Women. *Mol Endocrinol* 20: 437–443.
- [77] Liu S, Huang C, Li D, Ren W, Zhang H, Qi M, Li X, Yu L (2007) Molecular cloning and expression analysis of a new gene for short- chain dehydrogenase/reductase 9. *Acta Biochim Plonica Commun* 54: 213–218.
- [78] Su W, Wang Y, Jia X, Wu W, Li L, Tian X, Li S, Wang C, Xu H, Cao J, Han Q, Xu S, Chen Y, Zhong Y, Zhang X, Liu P, Gustafsson J-A, Guan Y (2014) Comparative proteomic study reveals 17 β -HSD13 as a pathogenic protein in nonalcoholic fatty liver disease. *Proc Natl Acad Sci* 111: 11437–11442.
- [79] Casey ML, MacDonald PC, Andersson S (1994) 17 β -Hydroxysteroid dehydrogenase type 2: chromosomal assignment and progestin regulation of gene expression in human endometrium. *J Clin Invest* 94: 2135–2141.
- [80] Moghrabi N, Head JR, Andersson S (1997) Cell Type-Specific Expression of 17 β -Hydroxysteroid Dehydrogenase Type 2 in Human Placenta and Fetal Liver. *J Clin Endocrinol Metab* 82: 3872–3878.
- [81] Mustonen M V, Poutanen MH, Kellokumpu S, de Launoit Y, Isomaa V V, Vihko RK, Vihko PT (1998) Mouse 17 β -hydroxysteroid dehydrogenase type 2 mRNA is predominantly expressed in hepatocytes and in surface epithelial cells of the gastrointestinal and urinary tracts. *J Mol Endocrinol* 20: 67–74.
- [82] Mustonen M, Poutanen M, Chotteau-Lelievre A, De Launoit Y, Isomaa V, Vainio S, Vihko R, Vihko P (1997) Ontogeny of 17 β -hydroxysteroid dehydrogenase type 2 mRNA expression in the developing mouse placenta and fetus. *Mol Cell Endocrinol* 134: 33–40.

- [83] Poirier D, Bydal P, Tremblay MR, Sam K-M, Luu-The V (2001) Inhibitors of type II 17 β -hydroxysteroid dehydrogenase. *Mol Cell Endocrinol* 171: 119–128.
- [84] Day J. M., Tutill H. J. PA (2010) 17 β -Hydroxysteroid dehydrogenase inhibitors. *Minerva Endocrinol* 35: 87–108.
- [85] Felson DT, Zhang Y, Hannan MT, Kiel DP, Wilson P, Anderson JJ (1993) The Effect of Postmenopausal Estrogen Therapy on Bone Density in Elderly Women. *N Engl J Med* 329: 1141–1146.
- [86] Chen C-L, Weiss NS, Newcomb P, Barlow W, White E (2002) Hormone Replacement Therapy in Relation to Breast Cancer. *JAMA* 287: 734.
- [87] Gargano EM, Allegretta G, Perspicace E, Carotti A, Van Koppen C, Frotscher M, Marchais-Oberwinkler S, Hartmann RW (2015) 17 β -Hydroxysteroid Dehydrogenase Type 2 Inhibition: Discovery of Selective and Metabolically Stable Compounds Inhibiting Both the Human Enzyme and Its Murine Ortholog. *PLoS One* 10: e0134754.
- [88] Spadaro A, Negri M, Marchais-Oberwinkler S, Bey E, Frotscher M (2012) Hydroxybenzothiazoles as New Nonsteroidal Inhibitors of 17 β -Hydroxysteroid Dehydrogenase Type 1 (17 β -HSD1). *PLoS One* 7. doi:10.1371/journal.pone.0029252
- [89] Perspicace E, Giorgio A, Carotti A, Marchais-Oberwinkler S, Hartmann RW (2013) Novel N-methylsulfonamide and retro-N-methylsulfonamide derivatives as 17 β -hydroxysteroid dehydrogenase type 2 (17 β -HSD2) inhibitors with good ADME-related physicochemical parameters. *Eur J Med Chem* 69: 201–215.
- [90] Marchais-Oberwinkler S, Xu K, Wetzel M, Perspicace E, Negri M, Meyer A, Odermatt A, Möller G, Adamski J, Hartmann RW (2013) Structural optimization of 2,5-thiophene amides as highly potent and selective 17 β -hydroxysteroid dehydrogenase type 2 inhibitors for the treatment of osteoporosis. *J Med Chem* 56: 167–181.
- [91] Gargano EM, Perspicace E, Hanke N, Carotti A, Marchais-Oberwinkler S, Hartmann RW (2014) Metabolic stability optimization and metabolite identification of 2,5-thiophene amide 17 β -hydroxysteroid dehydrogenase type 2 inhibitors. *Eur J Med Chem* 87: 203–219.
- [92] Gargano EM, Perspicace E, Carotti A, Marchais-Oberwinkler S, Hartmann RW (2016) Addressing cytotoxicity of 1,4-biphenyl amide derivatives: Discovery of new potent and selective 17 β -hydroxysteroid dehydrogenase type 2 inhibitors. *Bioorg Med Chem Lett* 26: 21–24.
- [93] Du Yan S, Fu J, Soto C, Chen X, Zhu H, Al-Mohanna F, Collison K, Zhu A, Stern E, Saido T, Tohyama M, Ogawa S, Roher A, Stern D (1997) An intracellular protein that binds amyloid- β peptide and mediates neurotoxicity in Alzheimer's disease. *Nature* 389: 689–695.
- [94] Kissinger CR, Rejto PA, Pelletier LA, Thomson JA, Showalter RE, Abreo MA, Agree CS, Margosiak S, Meng JJ, Aust RM, Vanderpool D, Li B, Tempczyk-Russell A, Villafranca JE (2004) Crystal Structure of Human ABAD/HSD10 with a Bound Inhibitor: Implications for Design of Alzheimer's Disease Therapeutics. *J Mol Biol* 342: 943–952.
- [95] Oppermann UC, Salim S, Tjernberg LO, Terenius L, Jörnvall H (1999) Binding of amyloid beta-peptide to mitochondrial hydroxyacyl-CoA dehydrogenase (ERAB): regulation of an

- SDR enzyme activity with implications for apoptosis in Alzheimer's disease. *FEBS Lett* 451: 238–242.
- [96] He XY, Merz G, Yang YZ, Mehta P, Schulz H, Yang SY (2001) Characterization and localization of human type10 17 β -hydroxysteroid dehydrogenase. *Eur J Biochem* 268: 4899–4907.
- [97] Yang S-Y, He X-Y, Schulz H (2005) Multiple functions of type 10 17 β -hydroxysteroid dehydrogenase. *Trends Endocrinol Metab* 16: 167–175.
- [98] Chai Z, Brereton P, Suzuki T, Sasano H, Obeyesekere V, Escher G, Saffery R, Fuller P, Enriquez C, Krozowski Z (2003) 17 β -Hydroxysteroid Dehydrogenase Type XI Localizes to Human Steroidogenic Cells. *Endocrinology* 144: 2084–2091.
- [99] Motojima K (2004) 17 β -Hydroxysteroid dehydrogenase type 11 is a major peroxisome proliferator-activated receptor α -regulated gene in mouse intestine. *Eur J Biochem* 271: 4141–4146.
- [100] Haeseleer F, Palczewski K (2000) Short-chain dehydrogenases/reductases in retina. *Methods Enzymol* 316: 372–383.
- [101] Strausberg RL, Feingold EA, Grouse LH, Derge JG, Klausner RD, Collins FS, Wagner L, Shenmen CM, Schuler GD, Altschul SF, Zeeberg B, Buetow KH, Schaefer CF, Bhat NK, Hopkins RF, Jordan H, Moore T, Max SI, Wang J, et al. (2002) Generation and initial analysis of more than 15,000 full-length human and mouse cDNA sequences. *Proc Natl Acad Sci* 99: 16899–16903.
- [102] Homo sapiens hydroxysteroid (17-beta) dehydrogenase 14, mRNA (cDNA clone MGC:10685 IMAGE:4026397), complete cds CN - BC006283.2 (2006) Available at: <http://www.ncbi.nlm.nih.gov/nuccore/BC006283.2>
- [103] Sivik T, Vikingsson S, Gréen H, Jansson A (2012) Expression Patterns of 17 β -Hydroxysteroid Dehydrogenase 14 in Human Tissues. *Horm Metab Res* 44: 949–956.
- [104] Beck KR, Kaserer T, Schuster D, Odermatt A (2017) Virtual screening applications in short-chain dehydrogenase/reductase research. *J Steroid Biochem Mol Biol* 171: 157–177.
- [105] Halle B (2004) Biomolecular cryocrystallography: structural changes during flash-cooling. *Proc Natl Acad Sci USA* 101: 4793–4798.
- [106] Wlodawer A, Minor W, Dauter Z, Jaskolski M (2013) Protein crystallography for aspiring crystallographers or how to avoid pitfalls and traps in macromolecular structure determination. *FEBS J* 280: 5705–5736.
- [107] Shi Y (2014) A glimpse of structural biology through X-ray crystallography. *Cell* 159: 995–1014.
- [108] Wlodawer A, Minor W, Dauter Z, Jaskolski M (2008) Protein crystallography for non-crystallographers, or how to get the best (but not more) from published macromolecular structures. *FEBS J* 275: 1–21.
- [109] Hassell AM, An G, Bledsoe RK, Bynum JM, Luke H, Iii C, Deng S-JJ, Gampe RT, Grisard TE, Madauss KP, Nolte RT, Rocque WJ, Wang L, Weaver KL, Williams SP, Wisely GB, Xu R, Shewchuk LM (2007) Crystallization of protein–ligand complexes. *Acta Cryst* 63: 72–79.

- [110] Danley DE (2006) Crystallization to obtain protein–ligand complexes for structure-aided drug design. *Acta Cryst* 62: 569–575.
- [111] Ehrmann FR, Stojko J, Metz A, Ois Debaene F, Barandun LJ, Heine A, Diederich FO, Cianferani S, Reuter K, Klebe G (2017) Soaking suggests “alternative facts”: Only co-crystallization discloses major ligand-induced interface rearrangements of a homodimeric tRNA-binding protein indicating a novel mode-of-inhibition. *PLoS One* 12: e0175723.
- [112] Zheng H, Hou J, Zimmerman MD, Wlodawer A, Minor W (2014) The future of crystallography in drug discovery. *Expert Opin Drug Discov* 9: 125–137.
- [113] Scheilman JA (1997) Temperature, Stability, and the Hydrophobic Interaction. *Biophys J* 73: 2960–2964.
- [114] Privalov PL (1979) Stability of Proteins Small Globular Proteins. *Adv Protein Chem* 33: 167–241.
- [115] Lo M-C, Aulabaugh A, Jin G, Cowling R, Bard J, Malamas M, Ellestad G (2004) Evaluation of fluorescence-based thermal shift assays for hit identification in drug discovery. *Anal Biochem* 332: 153–159.
- [116] Vedadi M, Niesen FH, Allali-Hassani A, Fedorov OY, Finerty PJ, Wasney GA, Yeung R, Arrowsmith C, Ball LJ, Berglund H, Hui R, Marsden BD, Nordlund PR, Sundstrom M, Weigelt J, Edwards AM, Thornton JM (2006) Chemical screening methods to identify ligands that promote protein stability, protein crystallization, and structure determination. *Proc Natl Acad Sci* 103: 15835–15840.
- [117] Senisterra GA, Markin E, Yamazaki K, Hui R, Vedadi M, Awrey DE (2006) Screening for Ligands Using a Generic and High-Throughput Light-Scattering-Based Assay. *J Biomol Screen* 11: 940–948.
- [118] Matulis D, Kranz JK, Salemme FR, Todd MJ (2005) Thermodynamic Stability of Carbonic Anhydrase: Measurements of Binding Affinity and Stoichiometry Using ThermoFluor. *Biochemistry* 44: 5258–5266.
- [119] Niesen FH, Berglund H, Vedadi M (2007) The use of differential scanning fluorimetry to detect ligand interactions that promote protein stability. *Nat Protoc* 2: 2212–2221.
- [120] Lavinder JJ, Hari SB, Sullivan BJ, Magliery TJ (2009) High-Throughput Thermal Scanning: A General, Rapid Dye-Binding Thermal Shift Screen for Protein Engineering. *JACS Commun* 131: 3794–3795.
- [121] Lucet IS, Hildebrand JM, Czabotar PE, Zhang J-G, Nicola NA, Silke J, Babon JJ, Murphy JM (2005) Determination of Pseudokinase-ligand Interaction by a Fluorescence-based Thermal Shift Assay. *bio-protol* 4. Available at: <http://www.bio-protocol.org/e1135>
- [122] Cummings MD, Farnum MA, Nelen MI (2006) Universal Screening Methods and Applications of ThermoFluor®. *J Biomol Screen* 11: 854–863.
- [123] Saijo K, Collier JG, Li AC, Katzenellenbogen JA, Glass CK (2011) An ADIOL-ER β -CtBP transrepression pathway negatively regulates microglia-mediated inflammation. *Cell* 145: 584–595.

- [124] Frotscher M, Ziegler E, Marchais-Oberwinkler S, Kruchten P, Neugebauer A, Fetzter L, Scherer C, Müller-Vieira U, Messinger J, Thole H, Hartmann RW (2008) Design, synthesis, and biological evaluation of (hydroxyphenyl)naphthalene and -quinoline derivatives: potent and selective nonsteroidal inhibitors of 17 β -hydroxysteroid dehydrogenase type 1 (17 β -HSD1) for the treatment of estrogen-dependent disease. *J Med Chem* 51: 2158–2169.
- [125] Kruchten P, Werth R, Bey E, Oster A, Marchais-Oberwinkler S, Frotscher M, Hartmann RW (2009) Selective inhibition of 17 β -hydroxysteroid dehydrogenase type 1 (17 β -HSD1) reduces estrogen responsive cell growth of T47-D breast cancer cells. *J Steroid Biochem Mol Biol* 114: 200–206.
- [126] Bertolotti N, Braun F, Lepage M, Möller G, Adamski J, Heine A, Klebe G, Marchais-Oberwinkler S (2016) New Insights into Human 17 β -Hydroxysteroid Dehydrogenase Type 14: First Crystal Structures in Complex with a Steroidal Ligand and with a Potent Nonsteroidal Inhibitor. *J Med Chem* 59: 6961–6967.
- [127] Braun F, Bertolotti N, Möller G, Adamski J, Steinmetzer T, Salah M, Abdelsamie AS, van Koppen CJ, Heine A, Klebe G, Marchais-Oberwinkler S (2016) First Structure–Activity Relationship of 17 β -Hydroxysteroid Dehydrogenase Type 14 Nonsteroidal Inhibitors and Crystal Structures in Complex with the Enzyme. *J Med Chem* 59: 10719–10737.
- [128] Gekko K, Timasheff SN (1981) Mechanism of protein stabilization by glycerol: preferential hydration in glycerol-water mixtures. *Biochemistry* 20: 4667–4676.
- [129] Myers JS, Jakoby WB (1975) Glycerol as an agent eliciting small conformational changes in alcohol dehydrogenase. *J Biol Chem* 250: 3785–3789.
- [130] Bondos SE, Bicknell A (2003) Detection and prevention of protein aggregation before, during, and after purification. *Anal Biochem* 316: 223–231.
- [131] Rodgers DW (1994) Cryocrystallography. *Structure* 2: 1135–1140.
- [132] Collaborative Computational Project N 4 (1994) The CCP4 suite: programs for protein crystallography. *Acta Crystallogr D Biol Crystallogr* 50: 760–763.
- [133] Laskowski R a., MacArthur MW, Moss DS, Thornton JM (1993) PROCHECK: a program to check the stereochemical quality of protein structures. *J Appl Crystallogr* 26: 283–291.
- [134] Kleywegt GJ, Zou JY, Kjeldgaard M, Jones TA (2001) International Tables for Crystallography, Volume F. Crystallography of Biological Macromolecules (Rossmann, M.G. and Arnold, E.,)
- [135] Krissinel E, Henrick K (2007) Inference of Macromolecular Assemblies from Crystalline State. *J Mol Biol* 372: 774–797.
- [136] Kantardjieff KA, Rupp B (2003) Matthews coefficient probabilities: Improved estimates for unit cell contents of proteins, DNA, and protein–nucleic acid complex crystals. *Protein Sci* 12: 1865–1871.
- [137] Weichenberger CX, Rupp B (2014) Ten years of probabilistic estimates of biocrystal solvent content: new insights via nonparametric kernel density estimate. *Acta Crystallogr Sect D Biol Crystallogr* 70: 1579–1588.

- [138] Powell AJ, Read JA, Banfield MJ, Gunn-Moore F, Yan SD, Lustbader J, Stern AR, Stern DM, Brady RL (2000) Recognition of structurally diverse substrates by type II 3-hydroxyacyl-CoA dehydrogenase (HADH II)/Amyloid- β binding alcohol dehydrogenase (ABAD)1. *J Mol Biol* 303: 311–327.
- [139] Gangloff A, Shi R, Nahoum V, Lin S-X (2003) Pseudo-symmetry of C19 steroids, alternative binding orientations, and multispecificity in human estrogenic 17 β -hydroxysteroid dehydrogenase. *FASEB J Off Publ Fed Am Soc Exp Biol* 17: 274–276.
- [140] Gabadinho J, Beteva A, Guijarro M, Rey-Bakaikoa V, Spruce D, Bowler MW, Brockhauser S, Flot D, Gordon EJ, Hall DR, Lavault B, McCarthy AA, McCarthy J, Mitchell E, Monaco S, Mueller-Dieckmann C, Nurizzo D, Ravelli RBG, Thibault X, et al. (2010) MxCuBE: a synchrotron beamline control environment customized for macromolecular crystallography experiments. *J Synchrotron Radiat* 17: 700–707.
- [141] Mueller U, Darowski N, Fuchs MR, Förster R, Hellmig M, Paithankar KS, Pühringer S, Steffien M, Zocher G, Weiss MS (2012) Facilities for macromolecular crystallography at the Helmholtz-Zentrum Berlin. *J Synchrotron Radiat* 19: 442–449.
- [142] Kabsch W (2010) XDS. *Acta Crystallogr Sect D Biol Crystallogr* 66: 125–132.
- [143] McCoy AJ, Grosse-Kunstleve RW, Adams PD, Winn MD, Storoni LC, Read RJ (2007) Phaser crystallographic software. *J Appl Crystallogr* 40: 658–674.
- [144] Emsley P, Cowtan K (2004) Coot: model-building tools for molecular graphics. *Acta Crystallogr Sect D Biol Crystallogr* 60: 2126–2132.
- [145] Adams PD, Afonine P V., Bunkóczi G, Chen VB, Davis IW, Echols N, Headd JJ, Hung LW, Kapral GJ, Grosse-Kunstleve RW, McCoy AJ, Moriarty NW, Oeffner R, Read RJ, Richardson DC, Richardson JS, Terwilliger TC, Zwart PH (2010) PHENIX: A comprehensive Python-based system for macromolecular structure solution. *Acta Crystallogr Sect D Biol Crystallogr* 66: 213–221.
- [146] <http://www.molinspiration.com/>
- [147] Smart OS, Womack TO, Sharff A, Flensburg C, Keller P, Paciorek W, Vonrhein C, Bricogne G (2011) grade, version v1.102. <http://www.globalphasing.com>.
- [148] Painter J, Merritt EA (2006) TLSMD web server for the generation of multi-group TLS models. *J Appl Crystallogr* 39: 109–111.
- [149] Painter J, Merritt EA (2006) Optimal description of a protein structure in terms of multiple groups undergoing TLS motion. *Acta Crystallogr Sect D Biol Crystallogr* 62: 439–450.
- [150] Bey E, Marchais-Oberwinkler S, Negri M, Kruchten P, Oster A, Klein T, Spadaro A, Werth R, Frotscher M, Birk B, Hartmann RW (2009) New insights into the SAR and binding modes of bis(hydroxyphenyl)thiophenes and -benzenes: influence of additional substituents on 17 β -hydroxysteroid dehydrogenase type 1 (17 β -HSD1) inhibitory activity and selectivity. *J Med Chem* 52: 6724–6743.
- [151] Poirier D, Boivin RP, Tremblay MR, Bérubé M, Qiu W, Lin S-X (2005) Estradiol-adenosine hybrid compounds designed to inhibit type 1 17 β -hydroxysteroid dehydrogenase. *J Med Chem* 48: 8134–8147.

- [152] Maltais R, Ayan D, Trottier A, Barbeau X, Lagüe P, Bouchard J-E, Poirier D (2014) Discovery of a non-estrogenic irreversible inhibitor of 17 β -hydroxysteroid dehydrogenase type 1 from 3-substituted-16 β -(m-carbamoylbenzyl)-estradiol derivatives. *J Med Chem* 57: 204–222.
- [153] Maltais R, Trottier A, Barbeau X, Lagüe P, Perreault M, Thériault J-F, Lin S-X, Poirier D (2016) Impact of structural modifications at positions 13, 16 and 17 of 16 β -(m-carbamoylbenzyl)-estradiol on 17 β -hydroxysteroid dehydrogenase type 1 inhibition and estrogenic activity. *J Steroid Biochem Mol Biol* 161: 24–35.
- [154] Lilienkampf A, Karkola S, Alho-Richmond S, Koskimies P, Johansson N, Huhtinen K, Vihko K, Wähälä K (2009) Synthesis and biological evaluation of 17 β -hydroxysteroid dehydrogenase type 1 (17 β -HSD1) inhibitors based on a thieno[2,3-d]pyrimidin-4(3H)-one core. *J Med Chem* 52: 6660–6671.
- [155] Allan GM, Lawrence HR, Cornet J, Bubert C, Fischer DS, Vicker N, Smith A, Tutill HJ, Purohit A, Day JM, Mahon MF, Reed MJ, Potter BVL (2006) Modification of estrone at the 6, 16, and 17 positions: novel potent inhibitors of 17 β -hydroxysteroid dehydrogenase type 1. *J Med Chem* 49: 1325–1345.
- [156] Allan GM, Vicker N, Lawrence HR, Tutill HJ, Day JM, Huchet M, Ferrandis E, Reed MJ, Purohit A, Potter BVL (2008) Novel inhibitors of 17 β -hydroxysteroid dehydrogenase type 1: templates for design. *Bioorg Med Chem* 16: 4438–4456.
- [157] Schuster D, Nashev LG, Kirchmair J, Laggner C, Wolber G, Langer T, Odermatt A (2008) Discovery of nonsteroidal 17 β -hydroxysteroid dehydrogenase 1 inhibitors by pharmacophore-based screening of virtual compound libraries. *J Med Chem* 51: 4188–4199.
- [158] Starcević S, Brozic P, Turk S, Cesar J, Rizner TL, Gobec S (2011) Synthesis and biological evaluation of (6- and 7-phenyl) coumarin derivatives as selective nonsteroidal inhibitors of 17 β -hydroxysteroid dehydrogenase type 1. *J Med Chem* 54: 248–261.
- [159] Wetzel M, Marchais-Oberwinkler S, Hartmann RW (2011) 17 β -HSD2 inhibitors for the treatment of osteoporosis: Identification of a promising scaffold. *Bioorg Med Chem* 19: 807–815.
- [160] Xu K, Al-Soud YA, Wetzel M, Hartmann RW, Marchais-Oberwinkler S (2011) Triazole ring-opening leads to the discovery of potent nonsteroidal 17 β -hydroxysteroid dehydrogenase type 2 inhibitors. *Eur J Med Chem* 46: 5978–5990.
- [161] Stoffel-Wagner B, Watzka M, Steckelbroeck S, Schramm J, Bidlingmaier JF, Klingmüller D (1999) Expression of 17 β -hydroxysteroid dehydrogenase types 1, 2, 3 and 4 in the human temporal lobe. *J Endocrinol* 160: 119–126.
- [162] Veber DF, Johnson SR, Cheng H-Y, Smith BR, Ward KW, Kopple KD (2002) Molecular Properties That Influence the Oral Bioavailability of Drug Candidates. *J Med Chem* 45: 2615–2623.
- [163] Lipinski CA, Lombardo F, Dominy BW, Feeney PJ (2001) Experimental and computational approaches to estimate solubility and permeability in drug discovery and development settings. *Adv Drug Deliv Rev* 46: 3–26.
- [164] Pajouhesh H, Lenz GR (2005) Medicinal Chemical Properties of Successful Central Nervous System Drugs. *NeuroRx* 2: 541–553.

- [165] Morrison JF (1982) The slow-binding and slow, tight-binding inhibition of enzyme-catalysed reactions. *Trends Biochem Sci* 7: 102–105.
- [166] Morrison JF (1969) Kinetics of the reversible inhibition of enzyme-catalysed reactions by tight-binding inhibitors. *Biochim Biophys Acta* 185: 269–286.
- [167] Copeland RA (2000) *Enzymes: A Practical Introduction to Structure, Mechanism, and Data Analysis* (Wiley-VCH, New York). 2nd Ed.
- [168] Baell JB, Holloway GA (2010) New substructure filters for removal of pan assay interference compounds (PAINS) from screening libraries and for their exclusion in bioassays. *J Med Chem* 53: 2719–2740.
- [169] http://cbligand.org/PAINS/search_struct.php
- [170] Schweigert N, Zehnder AJB, Eggen RIL (2001) Chemical properties of catechols and their molecular modes of toxic action in cells, from microorganisms to mammals. *Environ Microbiol* 3: 81–91.
- [171] Emsley P, Lohkamp B, Scott WG, Cowtan K (2010) Features and development of *Coot*. *Acta Crystallogr Sect D Biol Crystallogr* 66: 486–501.
- [172] Eisenberg D, Schwarz E, Komaromy M, Wall R (1984) Analysis of membrane and surface protein sequences with the hydrophobic moment plot. *J Mol Biol* 179: 125–142.
- [173] Molecular Operating Environment (MOE), 2013.08; Chemical Computing Group Inc., 1010 Sherbooke St. West, Suite #910, Montreal, QC, Canada, H3A 2R7, 2016.
- [174] Kruchten P, Werth R, Marchais-Oberwinkler S, Frotscher M, Hartmann RW (2009) Development of a biological screening system for the evaluation of highly active and selective 17 β -HSD1-inhibitors as potential therapeutic agents. *Mol Cell Endocrinol* 301: 154–157.
- [175] Kruchten P (2009) Entwicklung eines Screeningsystems zur Identifizierung hochaktiver und selektiver Hemmstoffe der 17 β -Hydroxysteroid-Dehydrogenase Typ 1 (17 β -HSD1). Dissertation (Saarland University, Saarbrücken).
- [176] Wetzel M, Gargano EM, Hinsberger S, Marchais-Oberwinkler S, Hartmann RW (2012) Discovery of a new class of bicyclic substituted hydroxyphenylmethanones as 17 β -hydroxysteroid dehydrogenase type 2 (17 β -HSD2) inhibitors for the treatment of osteoporosis. *Eur J Med Chem* 47: 1–17.
- [177] Hwang C-C, Chang Y-H, Hsu C-N, Hsu H-H, Li C-W, Pon H-I (2005) Mechanistic roles of Ser-114, Tyr-155, and Lys-159 in 3 α -hydroxysteroid dehydrogenase/carbonyl reductase from *Comamonas testosteroni*. *J Biol Chem* 280: 3522–3528.
- [178] Bissantz C, Kuhn B, Stahl M (2010) A medicinal chemist's guide to molecular interactions. *J Med Chem* 53: 5061–5084.
- [179] Michiels PJA, Ludwig C, Stephan M, Fischer C, Möller G, Messinger J, van Dongen M, Thole H, Adamski J, Günther UL (2009) Ligand-based NMR spectra demonstrate an additional phytoestrogen binding site for 17 β -hydroxysteroid dehydrogenase type 1. *J Steroid Biochem Mol Biol* 117: 93–98.
- [180] Sheriff S (1993) Some methods for examining the interactions between two molecules. *Immunomethods* 3: 191–196.

- [181] Sheriff S, Hendrickson WA, Smith JL (1987) Structure of myohemerythrin in the azidomet state at 1.71.3Å resolution. *J Mol Biol* 197: 273–296.
- [182] Connolly, M. L. (1983) Analytical Molecular Surface Calculation. *J Appl Crystallogr* 16: 548–558
- [183] Connolly ML (1983) Solvent-accessible surfaces of proteins and nucleic acids. *Science* 221: 709–713.
- [184] Callaghan R, Luk F, Bebawy M (2014) Inhibition of the multidrug resistance P-glycoprotein: time for a change of strategy? *Drug Metab Dispos* 42: 623–631.
- [185] Patrick GL, Mourik T van (2017) *An Introduction to Medicinal Chemistry* ed Oxford (Oxford). 5th Edition
- [186] Neudert G, Klebe G (2011) fconv: format conversion, manipulation and feature computation of molecular data. *Bioinformatics* 27: 1021–1022.
- [187] Urquhart BL, Kim RB (2009) Blood-brain barrier transporters and response to CNS-active drugs. *Eur J Clin Pharmacol* 65: 1063–1070.
- [188] Sam KM, Boivin RP, Tremblay MR, Auger S, Poirier D (1998) C16 and C17 derivatives of estradiol as inhibitors of 17 beta-hydroxysteroid dehydrogenase type 1: chemical synthesis and structure-activity relationships. *Drug Des Discov* 15: 157–180.
- [189] Mosmann T (1983) Rapid colorimetric assay for cellular growth and survival: application to proliferation and cytotoxicity assays. *J Immunol Methods* 65: 55–63.
- [190] Pires A do RA, Lecerf-Schmidt F, Guragossian N, Pazinato J, Gozzi GJ, Winter E, Valdameri G, Veale A, Boumendjel A, Di Pietro A, Pérès B (2016) New, highly potent and non-toxic, chromone inhibitors of the human breast cancer resistance protein ABCG2. *Eur J Med Chem* 122: 291–301.
- [191] Mazumdar M, Fournier D, Zhu D-W, Cadot C, Poirier D, Lin S-X (2009) Binary and ternary crystal structure analyses of a novel inhibitor with 17β-HSD type 1: a lead compound for breast cancer therapy. *Biochem J* 424. Available at: <http://www.biochemj.org/content/424/3/357>
- [192] Qiu W, Campbell RL, Gangloff A, Dupuis P, Boivin RP, Martin R (2002) A concerted, rational design of 17b-hydroxysteroid dehydrogenase inhibitors: the complex structure with estradiol-adenosine hy. *FASEB J*. 16: 1829–1831
- [193] Sievers F, Wilm A, Dineen D, Gibson TJ, Karplus K, Li W, Lopez R, McWilliam H, Remmert M, Sö Ding J, Thompson JD, Higgins DG (2011) Fast, scalable generation of high-quality protein multiple sequence alignments using Clustal Omega. *Mol Syst Biol* 7: 539.
- [194] Goujon M, McWilliam H, Li W, Valentin F, Squizzato S, Paern J, Lopez R (2010) A new bioinformatics analysis tools framework at EMBL-EBI. *Nucleic Acids Res* 38: W695–W699.
- [195] McWilliam H, Li W, Uludag M, Squizzato S, Park YM, Buso N, Cowley AP, Lopez R (2013) Analysis Tool Web Services from the EMBL-EBI. *Nucleic Acids Res* 41: W597–W600.
- [196] Jones G, Willett P, Glen RC, Leach AR, Taylor R (1997) Development and validation of a genetic algorithm for flexible docking. *J Mol Biol* 267: 727–748.

- [197] Hosfield DJ, Wu Y, Skene RJ, Hilgers M, Jennings A, Snell GP, Aertgeerts K (2005) Conformational flexibility in crystal structures of human 11 β -hydroxysteroid dehydrogenase type I provide insights into glucocorticoid interconversion and enzyme regulation. *J Biol Chem* 280: 4639–4648.
- [198] Schiebel J, Krimmer SGG, Röwer K, Knörlein A, Wang X, Park AYY, Stieler M, Ehrmann FRR, Fu K, Radeva N, Krug M, Huschmann FUU, Glöckner S, Weiss MSS, Mueller U, Klebe G, Heine A, R??wer K, Kn??rlein A, et al. (2016) High-Throughput Crystallography: Reliable and Efficient Identification of Fragment Hits. *Structure* 24: 1398–1409.
- [199] Scott DE, Coyne AG, Hudson SA, Abell C (2012) Fragment-Based Approaches in Drug Discovery and Chemical Biology. *Biochemistry* 51: 4990–5003.
- [200] Murray CW, Verdonk ML, Rees DC (2012) Experiences in fragment-based drug discovery. *Trends Pharmacol Sci* 33: 224–232.
- [201] Radeva N, Schiebel J, Wang X, Krimmer SG, Fu K, Stieler M, Ehrmann FR, Metz A, Rickmeyer T, Betz M, Winquist J, Park AY, Huschmann FU, Weiss MS, Mueller U, Heine A, Klebe G (2016) Active Site Mapping of an Aspartic Protease by Multiple Fragment Crystal Structures: Versatile Warheads To Address a Catalytic Dyad. *J Med Chem* 59: 9743–9759.
- [202] Radeva N, Krimmer SG, Stieler M, Fu K, Wang X, Ehrmann FR, Metz A, Huschmann FU, Weiss MS, Mueller U, Schiebel J, Heine A, Klebe G (2016) Experimental Active-Site Mapping by Fragments: Hot Spots Remote from the Catalytic Center of Endothiapepsin. *J Med Chem* 59: 7561–7575.
- [203] Schiebel J, Radeva N, Krimmer SG, Wang X, Stieler M, Ehrmann FR, Fu K, Metz A, Huschmann FUFU, Weiss MS, Mueller U, Heine A, Klebe G (2016) Six Biophysical Screening Methods Miss a Large Proportion of Crystallographically Discovered Fragment Hits: A Case Study. *ACS Chem Biol* 11: 1693–1701.
- [204] Schiebel J, Radeva N, Köster H, Metz A, Krotzky T, Kuhnert M, Diederich WE, Heine A, Neumann L, Atmanene C, Roecklin D, Vivat-Hannah VV, Renaud JP, Meinecke R, Schlinck N, Sitte A, Popp F, Zeeb M, Klebe G, et al. (2015) One Question, Multiple Answers: Biochemical and Biophysical Screening Methods Retrieve Deviating Fragment Hit Lists. *ChemMedChem* 10: 1511–1521.

Acknowledgements

First and foremost, I thank my supervisor Prof. Gerhard Klebe for the fruitful discussions and for giving me the opportunity to prepare my thesis as a member of his research group. His persistent encouragement have been very helpful for me during these years.

I would like to express my deep appreciation to Dr. Sandrine Marchais-Oberwinkler, my second supervisor, for her constant support, not only on scientific matter. She has been always there on my side to listen and give advice.

Moreover, I am very grateful to Prof. Andreas Heine for introducing me to macromolecular X-ray crystallography and for the great amount of time he invested in me. Thank you for believing in me.

Also, I thank all my internal and external collaborators, especially Florian Braun for working so closely and fruitfully together with me. His collaboration has been essential for the success of this project. Further thanks go to Prof. R.W. Hartmann, Dr. Gabriele Möller, Prof. Jerzy Adamski, Aline Keils, Lorena Zara, Mahalia Lepage, Steffen Glöckner, Paige Grant, Jud Badran, Corey Taylor and Dr. Alexander Metz.

A special thank you goes to Dr. Stefan Krimmer for helping me out in so many ways that words are not able to describe. Without his constant support this thesis would not have been possible. I deeply thank Felix Terwesten and Phong Nguyen, not least for keeping the computer network running. I am grateful to Lydia Hartleben for her administrative support and to Christian Sohn and Steffi Dörr for their technical help.

I thank my friends and colleagues from the entire Klebe and Kolb labs for creating a friendly working atmosphere and for making working with them a great experience. I especially thank my girl Aline Keils, Manuel Neeb, Chris Rechlin, Florent Chevillard, Martin Stieler, Anna Sandner, Francesca Magari, Engi Hassan, Felix Terwesten, Corey Taylor, Alexander Metz, Tobias Wulsdorf, Jonathan Cramer and Jessico Desogus.

Last but not least, I thank my family for their constant support.

Curriculum Vitae

Personal Details

Name	Nicole Bertoletti
Date of birth	May 2 nd , 1988
Place of birth	Sarzana, Italy
Nationality	Italian

Education

10/2017 (expected)	PhD (Dr. rer. nat.) in Life Sciences Institute of Pharmaceutical Chemistry, Philipps University of Marburg, Germany
07/2013	State Examination, Board License as Pharmacist in Italy
04/2013	Laurea Magistrale in Pharmaceutical Chemistry and Technologies University of Pisa, Italy
2007–2013	Study of Pharmaceutical Chemistry and Technologies University of Pisa, Italy

Research Experience

since 01/2014	Dissertation Drug design group of Prof. Dr. Gerhard Klebe, Institute of Pharmaceutical Chemistry, Philipps University of Marburg, Germany
09/2013–12/2013	Internship Drug design group of Prof. Dr. Gerhard Klebe, Institute of Pharmaceutical Chemistry, Philipps University of Marburg, Germany
09/2012–04/2013	Master Thesis Molecular Modeling & Virtual Screening Laboratory of Prof. Dr. Tiziano Tuccinardi, University of Pisa, Italy Thesis title: "In silico optimization of Lactate Dehydrogenase inhibitors"

Professional Experience

01/2014–06/2017	Teaching Assistant , Philipps University of Marburg, Germany
05/2012–11/2012	Pharmacist Intern , "Farmacia Martignoni" drugstore in Fosdinovo, Italy

Journal Publications

- Braun F,^{||} Bertoletti N,^{||} Möller G, Adamski J, Steinmetzer T, Salah M, Abdelsamie A. S, van Koppen C. J, Heine A, Klebe G, Marchais-Oberwinkler S.
First Structure-Activity Relationship of 17 β -Hydroxysteroid Dehydrogenase Type 14 Nonsteroidal Inhibitors and Crystal Structures in Complex with the Enzyme.
J. Med. Chem **2016**, *59*, 10719–10737
- Bertoletti N,^{||} Braun F,^{||} Lepage M, Möller G, Adamski J, Heine A, Klebe G, Marchais-Oberwinkler S.
New Insights into Human 17 β -Hydroxysteroid Dehydrogenase Type 14: First Crystal Structures in Complex with a Steroidal Ligand and with a Potent Nonsteroidal Inhibitor
J. Med. Chem **2016**, *59*, 6961–6967

Oral Presentations

- **25th Annual Meeting of the German Crystallographic Society, March 27–30, 2017 in Karlsruhe, Germany**
5 min talk on "X-ray Crystallographic Fragment Screening and Hit Optimization"

Poster Presentations

- **24th Congress of the International Union of Crystallography, August 21–28, 2017 in Hyderabad, India**
Poster on "X-ray Crystallography: essential tool for protein characterization and ligand optimization"
- **25th Annual Meeting of the German Crystallographic Society, March 27–30, 2017 in Karlsruhe, Germany**
Poster on "X-ray Crystallographic Fragment Screening and Hit Optimization"
- **Eighth Joint BER II and BESSY II User Meeting, December 7–9, 2016 in Berlin, Germany**
Poster on "X-ray Crystallographic Fragment Screening for the Development of New h17beta-HSD14 Inhibitors"
- **DPHG Jahrestagung 2016 / Annual meeting, October 4–7, 2016 in Munich, Germany**
Poster on "Structure and Fragment Based Lead Discovery for New Potential h17beta-HSD14 Inhibitor"
- **EFMC-ISMC 2016 XXIV EFMC International Symposium on Medicinal Chemistry, August 28 –September 1, 2016 in Manchester, UK**
Poster on "Insight into the Structure of Human 17beta-Hydroxysteroid Dehydrogenase type 14"
- **Seventh Joint BER II and BESSY II User Meeting, December 9–10, 2015 in Berlin, Germany**
Poster on "Structure of 17beta-Hydroxysteroid Dehydrogenase 14 with First-in-Class Inhibitors"
- **DPHG Jahrestagung 2015 / Annual meeting, September 23–25, 2015 in Düsseldorf, Germany**
Poster on "Structure characterization of 17beta-hydroxysteroid dehydrogenase Type 14 and identification of the first inhibitors"

^{||} These authors contributed equally

Workshop Participations

- 12/2016 **Challenges in diffraction data processing - How to get the most out of your data**, Helmholtz-Zentrum Berlin, Germany
- 12/2015 **Tender X-rays in MX**, Helmholtz-Zentrum Berlin, Germany

Stipends & Awards

- 2017 **IUCr travel grant** from TPP labtech, DKG and from the DAAD to the 24th Congress and General Assembly of the International Union of Crystallography in Hyderabad, India
- 12/2015 **MX-Poster prize** at the Seventh Joint BER II and BESSY II User Meeting, December 9–10, 2015 in Berlin, Germany

Erklärung

Ich versichere, dass ich meine Dissertation

*“Structural Characterization of 17 β -Hydroxysteroid Dehydrogenase Type 14
and Inhibitor Optimization Using Crystallography and Computational Techniques “*

selbständig ohne unerlaubte Hilfe angefertigt und mich dabei keiner anderen als der von mir ausdrücklich bezeichneten Quellen bedient habe. Alle vollständig oder sinngemäß übernommenen sind Zitate als solche gekennzeichnet.

Die Dissertation wurde in der jetzigen oder einer ähnlichen Form noch bei keiner anderen Hochschule eingereicht und hat noch keinen sonstigen Prüfungszwecken gedient.

Marburg, den

.

(Nicole Bertoletti)